Water Quality Modeling for the Kennet and Avon Canal, a Navigational Canal in an Inland Catchment

Rebecca Zeckoski

St. Catharine's College

University of Cambridge

This dissertation is submitted for the degree of Doctor of Philosophy.

June 2010

Declarations

This dissertation is the result of my own work and includes nothing which is the outcome of work done in collaboration except where specifically indicated in the text.

This dissertation is not substantially the same as any that I have submitted, or, is being concurrently submitted for a degree or diploma or other qualification at the University of Cambridge or any other University or similar institution. No substantial part of my dissertation has already been submitted, or, is being concurrently submitted for any such degree, diploma or other qualification at the University of Cambridge or any other University or similar institution.

This dissertation does not exceed the word limit, being 53433 words in length, comprising 230 pages and including 93 figures and 39 tables.

_____

Rebecca W. Zeckoski

Acknowledgements

I am most grateful to Dr. Colin Neal (Centre for Ecology and Hydrology) and Dr. Andrew Wade (Reading University) for their inspiration on this project and supply of information crucial to the characterization of my model for the Kennet and Avon Canal.

I also acknowledge the kind assistance of Mr. Mike Lee (Hon. Engineer for the Kennet and Avon Canal), Ms. Alison Love (Environment Agency), and Mr. John Hallett (Environment Agency), who provided additional information, documents, and guided tours of the Kennet and Avon Canal.

Mr. Attila Lazar (University of Reading) generously shared data used in the calibration of his own model for the River Kennet.

Mr. & Mrs. Mick Berry, of Berries B&B in Hungerford, were most supportive during my trips to visit the canal, even allowing me use of their personal bicycle. My water sample collection would not have been possible without their support.

I appreciate the support and advice of my advisor, Mr. Allan McRobie, whose input was critical in defining the scope of the project, keeping my focus on the purpose of a PhD project, and encouraging me to get out in the field and get my hands dirty.

To my supervisor, Dr. Dongfang Liang, I owe much gratitude: for believing in me and helping to bring me to this great institution, for his constant support of myself and my project, and for his willingness to help in every way possible.

To my parents, Dr. & Mrs. W.R. Winfrey, who have always believed in me and encouraged my academic efforts.

And last but certainly not least, I am eternally grateful for the support and encouragement of my husband, Aaron Zeckoski, who sat with me through the long days and nights when I was convinced I would never finish, and who supported me both financially and emotionally throughout my research process.

Water Quality Modeling for the Kennet and Avon Canal, a Navigational Canal in an Inland Catchment

Rebecca Zeckoski

The Kennet and Avon Canal in southern England is experiencing severe water quality problems caused by inorganic sediment and algae. These water quality problems are affecting the angling sport of fishermen downstream of the confluence of the canal with the River Kennet. The Environment Agency has been called upon to remedy these issues, but before proceeding they desire a computer model capable of predicting the water quality impacts of various scenarios under consideration. No such model was available to them.

This project identified the key solids generation and transport processes to be included in a water quality model for inland navigational canals. Where available, equations from the literature describing relevant processes were used or modified for inclusion in a canal modeling algorithm. Where literature was not available, water quality samples were taken to characterize needed relationships. The final algorithm was coded and tested using a simplified dataset that allowed clear evaluation of the simulated processes.

After successful testing, the canal model was applied to the Kennet and Avon Canal. The time series predicted by the model were compared to observed hydrological, solids, and chlorophyll-a (representing algae) data at multiple points in the canal. The model adequately predicted all of these constituents at the monitored locations.

The final task in the project required evaluation of six management scenarios proposed by the Environment Agency to address the water quality problem. The model suggests that filtration or other treatment of water in the canal near the confluence with the river is the best management option, as it will address both the elevated inorganic sediment and algae concentrations at the most critical point in the canal. Less desirable options include efforts that only target inorganic sediment, which could increase algal concentrations by increasing light availability; and diversion of surface flows from the canal, which could possibly damage the hydrologic balance of the canal while encouraging undesirable algal growth.

Key Words: Canal, Hydrologic Model, Sediment Transport, Sediment Model, Algal Growth, Algal Model, Computer Model, Kennet & Avon Canal, River Kennet, England

Notation

Storage Subscripts

$_{alg}$ = parameter is related to dry algal mass

$_{coh}$ = parameter is related to inorganic cohesive sediment

$_{non}$ = parameter is related to inorganic non-cohesive sediment

$_{sed}$ = parameter is related to inorganic sediment

Inflow and Outflow Subscripts

$_{abs}$ = parameter is related to flows abstracted from the canal

$_{bio}$ = parameter is related to algal growth

$_{boat}$ = parameter is related to boat traffic

$_{dep}$ = parameter is related to inorganic sediment deposition

$_{evap}$ = parameter is related to evaporation

$_{ext}$ = parameter is related to external flows entering the canal

$_{leak}$ = parameter is related to flow through leaky lock gates

$_{lock}$ = parameter is related to lockage flow

$_{lockmove}$ = parameter is related to movement of lock gates

$_{prec}$ = parameter is related to precipitation

$_{runoff}$ = parameter is related to runoff from the surrounding catchment

$_{seep}$ = parameter is related to seepage through the canal walls

$_{w,lock}$ = parameter is related to 'weir' flow over the top of a lock gate

$_{weir}$ = parameter is related to flow through the overflow weir in the reach

Variables and Parameters

C_{chl} = conversion constant to convert Chlorophyll-a mass to dry algal mass (mg dry algal mass/mg Chl-a)

$C_{d,weir}$ = weir coefficient (Ø)

CS_{boat} = concentration of inorganic sediment disturbed by boat movement (mg/m^3)

D = water depth in a reach (m)

D_{lock} = height of lock gates above bottom of upstream canal reach (m)

E_{boat} = efficiency of boat movement (number of boats moving in opposite directions/total number of boats) (Ø)

ED = euphotic depth, the water depth at which the light intensity is 1% of the value just below the water surface (m)

F_{boat} = frequency of boat movement (boats/s)

H_{sides} = height of sides of overflow weir 'box' (m)

H_{weir} = distance from overflow weir crest to the bottom of the canal (m)

I = inflow of water (m^3/s)

ISS = inflow of solids (mg/s)

K = maximum supportable algal population (mg dry algal mass/m^3)

$K_{s,l}$ = Michaelis-Menten constant for light-limited growth (J/m^2s)

L = length of reach (m)

Leak = leakage rate ($m^3/m \cdot s$)

LI = light intensity (light available to algae) (J/m^2s)

L_{lock} = length of lock gates (m)

L_{weir} = length of overflow weir crest (m)

Q = outflow of water (m^3/s)

QSS = outflow of solids (mg/s)

S = storage of water in a reach (m^3)

SS = storage of solids in a reach (mg)

Seep = seepage rate (m^3/m^2s)

t = time (s)

TP = total phosphorus concentration (mg/m^3)

V_{ED} = volume of water in the euphotic depth (m^3)

V_{lock} = lockage volume (m^3)

v_b = velocity of boat (m/s)

v_w = velocity of water (m/s)

W = reach width (m)

w_s = fall velocity of inorganic sediment (m/s)

μ = (in algorithm description) specific growth rate of algae considering temperature, light availability, and phosphorus availability (1/s)

μ_{max} = specific growth rate of algae based on temperature and light availability (1/s)

$\mu_{max,T}$ = specific growth rate of algae based only on temperature (1/s)

Table of Contents

List of Tables

List of Figures

1. Introduction

1.1. Problem Statement

There are many canals and navigable waterways in the United Kingdom with the potential to contribute poor quality water to natural streams (Swanson et al. 2004). During the heyday of canals, circa 1840, nearly 4100 miles (6600 km) of inland waterways existed, including both canals and rivers that were made navigable (Hadfield 1981). Over the subsequent years, railroads and lorry traffic led to a decline in canal use, and by the time of the 1968 Transport Act, when all existing canals in Britain were classified into commercial waterways, cruiseways (for amenity use only), and remainder waterways, only 2000 miles (3220 km) remained (Kennet and Avon Canal Trust Ltd. 1981). Of these, 570 miles (917 km) were classified as 'remainder' waterways: not legally abandoned, but not financially maintained by the Government. In these waterways, private groups, such as the Kennet and Avon Canal Trust, frequently put forth their own money to contribute to the maintenance of the canals. The Government maintains 1071 miles (1724 km) of cruiseways. Thus private citizens and Government officials alike will benefit from computer models that can help them make choices about the best maintenance activities to pursue in inland waterways in light of environmental concerns.

The Environment Agency and local stakeholders have voiced specific concerns over pollution in the Kennet and Avon Canal, and in particular about the water quality problems it is causing in the neighboring River Kennet that originate at the river's confluence with the canal just below Copse Lock (Figure 1). Prior to the start of this research project, suspected issues contributing to the water quality problem in the canal included elevated algal growth, boat traffic, and lock operations. All these issues contribute to an elevated suspended solids concentration in the canal. As no computer model existed that could account for all these sources of pollution, the goal of this research project was to create such a canal model, capable of being used both in the Copse Lock area of the Kennet and Avon Canal and other navigational canals with similar water quality issues.

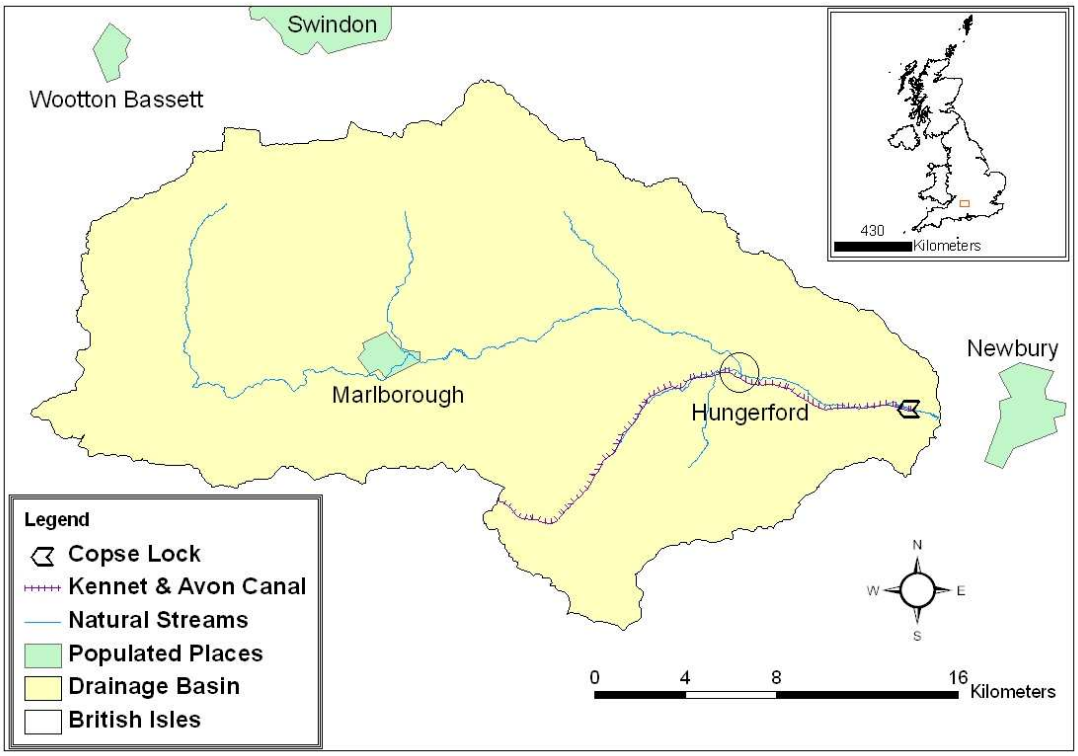

Figure 1. Location of the Kennet and Avon Canal. Hungerford is not large enough to be a 'populated place' but is an important location for monitoring of the canal and natural streams.

1.2. Research Objectives

Primary Objective: Determine and quantify the effect that canal operations have on water quality, specifically suspended solids concentrations, to include both inorganic sediment and algal processes. The desired output of this primary objective is a generic computer model of canals capable of representing these effects. The following tasks will be used to accomplish this objective:

Task 1: Identify the sources of sediment in a target canal that interacts with a river;

Task 2: Quantify the hydrological and water quality interactions between the canal and the natural landscape; and

Task 3: Develop and evaluate a computer model of canal processes and canal/river interactions.

S**econdary objective:** Recommend a course of action for the Environment Agency to address the water quality issues in the Kennet and Avon Canal and the River Kennet

by simulating alternative management scenarios with the new computer model. The following tasks will be used to accomplish this objective:

Task 1: Identify possible management scenarios for the Kennet and Avon Canal;

Task 2: Create mathematical representations of the management scenarios that can be simulated with a computer; and

Task 3: Enter the mathematical representation of each management scenario into the canal model to determine the water quality impacts of each scenario.

These tasks have been accomplished and objectives met by creating a standalone receiving water model capable of simulating the complex processes inherent to a canal. The guiding principle in developing the algorithms and needed inputs for the canal was to generate a model that could be easily parameterized without intensive monitoring studies. Thus, wherever possible, the intended inputs for the new canal model are drawn from readily available literature values, existing agency databases, or physical characteristics easily measured by a non-expert.

1.3. Thesis Layout

This thesis contains nine primary sections and additionally a reference list and appendices. The content of the remaining sections is outlined below.

Section 2 contains a review of literature and background information on canal operations and the study area.
Section 3 provides an overview of data sources used to parameterize the model.
Section 4 details algorithm development for the model.
Section 5 provides information regarding the testing and verification of the model.
Section 6 explains the use of an overland flow model to develop runoff inputs for the new canal model.
Section 7 provides a specific example of the model's application to the Kennet and Avon Canal through evaluation of the model output in comparison to observed data and subsequently in evaluating potential management options for the Kennet and Avon Canal.
Section 8 summarizes the project and describes the impact of this work.
Section 9 provides ideas for future research that would enhance this work.

2. Literature Review and Background Information

Before embarking on this study, it is necessary to present a background in basic canal operations, the mechanisms involved in sediment and algal generation and transport, existing canal modeling efforts, and details of the study area that served both as an example of typical canal processes and as a test case for the new canal model.

2.1. Overview of Canal Processes

Canals are essentially a series of impoundments ('reaches') separated by locks (Willby et al. 2001). Locks consist of a pair of gates that are a fairly standard distance apart for a given canal; the maximum acceptable boat size for a given canal is set based on the dimensions of the locks on the canal.

2.1.1. Locks

The purpose of a lock in a canal is to move a boat from one water elevation to another. The elevation change made possible by locks allows the reaches between locks to be fairly flat and easily navigable; this is often in contrast to a natural stream in the same topography, which would be too steep to be navigable. The interior of a typical lock is shown in Figure 2; schematics of a typical lock are given in Figure 3. From a plan view, it is evident that the lock gates form a convex angle against the direction of water movement. From an elevation view, it can be seen that past the upstream lock gates the bottom of the lock drops to the level of the downstream reach. The downstream lock gates (e.g., Figure 3) hold sluice doors near their bottoms to allow water to drain out of the lock as needed. The sluices for the upstream gates are located at the bottom of the canal wall (Figure 3); water flows through the sluice in the side of the canal and into the lock from an opening in the side of the lock wall. As a boat moves through a lock, it is necessary to completely fill or drain the lock (as appropriate) so the water level on both sides of the gates to be moved is equal; otherwise the water pressure behind the gates is too great for individuals to push the gates open.

Figure 2. Interior of a typical lock. Note cill.

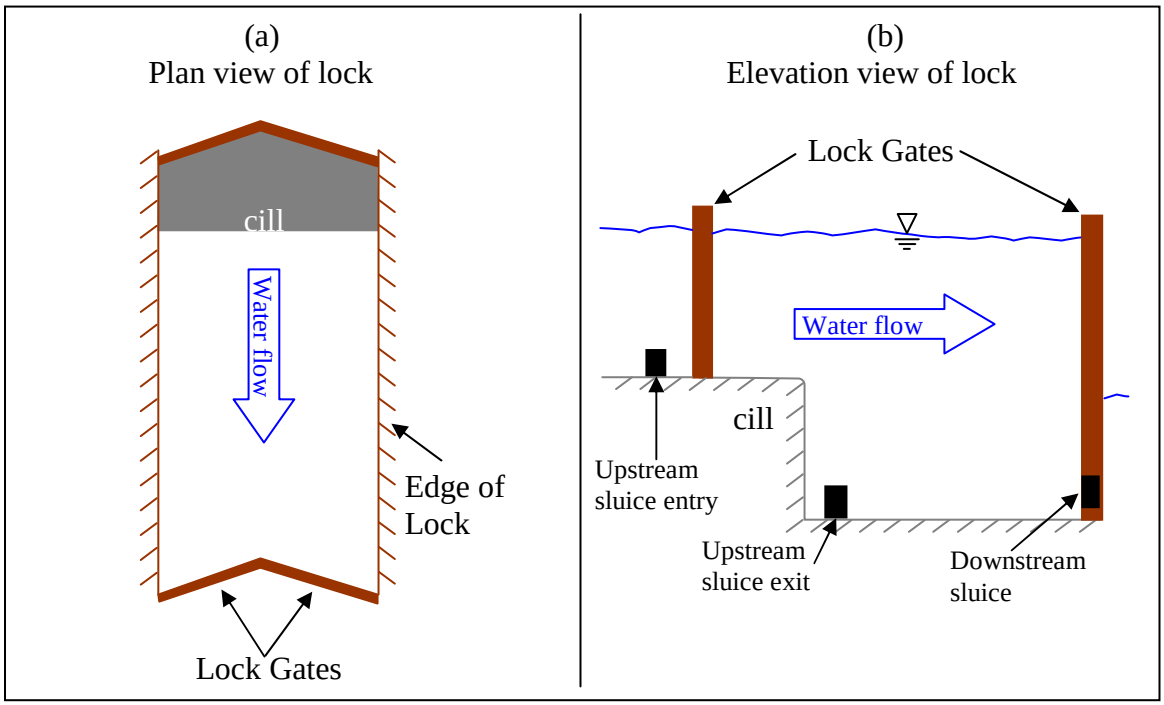

Figure 3. Plan (a) and elevation (b) views of a typical lock.

Canal users open and close the sluice doors as they move through the lock from one elevation to the next (Figure 4). Before entering the lock, the user opens the sluices on the same side of the lock as his boat is currently located, leaving them open until the water level equalizes, then closes the sluices. After the boat enters the lock, the opposite sluices are opened and again the boater waits until the water level in the lock

equalizes with that of his destination reach; finally the sluices are closed, the gates opened, and the boat moves on (closing the gates behind him) (Corrie 2002).

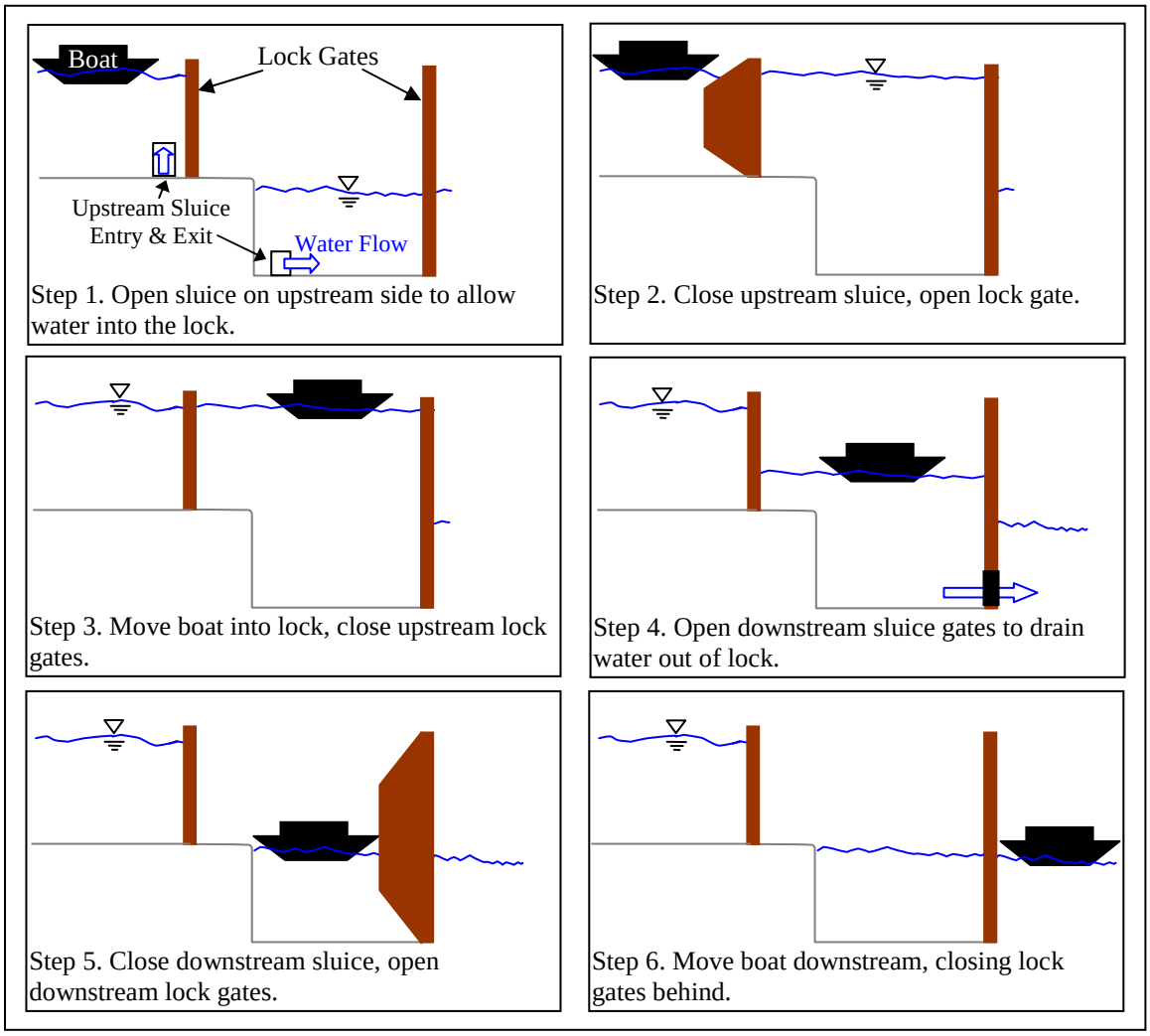

Figure 4. Typical lockage cycle for a boat moving downstream.

Lockages (the filling of a lock with water) are a major concern to canal engineers, as the significant amount of water lost from canal reaches due to lockages must be balanced by an external supply of water to the canal. The total amount of water lost during boat passage through a lock depends on the state of the lock when a boat approaches, which in turn is dependent on the direction the previous boat traveled compared to the direction the current boat is moving (Figure 5). Boats moving upstream must enter a drained lock, and boats moving downstream must enter a full lock; likewise, boats moving upstream leave a full lock, and boats moving downstream leave a drained lock. Thus, if boats move in sequence, heading the same direction (e.g., cases 3 and 4 in Figure 5), each boat passage draws a full lock volume from the upstream reach and deposits a full lock volume in the downstream reach. If

the boats moving through the lock are alternating directions (e.g., cases 1 and 2 in Figure 5), each boat passage will cause either a lock volume to be drawn from the upstream reach or a lock volume to be deposited in the downstream reach. It is evident that having boats move in alternate directions through a lock is an ideal situation, but it is difficult to force this in a real-world situation. Instead, canal engineers recommend that narrow boats travel together through a canal, sharing locks. This halves the amount of water needed for each individual boat, as the lockage only occurs once for the pair of boats, rather than once for each individual boat. Occasionally locks must be left empty after use; this requires an additional movement of water in each of the cases in Figure 5: boats moving downstream would always experience case 4 (they could not experience case 2), and boats moving upstream would experience case 1 with an additional drainage of the lock at the end.

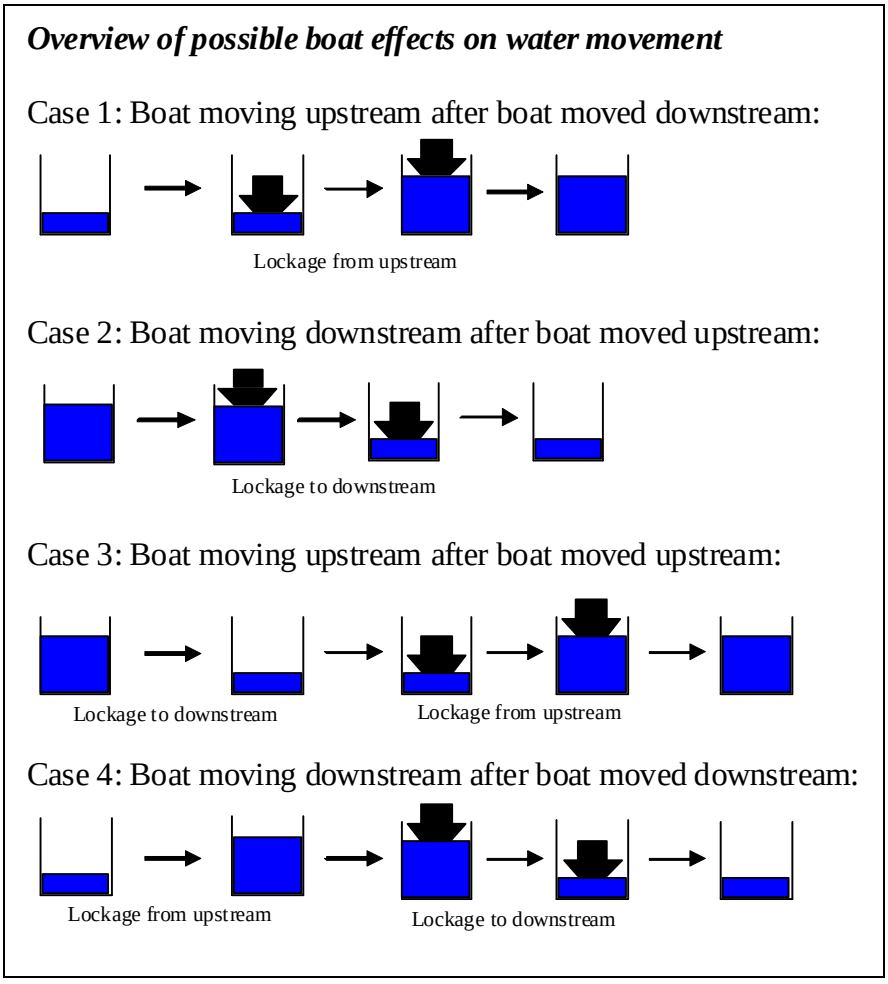

Figure 5. Illustration of possible water loss scenarios during lockages. (Rectangular containers indicate locks, black shape is a boat, blue fill indicates water level.)

In addition to water losses through lockages, locks control another important flow route through the canal: leakage. Excepting a short period right after they are installed, lock gates are typically leaky (Figure 6). This occurs for many reasons. The wood itself is weathered away after use and exposure to the high pressure of the canal water. Additionally, boats with single riders tend to push their way through the lock gates by pushing the bow of the boat against the closed gates to force them open and pass through. This permits the driver of the boat to exit the lock without leaving the boat to open the gates, but causes significant damage to the lock gates.

Figure 6. Typical leaking lock gates. Note reinforced center of gates where boats push in the left image.

2.1.2. Reaches

The reaches (impoundments) between the locks are often long; in a gently sloped landscape they may exceed 1.5 km. In a steep incline in the natural topography, however, they may be short. The shortest sections on the Kennet and Avon Canal (the canal chosen to test the new model) are in between locks in the steep flight of locks approaching the summit reach from the west, where the canal ascends approximately 75 m through 29 locks over the space of approximately 3 km (Kennet & Avon Canal Trust, 1999). The longest reach in the study area on the Kennet and Avon Canal is just over 1.5 km long. The canal sides are frequently elevated above the surrounding landscape, but also occur flush with the neighboring topography.

Overflow weirs in a canal reach are typically located in a side wall near the downstream lock (Figure 7). These weirs will typically discharge to the next lower lock or canal reach, although occasionally they may bypass a reach or discharge into a

neighboring body of water, depending on the needs of the canal or the constraints of design the engineers considered at that point during construction.

Figure 7. Typical overflow weirs on the Kennet and Avon Canal.

Unless the canal is lined by an impermeable material, water will seep through the canal walls. This can be a significant source of water loss, particularly in new canals where the pores in the soil lining the canal walls have not yet been clogged by fine particles (Minikin 1920).

The water level in a reach is generally controlled by three major factors: one input control and two output controls. First, a relatively large and constant source of water feeds the summit reach of the canal; this may be pumped from a reservoir or may come from a natural feeding stream. Although the source water is only directly input to the summit reach, it moves downstream through the exits from each reach to govern the total water input to each successive reach. Insufficient input to the summit reach will cause the water depth in all reaches to drop. Excessive input to the summit reach has little effect on water depth, as it will be channeled away by the second primary control on water depth: the overflow weirs. Given a sufficient input of water to the summit reach, the water level in each reach along the length of the canal is governed primarily by the height of the overflow weir in each reach. The overflow weirs are designed to carry all excess water above the desired depth to the next downstream reach. Thus, during normal steady-state operating conditions, the overflow weir determines the water level in the reach. However, should the input at the summit reach be too low, the water level will drop beneath the overflow weir crest and the overflow weir will no longer govern the water level in the reach. The last

major factor affecting water levels in the reach is boat traffic. The boat traffic directly affects water movement from one reach to the next as the boats move through locks at the upstream and downstream end of each reach. As the boats move through the locks, the volume of water needed to fill and/or empty the lock is removed from the upstream reach and deposited in the downstream reach. If these lockages are excessive, they may drain the water level in the reaches below the height of the overflow weirs, thus constituting a significant control on water levels during the peak boating season. These three factors in a canal are designed to balance each other: the source of water is designed to be large enough to counteract the water loss through expected lockages, leakage, and seepage; and the overflow weirs allow water to bypass the locks while boats are not traveling to prevent flooding or undesirable overtopping of lock gates.

2.1.3. Solids Considerations for a Canal

The generation and transport of solids in a canal can be considered a function of three primary processes: the underlying hydrology, boat traffic, and algal growth. With the exception of evaporative and seepage losses, solids will exit the reach at all locations that water exits the reach. The concentration of solids in the exiting flow may vary: in general, discharges that involve the whole water profile can be assumed to hold solids at the average concentration of the reach, whereas discharges from the top of the water profile will hold a concentration lower than the average concentration of the reach. The release of water into a reach during a lockage event or at the outlet of the overflow weir bypass is noticeably turbid; thus, any solids associated with the underlying hydrology flow can be considered well-mixed at the upstream end of the reach.

Boat passages generate sediment independently of the flow of water in the reach. This sediment generation is twofold: first, the boat propellers stir up sediment as the boat traverses the reach; and second, when the boat passes through the lock gates at either end of the reach, the movement of the lock gates near the canal bottom stirs up additional sediment. If the boat speed is high enough, it may additionally cause a wake that erodes earthen bank walls (Parchure et al., 2001); however, in general canal users are advised not to move so quickly that they might generate a wake.

Finally, algal growth can be an important contributor to solids concentration in the reach. Algal growth is negatively correlated with increased flow rate (Dickman 1969; Søballe and Kimmel 1987); canal reaches are essentially impoundments, with a low flow rate that encourages algal growth. Additionally, algal growth is enhanced by light and nutrient availability and water temperature (Eppley 1972). Historically, the construction of canals eliminated trees close to the water; typical usage patterns since their construction tend to keep the area surrounding a canal clear, historically for horses to pass on a towpath, and more recently for walkers and bikers to use former towpaths recreationally. As a result, light availability is typically high in a canal. This in turn leads to increased water temperature. All of these factors combine to provide a beneficial habitat for algal growth. Thus, although one might expect to see a decline in solids concentration in the still water of canals not experiencing boat traffic, it is common to see an increase in solids concentration in canal reaches as a result of algal growth.

All of these processes are described in more detail in the section on algorithm development (Section 4.2).

2.2. Inorganic Sediment

2.2.1. Types of Sediment

Inorganic sediment is typically classed into three general types: sand, silt, and clay. The divisions between these types of sediment are based on size: sand particles range from 0.02-2.0 mm in diameter, silt particles range from 0.002 to 0.02 mm in diameter, and clay particles are less than 0.002 mm in diameter. Further classification is possible: for example, sand can be broken into fine sand (0.02-0.2 mm) and coarse sand (0.2-2.0 mm); and larger particles can be defined, including gravels (>2.0 mm) and boulders (>1 m) (Brady and Weil 1996).

There are many soil properties tied to the particle size distribution, or texture, of the soil. Clays and silts have a larger charged surface area per unit weight and thus will hold more tightly to nutrients and pollutants than will sand. Small particles such as clays are easily splashed up by rainfall and can form a seal on the soil surface, reducing infiltration and increasing surface runoff in later rainfall events. The voids

between sand particles are larger than between clay particles, and thus infiltration is increased in sandy soil. Due to the minimal voids between clay particles and their ability to be compacted into a nearly watertight layer, compacted clays are often used as a sealing layer in landfills, reservoirs, and canals (Brady and Weil 1996).

In terms of water quality, the various particle sizes can be generally grouped into two categories: cohesive (particle size < 0.06 mm) and non-cohesive (Soulsby 1997). These categories of sediment behave differently while suspended in water: cohesive sediments, due to their high surface area and charge, have a tendency to attract each other and group together to form flocs (a process termed 'flocculation'). This process is affected by both physical and chemical parameters. Physically, increased sediment concentration increases the likelihood that a cohesive particle will randomly encounter another particle in the water, thus increasing flocculation (Mehta et al. 1989; Lau and Krishnappan 1992); to a certain extent, increased flow velocity can increase flocculation by moving particles about so that they encounter each other, but too vigorous a flow can have a negative effect by stressing the weak flocs so that they break apart (Baugh and Manning 2007). Water temperature and salinity affect the charge of the cohesive particles and thus their tendency to flocculate (Mehta et al. 1989; Lau 1994). By contrast, non-cohesive sediments have no tendency to flocculate and will behave independently of other particles suspended in the water column.

2.2.2. Sediment Transport and Fall Velocity

Sediment transport in streams has been well studied. A commonly accepted approach to modeling sediment transport utilizes the Krone-Partheniades method. This is used by the receiving water model in the Hydrological Simulation Program-Fortran (HSPF) (Bicknell et al. 2001), for example. In this method, suspension is calculated using a relationship developed by Partheniades (Equation 1) , and deposition is calculated using Krone's Equation (Equation 2) (Gerritsen et al. 2000). These equations use the relation of the bed shear stress to critical shear stress for deposition and scour to allow the total deposition or scour to scale from zero to the maximum possible deposition or an unlimited scour as the bed shear stress changes.

$$\frac{dC_{ero}}{dt} = \left(\frac{\tau_b}{\tau_{ero}} - 1 \right) \frac{E_o}{h} \quad \text{when } \tau_b > \tau_{ero} \tag{1}$$

$$\frac{dC_{dep}}{dt} = \left(1 - \frac{\tau_b}{\tau_{dep}}\right)\frac{C_{bed} w_s}{h} \quad \text{when } \tau_b < \tau_{dep} \tag{2}$$

Where: C_{ero} = concentration of sediment eroded (kg/m³);
C_{dep} = concentration of sediment deposited (kg/m³);
C_{bed} = suspended sediment concentration close to bed (kg/m³);
t = time (s);
τ_b = stress at bed (N/m²);
τ_{ero} = threshold stress for erosion (N/m²);
τ_{dep} = threshold stress for deposition (N/m²);
h = water depth (m);
w_s = fall velocity (m/s); and
E_o = erosion rate (kg $m^{-2}s^{-1}$).

Gerritsen and others (2000) suggest $\tau_{dep} = \tau_{ero} = 0.06$ N/m² and $E_o = 1$ kg $m^{-2}s^{-1}$ for their system, which consolidated all particle size classes into one for simulation. The scour calculation involves the estimation of an erosion rate per unit area, which can then be divided by the total depth to obtain an erosion rate per unit volume of water. This erosion rate will be site-specific and dependent on the material of the streambed.

Because the flow in a canal reach is typically low, scour due to flow velocity is negligible. There is some scour due to the propeller action of boat traffic, which will be discussed in greater detail later (Section 2.4); thus, erosion in a canal is typically independent of hydrology. Because the water is generally stagnant, the deposition of sediment in quiescent waters (Equation 3) is most important to the canal model.

Partheniades' deposition equation is actually a specific form of the more general equation (Equation 3) (Vanoni 1975).

$$\frac{\partial C}{\partial t} + \frac{\partial\left(\overline{w}C\right)}{\partial z} = 0 \tag{3}$$

Where: C = concentration of sediment (mass/length³);
t = time (time);
$\overline{w}$ = fall velocity (length/time); and
z = vertical position (length).

If $\overline{w}C$ represents the total mass settling flux (that is, the rate of sediment deposited over a unit area) and resuspension forces are ignored, mass conservation states that for a unit volume (the unit area multiplied by the affected depth *z*) the decrease in total sediment concentration over time (the first term of Equation 3) must be balanced out

by the amount of sediment that has deposited (the second term in Equation 3). If fall velocity is assumed not to change with depth ($\overline{w}$ = w_s) and flow is insignificant (τ_b = 0), Equation 3 can be simplified to Equation 2 to determine the total change in concentration over a depth *h*. Equation 3 also assumes that sediment concentration does not vary across the width of the stream.

The final component of Equations 1 and 2 is the shear stress. To simplify calculations in the Krone-Partheniades formulae, the relationship of the actual bed shear stress to critical deposition and scour shear stresses is used to estimate the amount of scour or deposition that would happen. If the bed shear stress is zero (that is, in perfectly still water), Equation 2 is equal to Equation 3 and sediment falls at the maximum velocity for still water (w_s). However, if there is some water movement, resuspension may occur, and the relationship $\left(1-\frac{\tau_b}{\tau_{dep}}\right)$ reduces the total deposition according to this water movement. Likewise, if the bed shear stress just reaches that needed for erosion, the shear stress term in Equation 1 is zero, and no erosion occurs. As the bed shear stress increases above the threshold value, erosion increases in an unlimited fashion. Later researchers (e.g., Gerritsen et al. 2000) modify the Partheniades formula to limit the total erosion according to the estimated sediment load available to be eroded.

The critical term to define in Equation 3 is the fall velocity, a key parameter into which much research effort has been invested. Two primary factors should influence the fall velocity: the weight of the sediment, being the primary force drawing the sediment down; and the viscosity of the water, being the primary force resisting the fall of sediment. The weight of the sediment can be described using a combination of the acceleration due to gravity, the diameter of the sediment (if sediment is assumed to be spherical), and the specific gravity of the sediment. Among others, Soulsby (1997) has experimented with equations using these components to represent observed data. It is generally accepted that the fall velocity of non-cohesive sediment is straightforward, commonly expressed as Equation 4 (Soulsby 1997).

$$w_s = \frac{\nu}{d}\left(\sqrt{10.36^2 + 1.049D_*^3} - 10.36\right) \qquad (4)$$

Where: w_s = fall velocity (m/s);
ν = kinematic viscosity of water (m^2/s);
d = diameter of sediment (m); and
D_* = dimensionless grain size (Equation 5).

$$D_* = \left[\frac{g(s-1)}{\nu^2}\right]^{1/3} d \quad (5)$$

Where: g = acceleration due to gravity (m/s^2); and
s = specific gravity of sediment (unitless).

Cohesive sediments such as silt and clay tend to flocculate in high sediment concentrations, thus increasing fall velocity over what one would normally expect using equations such as Equation 4, which assumes that grains of sediment will fall without interaction with each other (Vanoni 1975). The experiments of numerous researchers show that settling velocity for cohesive particles can vary with sediment concentration, temperature, water velocity, and salinity (Mehta et al. 1989; Lau and Krishnappan 1992; Lau 1994; Johansen and Larsen 1998; Milburn and Krishnappan 2003), which makes the fall velocity of the silt and clay particle size classes difficult to predict in a simple model. However, Equation 6 is a simple empirical model for cohesive sediments used by many researchers (e.g., Johansen and Larsen 1998). This equation clearly ties fall velocity to overall sediment concentration and attempts to encompass all other factors through the use of multiplicative and exponential constants. If sufficient detailed site-specific observations of fall velocity and concentration are available, Equation 6 has been found to be a good representation of reality (Johansen and Larsen 1998; Gerritsen et al. 2000; Baugh and Manning 2007).

$$w_s = k \cdot C^m \quad (6)$$

Where: k, m = constants estimated from regression against observed data.

Ideally, the settling velocity used in a water quality model should be measured on site or used as a calibration parameter for clay and silt particle size classes, enabling the characterization of Equation 6. However, practical applications of this method have obvious problems: when modeling an entire canal system (or a canal and its contributing catchment area), it is less likely that modelers would have the resources to properly characterize Equation 6 with site-specific data. Due to the difficulties in parameterizing equations such as Equation 6, Manning (2004) and Baugh and Manning (2007) have developed and tested an empirical model for cohesive sediment mass settling flux (MSF) using data from three sites in western Europe (Equation 7).

A key feature of Manning's work is the separation of cohesive particles into 'macroflocs' (flocs with diameter > 160 μm) and 'microflocs' (flocs with diameter < 160 μm). This separation allows a more precise estimation of overall fall velocity. Knowing that cohesive sediment fall velocity is dependent largely on sediment concentration and bed shear stress, Manning developed a set of empirical equations for the fall velocity of macroflocs (Equation 9) and microflocs (Equation 10). The total mass settling flux (as before, equal to $w_s \cdot C$) can then be calculated based on the relative contributions of macroflocs and microflocs (SPM_{ratio}) to the total concentration of suspended particulate matter (SPM, corresponds to C in previous equations).

$$MSF = \left[\left(1 - \frac{1}{1 + SPM_{ratio}}\right) \cdot \left(SPM \cdot w_{s,macro}\right)\right] + \left[\frac{1}{1 + SPM_{ratio}} \left(SPM \cdot w_{s,micro}\right)\right] \quad (7)$$

Where: MSF = mass settling flux (mg/m²s) = $w_s C$;
SPM = suspended particulate matter concentration (mg/L) = C;
SPM_{ratio} = ratio of suspended macroflocs to suspended microflocs (Equation 8);
$w_{s,macro}$ = settling velocity of macroflocs (Equation 9) (mm/s); and
$w_{s,micro}$ = settling velocity of microflocs (Equation 10) (mm/s).

$$SPM_{ratio} = 0.815 + 0.00318 \cdot SPM - 0.00000014 \cdot SPM^2 \quad (8)$$

$$w_{s,macro} = \begin{cases} 0.644 + 0.000471 \cdot SPM + 9.36 \cdot \tau - 13.1 \cdot \tau^2 & 0.04 < \tau < 0.7 \\ 3.96 + 0.000346 \cdot SPM - 4.38 \cdot \tau + 1.33 \cdot \tau^2 & 0.6 < \tau < 1.5 \\ 1.18 + 0.000303 \cdot SPM - 0.491 \cdot \tau + 0.057 \cdot \tau^2 & 1.4 < \tau < 5 \end{cases} \quad (9)$$

Where: τ = shear stress (N/m²).

$$w_{s,micro} = \begin{cases} 0.244 + 3.25 \cdot \tau - 3.71 \cdot \tau^2 & 0.04 < \tau < 0.55 \\ 0.65 \cdot \tau^{-0.541} & 0.51 < \tau < 10 \end{cases} \quad (10)$$

The macrofloc equations fit the measured data with an R^2 of 0.9-0.99. The microfloc equations fit the measured data with an R^2 of 0.73-0.75. The SPM_{ratio} equation fits Manning's data with an R^2 of 0.73. Manning's intent was that the equations should be universally applicable.

2.3. Algae

In addition to inorganic sediment, organic solids will influence the overall solids concentration in a reach. Organic solids in a canal may include detritus from the land

surface, fecal material from people and animals with access to the canal, and vegetation growing in the canal. Out of all these sources, the growth of algae (a form of vegetation) in a canal reach is of greatest concern. Unlike other sources of organic material, algae are living and will reproduce in the water, potentially providing an increasing impact on water quality in a canal.

2.3.1. Abundance and Chemical Composition

The algae (or phytoplankton) in a body of water typically consist of a multitude of species. Some species are adapted to high nutrient conditions, some to low, and thus there is a gradual progression in the abundance of individual species as the growth season progresses from the high nutrient conditions of the spring to the low nutrient conditions of the autumn (Rodhe 1948; Fogg 1965). Each of these species has a slightly different chemical composition. However, on the whole, it has been found that the chemical makeup, in terms of carbon (C), nitrogen (N), and phosphorus (P), is generally uniform in a multi-species population of algae ($C_{106}N_{16}P$) (Fleming 1940; Søballe and Threlkeld 1985); that the relative abundance of these elements in algal biomass is very similar to the relative abundance of these elements in sea water (Redfield 1958); and that the relative abundance of these elements in algal biomass may be more closely tied to environmental conditions than to species composition (Fogg 1965).

When monitoring for algae, water is typically analyzed for the presence of chlorophyll-a ($C_{55}H_{72}O_5N_4Mg$) (Chl-a), rather than biomass or volume of algal cells. Thus, a conversion is required when modeling the transport of biomass if one is to compare model results to observed data. Numerous authors have provided estimates for the relationship between chlorophyll-a and either live biomass, dry weight, or carbon. These are summarized in Table 1. Utilizing the various factors shown in Table 1, the ratio of the dry weight of the cell to chlorophyll-a content varies from 6.7 (111 mg biomass/mg Chl-a * 0.06 mg dry weight/mg live biomass) to 1861 (186.1 mg C/mg Chl-a * 10 mg dry weight/mg C). Using the dry weight:C estimate of Fleming, the average reported dry weight:chl-a ratio is 107 mg dry weight/mg Chl-a; the median value is 65. The dry weight is desired as it provides an estimate of algal contribution to measured suspended solids concentrations, which are estimated through oven-drying of the solids sample.

Table 1. Estimators of the proportion of chlorophyll-a (Chl-a) content in algae.

Mass Ratio	Condition	Ratio Value	Source
C:Chl-a	Batch Culture	11.8, 19	(Thomas and Dodson 1972)
	Chemostat	34.9, 61.8, 53.6, 24.0, 15.8	(Thomas and Dodson 1972)
	Vigorously Growing	25	(Antia et al. 1963)
	Unhealthy	60	(Antia et al. 1963)
	--	9-186.1	(Berman and Pollingher 1974)
	--	30, 60, 90, 120	(Eppley 1972)
	--	51	(Wienke and Cloern 1987)
	--	25-100	(Strickland and Parsons 1968)
Biomass:Chl-a	Algal Bloom	303	(Berman and Pollingher 1974)
	Otherwise	244	(Berman and Pollingher 1974)
	All Conditions	111-1000	(Berman and Pollingher 1974)
Biomass:C	--	10	(Berman and Pollingher 1974; Vollenweider 1974)
	--	37	(Fleming 1940)
Dry Weight:C	--	1.7-10	(Soeder et al. 1974)
	--	2.3	(Fleming 1940)
Biomass:Dry Weight	--	16	(Fleming 1940)

The varied relationship between chlorophyll-a and biomass is dependent not only upon the specific type of species present (Berman and Pollingher 1974; Malone et al. 1979), but also upon the environment surrounding the algae (Mullin et al. 1966). Thomas and Dodson (1972) found that chlorophyll-a per algal cell increased as growth rate increased; Antia and others (Antia et al. 1963) found that chlorophyll-a per algal cell decreased with decreased nutrient availability. Thus, although an estimate may be made for an average conversion between algal mass and chlorophyll-a concentration, the true relationship will be varied and will cause observed chlorophyll-a data to appear scattered around any modeled chlorophyll-a concentrations calculated from algal weight; in the evaluation of several nutrient-chlorophyll models, Brown and others (2000) found that the best model had an

interval of 30-325% in predicting chlorophyll-a concentrations at the 95% confidence level.

It has been suggested that the type of nutrient-limited growth phytoplankton are experiencing can be defined according to the ratio of nutrients in their bodies compared to the nutrient ratio in the water: thus, an N:P molar ratio in the water of 20 is considered ideal (Cooper 1937), and Dillon and Rigler (1974) suggest that N:P ratios above 12 are indicative of phosphorus-limited conditions. These correspond to the ratios of N and P in phytoplankton biomass: several authors (Fleming 1940; Antia et al. 1963; Vollenweider 1974; Reid and Hamilton 2007) describe the ideal phytoplankton N:P molar ratio as somewhere between 10 and 20. As phosphorus is commonly the limiting nutrient in the environment, several researchers (Vollenweider, 1976; Schindler, 1978; Jones and Bachmann, 1976; Dillon and Rigler, 1974) have found phosphorus to be the key factor affecting algal abundance, with variations in phosphorus levels accounting for between 83 and 95% of the variation in algal concentration in the waters studied. The equations developed by several authors to describe this relationship are listed below (Equations 11 – 17) and plotted in Figure 8.

Equation 11 was developed by Dillon and Rigler (1974).

$$\log_{10}[Chl-a] = 1.449\log_{10}[P] - 1.136 \quad (11)$$

Where: [Chl-a]= concentration of summer average chlorophyll-a (mg/m³); and
[P] = total phosphorus concentration (mg/m³).

Equation 12 was developed by Jones and Bachmann (1976).

$$\log[Chl-a] = 1.46\log[P] - 1.09 \quad (12)$$

Equation 13 was developed by Schindler (1978)

$$\log[Chl-a_{ann}] = 1.213\log[P_{ann}] - 0.848 \quad (13)$$

Where: [Chl-a_{ann}]= average annual chlorophyll-a concentration (mg/m³); and
[P_{ann}]= mean annual total phosphorus concentration (mg/m³).

Equation 14 was developed by Walker (1984).

$$\log[Chl-a] = \log[P] - 0.55 \quad (14)$$

Brown and others (2000) generated both annual (Equation 15) and growing season (Equation 16) equations.

$$\log[Chl-a_{ann}] = 1.053\log[P_{ann}] - 0.369 \quad (15)$$

$$\log[Chl-a] = 1.03\log[P] - 0.299 \quad (16)$$

Pridmore and McBride (1984) provide Equation 17 as part of their predictive model for algal growth.

$$\log[Chl-a_{max}] = 1.178\log[P] - 0.389 \quad (17)$$

Where: [Chl-a_{max}] = maximum chlorophyll-a concentration (mg/m³).

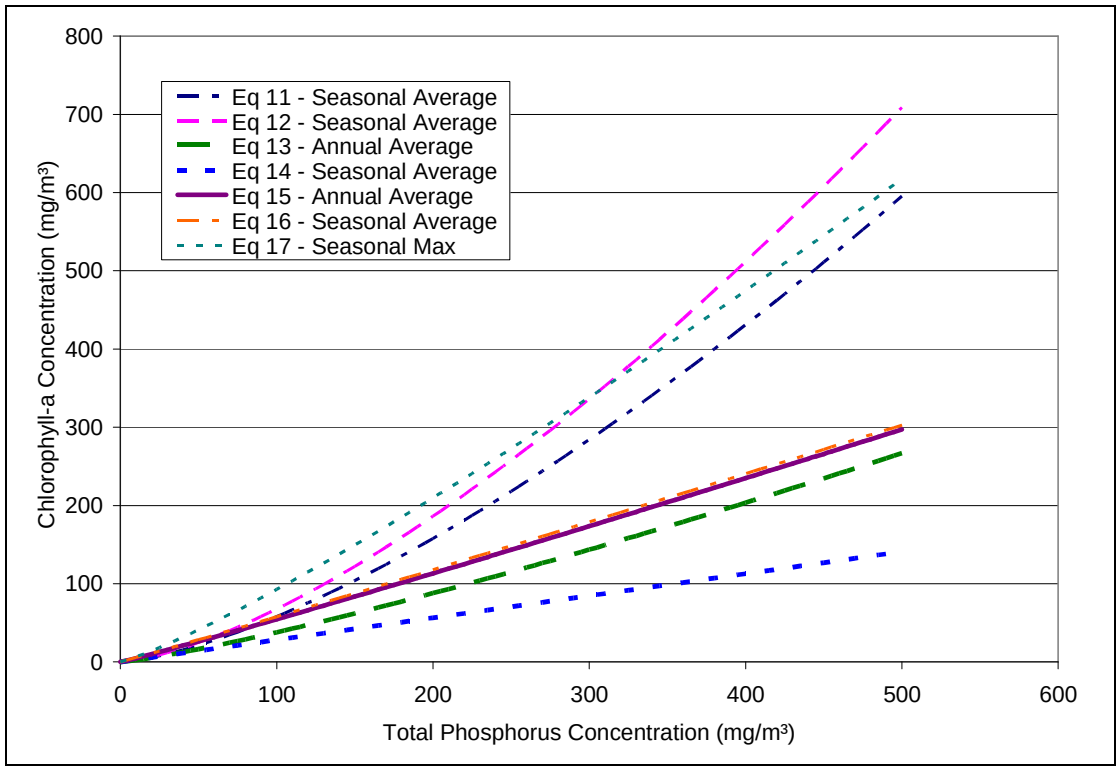

Figure 8. Relationships between phosphorus and chlorophyll-a concentrations.

2.3.2. Growth and Transport

In general, the growth of algae in a reach is dependent upon many factors, including water temperature; flow rate; and the availability of light, nutrients, carbon, oxygen, and silicon (Goldman et al. 1968; Eppley 1972; Dillon and Rigler 1974; Jones and Bachmann 1976; Vollenweider 1976; Schindler 1978; Kimmel et al. 1990; Reid and Hamilton 2007). Light, water temperature, and phosphorus concentration have a positive effect on algal growth in typical environmental conditions. In contrast, flow rate is inhibitory to growth in a reach in two ways: first, algae grow best in still water;

and second, what algae do grow in moving water will be more rapidly flushed out of a reach with increasing flow rate (Fogg 1965; Kimmel et al. 1990).

Eppley and Sloan (1966) (Equation 18) and later Eppley (1972) (Equation 19) found that a cap on the maximum specific growth rate for algae under ideal light and nutrient conditions could be defined according to water temperature (Figure 9).

$$\mu = 0.525 * 1.086^{T} \quad (18)$$

$$\mu = 0.851 * 1.066^{T} \quad (19)$$

Where: μ = maximum specific growth rate (doublings/day); and
T = water temperature (ºC).

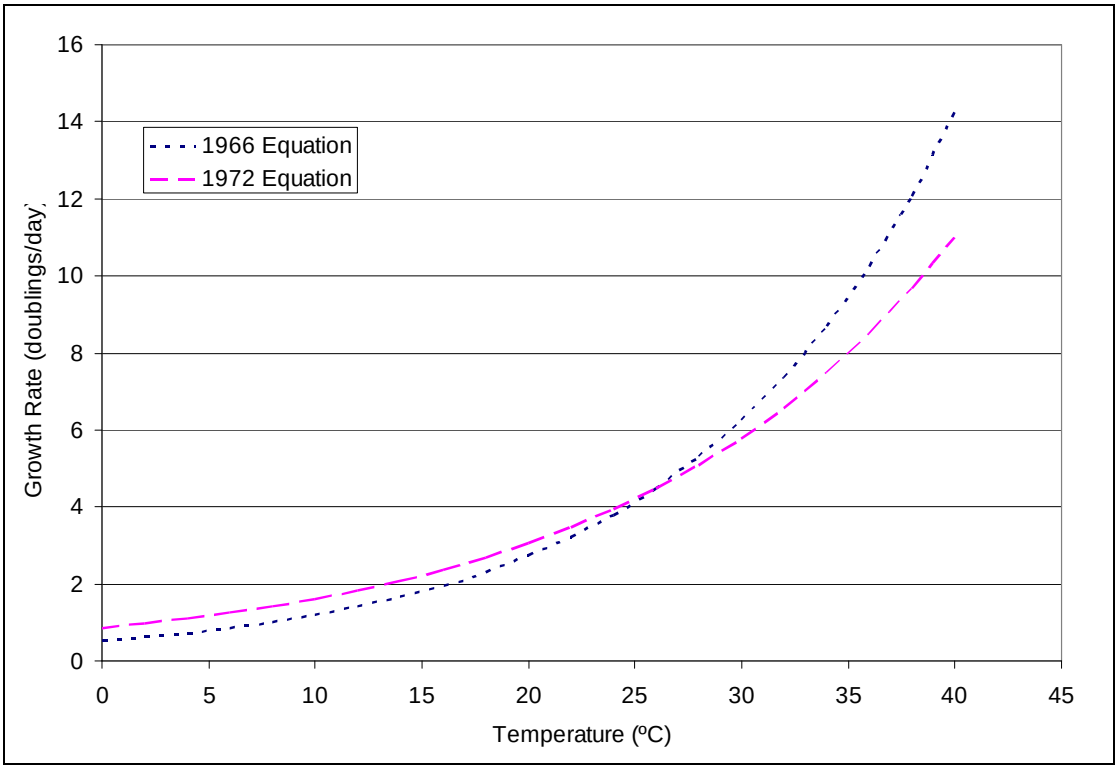

Figure 9. Maximum specific growth rate based on water temperature.

Equation 18 was developed based on the work of Talling (1955), who evaluated the relative growth rate of *Asterionella formosa* collected from Lake Windermere, England in 1952. However, Eppley and Sloan (1966) found this equation to overestimate growth rate at low and high temperatures for their culture of *Dunaliella tertiolecta*. This likely provided the impetus for the later development of Equation 19, which was created by analyzing about 200 samples from a wide range of researchers; as such, it is more representative than the 1966 equation, which was developed based

on the work of one researcher on one species of algae. Eppley (1972) found that the specific growth rate increased exponentially up to a temperature of 40ºC, and though his work focused primarily on organisms in the sea, he reported no noticeable variability in growth rate for freshwater organisms (compared to marine organisms), nor any variability between species. Where observed growth rates fall below the rate suggested by Equation 19, Eppley suggested that other factors – for example, light or nutrient availability – were limiting the growth rate such that it did not achieve its potential.

Solar radiation (light) is crucial for the growth of algae – phytoplankton, being plants, require sunlight to produce energy. A common term used when discussing light availability for algae is the euphotic depth – the depth below which photosynthesis is not possible. This depth is typically defined as the depth at which the light intensity is 1% of the value at the water surface (Reynolds 1984; Lee and Rast 1997). Beer's Law (Equation 20) gives a relationship useful in defining the euphotic depth. If the light intensity at the euphotic depth is $1/100^{th}$ of the light intensity at the water surface, then Equation 20 applied when the depth equals the euphotic depth simplifies to Equation 21.

$$I(z) = I(0)e^{-\eta z} \tag{20}$$

Where: I(z) = light intensity at depth z (percent);
I(0) = light intensity at water surface (100%);
η = light extinction coefficient (m^{-1}); and
z = depth (m).

$$z_{eu} = \frac{(\ln(100) - \ln(1))}{\eta} = \frac{4.60517}{\eta} \tag{21}$$

Where: z_{eu} = euphotic depth (m).

Many researchers have investigated the final piece of the equation: the light extinction coefficient. The total light extinction coefficient has been estimated between 1.56-7.93 m^{-1} (Reynolds 1984; Lee and Rast 1997); attempts have also been made to develop regression equations to dynamically predict the light extinction coefficient based on the concentration of various types of solids; these equations all follow the general formula given in Equation 22. The light extinction rate is dependent, at a minimum, on the light extinction due to the water itself, shading from

suspended solids, and self-shading by other algae. Many equations attempt to quantify the effects of organic matter as well. A list of the coefficients for Equation 22 found by various researchers is given in Table 2.

$$\eta = \eta_w + \eta_s[SS] + \eta_a[A\text{lg}] + \eta_o[OM] \quad (22)$$

Where: η_w = base light extinction coefficient due to water (1/m);
η_s = light extinction due to inorganic sediment (m^2 mg^{-1});
[SS] = concentration of inorganic sediment (mg/L);
η_a = light extinction due to algae (m^2 mg Chl-a^{-1});
[Alg] = concentration of algae (mg/L);
η_o = light extinction due to organic matter (m^2 mg^{-1});
[OM] = concentration of organic matter (mg/L).

Table 2. Regressed coefficients for Equation 22 presented by various authors.

η_w (m^{-1})	η_s (m^2 mg^{-1})	η_a (m^2 mg Chl-a^{-1})	η_o (m^2 mg^{-1})	Source
0.02-0.2*		0.006-0.02		(Reynolds 1984)
2.99	12.0	0.020	2.25	(Lee and Rast 1997)†
0	52	0.031	174	(DiToro 1978)‡
1.337	19	0.015	54	(Blom et al. 1994)‡
0.627	25	0.021	49	(Buiteveld 1995)‡¶
0.877	25	0.022	8	(Bakema 1988)‡
0.513	44	0.023	27	
1.020	76	0.017	58	
-0.259	10	0.035	8	
1.666	50	-0.027	83	
0.865	137	0.012	75	
§	62.6	0.0335	45.4	(Zhang et al. 2006)

* Includes effects of water, sediment, and organic matter
† Also included a term for color, 0.00113 (platinum-cobalt units)$^{-1}$ m^{-1}
‡ As cited by Van Duin et al. (2001)
¶ Also included a term for absorption due to Gilvin at 380 nm, 0.050 (absorption coefficient)$^{-1}$ m^{-1}
§ η_s, η_a, η_o regressed separately with intercepts of 1.6068, 3.1924, and 4.3433 m^{-1}, respectively

The relationships presented in Equations 21 and 22 and Table 2 can be used to define the amount of light available for algal growth. Once the light availability is known, the growth rate can be calculated or modified from a maximum rate. Some researchers have used Michaelis-Menten kinetics to define the effect of light intensity on algal growth rate (Equation 23) (e.g., Eppley and Sloan 1966; Bicknell et al. 2001). This relationship requires definition of a 'half-saturation' constant, the value of light intensity that yields a growth rate equal to half the maximum growth rate possible under the remaining environmental conditions (e.g., temperature). The growth rate multiplier based on light availability increases quickly at first, when light availability

is low and limiting, but reaches an asymptote of unity when light availability exceeds the maximum usable by the algae under the remaining environmental conditions (Figure 10).

$$GRM = \frac{LI}{K_{s,l} + LI} \tag{23}$$

Where: GRM = growth rate multiplier (unitless);
LI = light intensity (J/m²s); and
$K_{s,l}$ = half-saturation constant for light-limited growth (J/m²s).

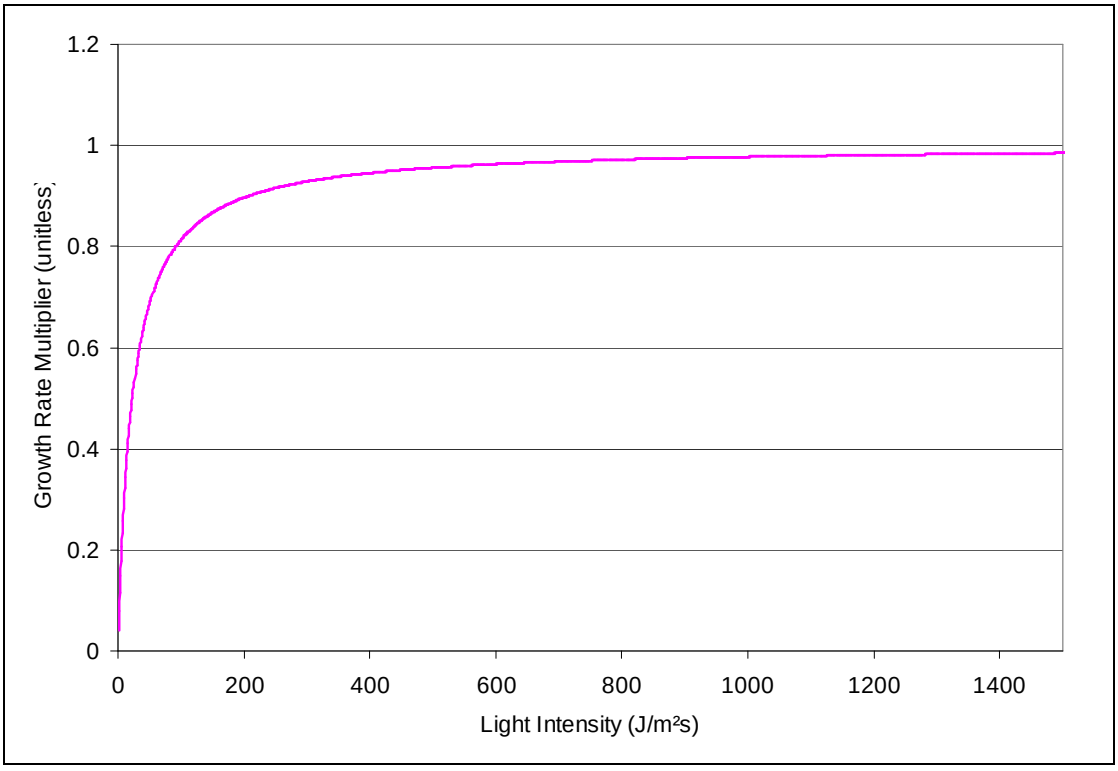

Figure 10. Michaelis-Menten relationship for light intensity given a half saturation constant of 23.012 J/m²s.

Bicknell and others (2001) suggest a value for $K_{s,l}$ of 23.012 J/m²s; Eppley and Sloan (1966) suggest a value for $K_{s,l}$ of 10.46 J/m²s.

As was described in Section 2.3.1 on algal abundance, the maximum and average supportable algal populations, as represented by chlorophyll-a concentration, are closely tied to phosphorus concentration. Some researchers, recognizing this, have used the supportable population based on phosphorus concentration as a cap on algal growth, slowing the rate of growth as this maximum supportable population is approached and causing death to occur should the maximum supportable population

be exceeded (e.g., Pridmore and McBride 1984) (Equation 24). Other researchers (e.g., Bicknell et al. 2001) again use Michaelis-Menten kinetics to predict a growth rate limited by phosphorus concentration. The disadvantage of the Michaelis-Menten model is that although it can slow the rate of growth, it cannot cause a decline in the algal population if the phosphorus level drops, and thus if death is not considered separately, the population would, at best, stagnate, rather than dropping to a level supportable by the current phosphorus concentration. For this reason, if death is not considered separately, Equation 24 is preferable.

$$GRM = \frac{K - B}{K} \tag{24}$$

Where: K = maximum supportable algal concentration based on current phosphorus level (mg/m^3) (Figure 8); and
B = algal concentration (mg/m^3).

Finally, flow rate has been shown to have a significant effect on algal biomass (Søballe and Threlkeld 1985; Kimmel et al. 1990; Reid and Hamilton 2007). Algae grow preferentially in more stagnant water, and increased flow rates flush the algae out of a water body. Equations 25 (Lucas et al. 2009) and 26 (Pridmore and McBride 1984) show how some researchers have attempted to correlate flow rate with algal abundance or growth rate. Equations 25 and 26 are conceptual models that follow the same basic principle of mass conservation: the change in biomass must be equal to the inflows minus the outflows, plus growth. For Lucas' model, the effect of flow rate is incorporated into the time available for growth and loss: a higher flow velocity causes the time for growth to reduce, which reduces the amount of biomass that can grow; it also reduces the amount of time available for loss. They emphasize that their model is developed assuming plug flow and uniformity of environmental conditions along the *x* direction. Pridmore and McBride's model incorporates the flow rate through a flushing of organisms, which reduces the biomass concentration available to grow. They developed their model for impoundments with short retention times, where they could assume the inflow and outflow rates were equal and that the volume of the impoundment did not change. These are slightly different approaches to the same problem. Lucas and others tested their model on nine datasets collected from six locations; where their underlying assumptions of plug flow and uniformity were met, the model predicted well, but for systems where the assumptions were violated (in two tidal lakes), the model did not predict adequately. Pridmore and McBride tested

their equation on two hydro-electric impoundments in New Zealand with retention times of 3.2 and 8.4 days and volumes of 70 and 45 m³.

$$B_{out} = B_{in} \exp\left(\frac{\mu_{growth} - \mu_{loss}}{u} x \right) \quad (25)$$

Where: B_{out} = algal biomass concentration (µg Chl-a/L or cells/L);
B_{in} = algal biomass concentration entering the system at inlet (x=0) (µg Chl-a/L or cells/L);
x = distance downstream from inlet (m);
μ_{growth}= algal specific growth rate (1/d);
μ_{loss} = sum of specific loss rates due to biological and physical processes (1/d); and
u = characteristic velocity along the primary flow direction (m/d).

$$\frac{dB}{dt} = \frac{Q}{V}(b - B) + \mu B \quad (26)$$

Where: B = average phytoplankton concentration in impoundment (mass/length³);
b = average phytoplankton concentration in inflow (mass/length³);
t = time at which B is measured (time);
Q = flow of water (length³/time);
V = impoundment volume (length³); and
µ = net growth rate of individual algal cells ($time^{-1}$).

As previously mentioned, Pridmore and McBride cap growth in their model through consideration of a maximum growth rate supportable by the phosphorus concentration (Equation 27). Equation 27 also allows a negative growth rate, should the existing population exceed the population supportable by the current phosphorus concentration.

$$\mu = \mu_{max}\left(\frac{K - B}{K} \right) \quad (27)$$

Where: μ_{max} = maximal specific growth rate of phytoplankton under existing light and temperature conditions ($time^{-1}$); and
K = theoretical maximum phytoplankton concentration ($mass/length^3$), determined from Equation 17.

Algae tend to remain suspended in the water column (Fogg 1965; Malone 1980); because they are suspended, they move through a hydrologic system as the water moves. This was captured in Pridmore and McBride's equation (Equation 26), which

simply assigned the concentration of algae to inflow and outflow of water to determine the mass of algae transported. Thus the transport of algae is rather simplistic in nature; the complexity lies in the prediction of their growth.

2.4. Canal Process Modeling

2.4.1. Canal Modeling

Although many hydrodynamic models exist for riverine systems, few canal models exist (Heatlie et al. 2007). In particular, while modeling efforts have been undertaken for irrigation and drainage canals (Sutcliffe and Parks 1987; Misra et al. 1991; Lal 2001), there seems to be a dearth of research on canals used for navigation. Some well-known canals (e.g., Venice and Suez) have been modeled, but have very different drivers on hydrology than do inland waterways. One study (Heatlie et al. 2007) does model a navigational canal similar to the study region, but with a different goal. In addition to these large-scale modeling studies, there are a few monitoring and regression studies that have gathered data of specific relevance to the current modeling effort.

Venice, Italy, is located on a series of small islands inside a lagoon. A network of nearly 160 canals forms the 'streets' of the city. Knowledge of the sedimentation rates within the canal network is of vital importance, to ensure that dredging happens as needed to keep the canals navigable. Coraci and others (2007) undertook a study to develop a detailed model of the Venice canal network in order to predict sedimentation rates therein. They coupled a finite element model using shallow water equations with a 2-D link-node model to represent the system. The finite element model was used to represent the flow in the lagoon, driven by tidal action; outputs from this model were then used as boundary conditions for the link-node model of the canal network. Simulation of water levels with this coupled system was excellent; sediment simulation was acceptable, though not as good, being heavily dependent on parameters (such as lagoon sediment input, building erosion, and sewage outfalls) that were difficult to quantify. Additionally, the modelers did not attempt to quantify sediment sourced from "boat traffic or other anthropogenic influences" (Coraci et al. 2007). Due to the nature of the system, it was not necessary to include a

representation for catchment contributions or for structures (e.g., locks) commonly found in inland navigational canals.

In a similar manner to Venice, where the hydrodynamics are primarily a function of water levels in the lagoon, the hydrodynamics of the Suez Canal are driven primarily by the mean sea level in the water bodies at each end of the canal (Abril and Abdel-Aal 2000). Abril and Abdel-Aal used a 1-D model based on the momentum equation to represent hydrology within the Suez Canal. While the authors acknowledge that boat movements will have an effect on sediment concentrations, they report that the primary influence on sediment concentrations in the Suez Canal is the water movement caused by tidal changes in the velocity of water, which affects settling and resuspension within the canal (Abril and Abdel-Aal 2000). Therefore they make no accounting for boat traffic.

A recent study used the ISIS model (Wallingford Software 2008) to characterize the Manchester Ship Canal in northern England (Heatlie et al. 2007). This canal contained five ponds and three riverine interactions; the primary focus of the modeling study was the use of the canal for flood control. The authors developed a method to represent an automated sluice control system within ISIS and successfully represented the hydrology in the canal. Although they proposed using the sediment module of ISIS at a later date to evaluate changes in flood risk due to dredging activities, they did not run the sediment module in their study (Heatlie et al. 2007). British Waterways also used ISIS to assist in their efforts to quantify a range of Manning's roughness coefficients for use in hydraulic modeling of canals (Dun 2006). The British Waterways study was conducted on single sections of canals – that is, the study segments did not include locks.

2.4.2. Modeling of Boat Traffic Effects

Murphy and Eaton (1983) evaluated the effects of boat traffic on macrophyte growth in several canals across England. They found a strong correlation between boat movements and turbidity measured at 55 sites ($p \leq 0.001$, correlation coefficient = 0.67) (Equation 28) for an average channel 1 km long, 10 m wide, and 1 m deep (Murphy and Eaton 1983).

$$\ln(t) = 0.6 \cdot \ln(T) - 1.68 \quad (28)$$

Where: t = mean turbidity as TSS (g/m³); and
T = annual traffic (movements/(ha·m·year)) (Equation 29).

$$T = \frac{10 \cdot L \cdot R}{w \cdot d} \quad (29)$$

Where: L = lockages (lock operated through filling and emptying cycle) per year;
R = boat to lockage ratio;
w = mean canal width at measuring point (m); and
d = mean canal depth at measuring point (m).

Hilton and Phillips (1982) also investigated boat traffic effects on turbidity. They reported that suspended sediment concentrations in trafficked waterways originated both from elevated phytoplankton levels and turbidity generated by boat movements, and that the division between the two was still in need of research. They recorded continuous and nearly-continuous turbidity at two sites on the River Ant, and found a visible correlation between boat activity and turbidity. With the assumption that settlement follows an exponential decay model, they developed Equations 30 and 31 to predict suspended solids mass and concentration in trafficked waters. At a given point in time, these equations sum the individual contributions from each boat that has passed, taking into account the deposition that has occurred since the time each individual boat passed.

$$T_{total} = T \cdot \sum_{p=1}^{p=n} e^{-k(\tau - t_p)} \quad (30)$$

$$T_{mean} = T_0 \cdot \sum_{p=1}^{p=n} e^{-k(\tau - t_p)} + T_B \quad (31)$$

Where: T_{total} = total mass of suspended solids in the water column over 1 meter of bank length (g/m);
T = mass of solids induced by a single boat passage (g/m travelled);
n = number of boats;
k = settlement rate coefficient;
τ = time of sampling, counted from arbitrary starting time;
t_p = time of passage of the p^{th} boat, counted from the same arbitrary starting time as τ;
T_{mean} = concentration of suspended solids (g/m³);
T_0 = T/A = suspended sediment concentration generated by passage of a single boat (g/m³);
A = cross-sectional area of river, m²; and
T_B = background suspended solids concentration when there is no boat activity (g/m³).

Although Equations 30 and 31 are designed for measured concentrations of suspended sediment in g/m³, the data available to the researchers (and the final values they report) were given in turbidity units of FTU. Hilton and Phillips (1982) tested their equations on two reaches on the River Ant, and found values for k of 0.0146 and 0.012 and values for T_0 of 0.156 and 0.148 FTU. Due to the differences in the reaches tested, they did not expect the values for k and T_0 to vary much if the model was extended to other rivers. The researchers cautioned that time steps of 5-60 minutes were tested in their model development, but longer time steps were not, and the model might not be suitable for time steps of greater than one hour. Finally, Hilton and Phillips concluded that solids resuspended by boat traffic were unlikely to build up over time, as their model suggested that even concentrations generated during times of peak boat traffic should return to normal within 5.5 hours.

2.5. Study Area

The Kennet and Avon Canal was chosen as the site for demonstration of this model, predominantly due to the tense political climate around the canal and resulting need for a computer model capable of predicting solids loads from the canal. The canal discharges into the visually pristine River Kennet, creating water quality problems that have outraged local anglers (Kennet Chalkstream Monitoring Group 2008). The Environment Agency is considering numerous management options to address the water quality problem in the River Kennet caused by the canal, but they desire a model capable of predicting the outcomes of these options before committing funds to any restoration efforts. The use of the Kennet and Avon Canal as the study site has the added benefit of the availability of varied spatial water quality data collected by the Centre for Ecology and Hydrology (CEH).

2.5.1. Description

The full length of the Kennet and Avon Canal runs 140 km from Bristol to Reading in southern England (Corrie 2002); the study area for this research project extends 21 km from the summit reach eastward to Copse Lock, where the natural course of the River Kennet merges with the canal (Figure 1, page 22). (In Figure 1, although the town of Hungerford is not large enough to be a 'populated place' by mapping standards, it is an important sampling location where the River Dun, the River Kennet, and the

Kennet and Avon Canal run nearly parallel before the convergence of the former two; thus Hungerford is noted in Figure 1 to aid in later discussion.) Copse Lock is the site of concern for anglers, the point where the slug of sediment carried by the canal enters the pristine River Kennet (Figure 11). Up until this point, the river and canal parallel each other, but have only minimal interaction, insufficient to cause water quality problems in the river.

Figure 11. Confluence of the Kennet and Avon Canal with the River Kennet. The canal enters from the lock visible in the top right of the photo; the river enters from the bottom right of the photo.

The study section of the canal contains 26 locks (and thus 25 reaches between the locks, plus the summit reach, for a total of 26 reaches), starting with lock number 55 (Crofton Top Lock) to the west and ending with lock number 80 (Copse Lock) to the east (Figure 12, Figure 13). To the south and west of Hungerford, the canal parallels the River Dun; to the east of Hungerford, after the Dun joins the Kennet, the canal parallels the River Kennet. Two major surface streams contribute flow to the canal in this section: Froxfield Stream deposits approximately a quarter of its flow into the canal through a control structure (the remainder flows in a culvert underneath the canal to join the Dun), and Shalbourne Brook contributes all of its flow to the canal, though a large portion of it is removed via a weir on the opposite side of its entry point on the canal (National Rivers Authority 1992). Additionally, generally small amounts of water are drawn at various points from the River Dun and the River

Kennet and deposited in the canal (National Rivers Authority 1992). The majority of the flow in the canal is provided via the summit reach, to which the Crofton Pumping Station (Figure 12) pumps water at a variable rate (but minimum of 125 L/s (personal communication, pumping station engineer, 15 September 2009)) year-round. The water pumped at Crofton is drawn from nearby Wilton Water, a manmade reservoir designed for this purpose.

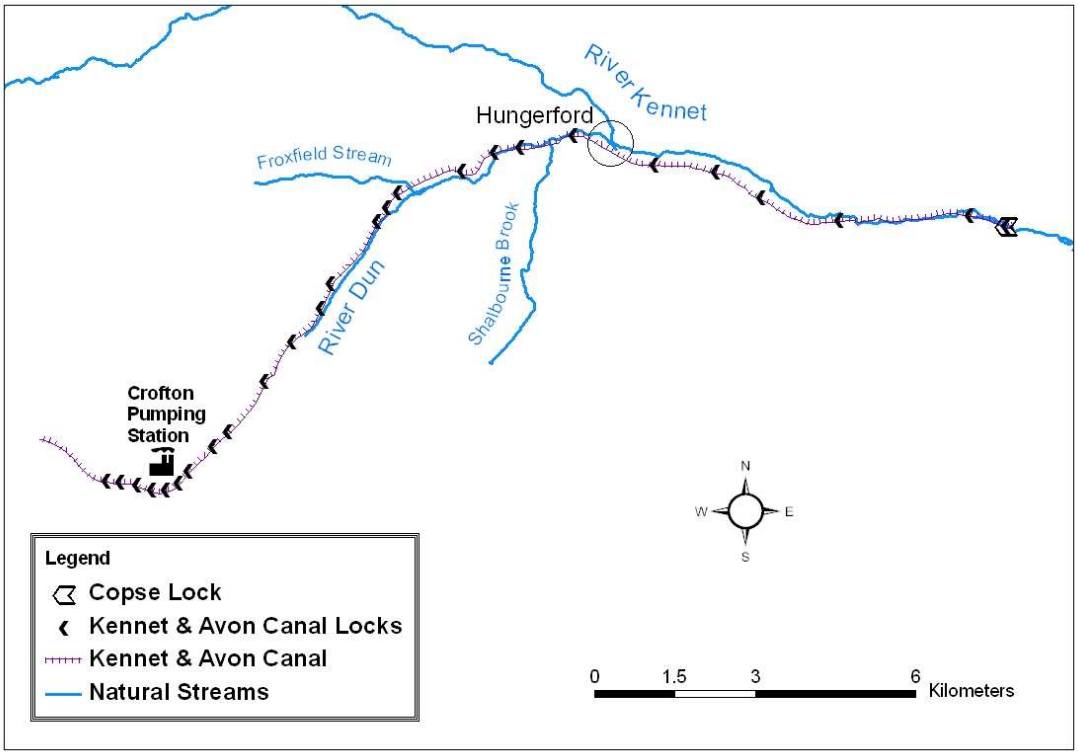

Figure 12. Locks on the Kennet and Avon Canal.

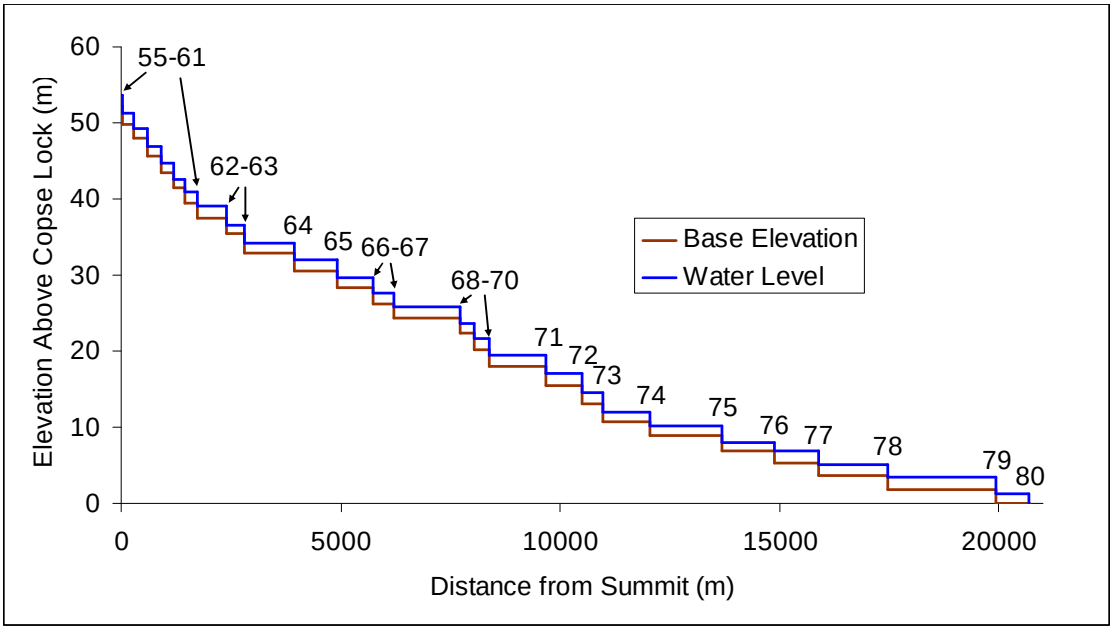

Figure 13. Elevation and water depth along the study section of the Kennet and Avon Canal. Distances and elevations approximate. Numbers correspond to lock numbers.

Though the major flows come from the aforementioned water bodies, runoff from the land surface does have the potential to enter the canal; as a result, it is important to understand the nature of the drainage area surrounding the canal and the river. This area is predominantly agricultural (Figure 14), with a loamy soil texture, roughly 30% sand, 45% silt, and 25% clay (Jarvis et al. 1979; Jarvis et al. 1984).

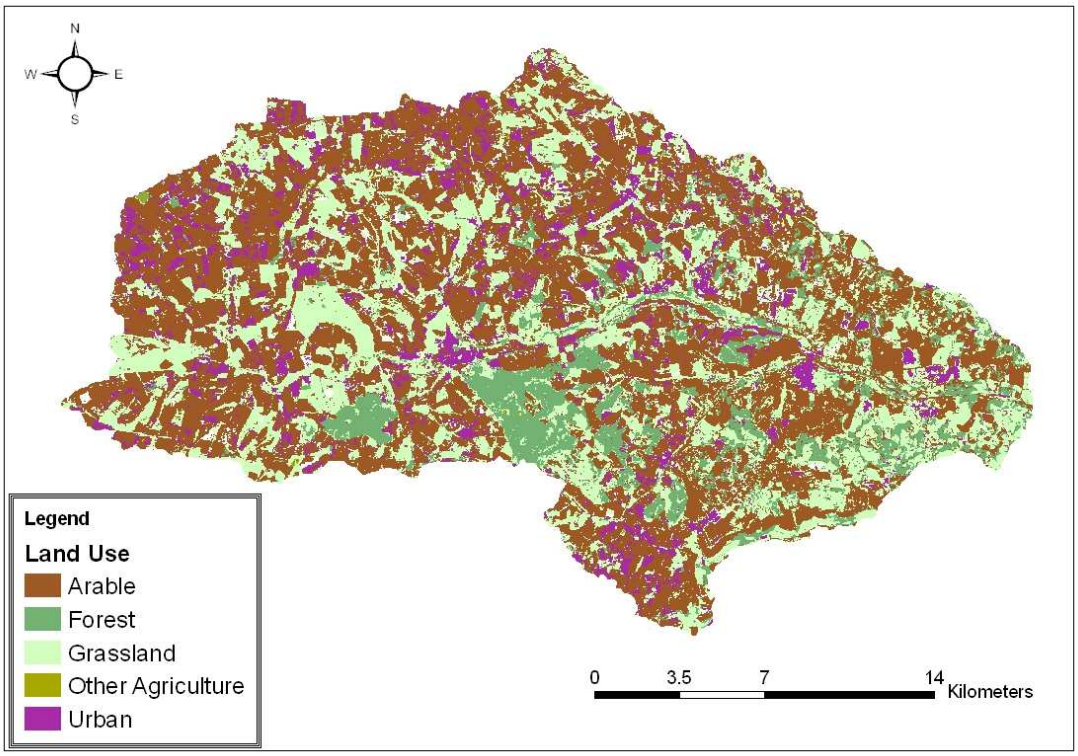

Figure 14. Land uses in the Kennet Catchment. Data obtained via Dr. Andrew Wade (University of Reading), originally from the Institute for Terrestrial Ecology.

2.5.2. History

As might be expected with a nearly 200-year-old structure, the Kennet and Avon Canal has had a colorful history. After experiencing financial difficulties that delayed its completion, it experienced its heyday in the early 1800s, followed by a substantial decline beginning in the mid-1800s when the nearby Great Western Railway was completed, with net deficits recorded beginning in 1877. Around the time of the world wars, the improvement in road transport delivered another blow to the canal, and throughout the 1900s it struggled to maintain its existence (Clew 1973). Various sections of the canal became impassable in the 1900s due to lack of maintenance; 13 km of canal between Newbury and Reading were closed in 1950 (Clew 1973; West Berkshire Heritage Service 1999). The entire canal reopened in 1990 thanks to the volunteer efforts of the Kennet and Avon Canal Trust. Today it exists primarily as a recreational canal, with very little of the commercial traffic that dominated its early years (Neal et al. 2007); however, the reopening of the canal has caused difficulties with local anglers (Halcrow Group Limited 2007), as a profitable fishery developed on the pristine River Kennet in the years of the canal's disuse.

2.5.3. Water Chemistry Assumptions

Certain assumptions were made in Section 2.3.2 in the investigations of relevant processes for canal modeling. First, it was assumed that phosphorus would be the limiting nutrient in any system studied. Second, it was assumed that Eppley's relationship for temperature (Equation 19) would be valid (that is, that the water temperature would be below 40ºC at all times). Data from Neal et al. (2006b) support both of these assumptions for the Kennet and Avon Canal.

The average N:P weight ratio for the Kennet and Avon Canal is 28.8, yielding an N:P molar ratio of 63.7. This is much greater than the 'ideal' molar ratio (20) given by Cooper (1937) and the P-limited ratio (12) given by Dillon and Rigler (1974), indicating that in terms of nutrients, algal growth is P-limited. Measured water temperatures in the Kennet and Avon Canal range from 1.5 to 22.7ºC, well below the 40ºC threshold established by Eppley (1972) for the use of his equation to predict maximum algal growth rate (Equation 19).

2.6. Summary

Many of the components needed to create a canal model currently exist: sediment deposition has been characterized, a multitude of formulae for algal growth are available, and observations of canal processes and consultation with experts provide a good background on the hydrologic processes that must be considered. However, no model currently exists that specifically addresses all the issues needed for a water quality study of an inland navigational canal: in particular, the issues of boat-generated sediment, lockages, and algal growth are not included in existing models. The selected length of the Kennet and Avon Canal includes boat traffic, lockages, overflow weirs, leakage, algal growth, and interactions with the surrounding natural environment and as such provides a suitable setting for development and testing of a new computer-based canal model.

3. Data Collection & Analysis

3.1. Introduction

The development of the canal model required data from numerous sources. Sources of existing data included other researchers, government agencies, and internet databases. Other data were not available and had to be collected specifically for this study.

3.2. Field Surveys

Two field surveys were conducted to collect data from the canal that were not available from an existing source. The first of these surveys was held in August 2008 and the second in September 2009. Water quality samples were collected on both occasions. In August only, latitude and longitude information for the canal was collected; in September only, weir dimensions were collected. On both occasions, consultation with knowledgeable persons provided further information on the canal.

3.2.1. Water Quality Samples

Water quality samples were collected from the canal in an effort to quantify the amount of sediment disturbed by the passage of boats and the opening and closing of lock gates. Samples were collected immediately before and after boat passage and likewise immediately before and after lock gate movement. During the August sampling, the boat and lock samples were often taken in series – that is, before a boat approached the lock, after the boat passed but before the lock gate closed, after the lock gate closed, and then the reverse process as the boat exited the lock.

The water quality samples were collected with a simple apparatus (Figure 15). This apparatus consisted of a 100 mL container, a weight to pull the container down into the water column, and a float to keep the sampling container at the correct depth (0.3 m) while sampling. The container was lowered (preferably from a bridge, occasionally thrown from the side of the canal) into the center of the canal, held under water for a few seconds, and retrieved. The sample was immediately transferred to

100-mL container with a screw lid and labeled with the time and date of collection and a unique identifying code used later during laboratory analysis.

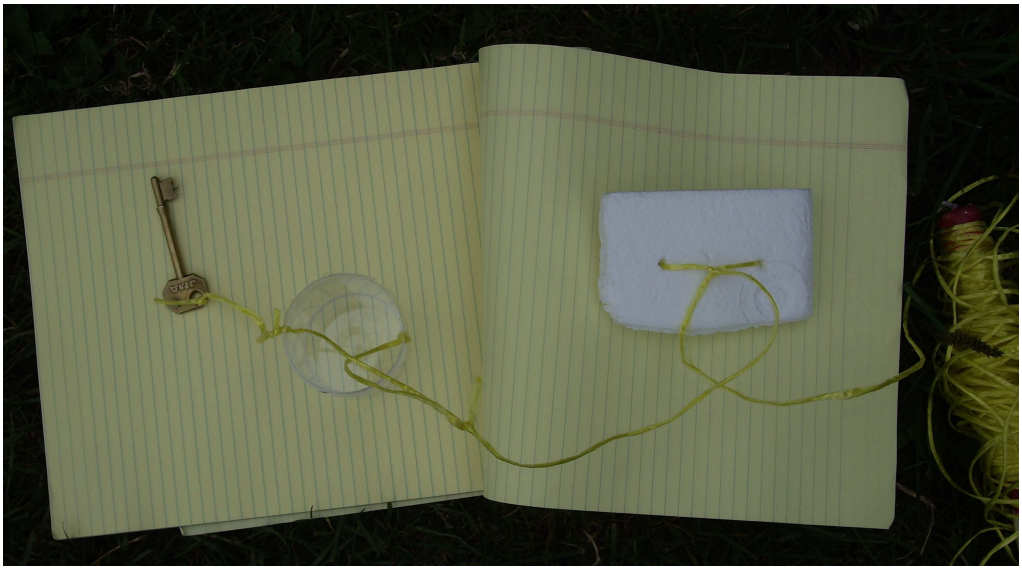

Figure 15. Sampling apparatus.

In total, samples were collected surrounding the passage of 24 boats: 10 in August 2008 and 14 in September 2009. Samples were collected surrounding 14 lock movements in August 2008.

3.2.2. Physical Characteristics

As lock locations and dimensions were not forthcoming from government agencies, it was necessary to collect information on both directly from the canal. The location of each lock on the study section was determined via personal survey using a handheld Global Positioning System (GPS) receiver (Garmin eTrex Vista HCx). The GPS receiver was also used to record the track of the old horse towpath along the canal, as an electronic map of the canal was not available. These data were imported into a Geographic Information System (GIS) (ESRI ArcGIS 9.2) for analysis. The results of both of these efforts were displayed previously as "Kennet & Avon Canal Locks" and "Kennet & Avon Canal" in Figure 12. These data were later used to calculate the lengths of the reaches between each lock and to determine to which reach various external sources (streams, sewage treatment works) contributed (described in Section 7.1.2).

In September of 2009, dimensions of lock gates and overflow weirs (bypassing lock gates) were measured using a 100-ft measuring tape. Notes were also taken regarding

any instructions to leave locks empty after use. The details of these measurements are included in Table 3 and in relevant sections throughout this report. On average, lock gates were 2.6 m long; overflow weir lengths varied greatly, with average weir boxes at locks (e.g., left photo, Figure 7) being 1.6 m long with a height of 16 cm and average culverted weirs (e.g., right photo, Figure 7) having an initial weir length of 6.3 m followed by a 62 cm diameter culvert.

Table 3. Reach and lock dimensions collected in September 2009. (continues next page)

Downstream Lock Number	Length of One Lock Gate (m)	Weir Length(s) (m)	Height of Weir Box (cm)	Leave Lock Empty?
55	2.69	2.4	14	Yes
56	2.64	0.91 0.91	33 33	Yes
57	2.44	0.94 0.94	20	Yes
58	2.59	1.1 1.1	18 18	Yes
59	2.67	2.0 2.0	18	Yes
60	2.69	2.3 2.3	23 23	No
61	2.59	2.1	18	No
62	2.67	1.9 1.9	20 20	No
63	2.74	2.2 2.2	20 20	No
64	2.72	2.0 2.0 6.7	20 20 ∞[†]	No
65	2.74	1.7 1.7	20 20	No
66	2.59	1.9 1.9 1.7	19 19 38	No
67	2.67	2.0 2.0	15 15	No
68	2.59	1.7 1.7	20 20	No
69	2.77	1.9	43	No
70	2.74	2.1 2.1	24	No
71	2.59	2.5	∞	No
72	2.74	1.2 1.2 7.7 (0.66)[‡]	15 15 74	Yes

Downstream Lock Number	Length of One Lock Gate (m)	Weir Length(s) (m)	Height of Weir Box (cm)	Leave Lock Empty?
73	2.57	1.4 1.4 3.2 (0.74)	20 20 74	No
74	2.62	1.5 1.5 7.8 (0.46)	13 13 46	No
75	2.69	1.6 1.6 8.8 (0.74)	23 23 74	No
76	2.69	1.7 1.7 6.7 (0.61)	13 13 61	No
77	2.54	1.5 1.5 9.0	18 18 18	No
78	2.74	n/a[¶]	∞	No
79	2.59	1.4 1.4 3.7 (0.43)	15 15 43	No
80	2.44	1.4 1.4	18 18	No

[†] Where weir height is given as ∞, the weir has no top (i.e., it is just a weir, no box).
[‡] Where a number is given in parentheses, the weir box consists of a long weir crest flowing into a box that discharges through a culvert (Figure 16); the number not in parentheses is the weir crest and the number in parentheses is the diameter of the culvert.
[¶] The overflow weir for this section is out of sight on private property at Kintbury Mill; estimates were later made from aerial photos that the weir length was 9.1 m and the weir had no top.

Figure 16. Example of complicated weir box.

3.2.3. Laboratory Analysis

Upon return to Cambridge after collecting water samples, the samples were refrigerated and analyzed within three days. Sample volume was measured and samples were filtered through use of a vacuum filtration system with a 47 mm diameter 0.4 μm cyclopore track etched membrane filter (Whatman brand). After filtration, samples were dried at 105ºC for two hours. The weight of each filter paper was recorded prior to analysis, and compared to the post-drying weight of solids and filter to determine the weight of dry solids in each sample. The solids concentration was determined as the quotient of the dry solids weight and the original sample volume.

The concentration of sediment disturbed by boat passage was determined by comparing the pre- and post-boat passage concentrations (Table 4). Likewise, the concentration of sediment disturbed by lock gate movement was determined by

comparing the pre- and post-lock gate movement concentrations (Table 5). In the case where these comparisons resulted in a negative concentration change, it is assumed that the turbulence generated by the boats or lock gates temporarily drew water of lower sediment concentration into the center sampling location in the canal.

The full details of the calculated sediment concentrations are included in Table 4 and Table 5; in summary, excluding outliers, the average concentration of sediment stirred up by boat passage was 23 mg/L (median 18 mg/L, range 1.8 mg/L to 70 mg/L); and by lock movements, 7.3 mg/L.

Table 4. Sediment concentration increases due to boat passage.

Collection Period	Boat Width	Sediment Concentration (mg/L)
2008	Wide	36.8
2008	Narrow	8.5/0.4[†]
2008	Two Narrow	14.0/-1.7/-2.8
2008	Narrow	31.5
2008	Narrow	12.1
2008	Narrow	23.3/8.9
2008	Narrow	147.8
2008	Not Recorded	149.8
2008	Not Recorded	22.3
2009	Wide	259.3
2009	Narrow	3.2
2009	Narrow	10.3
2009	Narrow	27.6
2009	Narrow	4.6
2009	Two Narrow	1.8
2009	Narrow	12.1
2009	Wide	193.8
2009	Narrow	44.3
2009	Narrow	70
2009	Narrow	2.1
2009	Wide	61.7
2009	Narrow	26.8

[†]Where multiple numbers are listed, they reflect samples taken surrounding the same boat at different stages of the lockage process. The first number – taken before the boat moved into the lock – is considered most accurate.

Table 5. Sediment concentration increases due to lock gate movements (mg/L).

70.3	-5.9	19.7
5.2	-7.3	-6.3
-12.9	-1.7	-12.1
-25.0	-3.9	-6.2
0.1	87.7	

3.3. Aerial Photography

A bird's-eye view of the canal was used to estimate reach widths, the area in the canal affected by boat-disturbed sediment, and shading of each canal reach. Aerial photos were obtained from Bing.com (© 2010, Microsoft Corporation, NAVTEQ, Intermap, and Getmapping plc) for use in this analysis.

Because dimensions of the canal were not forthcoming from any Government agency, canal widths were estimated from aerial photography; information from the literature suggests a typical width for all 107 reaches of the canal of 40ft (12.2m) (West Berkshire Heritage Service 1999); this is consistent with the widths measured for individual reaches in the study length, which ranged from 7.4 m to 13.3 m.

The laboratory analysis provided a concentration of sediment suspended by boat passage; in order to appropriately model sediment transport, a volume of affected water was needed to obtain the total mass of sediment suspended. This was nearly impossible to estimate from a ground perspective; however, aerial photos clearly show the affected width to be approximately that of the boat (Figure 17). It is assumed, as the sediment is stirred up from the bottom of the canal, that the sediment load is evenly distributed from the bottom of the canal to the surface, roughly in a rectangular cross-section.

Figure 17. Aerial photo of boat and sediment plume on the Kennet and Avon Canal. From bing.com, © 2010, Microsoft Corporation, NAVTEQ, Intermap, and Getmapping plc.

Because the aerial photos clearly showed the tree cover over each canal reach, they were also used to estimate the percentage of each canal reach shaded from the sun. This was done by first importing the aerial photos to a GIS program, then outlining the total reach surface area and the reach surface area not covered by trees, then using those areas to compute the fraction of the surface area not shaded by trees.

3.4. Agency Data

The cooperation of several Government and private agencies was essential to the completion of this work. In particular, personnel from the Environment Agency, British Waterways, the Centre for Ecology and Hydrology, the University of Reading, and the Kennet and Avon Canal Trust provided crucial information for the development and testing of the canal model.

The Environment Agency provided information on sewage treatment works in the Kennet catchment (Figure 18). These data included locations of the facilities and monitored concentrations of sediment in the facilities' outfalls. Additionally, the Environment Agency provided monitored flows in the river at the Marlborough station (Figure 18), used to calibrate the overland flow model used to generate runoff

inputs to the new canal model. Perhaps most importantly, the Environment Agency provided details of previous studies and surveys conducted on the canal that identified areas of interaction between the canal and the river (National Rivers Authority 1992; Halcrow Group Limited 2007).

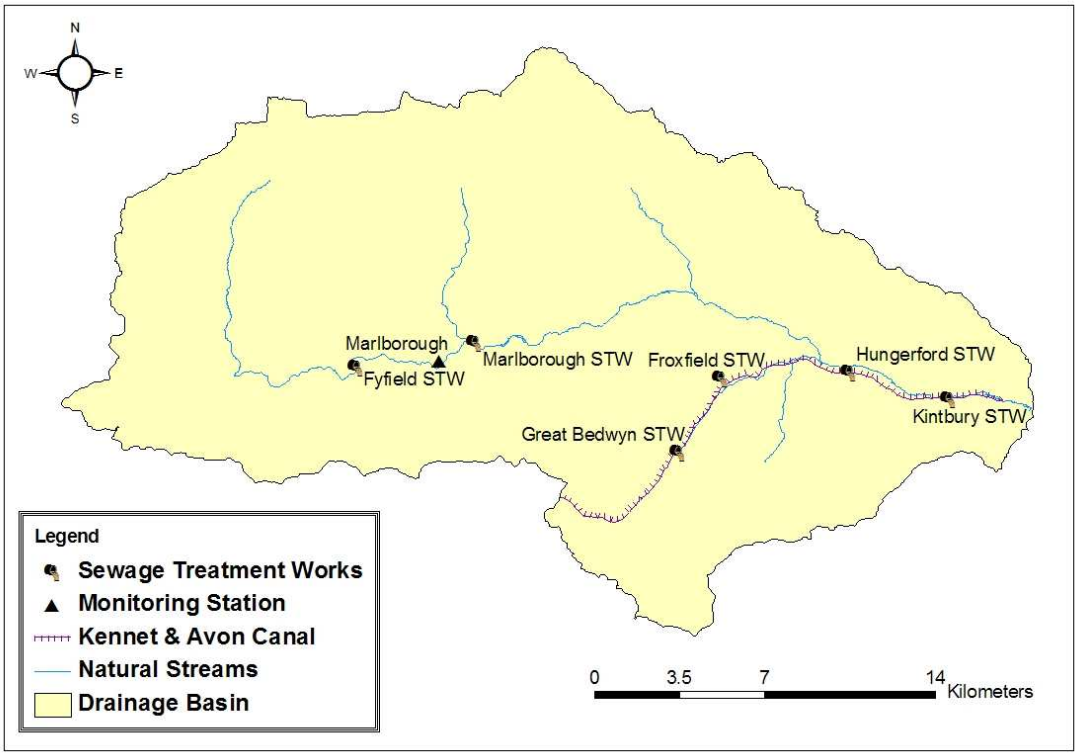

Figure 18. Sewage treatment works and hydrological monitoring station, data from which were provided by the Environment Agency.

British Waterways provided information on the height of the overflow weirs in the canal, lockage rates, and limited flow data recorded in the canal. The heights of overflow weir crests above the bottom of the canal ranged from 1.10 m to 1.53 m. An annual count of lockages at multiple locations on the canal (Figure 19) is shown in Table 6; Lock 85 is outside the study area, but data from this lock were used to estimate lockages at the lower locks on the study area. A representative distribution of lockages throughout the year based on data compiled from multiple canals in England was also available, shown in Figure 20. Flow data on the canal were only available for the modeling period at the Picketfield weir bypass (bypassing Lock 71).

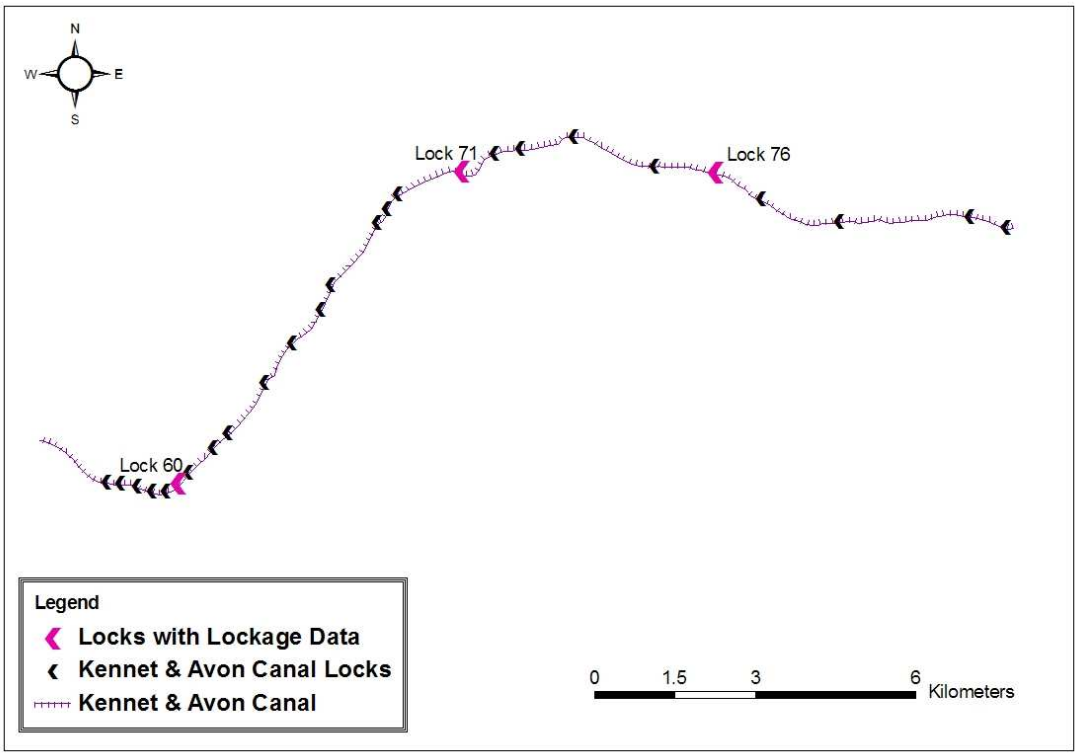

Figure 19. Location of information available from British Waterways – lockage data were available from the labeled locks, and flow data were available from the bypass at Lock 71.

Table 6. Lockages by year for four locks on the Kennet and Avon Canal.

	Lockages					
Lock	**2000**	**2001**	**2002**	**2003**	**2004**	**2005**
60	1862	1976				
71	1938	1892	1822	1915	2407	
76				2367	2443	2345
85	2261	2423	2750	2858	2950	2831

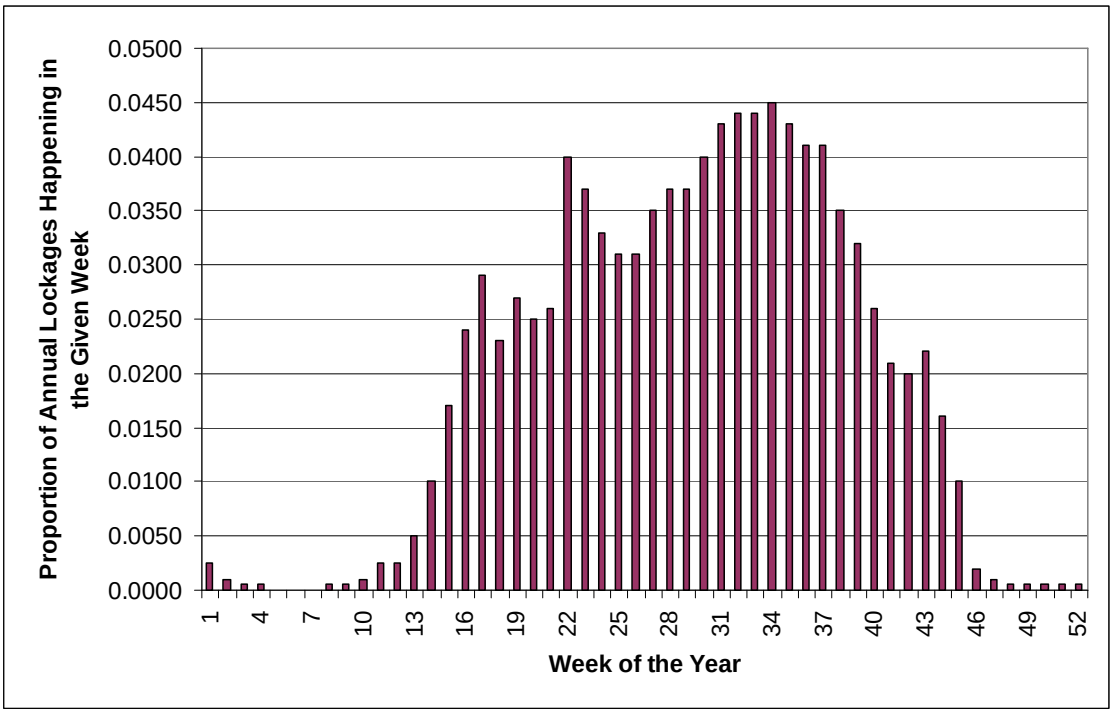

Figure 20. Weekly distribution of lockages.

Dr. Colin Neal at the Centre for Ecology and Hydrology provided sediment concentrations, phosphorus concentrations, and chlorophyll-a concentrations recorded over varying periods of time at multiple stations on the canal and the river (Figure 21) (Neal et al. 2000; Neal et al. 2006a; Neal et al. 2006b; Neal et al. 2007; and unpublished data). Observations made on the canal were used to verify the accuracy of the new canal model, and observations made on the river were used to calibrate the overland flow model used to provide runoff input to the canal model. Sediment and phosphorus data were also available from Dr. Neal for the Wilton Water reservoir supplying the canal.

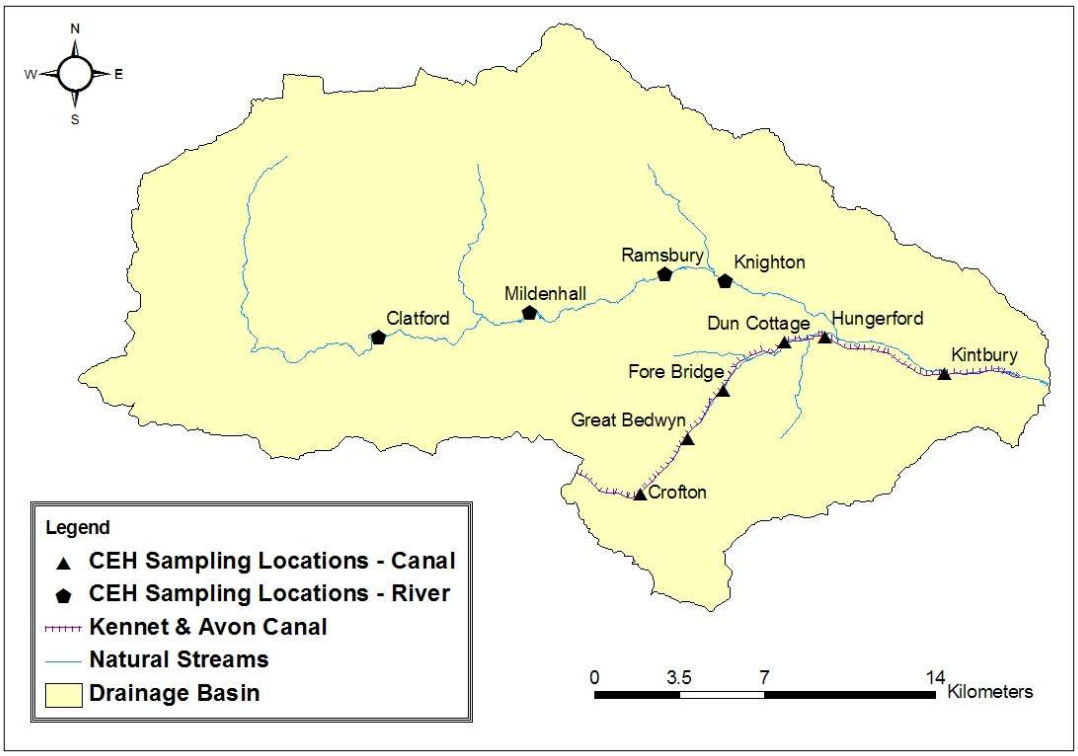

Figure 21. Centre for Ecology and Hydrology (CEH) sampling locations.

Dr. Andrew Wade and Mr. Attila Lazar (PhD candidate) at the University of Reading provided information on sewage treatment work flow rates and flow-velocity relationships for the River Kennet needed for the runoff model. They had previously gathered these data for their modeling efforts for the river.

Mr. Mike Lee, Hon. Engineer for the Kennet & Avon Canal Trust, provided a detailed map of the canal that included the lengths and depths of the locks. He also provided background information on the canal and the operation of the Crofton Pumping Station.

3.5. Summary

The data collected as described in this section of the report provided the needed inputs for the final canal model described later in Section 6. Estimates of sediment disturbed by boat passage provide a valuable contribution to the literature, which is noticeably deficient in that regard. Communication with local experts and agencies provided a much-needed background to help understand the canal, in addition to the data needed for parameterization and testing of the canal model.

4. Canal Model Development

4.1. Introduction

As has been mentioned previously, the goal of this project is to develop a computer model capable of predicting the multiple processes unique to a canal model, while retaining an ease of parameterization to make the model usable by agency personnel who may not be familiar with the intricacies of hydrologic modeling and usable in areas where intensive monitoring is not available.

4.2. Algorithm Development

Solids generation and transport in canals differs from what one might expect in a lake or river. Rivers have a high flushing rate and lakes tend to be stagnant enough to act as settling basins; however, canals are somewhere in the middle, essentially a series of impoundments with a 'short' water transit time. Although canals have a much lower flow rate than rivers, it is not so low that the individual 'impoundments' can be considered completely stagnant.

Boat traffic in canals dominates both the hydrology and sediment generation and transport in canals. Boat traffic serves two functions of interest – first, it increases the flow rate over an otherwise low rate as the boats remove large volumes of water from each impoundment ('reach') as they pass through locks; second, the boats themselves stir up noticeable quantities of solids (Figure 17, page 63). The subsections of Section 4.2 describe the key processes in canal operations and those that are considered as part of the canal model, illustrated in Figure 22. In summary, the suspended solids concentration in a reach is a function of the underlying hydrology, boat movements, and factors affecting algal growth. It is additionally affected by sources and sinks external to the model. Three types of solids will be tracked in the solids calculations: biological (i.e., algae), inorganic cohesive sediment, and inorganic non-cohesive sediment. The specific processes modeled include:

- Water and solids flow through the overflow weirs (I_{weir}, Q_{weir}, ISS_{weir}, QSS_{weir})
- Water and solids flow occurring with lockages (I_{lock}, Q_{lock}, ISS_{lock}, QSS_{lock})

- Water and solids flow associated with overtopping of lock gates ($I_{w,lock}$, $Q_{w,lock}$, $ISS_{w,lock}$, $QSS_{w,lock}$)
- Water and solids flow associated with lock leakage (I_{leak}, Q_{leak}, ISS_{leak}, QSS_{leak})
- Seepage of water through the sides of the canal (Q_{seep})
- Sediment disturbance caused by boat propellers (ISS_{boat}) and lock movements ($ISS_{lockmove}$)
- Biological solids generation in terms of algal growth (ISS_{bio})
- Deposition of sediment along the length of the reach (QSS_{dep})
- External influences on water and solids quantities in the canal reaches (I_{ext}, Q_{abs}, I_{runoff}, I_{prec}, Q_{evap}, ISS_{runoff}, ISS_{ext}, QSS_{abs})

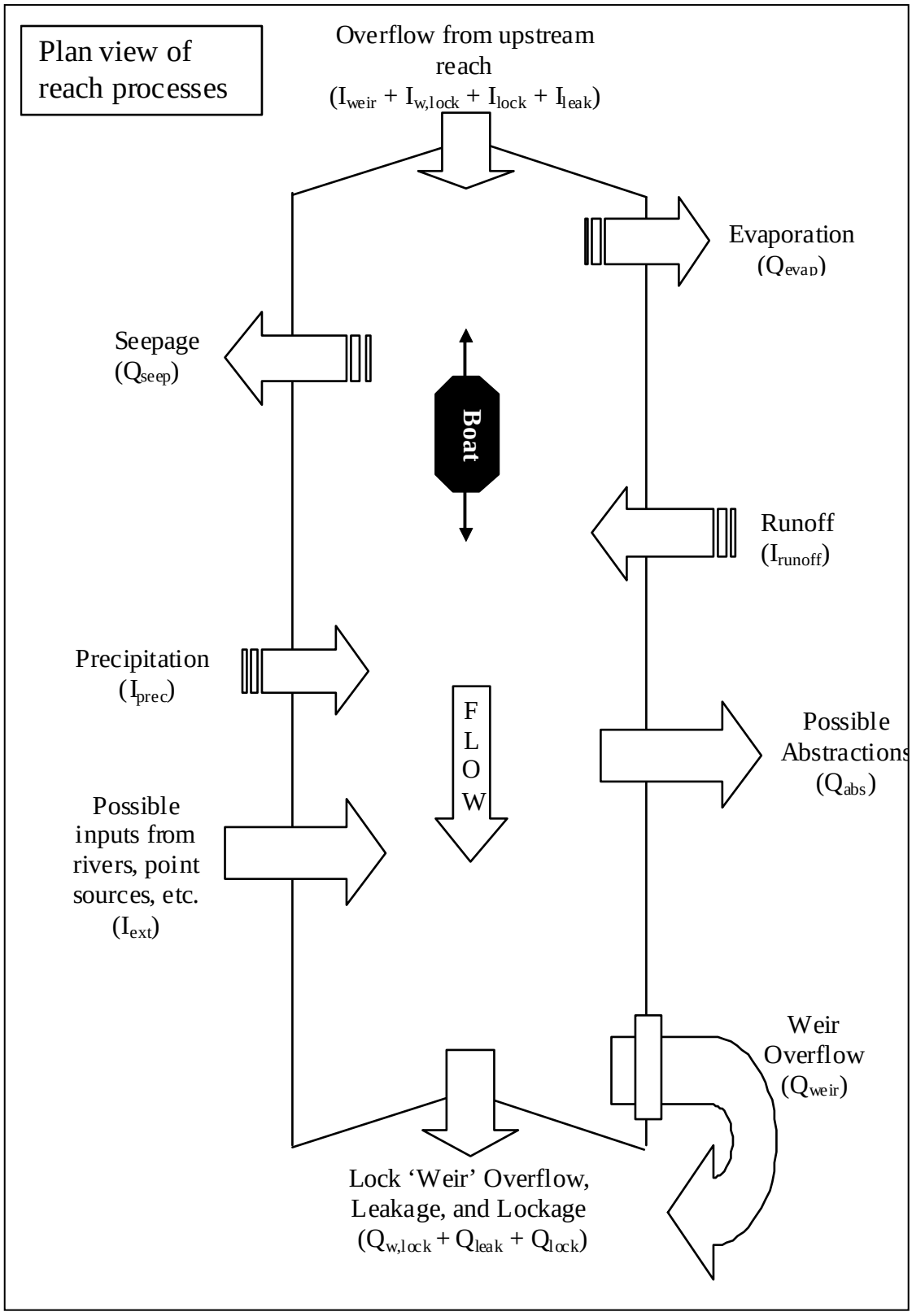

Figure 22. Plan view of reach processes.

Equation 32 is the basic governing equation for the hydrology calculations:

$$\frac{dS}{dt} = I(t) - Q(t) \tag{32}$$

Where: S = water storage in the canal reach (m^3);
I = water inflow to the reach as a function of time (m^3/s);
Q = water outflow from the reach as a function of time (m^3/s); and
t = time (s).

This is a basic continuity equation in use by numerous existing hydrologic models (e.g., HSPF (Bicknell et al. 2001) and INCA (Wade et al. 2002)); however, the characteristics of the inflows and outflows will be unique to the canal model.

Similarly, equation 33 is the basic governing equation for the solids calculations.

$$\frac{dSS}{dt} = ISS(t) - QSS(t) \tag{33}$$

Where: SS = sediment storage in the canal reach (mg);
ISS = sediment inflow to the reach as a function of time (mg/s); and
QSS = sediment outflow from the reach as a function of time (mg/s).

The components of inflow (I(t) and ISS(t)) and outflow (Q(t) and QSS(t)) are described in the following sections. Note that in each category of flow, the outflow of water and solids from the upstream reach(es) becomes the inflow to the downstream reach. This is done individually for each component of outflow and inflow; thus, Q_{weir}, Q_{lock}, $Q_{w,lock}$, and Q_{leak} for an upstream reach are routed separately to I_{weir}, I_{lock}, $I_{w,lock}$, and I_{leak}, respectively, for the downstream reach. The solids processes follow the same pattern.

4.2.1. Simplifying Assumptions

The basic system simulated is a series of reaches, within which solids are assumed completely mixed (except as detailed in the following sections). Each reach has four basic state variables – water storage, cohesive sediment storage, non-cohesive sediment storage, and algal storage. Equations 32 and 33 are applied to the state variables in each reach to determine the inflows and outflows at each time step.

It is assumed that the primary sources of sediment in the reach are the boats and upstream canal reaches, as opposed to runoff or external inputs; thus, the potential distribution of runoff and external inputs along the canal length is not considered in the deposition calculations.

It is assumed that the potential elevation of the canal sides above the neighboring topography does not affect the potential for runoff to enter the reach. Although surface runoff may be retarded by elevated earthen walls, interflow and groundwater flow into the reach may still occur.

It is assumed that the water temperature in the canal will not be so hot as to kill the algae in a reach and that the diversity of algal species is great enough that the general algal response to increased phosphorus concentrations is a positive one. Although some researchers like Rodhe (1948) have found a small number of species that were adversely affected by high concentrations of phosphorus, the hot water and low diversity conditions required as habitat for those species are considered unlikely to occur in an average inland navigational canal. Most researchers have found a positive relationship between algal growth and phosphorus concentration, as described previously in Section 2.3.2.

A few minor processes assumed insignificant in a typical navigational canal will not be modeled. Because boat operators are instructed not to cause a wake, the erosion of banks by wake effects is not considered. Because the flow rate in the canal is low, scour of the sides and bottom of the canal is not considered (except in conjunction with boat propellers and lock gates).

4.2.2. Hydrologic Algorithm

The hydrologic algorithm for the canal model quantifies the relationships unique to canals: lockages, weir flows, over-lock flows, seepage losses, and leakage. Because the reaches between locks are designed to be level, flow due to the slope of the stream is insignificant in comparison to these other flows, and thus a typical hydrologic model based on slope and roughness is inapplicable for these purposes.

The components of hydrologic inflow (I(t)) are precipitation, runoff, external sources, weir flows from upstream reaches, over-lock-gate flows from upstream reaches, lockages from upstream locks, and leakage from upstream locks. The components of hydrologic outflow (Q(t)) are evaporation, external abstractions, seepage, weir flows, over-lock-gate-flows, lockages to downstream locks, and leakage through downstream locks. Most of these flows are time-dependent and many also depend on the water storage in the reach. The methods by which each of these processes is represented in the canal model are described in this section.

4.2.2.1. Weir Flow

An overflow weir is typically positioned in the side of a canal wall to maintain a desired water level in the canal reach. It may take the form of a box cut in the side of the canal or it may be a long weir with no significant overhang (Figure 7, page 29, left and right images, respectively). The hydrology of the weir is governed by basic weir flow and orifice flow equations; while the weir opening is not completely submerged, Equation 34 for weir flow is used; if it becomes submerged, Equation 35 for orifice flow is used. Daugherty (1937) developed equation 35 as an orifice flow equation for low head conditions and as such it provides a smooth transition between typical weir flow and orifice flow equations. The smooth transition is necessary for the use of Newton's Method to solve the system of equations (described in more detail in Section 4.2.6). Water that exits a reach through a weir will become an inflow to the next downstream reach.

$$Q_{weir} = \frac{2}{3} C_{d,weir} \left(L_{weir} - 0.2H_{weir}\right)\sqrt{2g}\, H_{weir}^{3/2} \tag{34}$$

$$Q_{weir} = \frac{2}{3} C_{d,weir} L_{weir} \sqrt{2g}\left(H_{weir}^{1.5} - \left(H_{weir} - H_{sides}\right)^{1.5}\right) \tag{35}$$

Where: $C_{d,weir}$= weir discharge coefficient (unitless);
g = acceleration due to gravity (m/s²);
L_{weir} = length of weir crest (m);
H_{weir} = depth of water above weir crest (m); and
H_{sides} = height of sides of weir box (m).

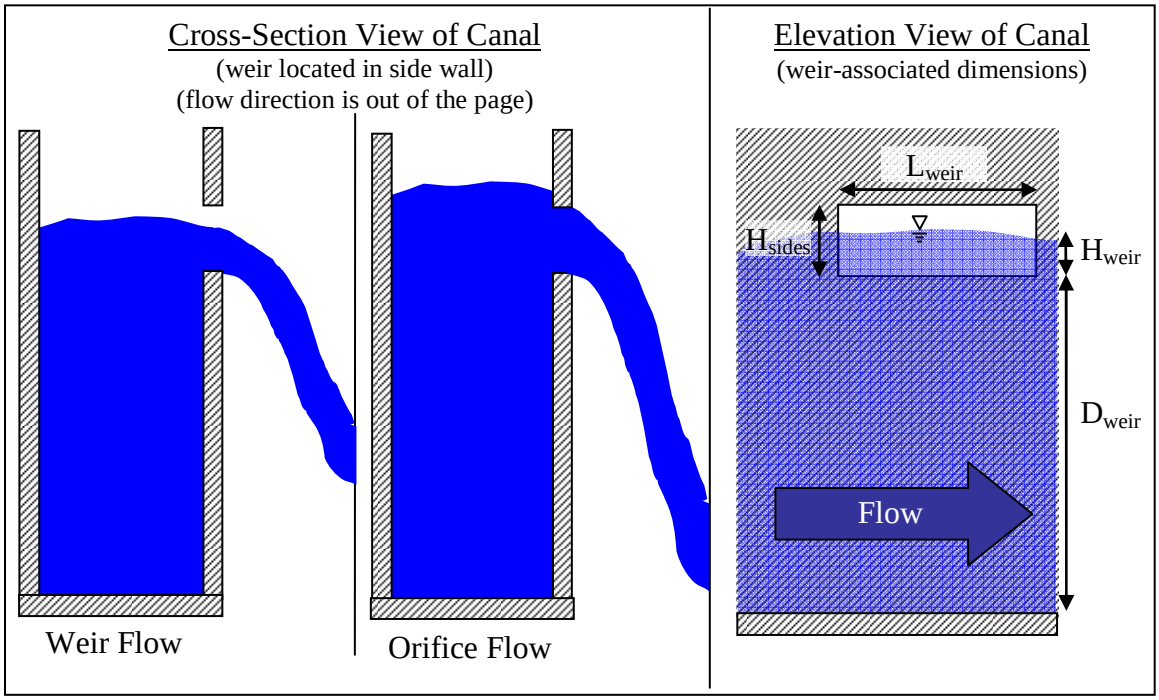

Figure 23. Illustration of typical canal overflow weir.

4.2.2.2. Lock-Associated Flows

The locks in a canal have several effects on flow. In addition to maintaining the reach impoundments while lock gates are closed, the most obvious effect is the water flow associated with a boat passage (Figure 4, page 26), which drives the primary outflow of the reach when boats are present. Not as obvious are the flows that occur due to leakage and overtopping of the lock gates.

During boat passage through a lock, a volume of water equal to the volume of the lock will be either taken from the upstream reach, deposited to the downstream reach, or both (Figure 5, page 27). Equation 36 describes this scenario.

$$Q_{lock} = \left[(1 - E_{boat}) + \frac{E_{boat}}{2} \right] * F_{boat} * V_{lock} \qquad (36)$$

Where: E_{boat} = efficiency of boat movement: that is, what portion of canal traffic follows case 1 or 2 in Figure 5 rather than case 3 or 4 (unitless);
F_{boat} = frequency of boat movement (boats/s); and
V_{lock} = volume of lock (m^3/boat).

The term $(1-E_{boat})$ in Equation 36 represents the boats moving through the lock sequentially in the same direction (that is, cases 3 and 4 in Figure 5, page 27); the term $E_{boat}/2$ in Equation 36 represents the boats moving through the lock sequentially

in opposite directions (that is, cases 1 and 2 in Figure 5). An entire lock volume is lost from the reach every time a boat passes going the same direction as the previous boat to pass the lock, but the same volume is lost only every other time a boat passes going the opposite direction of the previous boat to pass the lock.

Recalling Section 2.1.1, leakage occurs through lock gates that are weathered or damaged by use. A leakage rate must be estimated as a function of depth for input to the model; this leakage rate becomes the component of Q(t) related to lock leakage, Q_{leak} (Equation 37).

$$Q_{leak} = Leak * Min(D, D_{lock}) \quad (37)$$

Where: Leak = leakage rate ($m^3/m/s$);
D = water depth in canal reach (m); and
D_{lock} = height of lock gates (m).

The inclusion of depth in Equation 37 allows the discharge rate to scale based on the depth of water behind the lock gates.

On infrequent occasions, water may overtop the lock gates, causing weir flow (Figure 24). It is likely this would only happen in the case of extreme rainfall and flooding; however, a canal experiencing management or design problems may also experience over-lock-gate flow. When it does occur, this overtopping of a lock gate will experience non-contracted weir flow (Henderson 1966), as given in Equation 38.

$$Q_{w,lock} = \frac{2}{3} C_{d,weir} L_{lock} \sqrt{2g} H_{lock}^{3/2} \quad (38)$$

Where: L_{lock} = length of lock gates (m); and
H_{lock} = water depth above lock gates (m).

Note that because there is no ‘top’ to the lock gate weir flow, it will not switch to orifice flow at any point. Water that overtops the lock gates is assumed to enter the downstream reach in short order, either because the lock itself is already full, or through leakage in the downstream gates.

Figure 24. Water overtopping lock gates during a period of high flow.

4.2.2.3. Seepage

Seepage (Equation 39) is dependent on a seepage rate and the wetted surface area of the reach, which in turn can be determined by the model from the storage in the reach.

$$Q_{seep} = Seep * WSA \quad (39)$$

Where: Seep = rate of seepage (m/s); and
WSA= wetted surface area of the reach (m²).

Put briefly, this equation uses a constant rate of seepage, ideally determined based on the characteristics of the material lining the canal. This seepage rate is applied to the entire water-covered surface of the walls and bottom of the reach (the wetted surface area).

4.2.2.4. External Sources and Sinks

There are several processes that occur independently of the flow rate and flow depth in the reach. These include precipitation, runoff, point source inputs, abstractions, and evaporation. All of these processes must be input as a time series of values. Precipitation and evaporation are described by equations 40 and 41, respectively.

$$I_{prec} = PREC * SA \quad (40)$$

$$Q_{evap} = PE * SA \quad (41)$$

Where: PREC = precipitation rate (m/s);
SA = reach surface area (m²); and
PE = potential evaporation (m/s).

Evaporation can only happen when there is water in the reach (i.e., storage is greater than zero); this should always be the case in a properly modeled canal but regardless is checked in the model before applying the equation. Point source inputs (I_{ext}), hydrologic abstractions (Q_{abs}), and runoff (I_{runoff}) must be obtained from appropriate sources; these will likely be regulating agencies for I_{ext} and Q_{abs} and a separate catchment model for I_{runoff}. The sources used for the current application are detailed further in the section on model application (Section 7.1, page 126).

4.2.3. Inorganic Sediment Algorithm

Inorganic sediment is tracked in two classes: cohesive and non-cohesive. With the exception of fall velocity, these two classes of sediment can be described by the same basic equations. The components of inflow (ISS(t)) for inorganic sediment include boat generated sediment in addition to inputs associated with the water inflows to the reach. The components of outflow (QSS(t)) for inorganic sediment include deposition in addition to the outputs associated with the water outflows from the reach.

4.2.3.1. Deposition

The inorganic sediment in the reach will undergo deposition during each time step. The inorganic sediment deposition comprises QSS_{dep}, a component of QSS(t). The basic deposition formula is given as Equation 42.

$$\frac{dSS}{dt} = -\frac{w_s SS}{D} \tag{42}$$

Where: w_s = fall velocity of sediment (m/s).

It is evident that the solution to Equation 42 yields a relationship wherein deposition causes the remaining sediment in suspension to decay exponentially with time. Because the solution to Equation 42 actually yields the remaining suspended sediment after deposition has occurred, the deposited sediment load (QSS_{dep} (mg/s)) equals the existing suspended sediment load less the SS calculated from Equation 42. Although Equation 42 is readily solved analytically, the numerical solution is unstable when the time increment is large; therefore, the actual code of the model includes $1 - e^{-w_s t/D}$ as a term of QSS(t) rather than including the pure differential form as a decay term as given above.

The fall velocity (w_s) used in Equation 42 is calculated differently for cohesive and non-cohesive sediments. Non-cohesive sediment fall velocity is a straightforward function of particle diameters (Equation 4, Section 2.2). Because in-situ measurement of fall velocity for cohesive sediments is not practical for large-scale modeling projects, the relationship developed by Manning (2004) will be used to estimate the fall velocity for cohesive particles (Equations 7 - 10). This estimates the overall fall velocity based solely on suspended cohesive sediment concentration and shear stress near the bed. The adaptation of Manning's methods for use in the canal model is described in greater detail in Appendix A.1.

4.2.3.2. Boat-Associated Processes

As aptly pointed out by Copeland and others (2001), boats do not introduce sediment into the canal, but rather resuspend the sediment that has been previously deposited by other means. In the canal model, it is assumed that a plentiful supply of sediment exists in the canal, both as a result of earthen canal walls and from sediment carried into the reach from the land surface and external sources.

Boats will suspend a plume of sediment (Figure 17, pg. 63) as they travel down the reach. This plume is primarily generated by scour of the canal bottom caused by the turbulence generated by the propellers. An estimate of the sediment concentration generated by boats must be made, for example as a result of on-site sampling as described in Section 3.2.1. Once this estimate is provided, the sediment generated by a boat is a straightforward calculation (Equation 43).

$$ISS_{boat} = F_{reach} * CS_{boat} * L * D * B_{wid} \quad (43)$$

Where: F_{reach} = rate of boat passage in the reach (boats/s);
CS_{boat} = suspended sediment concentration generated by boat propellers (mg/m³•boat);
L = reach length (m); and
B_{wid} = boat width, assumed to be equal to the width of sediment disturbance in the canal (see Section 3.3) (m).

Because the F_{boat} variable introduced earlier is a property of locks, not reaches, it is necessary to calculate F_{reach} based on the F_{boat}'s at the upstream and downstream locks in order to determine the frequency of boat movement in the reach itself. These values may not be the same, for example, if there is a winding hole in a reach where boats commonly turn around and return from whence they came. As a boat traverses

the reach, it will cause sediment production along the entire length of the reach, and thus the concentration stirred up by the boat is multiplied by the volume of disturbed water in the reach (estimated as the product of reach length, reach depth, and boat width, as was described previously in Section 3.3) in order to obtain the total sediment load generated by boats as they traverse the reach. A concentration is used to generate a sediment load because it is considered more easily measured than the multitude of parameters needed to directly compute a load (for example, by using the model of Maynord and others (2004) to compute bedload generated by boat propellers).

Boats will also affect the sediment passing through weirs on the reach. The flow through overflow weirs or over the top of lock gates is typically only a few centimeters deep. When the reach is unaffected by boats, the concentration of sediment in the top few centimeters of flow will be lower than the average concentration in the reach. However, as a boat passes the lock gates or the overflow weir, it will stir up sediment and cause a fully mixed solution again, which will begin to deposit as the boat moves farther away from the point of interest (Figure 25). This means that the concentration of sediment shortly after boat passage in the top few centimeters of flow will be elevated compared to what would be expected considering only suspension and deposition operating on sediment entering the upstream end of the reach (this latter process will be described in the next subsection).

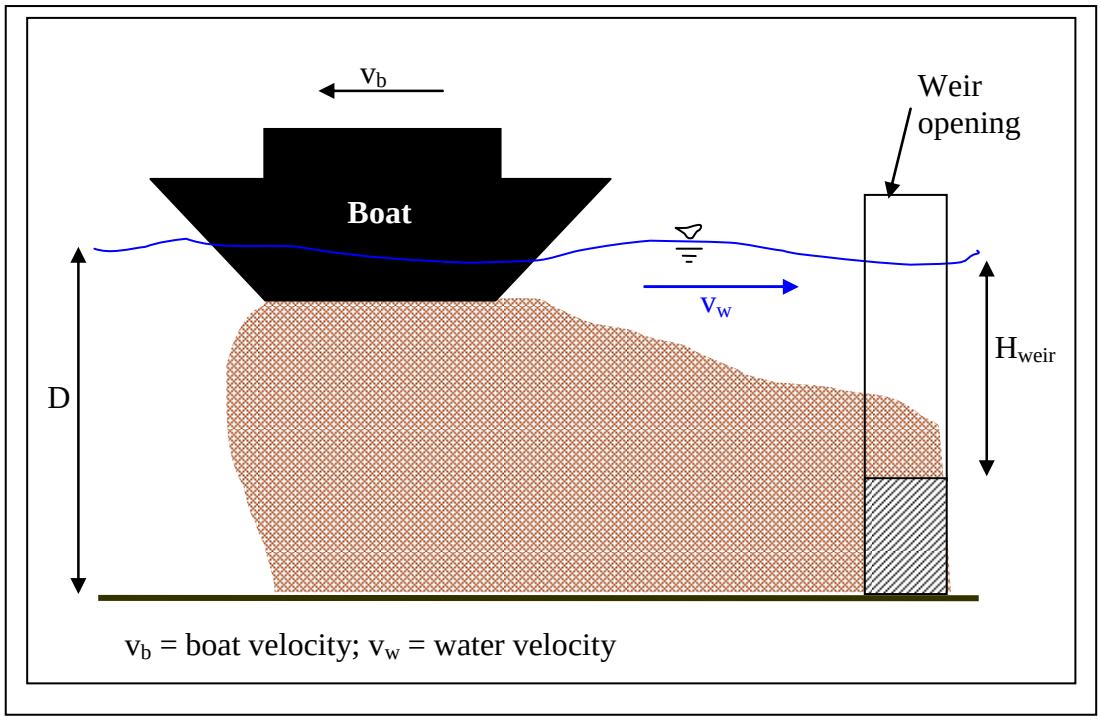

Figure 25. Elevation view of canal showing concentration profile for sediment generated by a boat as it passes a weir. Not to scale. Brown shading represents suspended sediment.

As time passes, sediment will move horizontally due to the effects of water movement and vertically due to the pull of gravity. The vertical movement is expected in Equation 42, but the horizontal movement is not. Therefore, in order to model the sediment suspended in the cross-section of the overflow weir, the time parameter in the solution to the deposition equation (Equation 42) must be modified to account for the effect of water movement. The modification must ensure that when the actual time is put into Equation 42, the model 'sees' a time adjusted for flow velocity. In short, the time parameter must change to account for water and boat velocities. Thus, Equation 44 describes the sediment generated by boat movement past a point of interest (that is, an overflow weir or a lock gate). The derivation of Equation 44 is provided in detail in Appendix A.1.

$$BSS = Q_{weir} \int_0^{t_3} CS_{boat} * e^{\frac{-w_s}{H_{weir}}\left(1+\frac{v_w}{v_b}\right)t}\, dt \qquad (44)$$

Where: BSS = suspended sediment generated by boat passage that is lost through an overflow weir or over top a lock gate (mg/boat);
v_w = water velocity (m/s);
v_b = boat velocity (m/s); and
t_3 = time for boat-generated sediment concentration to become negligible at the crest of the weir or top of the lock gates (s).

The boat suspended sediment (BSS) is the total sediment load passing over the weir sill or lock gate between the time when the boat passes (t = 0) and the time when the concentration above the weir crest or lock gate becomes negligible (t = t_3). This end time, t_3, is determined by setting the exponential part of the solution to Equation 42 to nearly zero (i.e., 0.0001). Typical t_3 values will be much less than the model time step (t_3 ~ 0.5-1hr for cohesives, 0.5-1min for noncohesives; model time step = 1 day). It should be emphasized that individual boat traffic is not modeled; rather, Equation 44 is used to calculate the contribution from a representative boat on the reach, and F_{boat} is used to determine how many BSS's should be included in each time step. The sediment disturbed by each of the passing boats is assumed to fall below the crest of the weir within one model time step; in a typical canal, there is no boat traffic for the last several hours of the day, such that all sediment generated by a boat will deposit below the crest of the weir before the next day begins, so this assumption is consistent with reality. The model set up does allow smaller time steps, but these should be chosen with care and attention to the expected values for t_3. The BSS will be incorporated into the weir transport in Section 4.2.3.3, where it is transformed to a rate (per time) through incorporation of the frequency of boat passage.

4.2.3.3. Weir-Associated Processes

There is significant turbulence associated with the inflow of sediment to a reach from upstream sources, whether the source is the outflow of the upstream overflow weir, leakage, or lockage. However, because the depth of water over the weir is often of the order of only 5cm or less (compared to a canal depth of approximately 1.5m), it is necessary to consider that the solids that were fully mixed at the upstream end of the reach may have settled out of the top few centimeters of the water column and thus not have the potential to exit the reach via the overflow weir (Figure 26). This is considered in Equation 45.

$$QSS_{weir} = F_{boat} * BSS + Q_{weir} * \frac{SS - ISS_{boat} \cdot \Delta t}{S} * e^{\frac{-w_s}{H_{weir}} \frac{L - x_{weir}}{v_w}} \qquad (45)$$

Where: Δt = model time step (s); and
x_{weir} = distance from upstream end of reach to weir location (m).

Note that F_{boat} is used in this case to affect BSS rather than F_{reach} (used in Equation 43) because most overflow/bypass weirs are located very close to the downstream lock

gate, and therefore the frequency of boat passage at the downstream lock gate is most representative of the boat traffic past an overflow weir.

In Equation 45, the first term accounts for the sediment stirred up by boats that passes through the weir. This term accounts for **all** boat-generated sediment (ISS_{boat}) that can possibly pass through the weir, as the time for the ISS_{boat} sediment to deposit below the weir height is considered as part of BSS. The second term accounts for the sediment from sources other than ISS_{boat} that passes through the weir during periods not affected by boat traffic. The $(L-x_{weir})/v_w$ term in the exponent represents the time it takes water to travel the length of the reach, and thus the time that sediment entering the reach at the turbulent upstream extent has to settle out of the water column. Thus ISS_{boat} is subtracted from the total sediment store in the second term so as not to double-count the sediment generated by boat traffic that was already considered in the first term. In practice, the second term of the equation is nearly always zero for the reach lengths considered in the Kennet and Avon Canal, and thus it may be appropriate in most cases to simplify Equation 45 to include contributions from boat passage only.

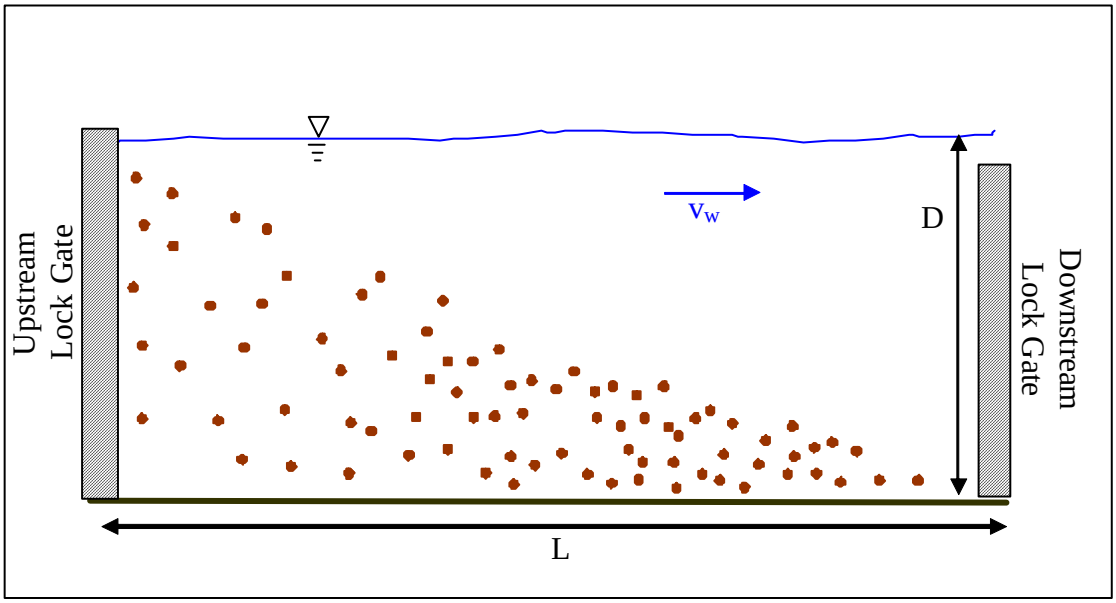

Figure 26. Elevation view of reach showing an idealized settling pattern for sediment traveling downstream. Brown dots represent sediment.

4.2.3.4. Lock-Associated Processes

As a lock is being drained to allow boat passage, water is typically released with great turbulence into the downstream reach. The sediment that moves downstream with

this water is assumed fully mixed, due to the turbulence in the released water. The sediment that moves with the water that fills the lock is also assumed fully mixed, as the water that fills a lock is drawn from near the bottom of the water column (Figure 4, page 26) and the water entering the lock also enters with a high turbulence. Thus, the sediment leaving the canal reach via lockages will do so at the average concentration of the reach, as described by Equation 46.

$$QSS_{lock} = Q_{lock} * \frac{SS}{S} \qquad (46)$$

When the lock gates open to allow boats to pass, a certain amount of sediment will be stirred up as the bottoms of the gates move across the bottom of the canal. The sediment will be disturbed in the pattern outlined in Figure 27.

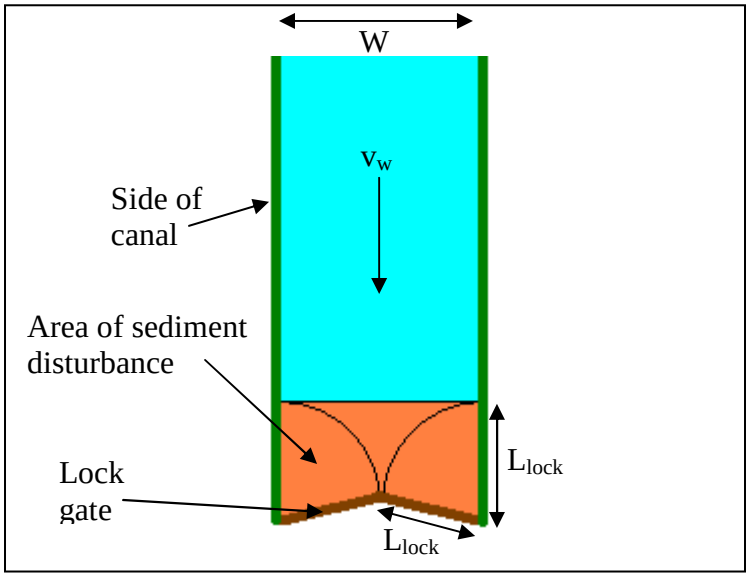

Figure 27. Plan view of lock gates and sediment disturbance caused by gate movement.

The orange area of disturbance in Figure 27 is the area that the lock gates disturb as they move from their closed position (shown) to their fully open position. When the lock gates are fully open, they are flush with the side of the canal. Assuming a significant amount of turbulence is generated, the sediment can be assumed fully mixed in the volume of water with the footprint of the orange area in Figure 27. If the sediment disturbed by the gates is considered to manifest itself as a constant concentration over the volume disturbed (with the orange footprint in Figure 27), Equation 47 describes the sediment input to the reach by lock gate movement.

$$ISS_{lockmove} = F_{boat} * CS_{lock} * L_{lock} * W * D \quad (47)$$

Where: CS_{lock} = concentration of sediment generated by lock gate movements (mg/m³/boat).

This $ISS_{lockmove}$ must be calculated for each lock bounding the reach, using the F_{boat} and L_{lock} applicable to each lock. The variables L_{lock} * W * D represent the affected volume, while CS_{lock} is a measured increase in concentration of sediment associated with lock gate movements and F_{boat} equates to the frequency of lock movements, which occur whenever a boat passes.

Leaking flows through lock gates draw from the entire water column; thus, sediment leaving through leaky lock gates will do so at the average concentration of the reach, as described in Equation 48.

$$QSS_{leak} = Q_{leak} * \frac{SS}{S} \quad (48)$$

Sediment moving with water that overtops the lock gates will follow a similar pattern to that moving with water associated with overflow weirs (defined previously as Equation 45), considering both the deposition of sediment originating from upstream (second term) and the resuspension by boats (first term) (Equation 49).

$$QSS_{w,lock} = F_{boat} * BSS + Q_{w,lock} * \frac{SS - ISS_{boat}}{S} * e^{\frac{-w_s}{H_{lock}} \frac{L}{v_w}} \quad (49)$$

The components of this equation mirror the components of the similar overflow weir equation (Equation 45) with BSS from equation 45 calculated using H_{lock} instead of H_{weir}.

4.2.3.5. External Sources and Sinks

Point source (ISS_{ext}) and runoff (ISS_{runoff}) sediment inputs must be estimated from agency data and a separate surface model, respectively. Once estimated they can be used without modification. The sediment associated with abstractions is calculated according to the average concentration in the reach (Equation 50).

$$QSS_{abs} = Q_{abs} * \frac{SS}{S} \quad (50)$$

Note inclusion of the position of the intake pipe would unnecessarily complicate the model inputs and is not considered.

4.2.4. Algal Algorithm

Algae will generally leave the reach at any point water exits; thus, the components of outflow (QSS(t)) for algae follow all but the evaporation and seepage outflows for water. Research has shown that algae tend to keep themselves suspended in the water column (Fogg 1965; Malone 1980); for this reason, deposition of algae is not considered and algae are considered fully and uniformly suspended in the reach, to the depth that light penetrates. Algae will enter the reach (ISS(t)) with incoming water via all routes except precipitation and runoff. The continuity equation (Equation 33) for algae is modified to include a growth term, μSS.

4.2.4.1. Outflows

The profile of algal concentration in a reach might be considered to be the opposite of the sediment profile: where sediment deposits and thus leaves the top of the water column with a low-to-zero sediment concentration, algae can only grow to the depth that light penetrates in the reach and thus will leave a portion of water with low-to-zero concentration at the bottom of the water profile. The outflow of algae from a reach can be divided into two categories: the outflow that draws from the entire water column, and the outflow that draws only from the light-saturated portion of the water column. Before proceeding, it is useful to define the euphotic volume, V_{ED}, as in Equation 51.

$$V_{ED} = \begin{cases} S & ED \geq D \\ L * W * ED & ED < D \end{cases} \quad (51)$$

Where: V_{ED} = volume of water in the euphotic depth (m^3); and
ED = euphotic depth (depth of light penetration, described in more detail in Section 4.2.4.2) (m).

Where the outflow draws only from the light saturated portion of the water column, the algal outflow is simply a product of the concentration of algae in the light-saturated depth and the flow rate through a given exit (Equation 52).

$$QSS = Q * \frac{SS}{V_{ED}} \quad (52)$$

Where: QSS = generic algal outflow term (mg dry algal mass/s); and
Q = generic water outflow term (m^3/s).

The algal outflows that fall into this category are abstractions (QSS_{abs}), weir overflows (QSS_{weir}), and lock gate overflows ($QSS_{w,lock}$).

The remaining algal outflows (through lockage (QSS_{lock}) and leakage (QSS_{leak})) draw from the entire water column and must be treated differently. The turbulence associated with lockages implies that the algae entering and leaving a lock will be thoroughly mixed in the lockage water and can be represented by Equation 53.

$$QSS_{lock} = Q_{lock} * \frac{SS}{S} \tag{53}$$

Calculation of algal loss through leakage is somewhat more complicated and can be represented by Equation 54.

$$QSS_{leak} = Min\left(Max\left(ED - H_{lock}, 0\right), D_{lock}\right) \cdot Leak \cdot \frac{SS}{V_{ED}} \tag{54}$$

The term $Max(ED-H_{lock},0)$ accounts for the effect of over-lock-gate flow ($Q_{w,lock}$); if over-lock-gate flow is occurring, the euphotic depth might not extend below the top of the lock gate (and thus no algal outflow would occur due to leakage) (case (a) in Figure 28); if there is over-lock-gate flow but ED is greater than the depth of flow over the gate, algal flow through leakage would only occur for the portion of the euphotic depth that extends below the top of the lock gate (case (b) in Figure 28). If there is no flow over the top of the lock gate, H_{lock} is zero and the algal outflow occurs over the entire euphotic depth (case (c) in Figure 28); this latter case is the typical one, as $Q_{w,lock}$ is typically zero. The Min term addresses the case when the calculated euphotic depth exceeds the height of the lock gate; in this case, the result of the Max term must not be allowed to exceed the height of the lock gate, or the leakage rate will be overestimated when calculating algal outflow. (Note that when $ED<D_{lock}$ the leakage rate applied to the algal concentration is recalculated in Equation 54 (rather than using Q_{leak} from the hydrologic calculations) to encompass only the flow that contains algae.)

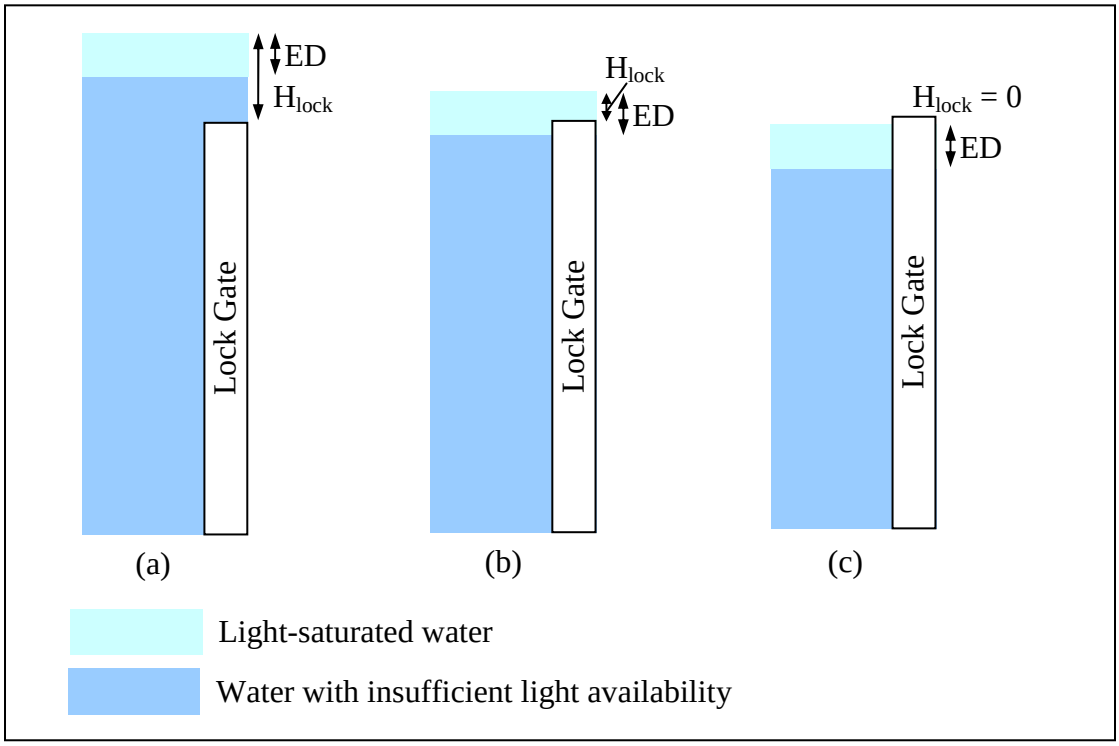

Figure 28. Possible euphotic depth (ED) and overlock depth (H_{lock}) scenarios: (a) ED<H_{lock}; (b) ED>H_{lock}>0; (c) H_{lock} = 0.

4.2.4.2. Algal Growth & Revised Continuity Equation

The continuity equation, with an added growth rate, has been used by previous phytoplankton researchers to model algal growth and transport (e.g., Pridmore and McBride (1984)). Equation 55 is the revised form of Equation 33 applicable to algal growth and transport.

$$\frac{dSS}{dt} = ISS(t) - QSS(t) + \mu \cdot SS \qquad (55)$$

Where: μ = algal growth rate (s^{-1}).

The factors affecting algal growth have been previously discussed (Section 2.3.2). In keeping with the primary factors found in the literature review, phosphorus concentration, temperature, light availability, and retention time are considered in the new canal model. A maximum growth rate is first calculated based on water temperature and then modified according to the other controlling factors to obtain 'μ' in Equation 55. This general method (starting from a base rate and modifying it) has been used in riverine models (e.g., HSPF (Bicknell et al. 2001)). The specific methods used to calculate growth rate are unique to the canal model, as detailed below.

The maximum growth rate limited by water temperature as given by Eppley (1972) (Equation 19) is modified for the canal model to yield a growth rate per second (Equation 56).

$$\mu_{\max,T} = \frac{\ln 2}{86400} * 0.851 * 1.066^{T} \quad (56)$$

Where: T = water temperature (ºC); and
$\mu_{max,T}$= maximum growth rate based on temperature (s^{-1}).

It is anticipated that daily water temperatures will be unavailable; thus, the canal model expects the user to provide parameters to characterize Equation 57 (Beer 2001) to provide water temperature for use in Equation 56.

$$T = T_{mean} + T_{mag} * \sin\left(\frac{2 * \pi}{365} * x + T_{phase}\right) \quad (57)$$

Where: T_{mean} = mean annual temperature (ºC);
T_{mag} = magnitude parameter for the temperature equation (ºC);
x = julian day; and
T_{phase} = phase parameter for the temperature equation (radians).

This sinusoidal curve provides a good fit to data collected on the canal – see, for example, Figure 29.

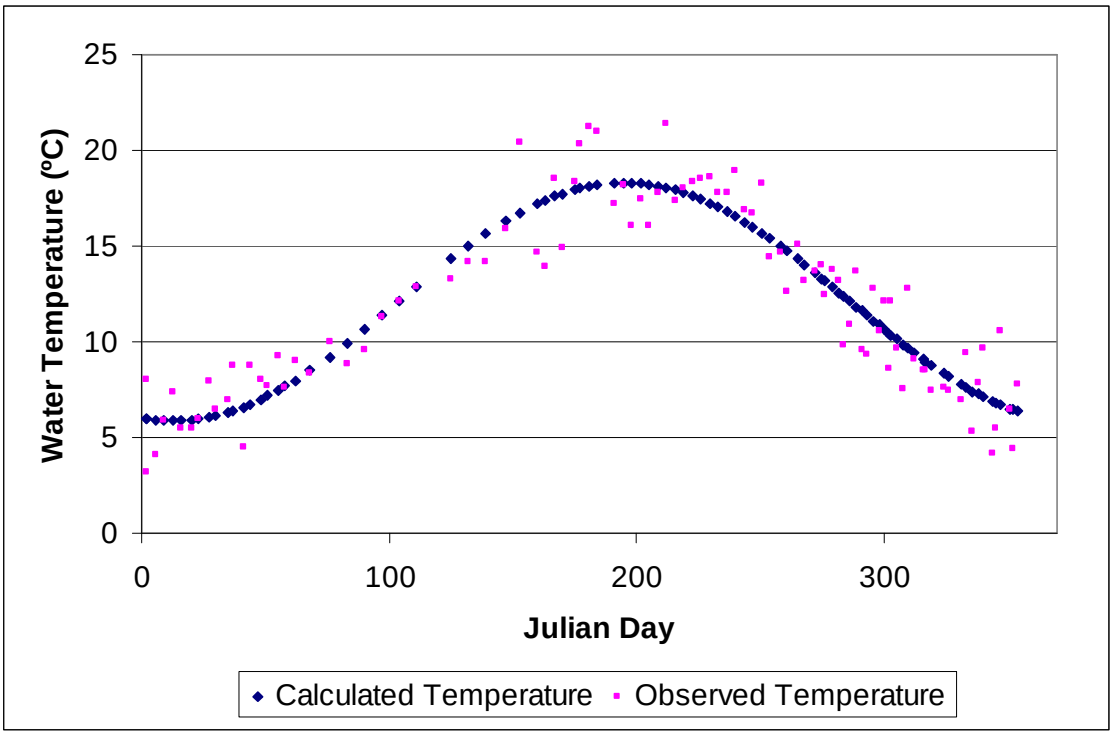

Figure 29. Equation 57 fit to observed data from the Kennet and Avon Canal.

The maximum growth rate for algae in the canal is then limited by light availability as described by Bicknell and others (2001) (Equation 58).

$$\mu_{max} = \frac{\mu_{max,T} * LI}{K_{s,l} + LI} \quad (58)$$

Where: μ_{max} = maximum growth rate based on temperature and light availability (s^{-1});
LI = light intensity (calculated as per the method in Appendix A.3) (J/m^2s); and
$K_{s,l}$ = Michaelis-Menten constant for light limited growth (J/m^2s).

Finally, the growth rate is limited according to phosphorus availability based on the equation developed by Pridmore and McBride (1984) (Equation 59) (the original equation was given in the literature review, Equation 27).

$$\mu = \mu_{max}\left(\frac{\frac{TP^{1.178}}{2.449} * C_{chl} - \frac{SS}{Vol_{ED}}}{\frac{TP^{1.178}}{2.449} * C_{chl}}\right) \quad (59)$$

Where: TP = total phosphorus concentration; and
C_{chl} = conversion from chlorophyll-a mass to dry algal biomass (mg dry algal mass/mg chlorophyll-a).

Equation 59 provides a final growth rate to be used in Equation 55. This final growth rate takes into account the primary algal growth factors of phosphorus availability, water temperature, and light availability. The effect of flow rate is captured in the inflow and outflow loads (ISS and QSS), which depend in the inflow and outflow rates of water for the reach.

4.2.5. Summary of Model Inputs and Variables

The parameters for the model are based on real physical and measureable characteristics; however, it is anticipated that many of the inputs will be difficult or prohibitively expensive to measure; in this latter case, it will be necessary to estimate values from the literature and/or alter the parameter during calibration. Table 7 summarizes the inputs that are anticipated to be readily measureable for a catchment; Table 8 summarizes the inputs that will likely need to be estimated from the literature and calibrated. In these tables, some variables appear that have not previously been discussed in Section 4.1; these are required for some of the background calculations discussed in Appendix A. Finally, Figure 30 summarizes the state variables that track along each time step and other variables calculated from them. As previously mentioned, there are four state variables that form the core of calculations in the canal model: hydrologic storage (S), non-cohesive sediment storage (SS_{non}), cohesive sediment storage (SS_{coh}), and algal storage (SS_{alg}). All inflows and outflows are based on these four core variables.

Some of the variables have quite a wide range based on literature information. The Sensitivity Analysis section (Section 5.3) will provide some useful information on parameters to which the model is sensitive and thus to which more attention in development should be given.

Table 7. Measureable Canal and Catchment Characteristics. (continues next page)

Variable Name	Description	Units	Source
PREC	Precipitation	m/s	Met Office
PE	Evaporation	m/s	Met Office
I_{runoff}	Runoff (surface and subsurface)	m^3/s	Hydrologic model (e.g., HSPF)
I_{ext}	External sources (e.g., STWs)	m^3/s	Regulatory agencies
Q_{abs}	External abstractions (e.g., WTWs)	m^3/s	Regulatory agencies
Reach Characteristics:			
L	Reach length	m	GIS analysis
W	Reach width	m	Canal regulatory agency, aerial photos, or measure
x_{weir}	Location of overflow weir along reach length	m	Canal regulatory agency or measure
D_{weir}	Height of overflow weir above reach bottom	m	Canal regulatory agency or measure
L_{weir}	Length of overflow weir crest	m	Canal regulatory agency or measure
H_{sides}	Height of sides of overflow weir box	m	Canal regulatory agency or measure
D_{lock}	Height of top of lock gate above the reach bottom	m	Canal regulatory agency or measure
T_{mean}	Mean water temperature	^oC	Measure
C_{rad}	Radiation coefficient to account for canal shading from vegetation etc.	Ø	Estimate from site visits, aerial photography
Lock Characteristics:			
Empty	Flag whether lock is intended to be left empty after use	Ø	Canal regulatory agency or signs on canal
V_{lock}	Volume of lock drained during a lockage	m^3	Canal regulatory agency
L_{lock}	Length of lock gates	m	Canal regulatory agency or measure
$CS_{lock,non}$	Concentration of non-cohesive sediment stirred up by lock gate movement	mg/m^3	Measure

Variable Name	Description	Units	Source
$CS_{lock,coh}$	Concentration of cohesive sediment stirred up by lock gate movement	mg/m³	Measure
F_{boat}	Frequency of boat passage	boats	Canal regulatory agency or measure
Sediment & Algal Constants:			
diam	Median sand diameter	m	Measure or pick from typical range (0.06-0.2mm) (Jarvis et al. 1979)
sg	Specific gravity of sand	Ø	Measure or use typical value (2.65) (Simons and Şentürk 1977)
$CS_{boat,non}$	Concentration of non-cohesive sediment stirred up by boats	mg/m³	Measure
$CS_{boat,coh}$	Concentration of cohesive sediment stirred up by boats	mg/m³	Measure
v_b	Average boat velocity	m/s	Canal regulatory agency
ISS_{runoff}	Sediment inputs from overland flow	mg/s	Hydrologic model (e.g., HSPF)
ISS_{ext}	Sediment and algal inputs from external sources (e.g., STWs)	mg/s	Regulatory agencies
TP	Total phosphorus concentration	mg/m³	Measure
RAD	Solar radiation	J/m²/s	Met Office
T_{mag}	Magnitude parameter for temperature equation (Equation 57)	ºC	Estimate by fitting monitored water temperature data to a sinusoidal curve
T_{phase}	Phase shift parameter for temperature equation (Equation 57)	radians	Estimate by fitting monitored water temperature data to a sinusoidal curve

Table 8. Estimated Canal and Catchment Characteristics.

Variable Name	Description	Recommended Value	Source
C_e	Evaporation correction factor, accounts for differences in pan evaporation vs. evaporation over larger surfaces	0.7	(Minikin 1920; Schwab et al. 1993)
$C_{d,weir}$	Weir discharge coefficient	0.611	(Henderson 1966)
Seep	Rate of seepage through canal walls	1.75×10^{-6} to 1.24×10^{-7} $m^3/m^2/s$	(Minikin 1920; Dun 2006)
E_{boat}	Efficiency of boat movement (i.e., how often does a boat approach a lock with the needed water entry level)	0.5	Estimate by watching locks for a while or talking to locals
Leak	Lock gate leakage	0.0301 $m^3/s \div D_{weir}$ ¶	(Dun 2006) (see also Minikin 1920; Pinkett 1995)
Up/Down	Fraction of boats moving upstream vs. downstream through a lock	0.5	Estimate by watching locks for a while or talking to locals
τ_{cd}	Critical shear stress for the deposition of sediment	0.06 $kg/m/s^2$	(Krone 1962) (as cited by Mehta et al. 1989)
$C_{d,drag}$	Drag coefficient	0.0025	(Soulsby 1997)
EXTB	Base light extinction coefficient used in light availability calculations	1 m^{-1}	Reynolds (1984) gives 1.02-1.22; Van Duin et al. (2001) give 0.513 to 1.666
$K_{s,l}$	Michaelis-Menton constant for light limited growth	23.012 $J/m^2/s$	Dugdale and MacIsaac (1971) give 0.033 Ly/min or 10% of radiation on clear day in mid-March
C_{chl}	Factor to convert Chlorophyll-a mass to dry weight biomass	60 mg dry algal mass/mg Chl-a	range of 10-372 as calculated from published data†
LITSED	Light extinction coefficient due to sediment	0.000025 m^2/mg	Van Duin et al. (2001) give 0.00001-0.000137 m^2 /mg
LITALG	Light extinction coefficient due to algae	0.00002 m^2/mg Chl-a	Van Duin et al. (2001) give 0.000012-0.000035 $m^2/\mu g$ Chl-a‡

† (Fleming 1940; Redfield 1958; Antia et al. 1963; Goldman et al. 1968; Strickland and Parsons 1968; Thomas and Dodson 1972; Berman and Pollingher 1974; Soeder et al. 1974; Vollenweider 1974; Malone et al. 1979; Malone 1980; Søballe and Threlkeld 1985; Wienke and Cloern 1987)

¶ Note that the leakage rate needs to be a flow rate per unit depth ($m^3/s/m$); because the expected depth in the reach is D_{weir}, divide the overall recommended leakage rate of 0.0301 m^3/s by the D_{weir} for each upstream section.

‡ Note Van Duin et al. (2001) incorrectly give units of mg/L for Chl-a concentration; the units for Chl-a concentration should be μg/L in their article.

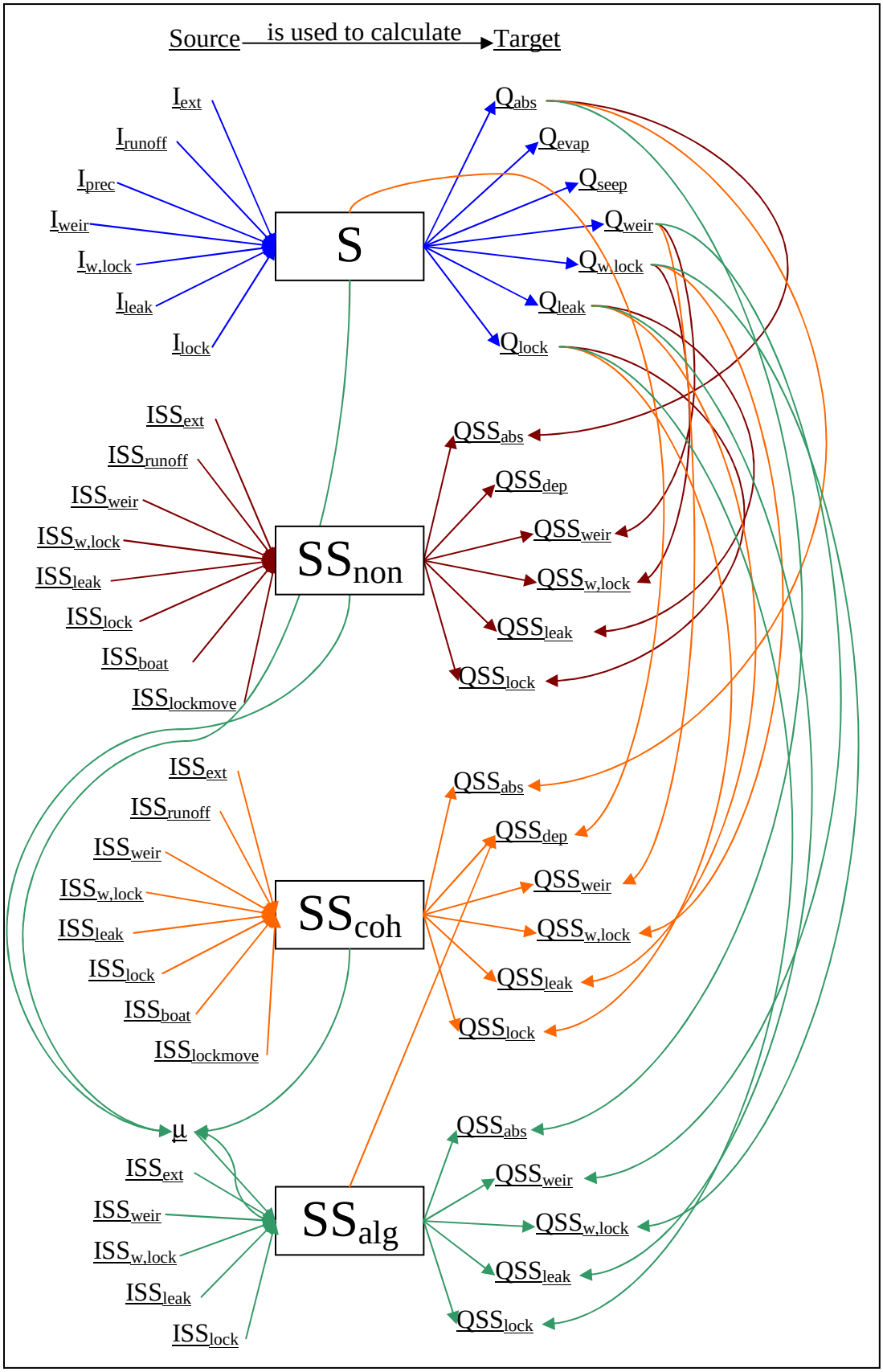

Figure 30. Relationships between state variables (Water Storage (S), Non-cohesive Sediment Storage (SS_{non}), Cohesive Sediment Storage (SS_{coh}), Algal Storage (SS_{alg})) and inflow and outflow variables. Color of line indicates classification of target variable.

Many of the relationships in Figure 30 are obvious connections: all outflow variables for a given classification of storage (water, non-cohesive sediment, cohesive sediment, or algae) are dependent on the state variable for that same classification of storage; solids outflows through various exits are dependent upon water outflows through the same exits, as the rate of water flow through the route determines the rate of loss through each exit. However, some of the connections may be less obvious. For example, μ is dependent on SS_{coh}, SS_{non}, and SS_{alg}, as all of these state variables affect the light availability for the algae. QSS_{dep} for cohesive sediments is dependent on SS_{coh} and SS_{alg} because these state variables affect flocculation and thus the fall velocity used to calculate QSS_{dep}. Algal growth rate (μ) and QSS_{dep} are dependent upon S because they are affected by the *concentration* of sediment and algae, not just the total quantity of the sediment and algae in the reach.

The web of relationships in Figure 30 complicates what might otherwise be a straightforward solution to the system of equations. For example, μ is dependent upon SS_{alg}, but SS_{alg} in turn cannot be determined until μ is known. Likewise, SS_{alg} affects QSS_{dep}, which is driven by SS_{coh}; but SS_{coh} affects μ and thus SS_{alg}. These issues force a nested approach to solution, described in the next section.

4.2.6. Solving the System of Equations

Considering the various factors described in the previous sections, the components of Equations 32, 33, and 55 are simply represented according to Equations 60-65. The subscript 'sed' indicates that the formulae are representative of both cohesive and non-cohesive sediment relationships.

$$I(t) = I_{weir} + I_{w,lock} + I_{lock} + I_{ext} + I_{runoff} + I_{prec} + I_{leak} \tag{60}$$

$$Q(t) = Q_{weir} + Q_{w,lock} + Q_{lock} + Q_{abs} + Q_{seep} + Q_{evap} + Q_{leak} \tag{61}$$

$$\begin{aligned} ISS_{sed}(t) = {} & ISS_{weir} + ISS_{w,lock} + ISS_{lock} + ISS_{runoff} \\ & + ISS_{boat} + ISS_{lockmove} + ISS_{ext} + ISS_{leak} \end{aligned} \tag{62}$$

$$QSS_{sed}(t) = QSS_{dep} + QSS_{weir} + QSS_{w,lock} + QSS_{lock} + QSS_{leak} + QSS_{abs} \tag{63}$$

$$ISS_{alg}(t) = ISS_{weir} + ISS_{w,lock} + ISS_{lock} + ISS_{ext} + ISS_{leak} \tag{64}$$

$$QSS_{alg}(t) = QSS_{weir} + QSS_{w,lock} + QSS_{lock} + QSS_{leak} + QSS_{abs} \tag{65}$$

Because Equations 32, 33, and 55 have no analytical solution (due to the complexity of their components), they must be solved using numerical methods. The canal model uses an implicit Euler method (Boyce and DiPrima 1986) to solve the equations, as in Equation 66 for the hydrology equations (the solids equations follow the same format).

$$S_{n+1} = S_n + \left[\frac{(I_n - Q_n) + (I_{n+1} - Q_{n+1})}{2}\right]\Delta t \qquad (66)$$

Where: n = subscript representing the previous model time step;
n+1 = subscript representing the current model time step; and
Δt = time that passes between model time steps (s).

The components of inflow are fixed at each time step, but most of the components of outflow are dependent upon the storage at each time step; therefore, this relationship does not have a straightforward solution, but must be solved via numerical methods. Newton's Method (Equation 67) was chosen for this purpose, for its simplicity in application and the fact that it does not require prior knowledge of the interval within which the solution to the equation must lie (something that would be nearly impossible to reliably determine for these equations) (Hamming 1973).

$$x_{i+1} = x_i - \frac{f(x_i)}{f'(x_i)} \qquad (67)$$

Where: x_{i+1} = next guess for the zero of f(x);
x_i = current guess for the zero of f(x); and
f(x) = the function whose zero is to be determined.

Under certain conditions it is not possible to use Newton's Method, and in these cases the Bisection Method (Hamming 1973) is used. These conditions are rare and typically involve limits of computer precision that cause Newton's Method to jump over the zero of the function. The Bisection Method is not used in the general case because of the difficulty of initially arriving at the opposite-signed estimates needed; however, in this particular case, such a bracket has been inadvertently found by Newton's Method as it jumps from a positive to negative f(x), thus enabling the use of the Bisection Method.

The Bisection Method starts with an x_1 and x_2 such that $f(x_1)\cdot f(x_2) < 0$. A value, x_3, is calculated as: $x_3 = x_1 + \frac{x_1 - x_2}{2}$; then a decision is made regarding the next value to choose based on the product of the function of x_1 and the function of x_3 according to Equation 68.

$$\text{If } f(x_1)\cdot f(x_3)\begin{cases} < 0, \text{ sign change in } (x_1, x_3), \text{set } x_2 = x_3, \text{repeat} \\ > 0, \text{ sign change in } (x_3, x_2), \text{set } x_1 = x_3, \text{repeat} \\ = 0, \text{ solution found } (x_3) \end{cases} \quad (68)$$

The f(x) function used for the bisection method is the same as that used for Newton's Method. Complete details on the solution to the system of equations are provided in Appendix Section A.4, pg. 207.

A final consideration for solution was the determination of the variables for the '0^{th}' time step – that is, the initial conditions. Because the water level in a canal is held mostly constant by design, the initial water storage is set at the design level – that is, $L\cdot W\cdot D_{weir}$. The initial outflows for the 0^{th} time step are calculated based on this storage. The inflows for each reach are simply the corresponding outflows from the next upstream reach (or 0, in the case of the summit reach), with the exception of I_{ext} and I_{runoff}, which are set to the values at the first time step as a simple approximation. Likewise, the water demands for Q_{evap} and Q_{abs} are set to the values at the first time step.

The initial conditions for the solids state variables were somewhat more complicated. For the sediment, because boat traffic is the primary driver of sediment concentration in a reach, the initial sediment storage is set to the storage generated by boat movement – that is, ISS_{boat} at time step 1. The initial storage of algae in the reach is calculated as half that supportable by the phosphorus concentration at time step 1, that is, $\frac{TP^{1.178}}{2.449} * \frac{C_{chl}}{2}$. Using half the population supportable by the phosphorus concentration gives a reasonable order of magnitude for the algal population while recognizing the population is unlikely to be at its fullest potential due to influences from light, temperature, and water flow. The remaining inflows and outflows for solids are calculated in the same manner as those for hydrology, based on the initial storages where appropriate and on the value for the first time stop where not.

Experimentation with the model showed that the effects of these choices of initial conditions vanished within a month of simulation, suggesting that with a sufficient 'start up' time for the model, any inaccuracies generated by these simplistic estimates of initial conditions will vanish.

4.2.7. Computer Programming

The algorithms listed in the previous section have been translated into computer code using the Visual Basic 2008 programming language (a component of Microsoft Visual Studio 2008, © 2007 Microsoft Corporation). A graphical user interface was created to aid the user in the input of the needed parameters.

In programming, objects were created to represent reaches and locks. The calculations for Newton's Method f(x) formulae have been isolated in individual subroutines. It is hoped that the modularization of the code will make it easily portable for any future model developers who may take interest in it.

5. Canal Model Verification

There is some discrepancy in the professional community regarding the definition of 'verification' vs. 'validation' of a model. In the context of this document, 'verification' is taken to mean the process by which model code is verified to be an accurate representation of an algorithm. That is, the verification process is meant to ensure there are no typographical errors in the code, that the code functions under all conditions without causing exceptions at run-time, and that the correctly coded algorithms predict model variables in a logical fashion. During the verification process for this model, extreme cases were also tested to ensure that the model algorithms continued to function as desired in extreme conditions. Validation, by contrast, is defined in this text to mean the process by which a calibration is proved valid, by using the calibrated model parameters to predict model output for a time period separate from that used for the calibration process and comparing that model output to observed values.

5.1. Code Verification

The canal model code was verified in stages. The hydrology component was verified initially and separately from the solids component. For each component, a simple set of inputs for a system of three locks and three reaches was tested (Figure 31); characteristics of the reaches and locks are listed in full in Appendix B, pg. 215. In the initial test, only meteorological inputs were included – no runoff or external source of flow was considered – this tested the code behavior in extreme low flow conditions. Following successful verification of the extreme condition, a full-blown scenario with more typical water levels was verified. This process ensured that the model would behave properly under all conditions.

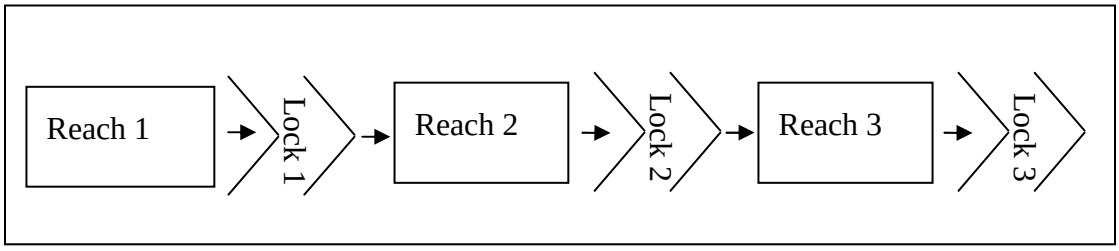

Figure 31. Simple canal system used to verify the model.

To complete the verification, the relationships described in Section 4.1 were input into an Excel spreadsheet to produce an expected set of output. By using Excel (rather than making calculations by hand), a long time period with varying hydrologic conditions could be tested while at the same time making all the intermediate steps transparent. The results of the simple hydrology and water quality models were compared to the same values calculated using the equations in Section 4.1 and Appendix Section A.4 in a Microsoft Excel spreadsheet, and investigation and correction of bugs continued until all components of inflow, outflow, and storage calculated by the Excel spreadsheet precisely matched those predicted by the canal model (with an allowed tolerance due to expected rounding errors).

It was noted during verification that an inaccuracy at the first timestep was generally rendered inconsequential to the results of the fifteenth and later time steps. This lends support to the idea that, given a sufficient (e.g., one month) startup time, inaccuracies in the initial state variable estimates will be irrelevant.

5.2. Algorithm Verification

Once the code was ensured bug-free via the process described in Section 5.1, the model output was evaluated to ensure that the algorithms predicted outflows of water and solids that made logical sense. For this test, the parameters for the top three reaches of the Kennet and Avon Canal were used, to ensure the input values were realistic. The development of these parameters will be discussed in detail in the section on model application (Section 7.1).

5.2.1. Storage Variables

Water storage in a reach is expected to remain fairly constant, at a level near D_{weir}. It may be slightly higher in the winter (when no lockage demands exist) and slightly lower in the summer (when lockages may draw the water level below that of D_{weir}), but to be a properly functioning canal, the water level should remain relatively constant. The canal model accurately generated this trend, as can be seen for the reach above Lock 57 in Figure 32. The storage in this reach when the water level is at D_{weir} is 3600 m³.

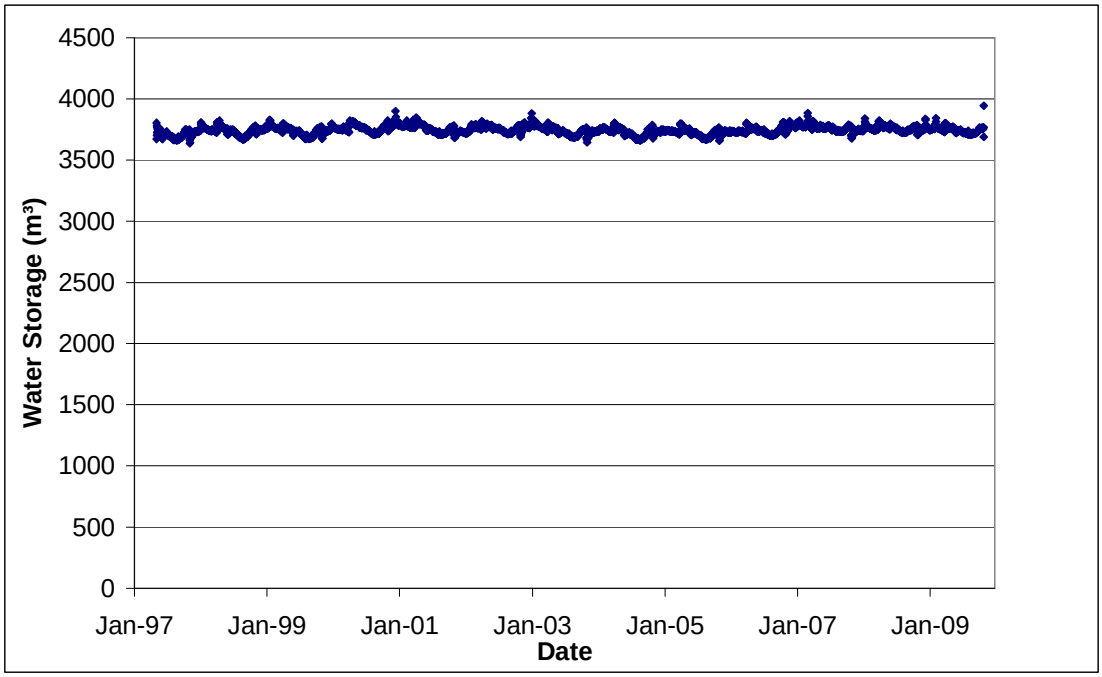

Figure 32. Modeled water storage in the reach above lock 57.

By contrast, the sediment and algae storages should vary greatly throughout the year. During the boating season in the late spring to early autumn, inorganic sediment concentrations will greatly increase compared to winter values due to the sediment stirred up by boat propellers. Algal growth in the summer far exceeds its growth in the winter due to increased water temperature and solar radiation in the summer. Thus, a nearly sinusoidal curve for solids is expected, as gradual increases in temperature, sunlight, and boat traffic in the spring cause corresponding increases in solids concentrations, eventually peaking in mid-summer and then falling off again gradually in the autumn. The model accurately predicted these trends (Figure 33).

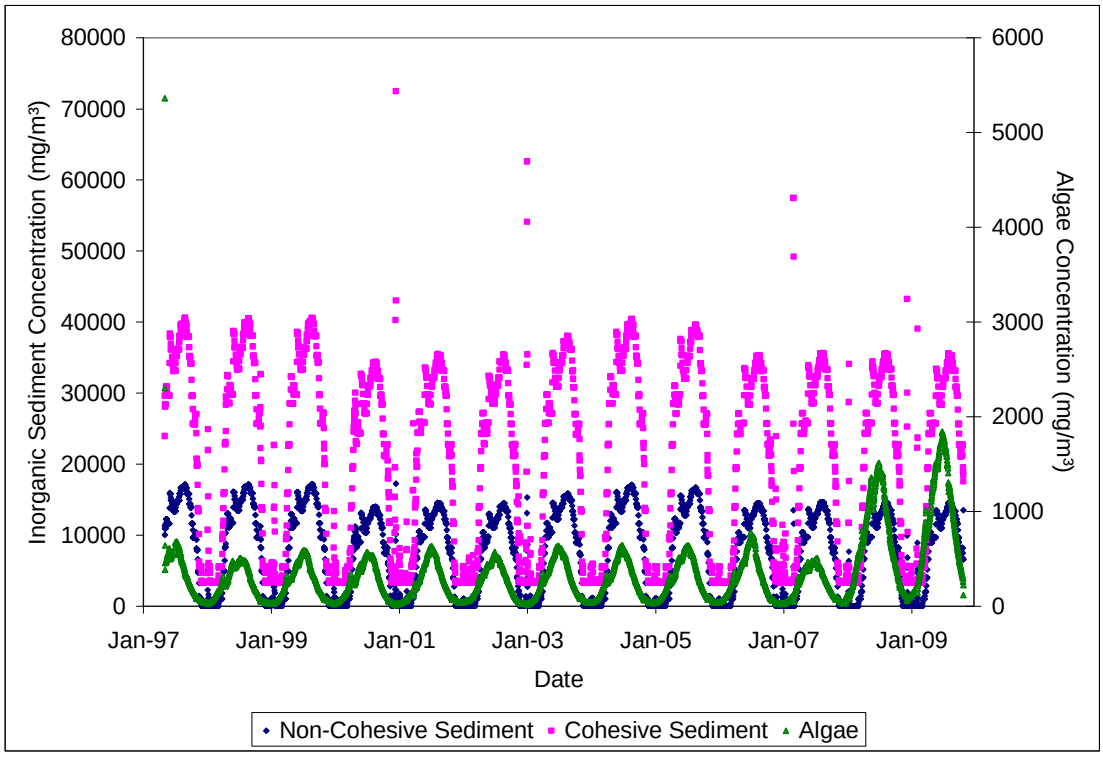

Figure 33. Modeled solids concentrations in reach above Lock 57.

Note that Figure 33 supports the previous conclusion that inaccuracies in initial storage estimates quickly vanish: the initial calculated algal concentration is more than twice any other value attained during the simulation, but after two time steps the algal concentration converges on a stable and appropriate trend for the remaining simulation.

5.2.2. Outflows

To a large extent, modeled outflows of all the constituents can be expected to follow the trends in storage illustrated previously.

Considering hydrology, it is expected that lockages will dominate flow in the summer, while weir flows will dominate in the winter. There should be little to no lockage flow in the winter, while weir flow will be slightly to greatly reduced during the summer. Flows such as leakage and seepages will vary slightly according to the overall reach storage; abstracted flows will remain constant all year; and evaporative outflows should peak in the summer and trough in the winter, though they are expected to be much lower than the rest of the outflows. Ideally over-lock flows will be insignificant year-round, but if present they should peak in the winter and be

unnoticeable in the summer. These expected trends are met by the model, as illustrated in Figure 34.

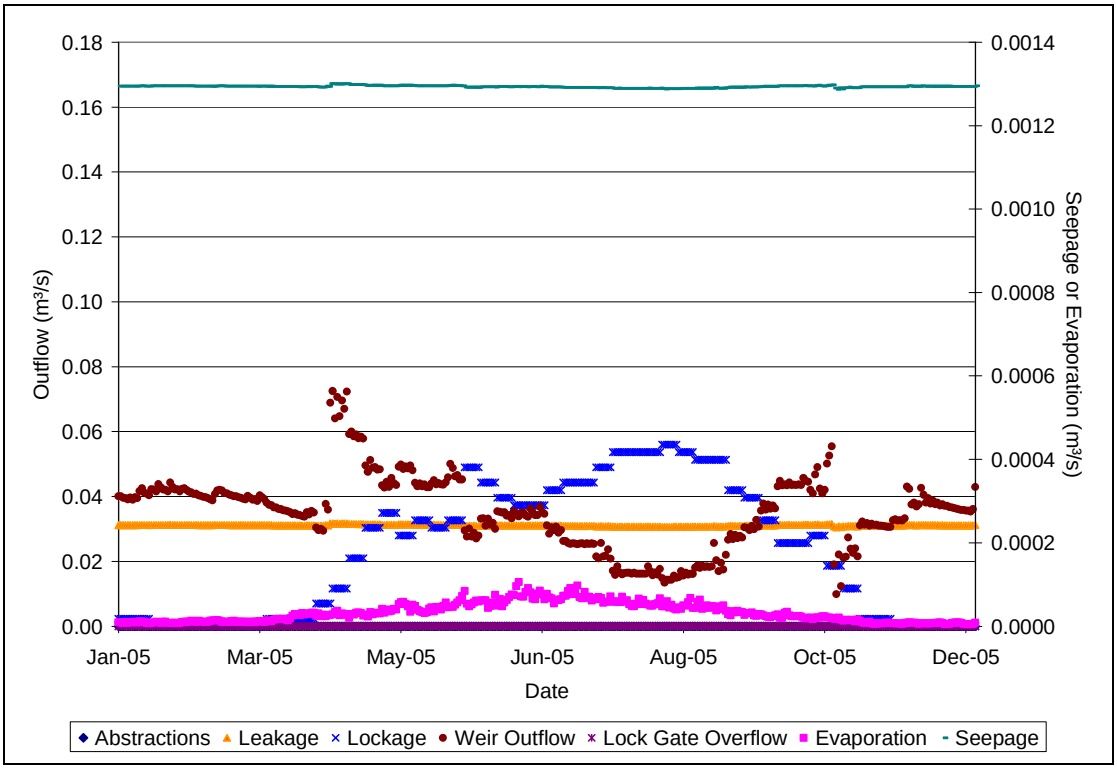

Figure 34. Modeled hydrologic outflows for the reach above Lock 57.

For clarity, Figure 34 shows only the outflows for 2005, so that the seasonal trends are evident. As expected, lockage outflows increase in the spring, peak in the summer, and are negligible in the winter. They also change in a step-wise fashion due to the estimation of F_{boat}, which is held constant on a weekly basis due to the resolution of the input data. Weir outflows are fairly constant while boat traffic is not present, but experience a short-lived peak at the beginning of the boating season when inflows to the summit reach have increased to their higher summer levels but the boating traffic is not yet plentiful enough to for lockages to demand the full increase in inflow. Seepage and leakage are relatively constant year-round, which is expected as the overall reach storage is nearly constant. Evaporative losses increase in the summer but are nearly non-existent in the winter. Lock gate overflows never occur, as expected. For this particular reach there are no abstractions, so the abstracted flows remain zero year-round.

Solids outflows should also follow a seasonal trend. Solids outflows must match the overall availability of solids, so in general all solids outflows in the winter months

should decline as the solids storage in the reach declines. Additionally, solids should move with the water – so the trends in the distribution of hydrologic outflows to various pathways should match the distribution of solids through the same pathways, with the exception of weir outflows of inorganic sediment. Although weir outflows are significant year-round for water, most inorganic sediment will settle out of the top of the water column from which the weir overflow draws, so weir overflows should be minimal for inorganic sediments. Finally, inorganic sediments experience an additional outflow route through sediment deposition; due to the length of the reach in question (322 m) and the fall velocity (~0.0005 m/s for cohesive sediment, ~0.026 m/s for non-cohesive sediment) and slow moving water (~0.009 m/s), a sizeable amount of inorganic sediment, particularly the non-cohesive variety, is expected to deposit out of the water column at each time step. These trends are accurately reproduced in the model for non-cohesive sediment (Figure 35), cohesive sediment (Figure 36), and algae (Figure 37).

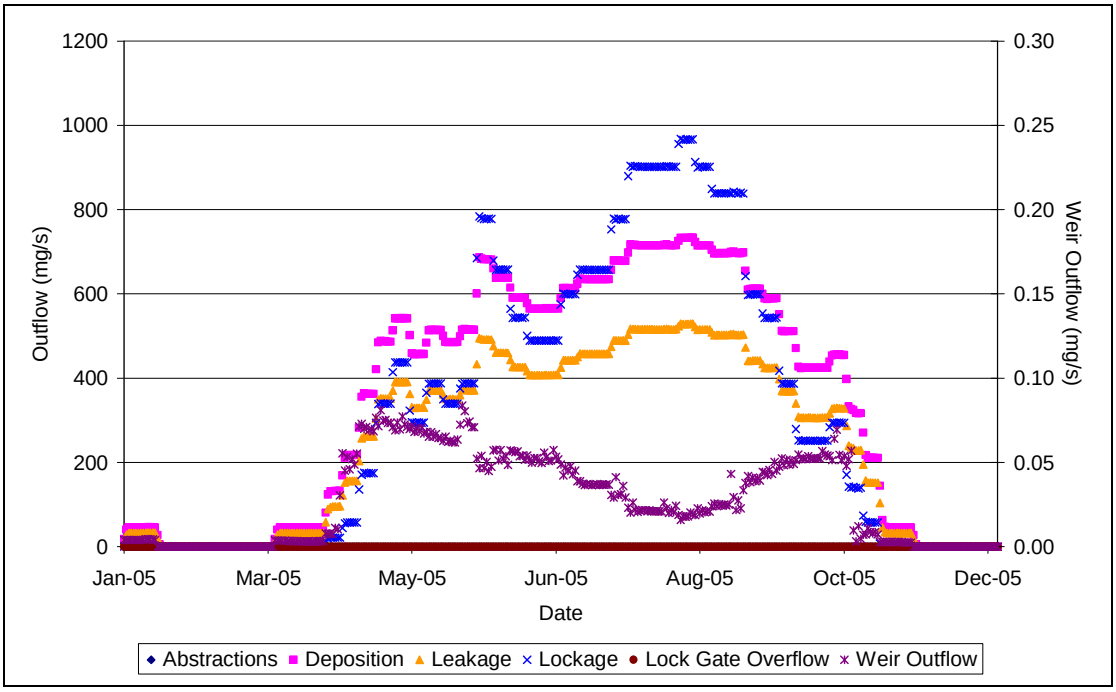

Figure 35. Modeled non-cohesive sediment outflows from the reach above Lock 57.

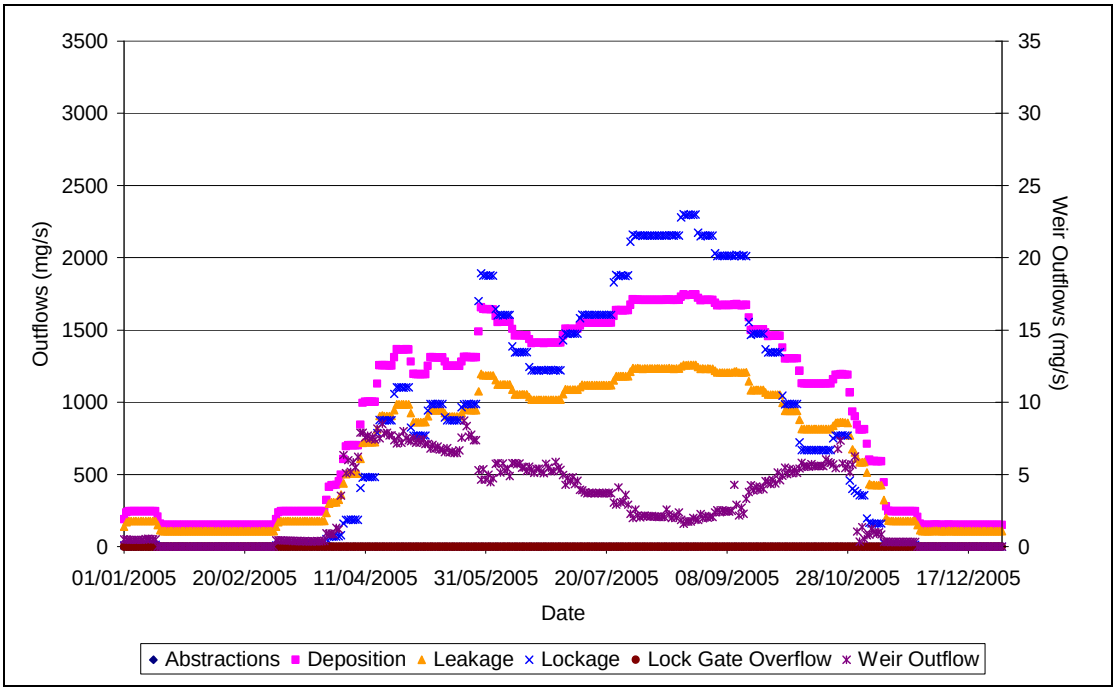

Figure 36. Modeled cohesive sediment outflows from the reach above Lock 57.

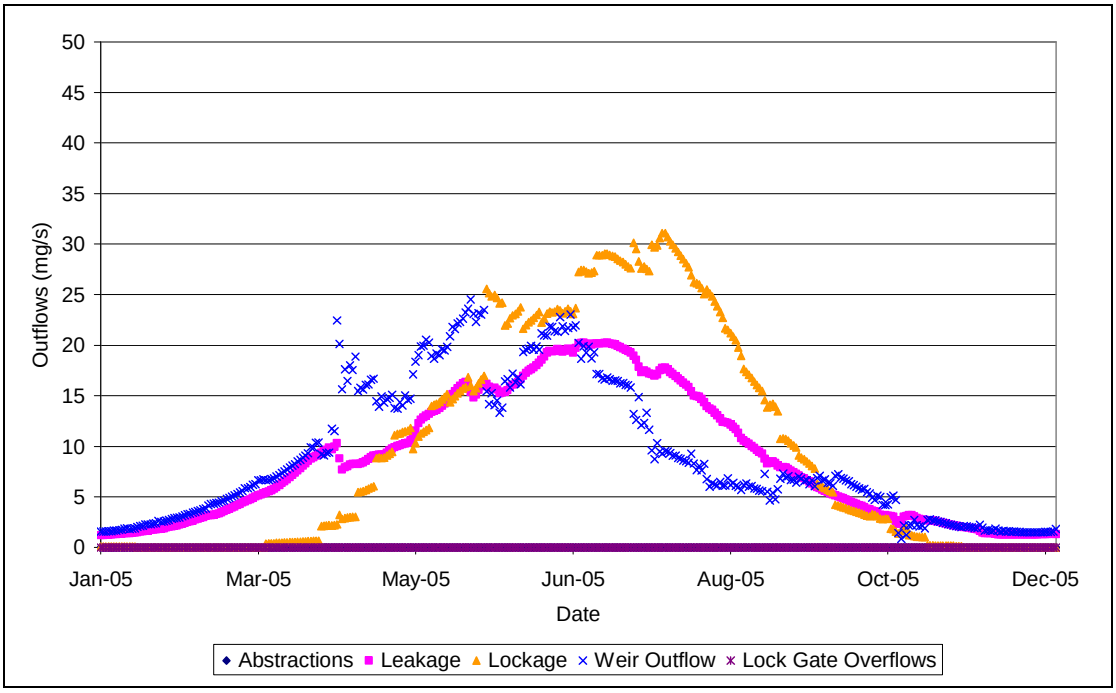

Figure 37. Modeled algal outflows from the reach above Lock 57.

The small peak in inorganic sediment concentrations seen in January is due to a small amount of boat traffic associated with the New Year holiday. Aside from this holiday, winter boat traffic is at or near zero. As expected, inorganic sediment outflows through the weir are negligible compared to outflows through other routes.

Algal outflows make a nearly perfect mirror of the overlay of relative hydrologic outflows (Figure 34) and algal concentration (Figure 33).

5.3. Sensitivity Analysis

A sensitivity analysis was conducted on the key parameters of the model to identify those parameters most influential on various aspects of model output. This is a useful exercise for multiple reasons: first, it adds confidence to the verification process to see the model respond to various changes in model parameters in an expected fashion; second, it allows current and future users of the model to identify parameters that may be most useful in calibration; third, in application of the model to find solutions to water quality problems, a sensitivity analysis run using model parameters similar to those correct for a target canal suggests which efforts may be most successful. Considering this latter benefit, the sensitivity analysis was run using an abbreviated and slightly modified set of input parameters from the final application described in Section 6. It should be understood that the precise values of sensitivities observed will change with a different set of inputs, and likewise future model users would benefit from running a new sensitivity analysis customized for their own situations. However, the relative importance of the parameters discussed in this section should provide a useful guide for all future users of the canal model.

5.3.1. Procedure

The sensitivity analysis was conducted for a three-reach system based generally on the top three reaches of the Kennet and Avon Canal. Modifications were made to the parameters later used in Section 6 to make the sensitivity analysis more representative of the full range of influential parameters, primarily moving abstraction demands and external inflows to occur in these three reaches where they previously did not. The model time span was set to a period of one year for the sensitivity analysis. Both the limited number of reaches and limited time span were chosen to allow the full sensitivity analysis to run in a reasonable amount of time: this setup allows one scenario of the sensitivity analysis to run in less than a minute, and the full 178 scenarios to run in 2 hours. Some of the scenarios caused extreme conditions to be simulated, slowing down execution as the numerical methods encountered greater difficulty in convergence.

The values of the parameters previously listed in Table 7 and Table 8 for the baseline scenario are listed in Table 25 - Table 28 in Appendix C. For the sensitivity analysis, these parameters were varied by ±25% and ±10% to generate a total of four sensitivity runs for each variable. This resulted in 178 different scenarios, including the baseline scenario and the scenario for Empty, which could not be varied by a percent, just simply set to false. For each of the 178 runs, statistics were computed for the following state variables and outflows for the downstream reach:

- Hydrologic Variables:
    - S (hydrologic storage)
    - D (water depth)
    - Q_{abs} (hydrologic outflow via abstractions)
    - Q_{weir} (hydrologic outflow via overflow weir)
    - $Q_{w,lock}$ (hydrologic outflow via lock overtopping)
    - Q_{seep} (hydrologic outflow via seepage)
    - Q_{leak} (hydrologic outflow via leakage)
    - Q_{lock} (hydrologic outflow via lockage)
    - Q_{evap} (hydrologic outflow via evaporation)
    - Q_{tot} (total hydrologic outflow)
- Concentration Variables:
    - $[SS_{non}]$ (concentration of non-cohesive sediment)
    - $[SS_{coh}]$ (concentration of cohesive sediment)
    - $[SS_{alg}]$ (concentration of algae)
- Sediment (cohesive and, separately, non-cohesive) Variables:
    - SS (sediment storage)
    - QSS_{abs} (sediment outflow via abstractions)
    - QSS_{weir} (sediment outflow via overflow weir)
    - $QSS_{w,lock}$ (sediment outflow via lock overtopping)
    - QSS_{dep} (sediment loss via deposition)
    - QSS_{leak} (sediment outflow via leakage)
    - QSS_{lock} (sediment outflow via lockage)
    - QSS_{tot} (total sediment outflow)
- Algae (Biological Solids) Variables:
    - SS (algal storage)

- QSS_{abs} (algal outflow via abstractions)
- QSS_{weir} (algal outflow via overflow weir)
- $QSS_{w,lock}$ (algal outflow via lock overtopping)
- QSS_{leak} (algal outflow via leakage)
- QSS_{lock} (algal outflow via lockage)
- QSS_{tot} (total algal outflow)
- ISS_{bio} (algal growth)

For each of these variables, the following statistics were calculated:

- Mean (total simulation) (Avg)
- Minimum (total simulation) (Min)
- Maximum (total simulation) (Max)
- 1st Quartile (total simulation) (1Q)
- Median (total simulation) (2Q)
- 3rd Quartile (total simulation) (3Q)
- Seasonal Means (Winter (W), Spring (Sp), Summer (Su), Autumn (A))

The sensitivity of model variables to the input parameters was calculated according to a simple formula used in previous model studies (Equation 69) (Byne 2000).

$$S_r = \left(\frac{O - O_b}{P - P_b}\right) \cdot \left(\frac{P_b}{O_b}\right) \tag{69}$$

Where: S_r = relative sensitivity of parameter;
O = output (model output for variables bulleted above);
P = input (model parameters in Table 7 and Table 8);
O_b = baseline output (model output for baseline run); and
P_b = baseline input (model parameters in Appendix C).

5.3.2. Results

The full results of the Sensitivity Analysis are given in Appendix D. The parameters to which the model is most sensitive are presented and discussed in the following sections. A positive sensitivity (S_r) indicates a positive correlation between the indicated parameter and the indicated variable; if the sensitivity is greater than 1, the change in the variable is greater, proportionally, than the change in the parameter.

5.3.2.1. Hydrologic Variables

The key parameters to which the hydrologic variables are sensitive are given in Table 9. A key parameter in this case is defined as one which has at least one sensitivity (S_r) at the -25%, -10%, 10%, or 25% level whose absolute value is greater than or equal to 0.5 for the mean statistic. The average sensitivities for each combination of parameter and statistic are calculated as the mean of the S_r values calculated at the -25%, -10%, 10%, and 25% levels.

Table 9. Key parameters to which the hydrologic variables are most sensitive.

Var.	Most Sig. Params.	Average Sensitivities									
		Avg	Max	Min	1Q	2Q	3Q	W	Sp	Su	A
S	L	1.00	1.00	0.99	1.00	1.00	1.00	1.00	1.00	1.00	1.00
	W	1.00	1.00	1.00	1.00	1.00	1.00	1.00	1.00	1.00	1.00
	D_{weir} †	0.93	0.80	0.95	0.96	0.94	0.92	0.91	0.91	0.95	0.95
	D_{lock} ‡	0.71	0.80	3.68	0.68	0.70	0.72	0.75	0.72	0.68	0.69
D	D_{weir} †	0.93	0.80	0.95	0.96	0.94	0.92	0.91	0.91	0.95	0.95
	D_{lock} ‡	0.71	0.80	3.68	0.68	0.70	0.72	0.75	0.72	0.68	0.69
Q_{abs}	Q_{abs}	1.00	1.00	1.00	1.00	1.00	1.00	1.00	1.00	1.00	1.00
Q_{weir}	I_{runoff}	0.64	0.84	3.82	0.60	0.63	0.65	0.73	0.58	0.78	0.48
	I_{ext}	2.44	0.60	14.96	4.53	2.42	1.75	1.34	2.00	4.96	3.45
	Q_{abs}	-0.50	-0.14	-5.50	-0.84	-0.50	-0.39	-0.36	-0.38	-0.93	-0.69
	D_{weir} †	-1.84	-2.43	-10.90	-1.52	-1.57	-1.79	-1.87	-1.82	-1.93	-1.75
	V_{lock}	-0.70	<0.01	-7.47	-1.87	-0.48	-0.30	-0.01	-0.47	-2.51	-1.08
	Leak	-0.92	-0.31	-9.19	-1.53	-0.93	-0.68	-0.67	-0.70	-1.65	-1.25
	F_{boat}	-0.68	0.00	-7.43	-1.93	-0.52	-0.28	0.00	-0.43	-2.48	-1.06
Q_{seep}	L	1.00	1.00	1.00	1.00	1.00	1.00	1.00	1.00	1.00	1.00
	W	0.73	0.72	0.73	0.73	0.73	0.73	0.73	0.73	0.73	0.73
	Seep	1.00	1.00	1.00	1.00	1.00	1.00	1.00	1.00	1.00	1.00
Q_{leak}	D_{weir} †	0.92	0.76	0.95	0.96	0.93	0.90	0.90	0.90	0.95	0.94
	D_{lock} ‡	0.74	0.87	3.68	0.71	0.74	0.76	0.79	0.76	0.70	0.71
	Leak	0.97	0.99	0.83	0.98	0.98	0.98	0.98	0.98	0.96	0.97
Q_{lock}	V_{lock}	1.00	1.00	0.00	1.00	1.00	1.00	1.00	1.00	1.00	1.00
	F_{boat}	0.97	1.08	0.00	0.00	1.00	1.05	0.00	0.93	0.99	0.99
Q_{evap}	PE	1.00	1.00	1.00	1.00	1.00	1.00	1.00	1.00	1.00	1.00
	L	1.00	1.00	1.00	1.00	1.00	1.00	1.00	1.00	1.00	1.00
	W	1.00	1.00	1.00	1.00	1.00	1.00	1.00	1.00	1.00	1.00
	C_e	1.00	1.00	1.00	1.00	1.00	1.00	1.00	1.00	1.00	1.00
Q_{tot}	I_{ext}	0.87	0.44	0.51	0.70	0.97	0.91	0.72	0.84	0.95	0.98

† Average sensitivity for D_{weir} ±10% and -25%; at D_{weir} +25%, the weir depth exceeded lock depth and caused an erroneous sensitivity

‡ Only significant at the -25% level, when $D_{lock} < D_{weir}$

Many of the relationships in Table 9 are expected, and support the verification of the model. Storage and depth are most dependent on the dimensions of the reach. Evaporative losses are dependent only upon those things that affect evaporation (potential evaporation, the coefficient of evaporation, and factors that contribute to the

water surface area in the reach); Q_{lock} is dependent on the volume of lockage and the frequency that lockages occur (represented by F_{boat}). The S_r values of zero seen for some statistics for Q_{lock} are expected, as there are some weeks of the year that have no boat traffic and thus no Q_{lock}. Q_{leak} is dependent on the leakage rate and the depth from which the leakage can draw, and shows sensitivity to external inflows only when they decrease to the point that the water level in the reach falls. Q_{seep} is sensitive to the components used to calculate the wetted surface area and the rate of seepage; it may be surprising that a representative of depth does not appear on the list for Q_{seep}; the model does show an average sensitivity of 0.25 to $D_{weir,}$ but because the wetted surface area of the sides of the canal is small compared to the wetted surface area of the bottom of the canal, it does not reach the requirements set for a 'key parameter.'

Q_{weir} is by far the most complex variable, being the primary route by which excess water leaves a reach. It is thus sensitive to any parameter that is a significant contributor to the inflow or outflow of water in the reach. Q_{weir}'s strong sensitivity to external inflows ($S_r = 2.44$) shows that changes in external inflow produce a change in weir outflow proportionally much greater than the inflow change. This is because any increase in inflow rate to the canal mostly exits the reach through the weir overflow, so that the overall storage is maintained at the desired level. In a properly balanced scenario, weir overflow should be minimal, as the input flows as designed should just balance the outflow demand from lockage, leakage, seepage, and evaporation. However, when the inflow rate increases, the outflow demands from lockage, leakage, seepage, and evaporation will not change; thus, all additional inflow will leave via the overflow weir (and perhaps over the lock gate, if the flow increase is very great). A small change in total inflow in this case results in a much greater change in weir outflow. For example, if total inflow is 10 m^3/s, and under normal conditions the weir overflow is 1 m^3/s, then a 10% increase in inflow (to 11 m^3/s) will result in a 100% increase in weir overflow (to 2 m^3/s). Likewise, decreasing the inflow will affect the weir flows firstly and most greatly – for the same scenario, but for a decrease of 10%, the weir overflow would decrease by 100% (to 0 m^3/s). The maximum value for Q_{weir} is expected to occur in the winter, when lockages are low and most water flows through the overflow weir, and thus the maximum Q_{weir} sensitivity is unaffected by changes in F_{boat}, the value of which parameter is near or equal to zero in the winter months.

As expected, Q_{tot} is dependent primarily upon the external inflow of water. Indeed, had Q_{tot} been dependent upon anything other than external inflows, runoff, or precipitation, it would indicate an error in the model, as the mass of water must be conserved, so assuming a minimal change in storage for the simulation period (as would be expected in a canal), the inflows from all sources should approximately equal the sum of the outflows from all sources. The variations in sensitivity to I_{ext} are due to the varying predominance of runoff sources. Although runoff sources are not so significant on an annual basis, they contribute significantly to the high flows, and thus have a much greater impact on the maximum Q_{tot} statistic than do the external flows.

5.3.2.2. Concentration Variables

The key parameters to which the solids concentration variables are sensitive are listed in Table 10. As with the hydrology variables, parameters to which the model is most sensitive are defined as those parameters for which the absolute value of one value of S_r for the mean statistic is greater than or equal to 0.5.

The sensitivity of the load variables to the model input parameters mirrors the sensitivity of the hydrology variables (Table 9) and that of the solids concentration of the reach (Table 10); therefore, the sensitivities of the load parameters are only included in Appendix D, as they would be repetitive here.

Table 10. Key parameters to which the solids concentrations are most sensitive.

Var.	Most Sig. Params.	Average Sensitivities									
		Avg	Max	Min	1Q	2Q	3Q	W	Sp	Su	A
$[SS_{non}]$	$CS_{boat,non}$	0.82	0.86	<0.01	0.62	0.79	0.85	0.13	0.82	0.85	0.84
	F_{boat}	0.61	0.60	0.00	0.00	0.71	0.68	<0.01	0.68	0.59	0.66
$[SS_{coh}]$	W	-0.45	-1.23	-1.04	-0.86	-0.54	-0.38	-1.05	-0.50	-0.36	-0.44
	$CS_{boat,coh}$	0.70	0.02	0.01	0.39	0.66	0.76	0.06	0.70	0.76	0.73
	F_{boat}	0.54	0.00	0.00	0.00	0.59	0.63	<0.01	0.59	0.55	0.59
$[SS_{alg}]$	I_{ext}	-1.57	-0.44	-[¶]	-1.31	-1.49	-1.57	-0.81	-1.48	-1.90	-1.55
	L	0.85	0.39	+[¶]	0.55	0.73	0.88	0.68	0.72	1.05	0.63
	W	1.00	0.38	+[¶]	0.58	0.80	1.05	0.67	0.81	1.29	0.76
	T_{mean}	0.60	0.05	0.00	0.36	0.53	0.69	0.13	0.54	0.84	0.47
	$ISS_{ext,alg}$	0.85	0.00	0.00	1.00	0.98	0.98	0.26	0.98	0.96	0.99
	EXTB	-0.47	-0.05	0.00	-0.39	-0.43	-0.54	-0.14	-0.42	-0.62	-0.45

[¶] Because the minimum algae concentration was nearly zero, extreme values of S_r were calculated whenever any change in minimum algae concentration was seen; therefore, this column is simply marked '+' or '-' to indicate a positive or negative correlation, respectively.

It is not surprising that the sediment concentrations are most sensitive to boat-related parameters – that is, the amount of sediment stirred up by the boats ($CS_{boat,non}$, $CS_{boat,coh}$) and the frequency of boat passage (F_{boat}). In a typical canal, it is expected that boat contributions to sediment will greatly exceed any contributions from runoff or external sources (this certainly appears to be the case from monitoring efforts in the Kennet and Avon Canal). Without boat traffic, any sediment that did enter the canal from an external source would quickly settle out in the near-stagnant water in the canal reaches. The sensitivity to boat width for cohesive sediment concentration occurs because the primary driver of sediment concentration – the concentration of sediment disturbed by boat traffic – is dependent upon the width of the boat rather than the width of the canal. The same load of sediment will be disturbed regardless of the canal width, so that the overall fully-mixed concentration will be lower when the reach width (and thus total water storage) is higher. The sensitivity to reach width (S_r = -0.42) is not quite as great for non-cohesive sediment because it falls more rapidly out of suspension.

Algal concentration is sensitive to many things. Unsurprisingly, parameters related to temperature, light intensity, and water velocity play key roles as represented by mean temperature (T_{mean}); the base water light extinction coefficient (EXTB); and external flow inputs (I_{ext}), respectively. Interestingly, parameters that affect the total storage of water in the reach (thus the total algal load) are also important – Length and Width. These factors affect Vol_{ED} used in equation 59 to calculate algal growth rate; all other things being equal, if Vol_{ED} increases, the concentration of algae decreases, the difference between the concentration of algae supportable by the total phosphorus concentration increases, and thus the multiplier for μ_{max} increases, causing a higher growth rate. Additionally, the greater width decreases the concentration of inorganic sediment, allowing more light to penetrate through the water and thus allowing a higher growth rate (μ_{max}).

As expected the algae input to the whole system ($ISS_{ext,alg}$) are an important influence on the algal concentration at the downstream reach: these provide the ‘seed’ for the entire system. However, it is interesting to note that as long as there is some sort of seed, its influence is less apparent farther down the reaches: during calibration of the

full 26-reach model, it was noted that changes in the input of algae to the summit reach had minimal effect at the calibration station 18 reaches downstream. That far downstream, as long as there is any seed at the summit reach, the concentration of algae in the reach becomes more dependent upon factors that influence the growth rate – temperature, light availability, and nutrient availability. Consider a case where the total growth is limited to 10 cells in a given reach by temperature, light, and nutrients; if the upstream reach provides 8 cells, only 2 more cells can grow in the current reach; if the upstream reach provides 6 cells, only 4 more cells can grow in the current reach. In both cases, the number of cells in the reach will be the maximum supportable by the environmental conditions – 10 cells. For the upstream reaches, the seed is still growing, and so considering the same environmental conditions: if 1 cell is input to the reach and only one doubling time passes, the reach will hold 2 cells at the end of the time step; if 2 cells are input, then the reach will hold 4 cells; it is not until the input exceeds 5 cells that the cap imposed by environmental conditions becomes important.

What is surprising in the algal sensitivities is that phosphorus and solar radiation do not make an appearance. They are somewhat influential with mean algae $S_r = 0.17$ for phosphorus and $S_r = 0.39$ for solar radiation. However, the water temperature, 'seed' algal input ($ISS_{ext,alg}$), and light extinction exert more control on the algal concentration in a reach typical of the Kennet and Avon Canal. This is due in part to the choice of the top three reaches for use in the sensitivity analysis; as will be discussed later (Section 7.2.4.3, page 156), in the upstream reaches of the canal the population is so low that it generally does not reach the cap imposed by phosphorus and is rather controlled by the seed of algae input at the summit reach.

6. Overland Flow Model

In order to adequately predict flow in the canal, it was necessary to use an existing overland flow model to generate runoff inputs for the canal model described in Section 4. No attempt was made to improve upon existing overland flow models, nor was it the intent of this project to develop or evaluate an existing overland flow model (although some comparisons have been made recently (Zeckoski et al. 2009)). The overland flow model was simply a tool used in generating necessary inputs to the canal model. The Hydrological Simulation Program-Fortran (HSPF) (Bicknell et al. 2001) was chosen for this purpose due to the researcher's familiarity with the model and thus the straightforward nature of obtaining the outputs from HSPF that would be needed for input to the canal model. The adequacy of predictions of the overland flow model was evaluated based on successful calibration of the model to points above the first primary intersection of the canal and the natural river.

6.1. Subcatchment Delineation for HSPF Calibration

The area above the confluence of the River Kennet with the Kennet and Avon Canal, contributing to the river, was subdivided into 13 subcatchments in order to perform the hydrology and sediment calibrations. The breaks in the subcatchments were largely dependent on the locations of the monitoring stations (Figure 38). The subcatchments also generally followed the delineation previously performed by Dr. Andrew Wade at the University of Reading for his work with the Integrated Catchments (INCA) model (Wade et al. 2002) so that the velocity-discharge relationships he developed for the INCA model could be used to create hydraulic function tables to represent the river in HSPF.

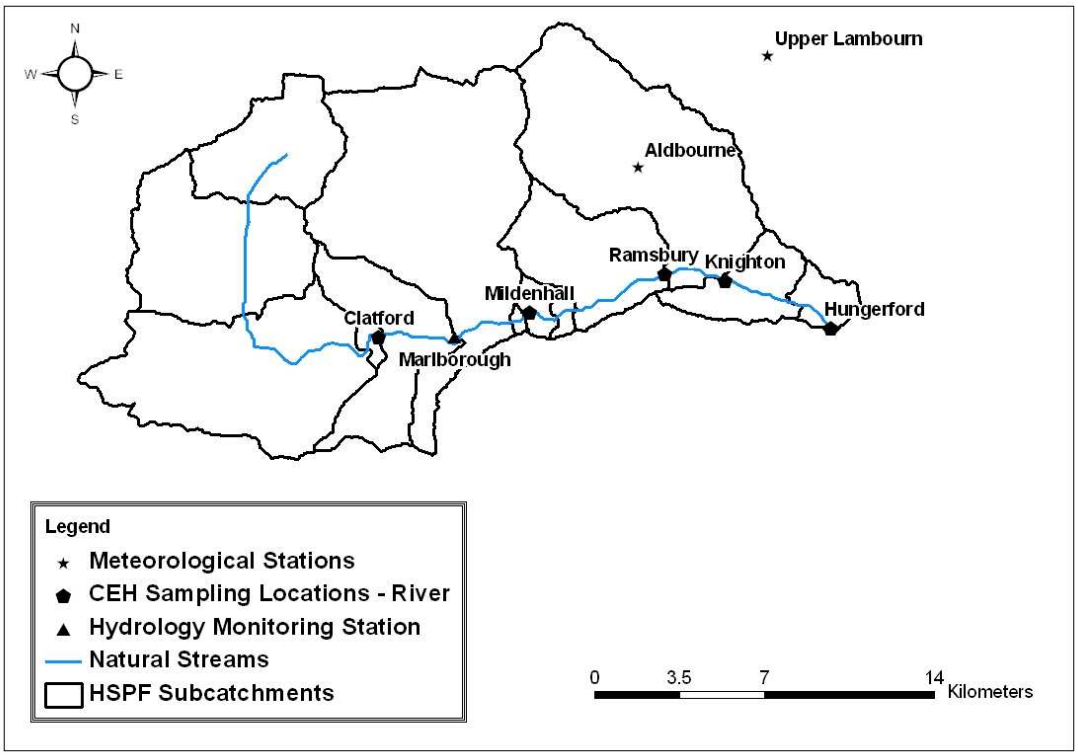

Figure 38. Subcatchment delineation for HSPF calibration.

6.2. Hydrology Calibration

6.2.1. Introduction

Hydrological calibration methods for HSPF are well established (Lumb et al. 1994; EPA 1999; EPA 2000; Kim et al. 2007a). To summarize, a hydrologic model calibration is evaluated based on seven metrics: total annual runoff, low flow recession, total of highest 10% of flows, total of lowest 50% of flows, storm peaks, seasonal volume, and summer storm volume. These latter two are seasonal metrics, ensuring that success in the remaining statistics is not achieved by improper distribution of high flows (e.g., compensating for low flows in summer by elevating flows in winter, thus achieving an acceptable total runoff metric). The seasonal volume metric is the difference between the summer and winter flow errors. The summer storm volume metric is the difference between the summer storm volume error and the total storm volume error (for all times of the year).

6.2.2. Calibration Station

In the case of the River Kennet, one station was available for calibration above the confluence of the river with the canal: Marlborough (Figure 38). The period of record for this station extended from 1972 to present. Being most relevant to the current work, the period of 1997-present was chosen for calibration and validation. This period also corresponded to the available data for sediment calibration. Calibration was performed on data from 1997-2003, and validation on data from 2004-2009.

6.2.3. Model Parameterization

HSPF model parameters were initially estimated using the guidance in BASINS Technical Note 6 (EPA 2000). This required information on land use, soils, and meteorology. Land use and soils were previously discussed in Section 2.5.1. Meteorological data were collected from the British Atmospheric Data Centre (http://badc.nerc.ac.uk/home/) for the stations Aldbourne (precipitation) (World Meteorological Organization (WMO) ID 266949) and Upper Lambourn (temperature) (WMO ID 268196) (Figure 38). The precipitation data were converted to appropriate units and entered as inputs to HSPF; the temperature data were used along with the catchment's latitude to estimate potential evaporation using the Hamon Potential Evapotranspiration method in the Watershed Data Management Utility (WDMUtil) program (Hummel et al. 2001) (a companion program to HSPF).

6.2.4. Results

After calibration, the HSPF metrics were satisfied for both the calibration and the validation periods (Table 11). The baseflow index was calculated as 0.94 for the calibration period and 0.95 for the validation period, compared to 0.94 predicted by the UK Hydrometric Register (Marsh and Hannaford 2008). A comparison of simulated and observed flows is provided in Figure 39 for the calibration period and Figure 40 for the validation period. A full list of the final calibrated parameters is provided in Appendix E.

Table 11. Results of HSPF hydrologic calibration and validation.

Metric	Acceptable Error Range	Error for Calibration Period	Error for Validation Period
Total Runoff	±10%	-6.6%	5.3%
Low Flow Recession	±0.01	0.01	0.01
Highest 10% of Flows	±15%	-14.1%	-3.2%
Lowest 50% of Flows	±10%	3.9%	1.5%
Storm Peaks	±15%	-13.3%	-10.8%
Seasonal Volume	±10%	8.1%	4.6%
Summer Storm Volume	±15%	-10%	-3.9%

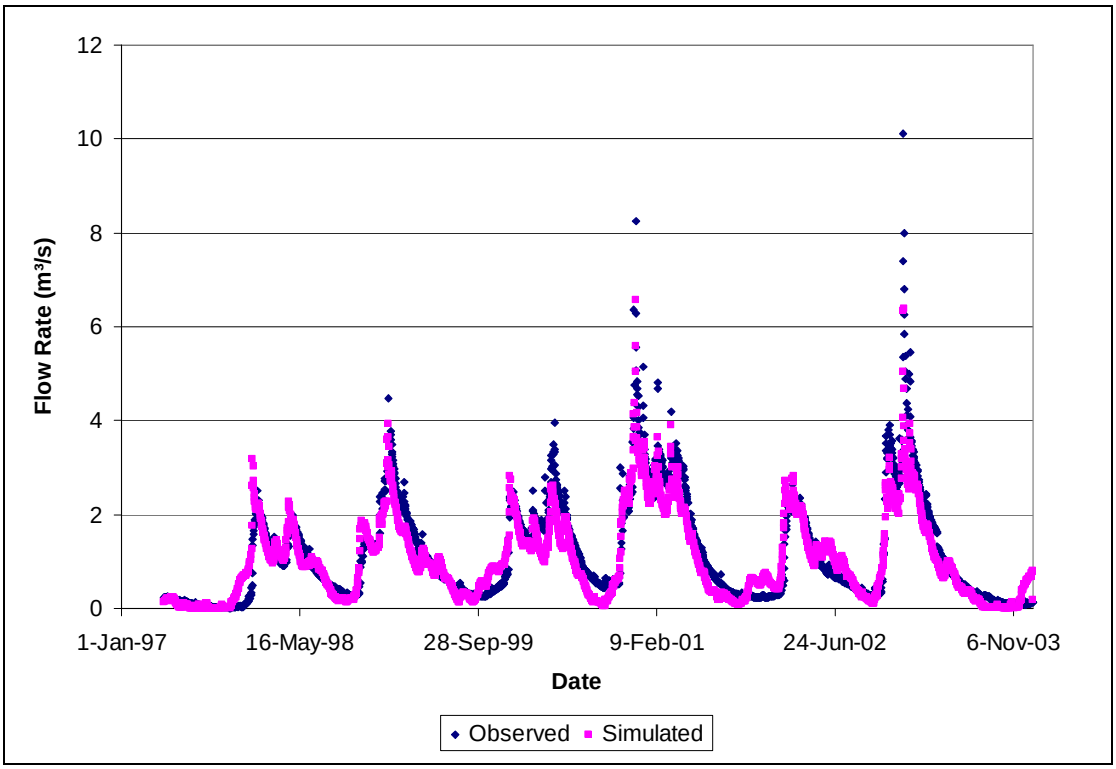

Figure 39. Observed and simulated flow rates for the Marlborough station on the River Kennet – calibration period.

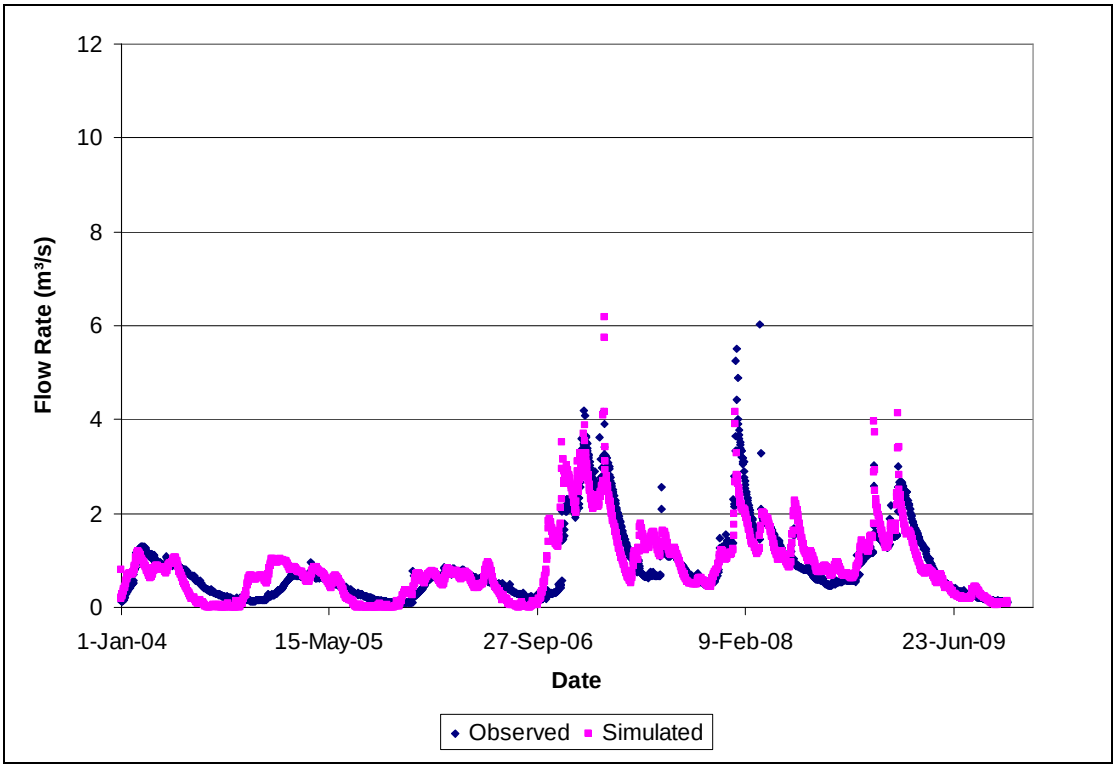

Figure 40. Observed and simulated flow rates for the Marlborough station on the River Kennet - validation period.

6.3. Sediment Calibration

6.3.1. Introduction

Compared to hydrologic calibration, sediment calibration for HSPF is less well defined in terms of both procedure and metrics. However, some guidance exists. The guidelines in BASINS Technical Note 8 (EPA 2006) were followed to estimate parameters, target parameters for calibration, and establish the sediment loading rate metric to assess the calibration. Additional metrics used to assess the sediment calibration included the 5-day window concept introduced by Kim and others (2007b) to calibrate to discontinuous data; the discrepancy ratio (van Rijn 1984; Winter 2007; Neumeier et al. 2008); and the Nash-Sutcliffe model efficiency (Benaman et al. 2005; Mishra et al. 2007; de Vente et al. 2008; Tyagi et al. 2008) based on monthly average concentrations. As is generally accepted (Soulsby 1997), sediment loads and concentrations are more difficult to predict than hydrologic data; therefore the satisfactory errors for the sediment calibration were less stringent than those for the hydrology calibration.

6.3.2. Setting Calibration Targets

HSPF produces two key variables used in the sediment calibration: an edge-of-stream load (model parameter SOSED) and an in-stream concentration of sediment (model parameter ROSED). It was necessary to set observed targets for each of these variables.

6.3.2.1. Edge-Of-Stream Load

BASINS Technical Note 8 (EPA 2006) suggests use of sediment loading rate as an initial assessment of a sediment model's performance, and specifically the model's ability to predict sediment washed off the land surface (as opposed to sediment scoured from the stream). This sediment washed off the land surface will have a greater effect on the canal model than the in-stream sediment concentration, and so determination of an appropriate 'observed' value for this target and minimization of the error in sediment loading rate was a high priority in calibration.

A sediment loading rate is a function of two processes. First, the sediment must be detached from the soil surface – either by raindrop impact or scour from surface runoff. Second, the sediment must be carried by surface runoff to the stream. This process is illustrated in Figure 41. Sediment detached by raindrop impact may fall on a portion of the land surface that has no flowing water, or it may land in flowing surface runoff and be carried to the stream. Sediment scoured by surface runoff may continue to be carried by the runoff, or it may be deposited as the rate of runoff slows due to the roughness of the land surface.

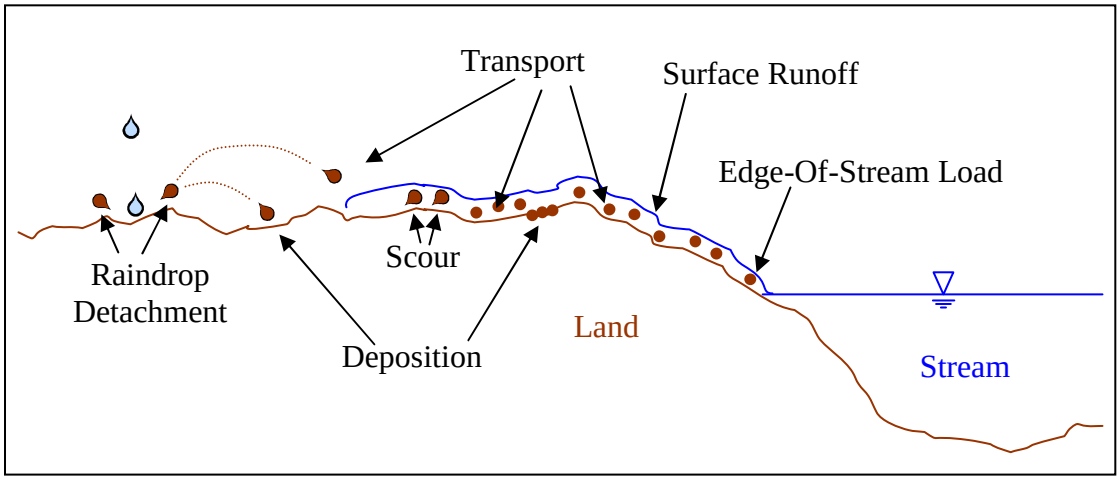

Figure 41. Sediment transport processes on the land surface. Brown dots and drops represent sediment.

The first component of the sediment loading rate, the expected soil detachment, was estimated from the Pan-European Soil Erosion Risk Assessment (PESERA) map (Kirkby et al. 2004) for the area contributing to each monitoring station used in calibration (see Figure 21, page 67). To determine the final target sediment loading rate, it was necessary to multiply this detachment by a sediment delivery ratio to determine how much of the detached sediment reaches the stream. The sediment delivery ratio is the ratio of sediment that reaches the edge of the stream to the total amount of sediment detached from the land surface. The sediment delivery ratio for this purpose was estimated based on the method of Roehl (1962) (Equation 70).

$$\log(SDR) = 1.91349 - 0.33852 \cdot \log(10 \cdot W) \quad (70)$$

Where: SDR = sediment delivery ratio (unitless); and
W = drainage area (square miles).

By multiplying the sediment detachment from PESERA by the sediment delivery ratio determined from Equation 70, an 'observed' (or more appropriately, expected) value is obtained that can be compared to HSPF edge-of-stream outputs from the land surface.

6.3.2.2. In-Stream Concentration

Data from the Centre for Ecology and Hydrology that were collected from the five stations on the River Kennet above the confluence of the river with the canal (Figure 38) were used as targets for the in-stream portion of the sediment calibration. These stations have varying periods of record as presented in Table 12. Because most

stations had a limited number of samples, calibration to a multitude of spatially distributed stations was performed in lieu of a calibration and validation at a single station.

Table 12. Periods of sediment data available at stations on the River Kennet.

Station Name	Period of Record	Number of Samples
Clatford	6/1997-9/2005	410
Mildenhall	6/1997-9/2005	417
Ramsbury	6/1997-2/2001	204
Knighton	6/1997-2/2001	204
Hungerford	8/2003-9/2005	107

It was assumed that the monitored concentrations at these stations were comparable in nature to the in-stream concentrations predicted by HSPF.

6.3.3. Establishing Metrics

Kim and others (2007b) introduced a 5-day window method of computing statistics for use in bacteria calibrations. Portions of this method were adapted here as well, as the difficulties and goal are the same for sediment predictions as with bacteria: there are a limited number of grab samples for a water quality constituent that varies greatly both spatially and temporally. Thus, an expectation that daily model output would be capable of predicting the precise observed value from a grab sample collected once a week (at best) is not reasonable. By looking at a 5-day window of simulated values surrounding each observation, a more reasonable comparison can be made. In particular, this allows focus of the statistics on the conditions unique to the observation dates – a particular benefit in this case, where the observed record misses entire seasons. Comparing yearly or simulation-long averages that capture all seasons to observed values that only represent some seasons would be erroneous.

In practice, the simulated values for two days before, one day before, the day of, one day after, and two days after each observation date were averaged to create a series of simulated 5-day window values – one 5-day window value for each observation date. Then the average and median of this series were calculated to compare with the average and median of the observed data.

The discrepancy ratio used by several researchers to evaluate sediment prediction capabilities is simply a ratio of an observed value to a simulated value – either on a daily (that is, each observation day) or monthly basis. If it is desired for all observed values to fall within a factor of 2 of the simulated values, then the desired discrepancy ratio range would run from ½ to 2. The factors used to define the limits on a desirable discrepancy ratio range in the literature from 1.5 to 10. Having established the desired factor, the next step is to determine what fraction of discrepancy ratios fall between the limits imposed by the desired factor. Typically, as the desired range decreases, so does the fraction of calculated discrepancy ratios that fall between the limits imposed by that range. As an example, Soulsby (1997) suggests that the best models are able to have 70% of their discrepancy ratios fall between 0.5 and 2. van Rijn (1984) provided an example of an acceptable model that had 76% of its discrepancy ratios falling between 0.5 and 2; 37% falling between 0.67 and 1.5; and 94% falling between 0.33 and 3. To evaluate the HSPF model calibration, discrepancy ratios were calculated for monthly average solids concentrations. The desired factor was set at 2 (providing a desired range of 0.5 to 2).

The Nash-Sutcliffe Model Efficiency (NSE) (Nash and Sutcliffe 1970) is perhaps one of the best known methods for evaluating prediction of flow from a hydrologic model. As mentioned in the introduction, this metric is also frequently used to evaluate a water quality model's predictive capability for sediment. The formula for the Nash-Sutcliffe Model Efficiency is given in Equation 71.

$$NSE = 1 - \frac{\sum_{i=1}^{N} \left(x_{oi} - x_{si} \right)^2}{\sum_{i=1}^{N} \left(x_{oi} - \bar{x} \right)^2} \qquad (71)$$

Where: NSE = Nash-Sutcliffe Model Efficiency (unitless);
N = number of observations;
x_{oi} = value of observation *i* (mg/L, in this case);
x_s = simulated value corresponding to observation *i* (mg/L); and
$\bar{x}$ = mean of observed values (mg/L).

By comparing the error between the observed and simulated data (numerator) to the error between the observed value and the mean of all observed values (denominator), the NSE allows the modeler to determine whether the model simulation is a better predictor of the observed condition than a simple use of the mean of observed values.

If the NSE is greater than zero, the error in the numerator is lower than the error in the denominator, and the model is a better predictor of reality than the mean of the observed values; if the NSE is less than zero, the error in the numerator is greater than the error in the denominator, and the mean of observed values is a better predictor than the model. This can be used on individual observations or an aggregate of observations – for example, an average daily value for the month. This average daily value each month is what was used in this case to evaluate HSPF's predictive capabilities.

The satisfactory error rates are summarized in Table 13. Because the prediction of sediment is inherently less certain than the prediction of hydrology, the allowed error bounds are less restrictive for the sediment calibration than they were for the hydrology calibration. In addition to the metrics listed in this section, a visual assessment of the goodness-of-fit was also conducted.

Table 13. Satisfactory errors for the metrics used in the calibration of the overland flow model for sediment.

Metric	Evaluation Criterion	Abbreviation
Sediment Loading Rate (tonnes/ha/yr)	±30%	SLR
5-Day Window Average (mg/L)	±30%	5DA
5-Day Window Median (mg/L)	±30%	5DM
Discrepancy Ratio (using factor of 2)	max[†]	DR
Nash-Sutcliffe Model Efficiency	max	NSE

[†] That is, maximize the percent of values with a discrepancy ratio between 0.5 and 2

6.3.4. Results

The sensitive parameters listed in BASINS Technical Note 8 (EPA 2006) were targeted for calibration and adjusted until they met the allowed errors for each metric. The final calibration results are listed in Table 14. Graphs of simulated and observed data are provided in Figure 42.

Table 14. HSPF sediment calibration results.

Station	Error			DR	NSE
	SLR	5DA	5DM		
Clatford	4%	-17%	2%	29%	0.11
Mildenhall	3%	26%	24%	59%	-0.17
Ramsbury	1%	5%	-20%	60%	-0.19
Knighton	-2%	7%	14%	62%	-0.01
Hungerford	-6%	29%	2%	65%	-1.77

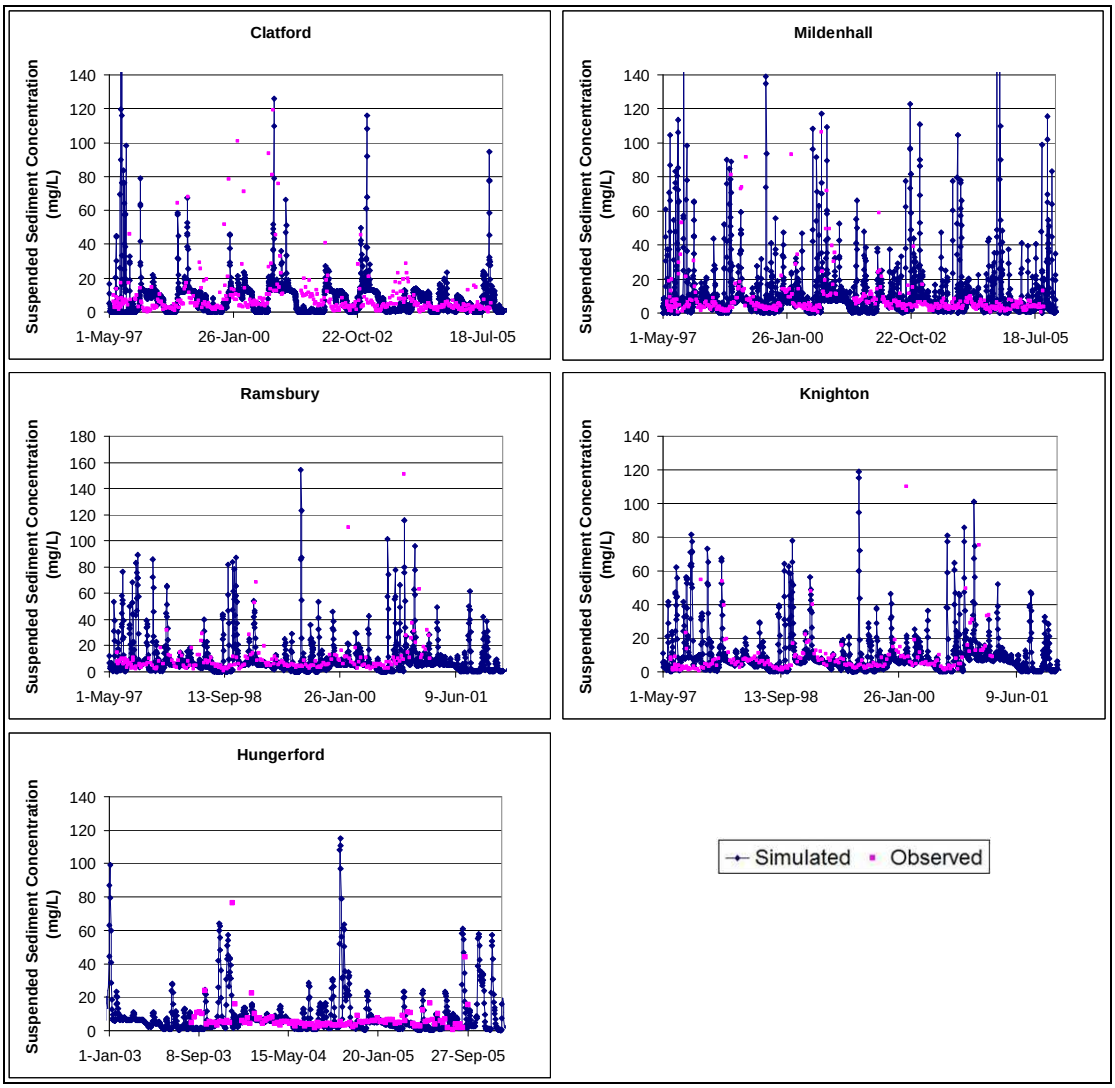

Figure 42. Results of HSPF sediment calibration for five stations on the River Kennet.

Overall the sediment predictions are good, particularly in the middle region, at Ramsbury and Knighton. After calibration, the 30% error targets for sediment loading rate, 5-day average, and 5-day median were met. The magnitudes of the sediment loading errors were all less than 10%; this is especially important, as the sediment loading from the land surface is the most crucial export from the overland flow model to the canal model. The percents of discrepancy ratios that fall between 0.5 and 2 are generally high, with the exception of the values predicted for Clatford. However, the Clatford station shows the best Nash-Sutcliffe model efficiency. Given how well all other calibration targets were met, the poor Nash-Sutcliffe model efficiency results for the remaining stations are surprising. However, as was previously mentioned, expecting a metric based upon a single value for the entire

simulation to perform well when one is comparing simulated results to observations based on (non-continuous) grab samples is optimistic. Note that the 5-day window metric, which compares a grab sample collected once a week to simulated values for a window surrounding the collection date, has very good results. Additionally, the visual comparison shows that the model is accurately predicting the average condition. The peaks predicted by the model would happen in association with storm events, and given that grab samples are not typically collected during storm events, one would not expect the monitored data to capture such peaks. The inclusion of the storm peaks in the simulated record forces a more variable condition than the ambient measurements would suggest, which in turn causes the mean of observed values to appear to be a better predictor than the simulated results. Considering all these issues and that all other metrics used to evaluate the calibration are good, the calibration is acceptable. The final calibrated parameters for HSPF are given in Appendix E.

7. Canal Model Application

To further demonstrate the use and reliability of the new canal model, it was applied to the Kennet and Avon Canal in Southern England (described in Section 2.5.1, pg. 21).

7.1. Inputs for Canal Model

The list of required inputs for the model was previously discussed (Section 4.2.5). In practice, these inputs can be generally divided into three categories: inputs from the overland flow model (runoff and sediment transported in runoff), time series inputs, and physical canal characteristics. In this section, the runoff inputs are treated separately, as they required greater effort involving parameterizing and calibrating a separate overland flow model. The time step for the canal model was set to one day to match the resolution of available input data.

7.1.1. Runoff Inputs

7.1.1.1. Modification of HSPF

The HSPF model as used in calibration (Section 6) only required subcatchment delineation for the River Kennet to Hungerford, the last station available before the confluence of the River Kennet and the Kennet and Avon Canal. To produce appropriate runoff inputs for the canal model, small subcatchments were created to contribute to each lock and were then further divided to separate drainage to the canal from drainage to the river to ensure the correct runoff could be apportioned to the canal. The first step in doing this was to use the digital elevation model (DEM) provided by Dr. Andrew Wade at the University of Reading (originally generated by the Centre for Ecology and Hydrology) to create new subcatchments with outlets at each lock location (Figure 43).

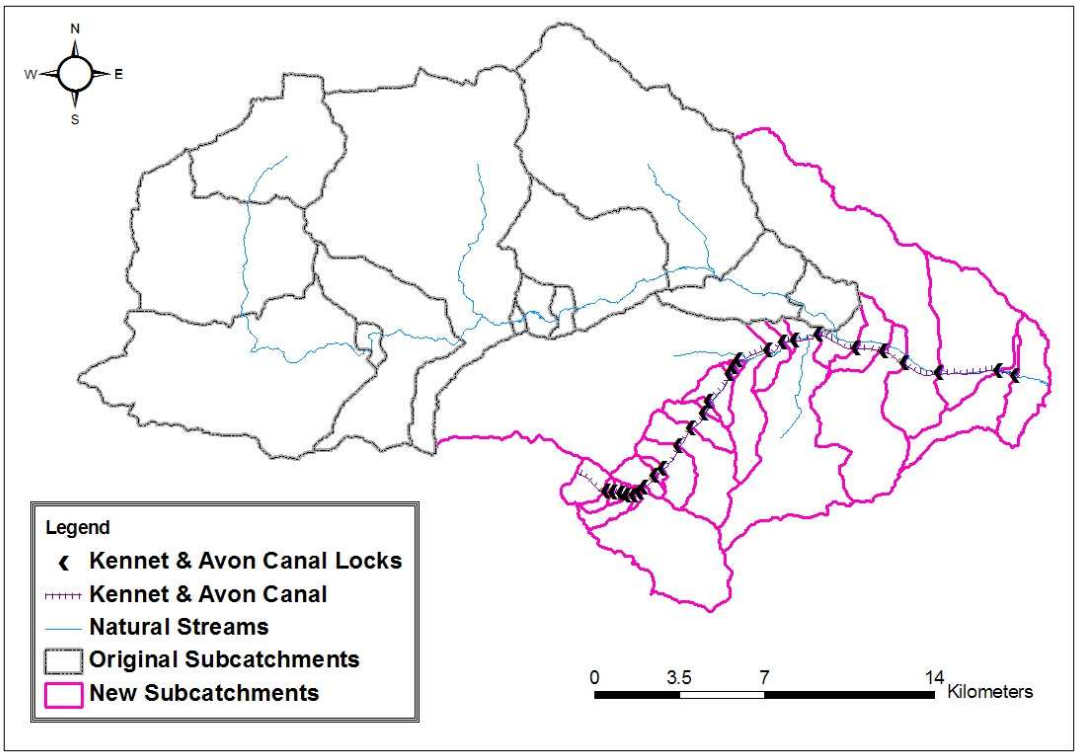

Figure 43. Intermediate subcatchment delineation, causing a break at each lock location.

After this was completed, the subcatchments were split along the line of the canal. The resulting polygons were then classified as contributing to the canal or contributing to the river depending on whether they fell on the canal side or the river side of the divide, respectively. This is illustrated in Figure 44; the final division is shown in Figure 45. It was assumed that any area between the canal and the river contributed to the river, as the canal was typically slightly elevated above the river.

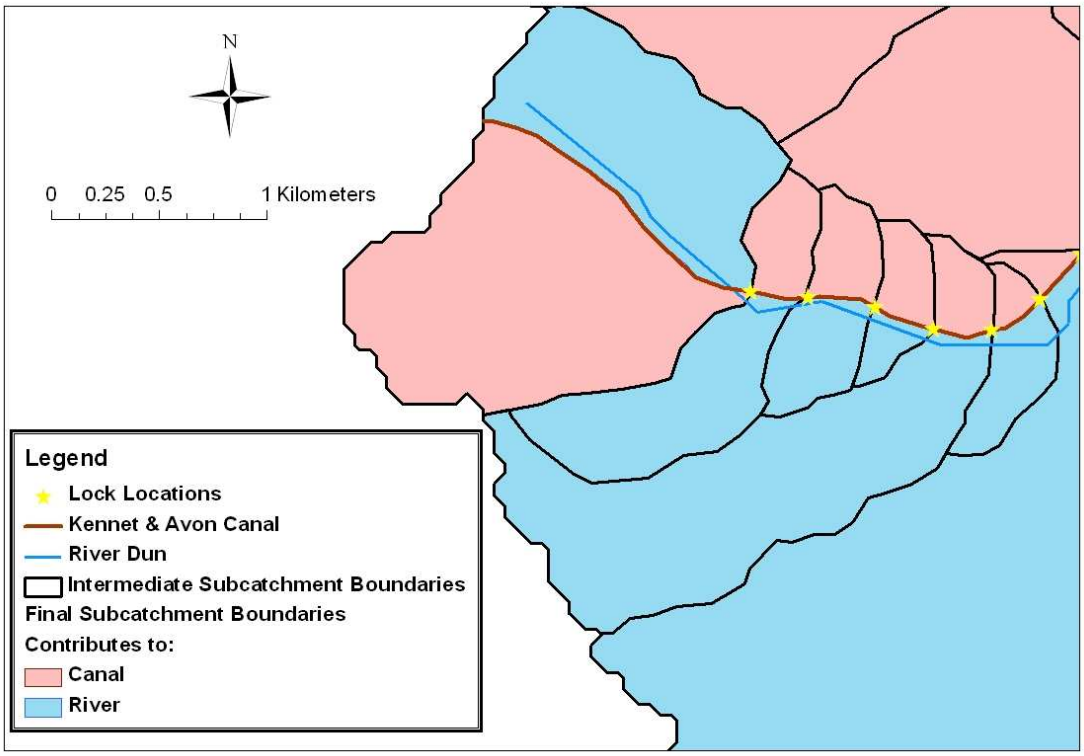

Figure 44. Close-up of subcatchment delineation according to whether it contributes to the river or canal. Drainage area that intercepts the canal before the river contributes to the canal; the remainder contributes to the river.

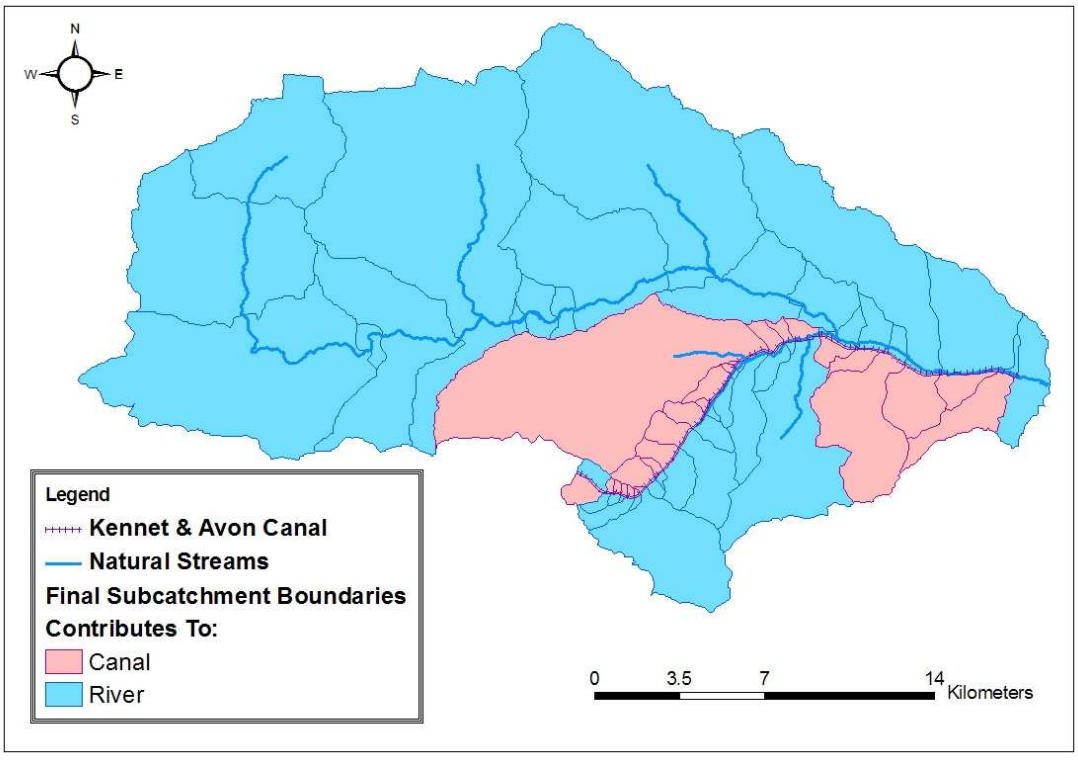

Figure 45. Final subcatchment delineation, splitting the intermediate subcatchments according to contribution to the canal or river.

After delineation, the previously calibrated parameters described in Appendix E were applied to the new subcatchments.

7.1.1.2. Data Used in Canal Model

The total runoff and sediment transported from the land surface were exported to text files from HSPF for each of the new subcatchments in Figure 45. These text files represented the total volume of flow (I_{runoff}) and mass of inorganic sediment (ISS_{runoff}) delivered from the land to each reach of the canal. In the case where a direct transfer of water from the River Dun or the River Kennet was made to the canal, the concentration of sediment in the water in the **river** predicted by HSPF was used to determine the load of sediment (ISS_{ext}) that should enter the canal at those points. The transfers of water (and thus sediment) from the River Dun or the River Kennet to the canal occurred in the reaches above Locks 68, 75, and 78.

7.1.2. Canal Data Processing

7.1.2.1. Time Series Processing

In addition to time series inputs also required or provided by the catchment model (e.g., precipitation, evaporation, runoff), the canal model required the following time series of data: solar radiation, total phosphorus, external inputs (water, sediment, algae), external abstractions, and frequency of boat movements. This section describes the development of each of these time series.

7.1.2.1.1. Solar Radiation

Solar radiation data were not readily available for the study area. However, solar radiation (exclusive of cloud cover) is a standard function of the latitude of a given region. Therefore, the relation developed by Hamon and others (1954) as implemented by the WDMUtil program (Hummel et al. 2001) was used to estimate solar radiation data for the study area. This method requires input of latitude and cloud cover. Although the latitude of the study area is approximately 51°24′N, solar radiation was estimated at 50°N as this is a limitation of the WDMUtil program. Cloud cover was estimated based on available hours of sunshine available from the MetOffice for a nearby station in Oxford (51°42′N) (MetOffice 2010) combined with

sun rise and set tables published by the United States Naval Observatory (U. S. Naval Observatory 2010).

7.1.2.1.2. Total Phosphorus Concentration

Total phosophorus concentration was estimated on a monthly basis from data collected by Colin Neal at the Centre for Ecology and Hydrology (Neal et al. 2006b) at the stations shown on the canal in Figure 21. The phosphorus concentration in each reach on the canal was estimated using data from the closest observation station. The phosphorus concentration for each month of simulation varied by reach and was the average of observed values for that month collected over the observation period. The average of observed monthly values was used in place of the actual values both because the observed record had many holes and because this minimized the effect of isolated extreme values, which were likely not representative of the entire observation period in which they were taken. There were three stations that did not have a record that included a minimum of one observed sample each month; where their records were incomplete (i.e., months with no observed data), an average of the concentration at all other stations was used to patch the missing month.

7.1.2.1.3. External Inputs and Abstractions

External inputs and abstractions of water were estimated primarily from a field survey conducted in 1992 (National Rivers Authority 1992) (henceforth 'the NRA report'). The exceptions were the input from streams directly to the canal (Froxfield Stream and Shalbourne Brook) and pumping from Crofton Pumping Station to the summit reach (see Figure 12, page 52 for stream and pumping station locations). These flows are significant contributors to the canal, and so more current information was used in their estimation.

The major input of water, pumped by the Crofton Pumping Station from Wilton Water Reservoir into the summit reach, was varied throughout the year based on personal communication with the Hon. Engineer for the Kennet and Avon Canal and with engineers at the Crofton Pumping Station. There is a constant 'baseflow' from the pumping station that is pumped year-round to compensate for leakage, seepage, and evaporative losses; this was estimated as 125 L/s. Additionally, a higher flow rate is pumped in the boating season to compensate for lockages; this was estimated as 80

L/s. The concentration of sediment in the feed water from Wilton Water was estimated as the monitored concentration of sediment in the reservoir (Neal et al. 2006b).

The concentration of algae in the feed water from Wilton Water was not available; however, visual inspection confirms that algae are present (Figure 46), and thus a method was devised to generate algal inputs from the feed water. First, the seasonal average TP concentration recorded by Colin Neal (Neal et al. 2006b) was used to calculate the seasonal maximum, mean annual, and summer average chlorophyll-a concentrations using the relationships described in Section 2.3.2. The seasonal maximum and summer average concentrations calculated using these methods ranged from 208 to 424 mg Chl-a/m^3; the mean annual concentrations ranged from 88 to 182 mg Chl-a/m^3. After calibration, 208 mg Chl-a/m^3 was chosen as the maximum chlorophyll-a concentration.

Figure 46. The outlet of Wilton Water Reservoir next to the Crofton Pumping Station. Note algal mat.

Next, the solar radiation data previously collected for direct input to the model were processed to create a time series indicating the fraction that each solar radiation daily value was of the maximum solar radiation for the simulation period. Then the chlorophyll-a concentration was distributed throughout the year according to this fractional solar radiation time series. This resulted in the maximum concentration

occurring in the summer (at the time of maximum solar radiation) and the minimum in the winter. The chlorophyll-a concentration was converted to algal biomass using the conversion factor used in the rest of the simulation (C_{chl}), estimation of which was described in Table 8. Finally, this value was multiplied by a fraction to account for the fact that the intake to the pumping station is located well beneath the water surface and likely at or below the euphotic depth. Reasoning that 1% or less of the algae would be expected to inhabit a depth where 1% or less of the incident light was available, and through experimentation with a few different fractions during calibration, 1% was chosen as the fraction for this purpose.

HSPF was used to estimate the flows from Froxfield Stream and Shalbourne Brook (for locations of these streams, see Figure 12, page 52). The NRA report indicated approximately three quarters of the flow from Froxfield Stream (51 L/s of a total streamflow of 66 L/s) passed through a control structure (Figure 47) that diverted the majority of the Froxfield Stream flow to the River Dun through a culvert passing underneath the canal. As a result, output from HSPF for the drainage area contributing to the reach above Lock 71 was divided: one quarter became input for the canal model, and three-quarters was redirected to the River Dun. This division was applied to both water and sediment outputs from HSPF. Shalbourne Brook enters the canal in its entirety, but an excess is taken off at the opposite side of that reach (above Lock 74). The input of water and sediment was estimated from HSPF runoff, and the output was set at the abstraction level indicated by the NRA report (0.5 L/s). The concentration of sediment in the abstracted water was estimated as the concentration of sediment in the canal reach.

Figure 47. Control structure to divert Froxfield Stream flow away from the canal.

On a few occasions – above locks 68, 75, and 78 – water is drawn from the River Dun or the River Kennet. The volumes of water input to the reach at these points were set at the values given in the NRA report: 0.014 m^3/s, 0.003 m^3/s, and 0.207 m^3/s, respectively. The concentration of sediment in the water from these external sources was set equal to the HSPF-modeled concentration of sediment in the corresponding river sections of the model setup shown in Figure 45.

Two sewage treatment works enter the canal: Great Bedwyn and Kintbury. These discharge to the canal above Lock 66 and Lock 79, respectively (see Figure 18, page 64). The volume of water entering from Great Bedwyn was estimated as 203.8 m^3/d as given by Neal and others (2005b). The volume of water entering from Kintbury was not readily available from any current source, but was estimated as 9 L/s by the NRA report; this value was used in the canal model. Concentrations of sediment in the sewage treatment works outfalls were available from the Environment Agency and were used as input to the canal model.

Whenever water was abstracted from the canal, at locations defined by the NRA report, it carried solids with it at a concentration equal to the concentration in the reach from which it was abstracted. Total abstractions were minimal, amounting to a total of 0.14 m^3/s over the entire length of the study section of the canal.

7.1.2.1.4. Boat Movements

Frequency of boat movement was estimated based on data supplied by Glenn Millar at British Waterways (Langridge 2004). These data included total lockages for the year for Locks 60, 71, 76, and 85 on the Kennet and Avon Canal as well as a typical weekly distribution for lockages averaged from data from multiple canals around Britain (Section 3.4). The annual data for the locks on the Kennet and Avon Canal were distributed to all locks on the study reach based on proximity to the monitored locks and the location of winding holes. In consideration of winding holes: a boat heading a particular direction in a canal will be forced to continue in that direction until it reaches a winding hole, a point in the canal wide enough to permit a canal boat to turn around. There are seven winding holes in the section of the canal being studied (Figure 48) (based on data extracted from Corrie (2002)). Using these data, it can be said with confidence that any boat traffic experienced by Lock 60 must also be experienced by locks 55-64; any boat traffic experienced by Lock 71 must also be experienced by locks 72-74; and any boat traffic experienced by Lock 76 must also be experienced by locks 77-78. For the intervening locks, best judgment and calibration were used to determine how to allocate the known boat movements. It was assumed that most boat traffic would originate from the east (and turn around to return there), so that boats passing through lock 60 would also pass through locks 61-80; boats passing through lock 71 would also pass through locks 72-80; etc. Thus, locks 65-71 and 75 were given the boat movements of Lock 71 and locks 79-80 were given the boat movements of Lock 85.

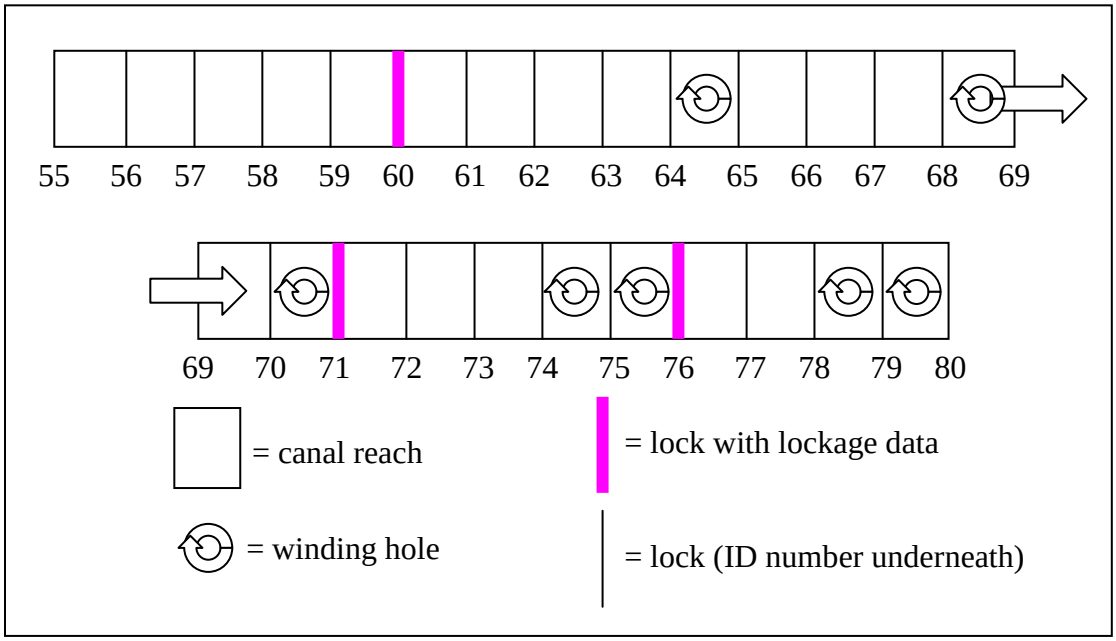

Figure 48. Schematic of winding hole locations in the study area.

The resulting annual lockage data were distributed throughout the year based on the weekly distribution provided by Glenn Millar. Annual lockage data were available only for 2000-2005; data for 1997-1999 were estimated as the maximum observed (as the hydrology of the canal clearly demonstrated increased lockage losses prior to 2000, causing a depression in total weir flow, Figure 47). Data for 2006-2009 were adjusted within the observed range given in 2000-2005 to achieve a successful validation. Because the lockage data were only known from 2000-2005, most confidence was held in model output from that period.

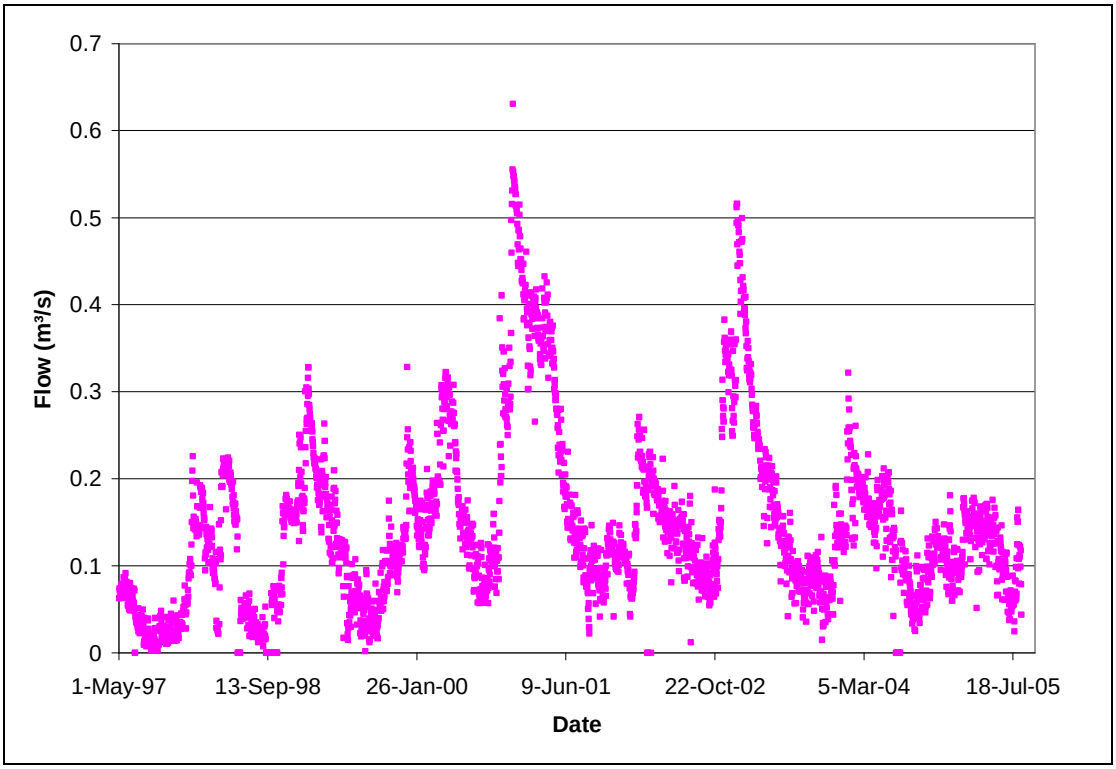

Figure 49. Observed flows collected at the bypass weir for the Picketfield Lock (Lock 71).

7.1.2.2. Reach and Lock Data

Where possible, the data for the locks and reaches were estimated as suggested in Table 7 and Table 8. Further details on the estimates are supplied in this section.

The reach data were determined as follows:

- Length: measured in GIS as the GPS-delineated towpath distance between locks
- Width: measured from aerial photographs
- x_{weir}: measured with tape measure
- D_{weir}: estimates provided by British Waterways (Fox 2010)
- L_{weir}: measured with tape measure
- H_{sides}: measured with tape measure
- D_{lock}: estimated to be 17.8 cm above D_{weir} (visual observation suggested the top of the lock gates was the width of a railroad tie above the permanent water level)
- $C_{d,weir}$: set at 0.611 as suggested by Henderson (1966)

- Seep: calibrated to 3.72 x 10^{-7} $m^3/m^2/s$; this is three times the value given by Dun (2006) and approximately one fifth of the value given by Minikin (1920) for old canals
- T_{mean}: average of water temperature data collected at multiple points in the canal by Colin Neal (Neal et al. 2006b)
- C_{rad}: estimated from aerial photos based on the fraction of canal visible (not covered by trees)

Data are summarized in Table 15 for each reach of the canal.

Table 15. Reach parameters for the Kennet and Avon Canal for input to the new canal model.

Reach ending in Lock	Length (m)	Width (m)	D_{weir} (m)	L_{weir} (m)	H_{sides} (cm)	D_{lock} (m)	T_{mean} (ºC)	C_{rad} (Ø)
55	18†	10.0	1.37	2.44	0.14	1.55	11.5	1.0
56	270.7	9.0	1.42	1.83	0.33	1.60	11.5	0.92
57	322.1	7.9	1.42	1.88	0.20	1.60	11.5	0.89
58	290.8	8.8	1.21	2.19	0.18	1.39	11.5	0.85
59	283.3	8.1	1.17	4.01	0.18	1.35	11.5	0.92
60	273.2	7.9	1.10	4.52	0.23	1.28	11.6	0.95
61	287.0	11.9	1.53	2.06	0.18	1.71	11.6	0.94
62	663.9	10.5	1.47	3.86	0.20	1.65	11.6	0.90
63	399.6	8.6	1.21	4.47	0.20	1.39	11.6	0.79
64	1145.8	10.5	1.17	10.67	0.20	1.35	11.6	0.69
65	954.1	11.4	1.40	3.45	0.20	1.58	11.6	0.88
66	821.9	10.5	1.23	5.51	0.19	1.41	12.0	0.86
67	485.1	10.2	1.37	3.96	0.15	1.55	12.3	0.73
68	1494.7	9.5	1.44	3.45	0.20	1.62	12.3	0.92
69	317.6	13.3	1.37	1.88	0.43	1.55	12.3	0.95
70	355.9	7.4	1.36	4.22	0.24	1.54	12.3	0.87
71	1297.9	8.8	1.37	2.54	∞	1.55	12.3	0.86
72	811.6	9.5	1.51	10.21	0.15	1.69	12.4	0.83
73	489.7	10.7	1.38	6.00	0.20	1.56	12.4	0.94
74	1065.3	10.0	1.34	10.81	0.13	1.52	12.4	0.91
75	1648.1	10.7	1.30	11.99	0.23	1.48	12.1	0.71
76	1176.4	10.7	1.12	10.06	0.13	1.30	12.1	0.72
77	1008.3	10.0	1.50	12.04	0.18	1.68	12.1	0.60
78	1573.6	10.7	1.55	9.14‡	∞	1.73	12.3	0.69
79	2483.8	10.0	1.54	6.56	0.15	1.72	12.3	0.79
80	743.4	10.2	1.19	2.90	0.18	1.37	12.3	0.74

† Estimated as the distance from the feeder from Crofton Pumping Station to the lock gates; water west of the inlet of the feeder flows to the west side of the canal.

‡ Weir was not visible from public land; estimated from aerial photos.

∞ Weir was open to the air (no top).

The lock data were determined as follows:

- Empty: based on instructions recorded in the field at each lock gate (e.g., Figure 50)
- E_{boat}: calibrated to 0.67
- V_{lock}: calculated from lock dimensions provided in a map from Mr. Mike Lee (Hon. Engineer for the Kennet and Avon Canal)
- L_{lock}: measured with tape measure
- Leak: set at 0.0301 m^3/s based on 2.6 ML/d given by Dun (2006); doubled for locks that were observed to be especially 'leaky' in the field (e.g., Figure 51)
- $CS_{lock,non}$ & $CS_{lock,coh}$: set at 7.3 mg/L (7300 mg/m^3) (the median of recorded values), allocated to non-cohesive (2000 mg/m^3) and cohesive (5300 mg/m^3) forms based on an area-weighted average soil texture in the catchment as determined from Jarvis et al. (1979; 1984)

The lock data are summarized in Table 16.

Figure 50. Example of instructions regarding lock emptying at a lock on the Kennet and Avon Canal.

Figure 51. Example of leaky lock gates.

Table 16. Lock parameters for the Kennet and Avon Canal for input to the new canal model.

Lock Number	Empty	V_{lock} (m^3)	L_{lock} (m)	Leak ($m^3/m/s$)
55	TRUE	173.02	5.38	0.0439
56	TRUE	229.27	5.28	0.0212
57	TRUE	201.52	4.88	0.0211
58	TRUE	219.38	5.18	0.0498
59	TRUE	223.54	5.34	0.0257
60	FALSE	205.85	5.38	0.0273
61	FALSE	200.55	5.18	0.0197
62	FALSE	180.79	5.34	0.0409
63	FALSE	211.49	5.48	0.0249
64	FALSE	240.35	5.44	0.0257
65	FALSE	234.86	5.48	0.0215
66	FALSE	226.91	5.18	0.0245
67	FALSE	210.11	5.34	0.0220
68	FALSE	180.96	5.18	0.0208
69	FALSE	208.36	5.54	0.0220
70	FALSE	212.99	5.48	0.0221
71	FALSE	212.76	5.18	0.0220
72	TRUE	248.53	5.48	0.0199
73	FALSE	249.93	5.14	0.0218
74	FALSE	241.73	5.24	0.0224
75	FALSE	172.76	5.38	0.0231
76	FALSE	209.91	5.38	0.0538
77	FALSE	149.87	5.08	0.0201
78	FALSE	174.45	5.48	0.0194
79	FALSE	175.27	5.18	0.0195
80	FALSE	181.76	4.88	0.0506

7.1.2.3. Constants

The various constant parameters (those that do not vary by reach, lock, or timestep) were determined in the following fashion:

- C_e: set at 0.7 as suggested by Schwab et al. (1993)
- diam: set at 0.0002 m as a mid-range point from the range given by Jarvis et al. (1979)
- sg: set at 2.65 as a standard accepted for fluvial sediment (Simons and Şentürk 1977)
- τ_{cd}: set at 0.06 $kg/m/s^2$ as given by Krone (1962) as cited by Mehta et al. (1989)
- $C_{d,drag}$: set at 0.0025 as suggested by Soulsby (1997)

- $CS_{boat,coh}$ & $CS_{boat,non}$: total calibrated to 13500 mg/m³ based on field measurements; distributed as described for $CS_{lock,coh}$ and $CS_{lock,non}$ (Section 7.1.2.2)
- v_b: 1.79 m/s provided in a map from Mr. Mike Lee (Hon. Engineer for the Kennet and Avon Canal)
- EXTB: calibrated to 1.67/m, within the ranges given by Reynolds (1984) and Van Duin et al. (2001)
- $K_{s,l}$: set at 23.012 J/m²s based on the recommendation of Dugdale and MacIsaac (1971)
- T_{mag} and T_{phase}: set to 6.54 and 4.46, the best fit parameters for Beer's (2001) model as fit to water temperature data collected in the canal by Colin Neal (Neal et al. 2006b)
- C_{chl}: set at 60 as a midrange of data calculated from the sources in Table 8
- LITSED: set at 0.000025 m²/mg based on range reported by Van Duin et al. (2001)
- LITALG: set at 0.00002 m²/mg Chl-a based on range reported by Van Duin et al. (2001)

7.2. Canal Model Calibration & Validation

7.2.1. Hydrology

Very little hydrology data are available on the Kennet and Avon Canal. The only data available are flows over a weir that bypasses Picketfield Lock (Lock 71) (Figure 19, page 65). As the dataset for comparison is so sparse, only a calibration was performed for hydrology on the canal; this calibration consisted of a visual evaluation coupled with a comparison of observed and simulated average and median values. This particular bypass flow is heavily influenced by input to the reach from Froxfield Stream, one-quarter of which flows into the canal near the top of the reach (Section 7.1.2.1). Thus, errors in the overland flow model propagate to this section of the canal model. Due to the lack of detail available and the concern of error propagation from the overland flow model, the acceptable error in the average and median comparison was set at ±15%.

The visual comparison of observed and simulated bypass weir flows around Lock 71 is presented in Figure 52. It is evident from the figure that there is generally a good agreement between the observed and simulated flows, particularly in the years where good lockage data are available (2000-2004, see Table 6). There is more confidence in the model predictions for this 2000-2004 period, as weir flows are noticeably influenced by lockages (with an S_r of -0.68 (Table 9)); thus, with greater confidence in lockages, there is greater confidence in weir flow. The good agreement of the modeled and observed data is further supported by the error in the average flow rates (10%) and median flow rates (9%).

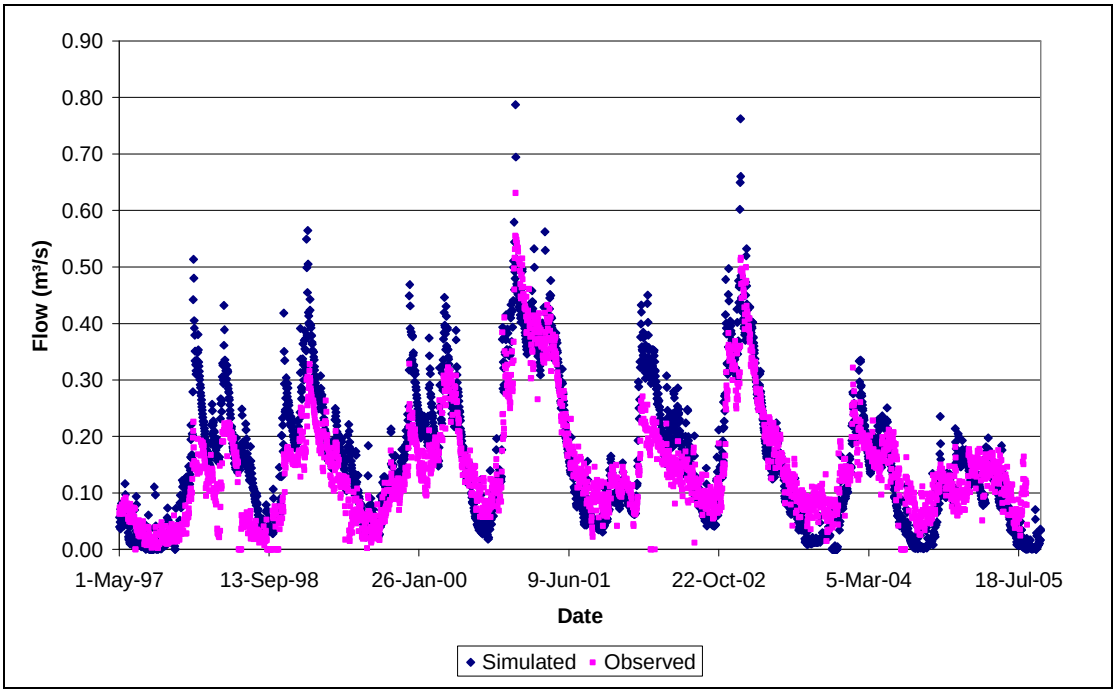

Figure 52. Simulated and observed flows at Picketfield Lock (Lock 71).

The successful calibration was obtained with minimal parameter adjustment from the initial estimates. The parameters adjusted were the input rates to the summit reach at Wilton Water and the seepage rates. Consultation with the literature, agencies, and canal engineers yielded a wide range of estimated flow to the summit reach, from an unlikely maximum of 250000 gal/hour (Kennet and Avon Canal Trust Ltd. 1999) (316 L/s), to rate of 14 ML/d (162 L/s) reported by British Waterways (very patchy data, only through 1998), to 2500 gal/min (189 L/s) and 125 L/s reported by canal engineers. Consultation with the engineers also suggested a variable rate, with additional pumping capacity of 80 L/s for the summer months. Each of these rates

was tried in the canal model, and the constant 125 L/s with a supplement of 80 L/s in the summer was accepted as it best matched the observed flow data. This rate was the one in which there was most confidence, as it was the rate reported by the engineer who operates the pumping station. Seepage estimates started at the low end of the range reported in the literature (Table 8) and were gradually adjusted upward until a successful calibration was obtained.

7.2.2. Total Solids

7.2.2.1. Observed Data

Total solids data were available at seven sites on the canal (Figure 21, page 67), collected by the Centre for Ecology and Hydrology. An initial data collection period spanned 1997-2002, with six individual stations recording data for 2-5 years within that time window (Neal et al. 2006c). A secondary collection period covered five stations for the period 2008-2009 (unpublished data obtained from Dr. Colin Neal, Centre for Ecology and Hydrology). Samples were collected at a sole station, Hungerford, for 2003-2007. The observed data did not differentiate between organic and inorganic solids; thus the observed data were compared to total simulated solids concentrations (non-cohesive sediment, cohesive sediment, and algal dry mass) in the canal at these seven locations. It was assumed that the observed data were representative of the average concentration of solids in the reach. The data from 1997-2005 were used in calibration; the data from 2006-2009 were used in validation. A summary of the data available at the seven stations is given in Table 17.

Table 17. Observed solids data available from the Kennet and Avon Canal.

Station Name	Period of Record	Number of Samples in Calibration Period	Number of Samples in Validation Period
Crofton	Feb 2000 – Feb 2002; Oct 2008 – Oct 2009	50	48
Great Bedwyn	Feb 2000 – Feb 2002	50	0
Fore Bridge	Feb 2000 – Feb 2002; Oct 2008 – Oct 2009	50	48
Dun Cottage	Feb 2000 – Dec 2001	49	0
Hungerford	Feb 2000 – Oct 2009	238	130
Kintbury	Feb 2000 – Feb 2002; Oct 2008 – Oct 2009	50	49
Copse Lock	Oct 2008 – Oct 2009	0	47

7.2.2.2. Calibration Methods and Results

The metrics considered for solids calibration and validation included the 5-day window average values (5DA) and a visual comparison. The percent of discrepancy ratios falling between 0.5 and 2 (DR) and Nash-Sutcliffe model efficiencies (NSE) were also calculated. The criterion for calibration acceptance was an error in the 5-day window average value prediction of ±30%; due to the previously mentioned uncertainty in boat movements after 2005, the criterion for validation acceptance was an error in the 5-day window average value prediction of ±40%. As with the runoff model calibration and validation, a larger DR and larger NSE are desired, while a minimal-magnitude 5DA is desired. The results of the successful calibration and validation of the canal model for the Kennet and Avon Canal are shown in Table 18.

Table 18. Results of suspended solids calibration for the canal model.

Station Name	Calibration			Validation		
	5DA	DR	NSE	5DA	DR	NSE
Crofton	15%	28%	-0.74	25%	54%	-0.26
Great Bedwyn	-8%	24%	-0.14	n/a	n/a	n/a
Fore Bridge	-29%	46%	0.12	-15%	56%	0.38
Dun Cottage	-17%	63%	0.69	n/a	n/a	n/a
Hungerford	1%	63%	-0.22	19%	62%	-0.03
Kintbury	5%	49%	-0.04	-1%	69%	0.48
Copse Lock	n/a	n/a	n/a	-26%	66%	0.44

n/a: data not available at this station in the designated period

The model agreement is further demonstrated in Figure 53 for calibration and Figure 54 for validation. In Figure 54, the predictions for Copse Lock appear low, relative to the observed values, compared with the predictions at the other stations. This may be a result of multiple factors, including the lack of data available for the calibration period which prevented locally specific calibration of model parameters. As with all the data, there is difficulty in comparing grab samples to daily average simulated values (and the 5DA metric, designed to overcome this difficulty, performs well); additionally, surface runoff may be impacting the area, and maneuvering at the winding hole in the reach above Copse Lock may mean both that boat traffic is under or over estimated and that peaks of sediment concentration may be produced in association with maneuvering efforts.

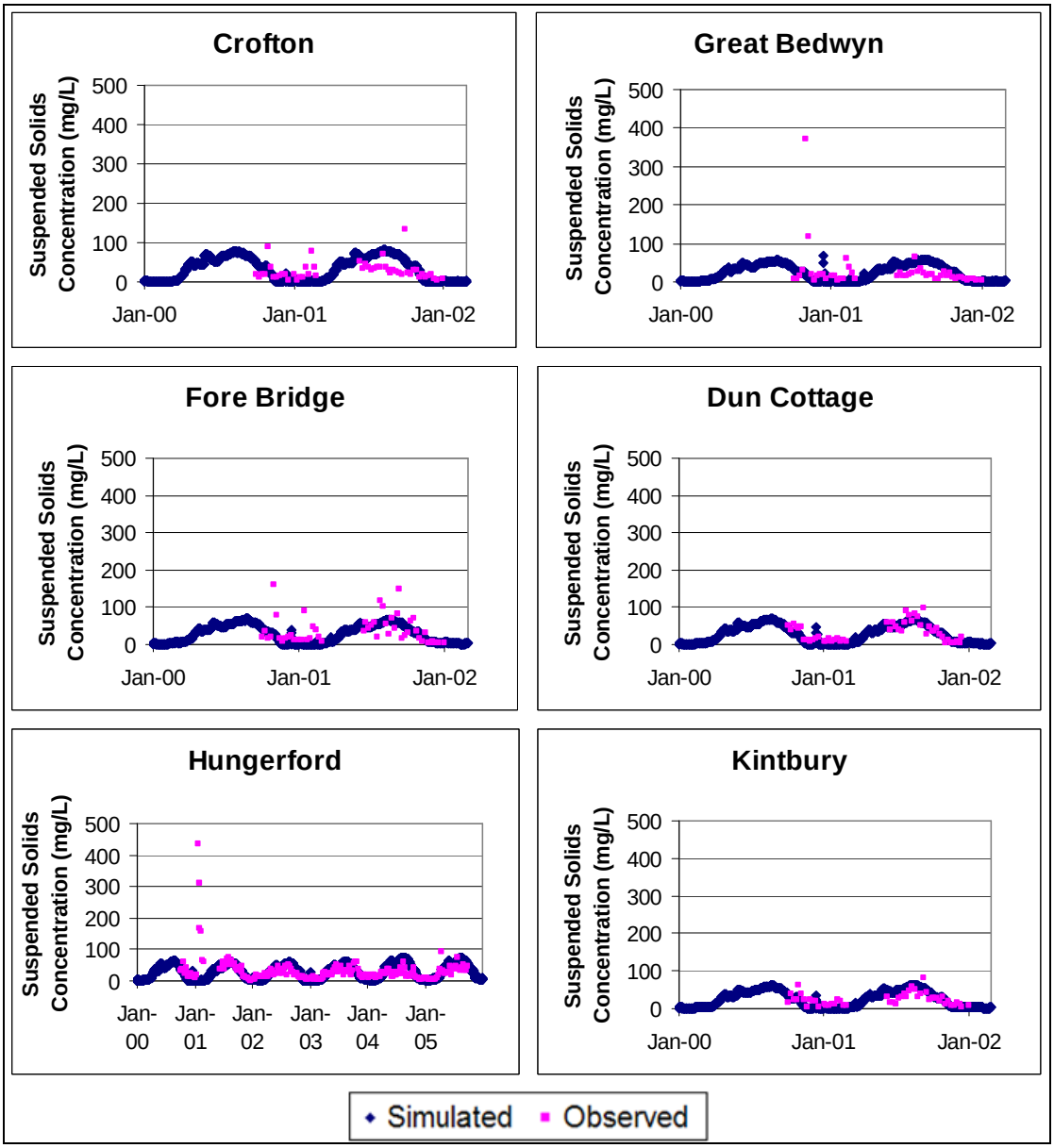

Figure 53. Calibrated model results compared with suspended solids concentrations measured in the Kennet and Avon Canal.

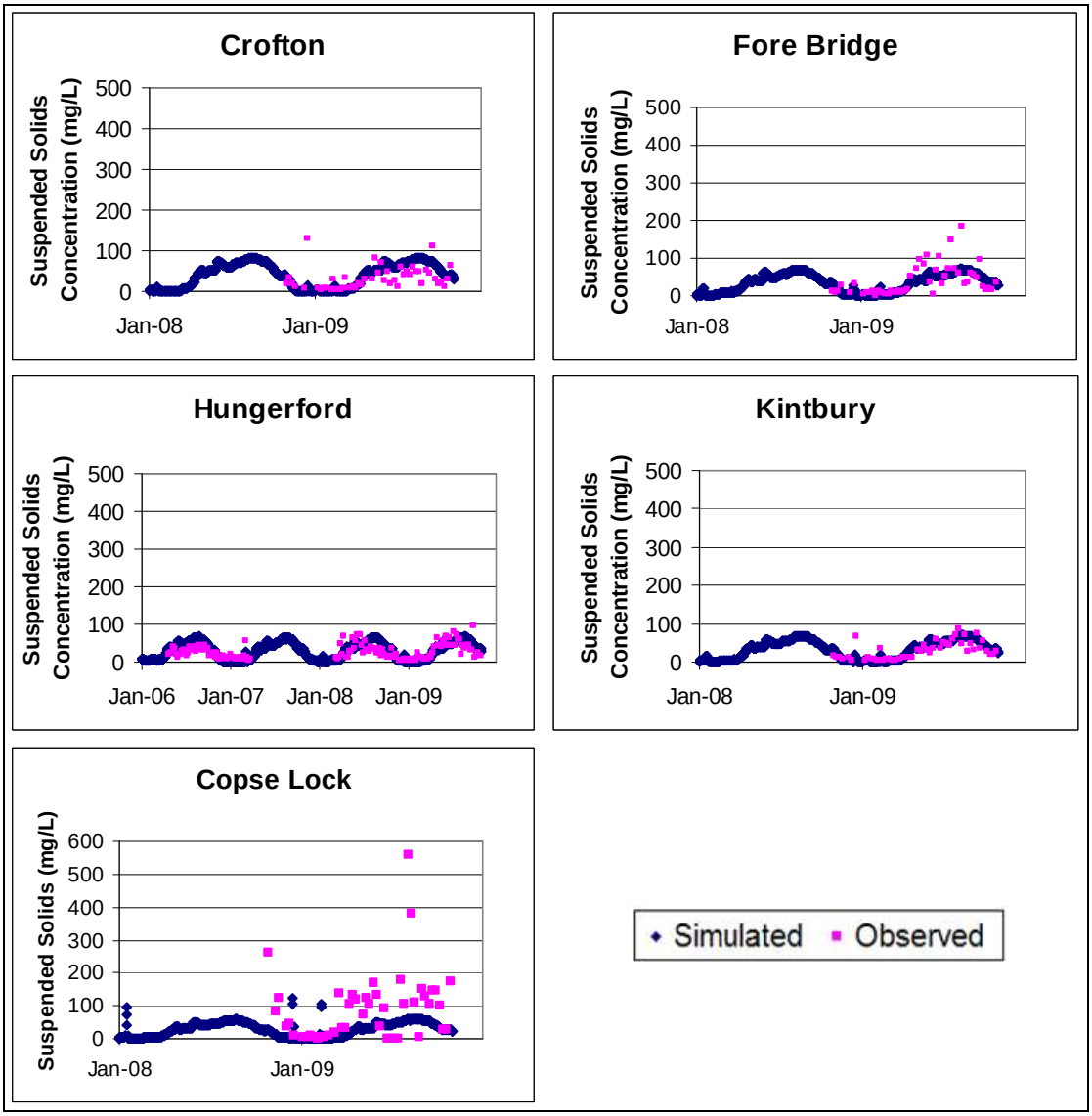

Figure 54. Validated model results compared with suspended solids concentrations measured in the Kennet and Avon Canal.

During the calibration of the solids model, the primary factors adjusted were the sediment stirred up by boat movements and the boat:lockage ratio (note that lockage data were provided by British Waterways, but had to be converted to number of boats by use of an unknown boat:lockage ratio). The boat:lockage ratio was suggested to be 2 by British Waterways; however, if this were the case, it would mean that each boat entered a lock going the opposite direction of the boat before it. A 100% efficiency of this sort seems extremely unlikely, and observations made while visiting the canal did not support an estimate of 100% efficiency. Therefore, this value was adjusted downward to a boat:lockage ratio of 1.5, corresponding to a 67% efficiency in lock usage. This matched the sediment data well and was supported by visual observations. The observed values of sediment concentration disturbed by boats

varied widely (Section 3.2.3 and Appendix Table 4); the initial value chosen was the median of the non-extreme values collected in September 2009, 12 mg/L; the values collected in September were considered more reliable because they were collected from a bridge, rather than near a lock where boat manuevers to enter the lock, the movement of the lock gates, and the increased flow of water due to lock filling may have had an unanticipated effect on the results. However, 12 mg/L proved to be too low, and was increased to 13.5 mg/L in the final calibration; an increase of this nature was supported by the samples collected in August 2008, which suggested an overall median of 18 mg/L.

7.2.3. Algae

Chlorophyll-a data, considered to be representative of algal concentration, were available at only 2 sites on the canal during the calibration period (Crofton and Hungerford, Figure 21, page 67), again collected by the Centre for Ecology and Hydrology (Neal et al. 2005a). All stations at which suspended solids data were collected during the validation period (Table 17) also collected chlorophyll-a data (unpublished, received from Dr. Colin Neal at the Centre for Ecology and Hydrology). Because the model predicts algal dry mass rather than chlorophyll-a concentration, the conversion factor used for equations in the model (C_{chl}, Table 8, page 93) was applied to the algal mass output to generate a time series of simulated chlorophyll-a concentrations. As this chlorophyll-a to algal mass ratio varies with a multitude of conditions (Section 2.3.1), and as algae are living organisms, a great deal of scatter is expected in the observed data compared to the modeled results. It was assumed for comparison purposes that the measured chlorophyll-a data were representative of the average chlorophyll-a concentration in the relative reaches.

As with suspended solids, the primary focus of the algal calibration was the 5-day window average value coupled with visual inspection. The 5-day window average was allowed to have an error of up to 50% during the calibration period, in consideration of the increased uncertainty associated with algal prediction. During the validation period the allowed error rate was increased to 60% to allow for increased uncertainty caused by lack of knowledge of any water quality conditions in the Wilton Water reservoir (and thus lack of knowledge of the ‘seed’ of algae entering the summit reach). The discrepancy ratios falling between 0.5 and 2 and the Nash-

Sutcliffe model efficiency were also considered. The results of the successful calibration and validation are shown in Table 19.

Table 19. Results of algal calibration for the canal model.

Station Name	Calibration			Validation		
	5DA	DR	NSE	5DA	DR	NSE
Crofton	28%	56%	0.24	-21%	54%	0.36
Fore Bridge	n/a	n/a	n/a	-24%	44%	0.25
Hungerford	22%	53%	0.14	6%	58%	0.38
Kintbury	n/a	n/a	n/a	-37%	20%	0.19
Copse Lock	n/a	n/a	n/a	-28%	51%	0.84

n/a: data not available at this station in the designated period

The fit of the model is additionally demonstrated in Figure 55 for calibration and Figure 56 for validation. As expected, there is considerable scatter about the relatively smooth simulated values, but the simulated values do reproduce the overall trend and thus will be useful in targeting scenarios to address the solids problem in the canal.

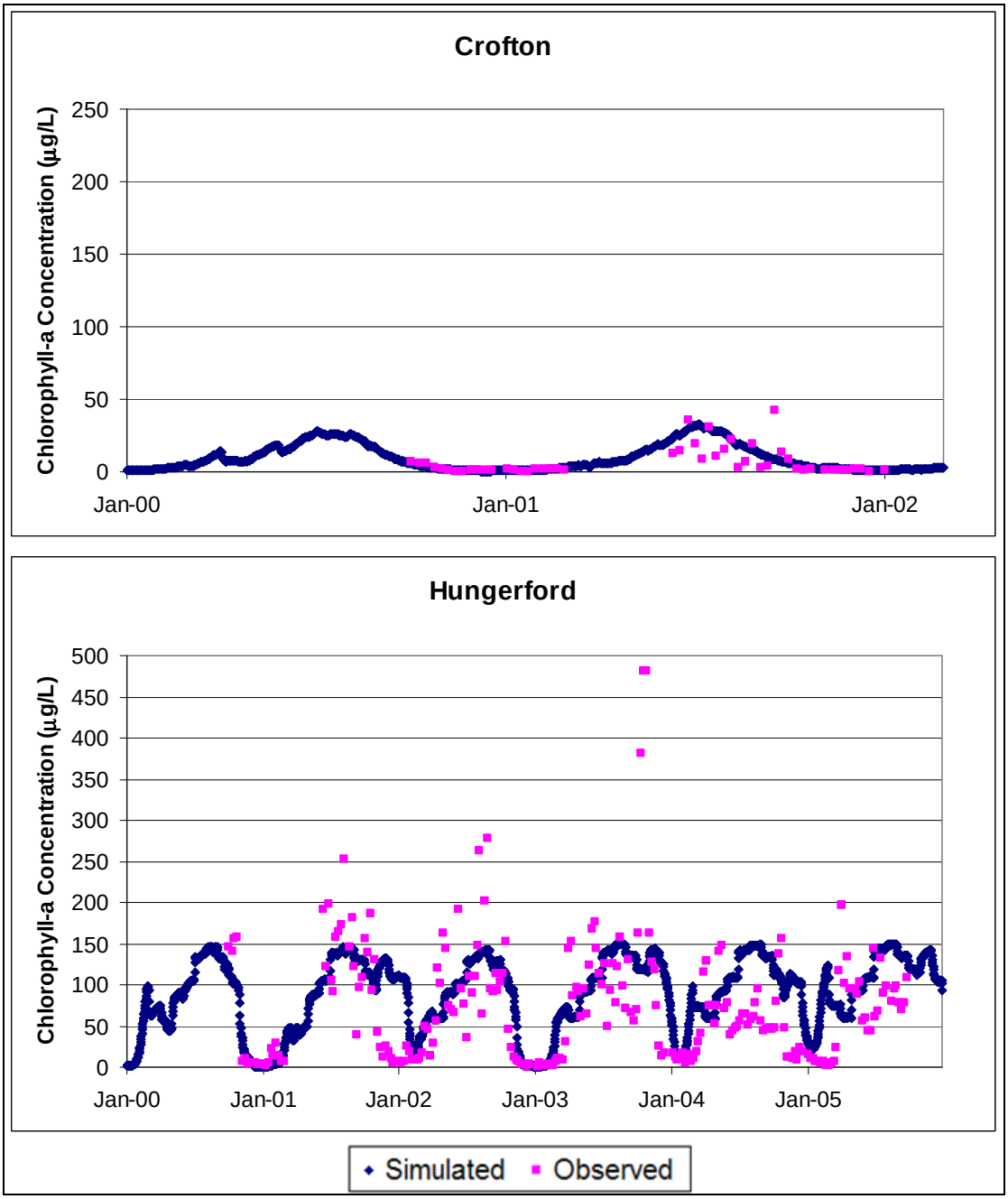

Figure 55. Calibrated model results compared with algal concentrations measured in the Kennet and Avon Canal.

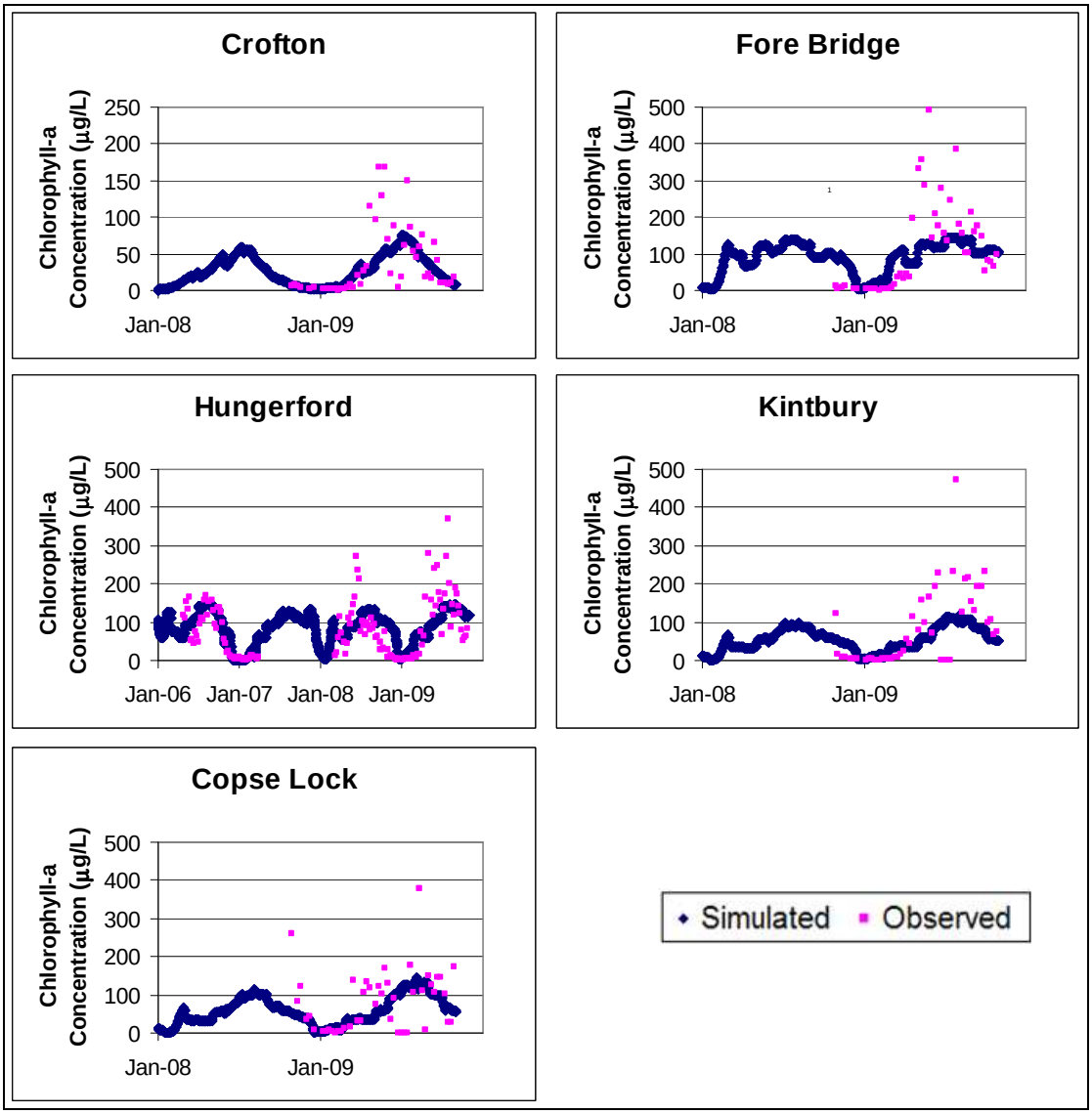

Figure 56. Validated model results compared with algal concentrations measured in the Kennet and Avon Canal.

The primary factor altered during calibration of the algal model was the base light extinction coefficient, which was increased from 1 to 1.67 to address a surge in algal growth modeled in the autumn after boat movements (and thus shading from sediment) decreased (no corresponding surge was seen in the observed data). Modeled algal concentrations were also considered in choosing the flow rate from the Crofton Pumping Station, as this flow rate had a great flushing effect on algal concentrations near the summit reach (e.g., at the Crofton station). During calibration, initial rough estimates associated with algae were further refined – the algal concentration in the feeder from Wilton Water was estimated to be a small percentage of the supportable population due to presumed water withdrawal from well below the water surface; and estimates of C_{rad} were determined geometrically through

measurement in ArcGIS rather than through rough visual observation as was done originally. A small attempt was made to address known changes in algal concentrations in the reservoir during the validation period by increasing the algal concentration in the feed water by a factor of 3 (compared to the calibration period), due to an algal bloom seen in the summers of 2008 and 2009 that local canal users claimed to be very unusual.

7.2.4. Analysis & Discussion

In addition to the metrics included in the previous sections, there are some revealing bits of information that can be extracted from the model output that will be useful in planning efforts.

7.2.4.1. Hydrology

Figure 57 (inflows) and Figure 58 (outflows) show the total hydrologic flows through various routes, summed for the entire simulation (recall that the study section of the canal covers the length from the reach above Lock 55 to the reach above Lock 80). It is clear from these figures that leakage and weir flow, being relatively constant through the year, cause the majority of flow in the Kennet and Avon Canal. Lockages provide significant flow in the summer months, but the constant flows through weirs and leakage in the full 12 months of the year outweigh the lockages on an annual basis. From a management perspective, it is clear that replacement and/or reinforcement of lock gates designed to address leakage problems could have great effect on the amount of water needed to maintain water levels in the canal, as the current flow into the summit reach is just above that needed to satisfy the leakage and lockage demands for the next six reaches.

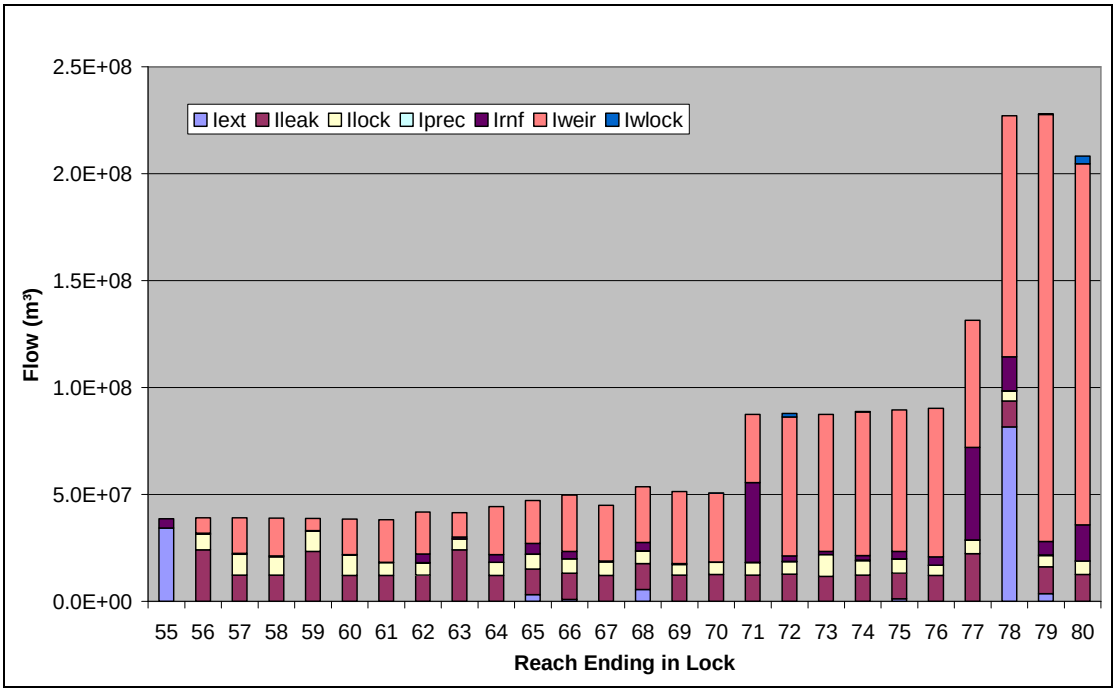

Figure 57. Relative contribution of various inflows to the total inflow into each reach of the Kennet and Avon Canal.

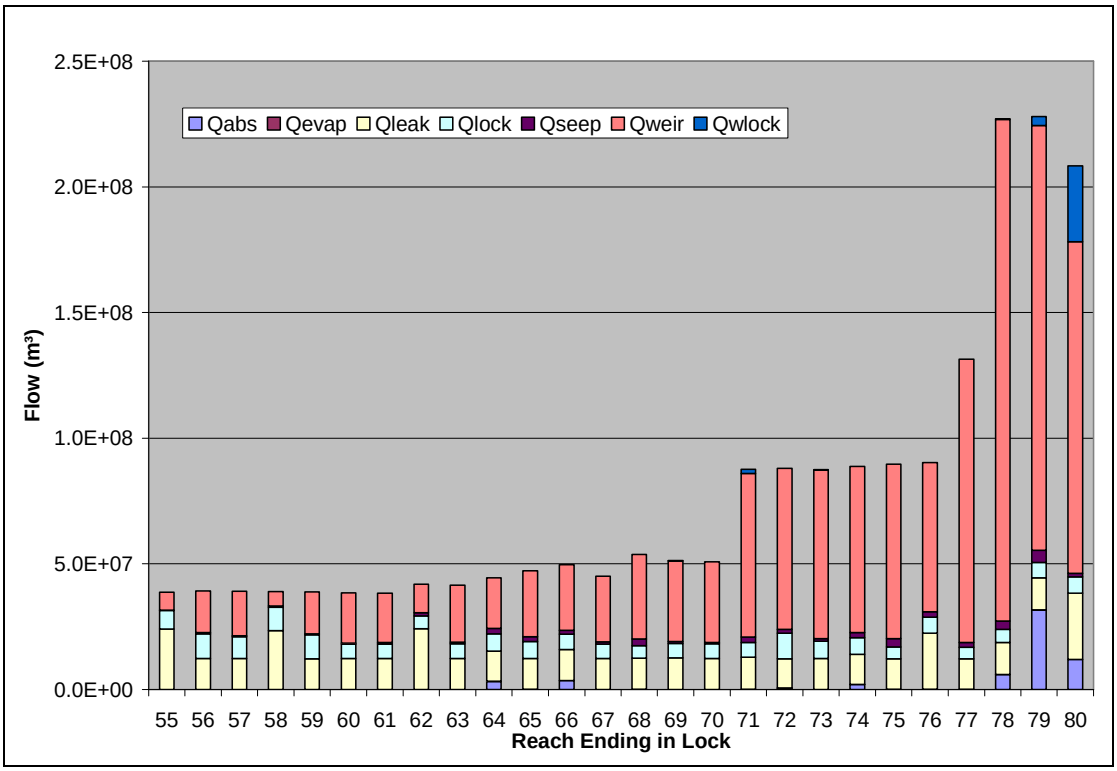

Figure 58. Relative contribution of various outflows to the total outflow from each reach of the Kennet and Avon Canal.

7.2.4.2. Inorganic Sediment

The inorganic sediment behaves as one might expect (non-cohesive inflows: Figure 59; non-cohesive outflows: Figure 60; cohesive inflows: Figure 61; cohesive outflows: Figure 62). Losses through the weir are minimal despite the major flow being through this route; this is because most of the suspended sediment in the reach deposits by the time it reaches the overflow weir, with the exception of that disturbed by boats in the immediate vicinity of the overflow weir. A large slug of sediment moves from one reach to the next with each lockage; this is expected as the water used to fill the lock is drawn from the bottom of the water profile. Additionally, this movement happens in direct association with the sediment disturbance caused by boat traffic. The other primary source of transfer from one lock to the next is through leakage, which again draws from the entire water column. These movements of sediment from one reach to the next are minor in comparison with the huge amounts of sediment disturbed by boats in passing. Likewise, the amount of sediment deposited out of suspension is the primary 'outflow' route for sediment in a given canal reach. There are only a few differences in the overall pattern for cohesive sediment vs. non-cohesive sediment: the cohesive sediments do have some outflows via the overflow weir, and external inflows are assumed to include cohesive sediments but not non-cohesive sediments. The total amount of sediment involved in transport is greater for cohesive than for non-cohesive sediment, principally due to the soil texture in the area (see Section 2.5.1), dominated by cohesive sediments.

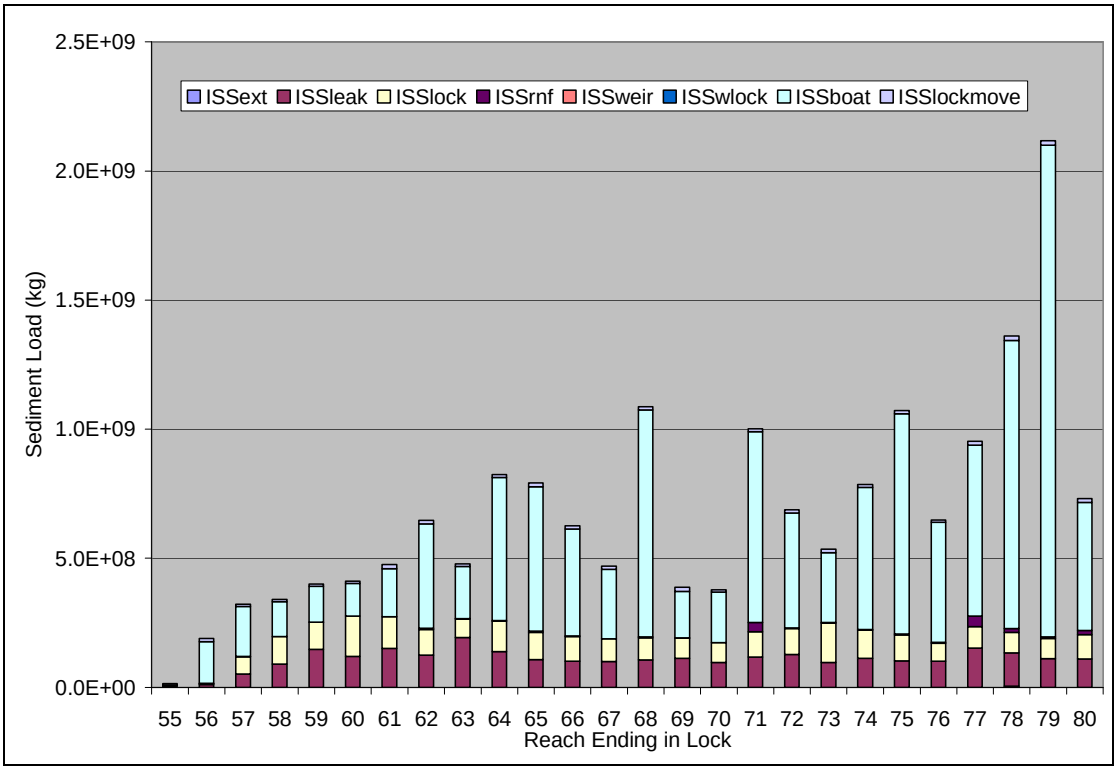

Figure 59. Breakdown of non-cohesive sediment inflows to each reach in the Kennet and Avon Canal.

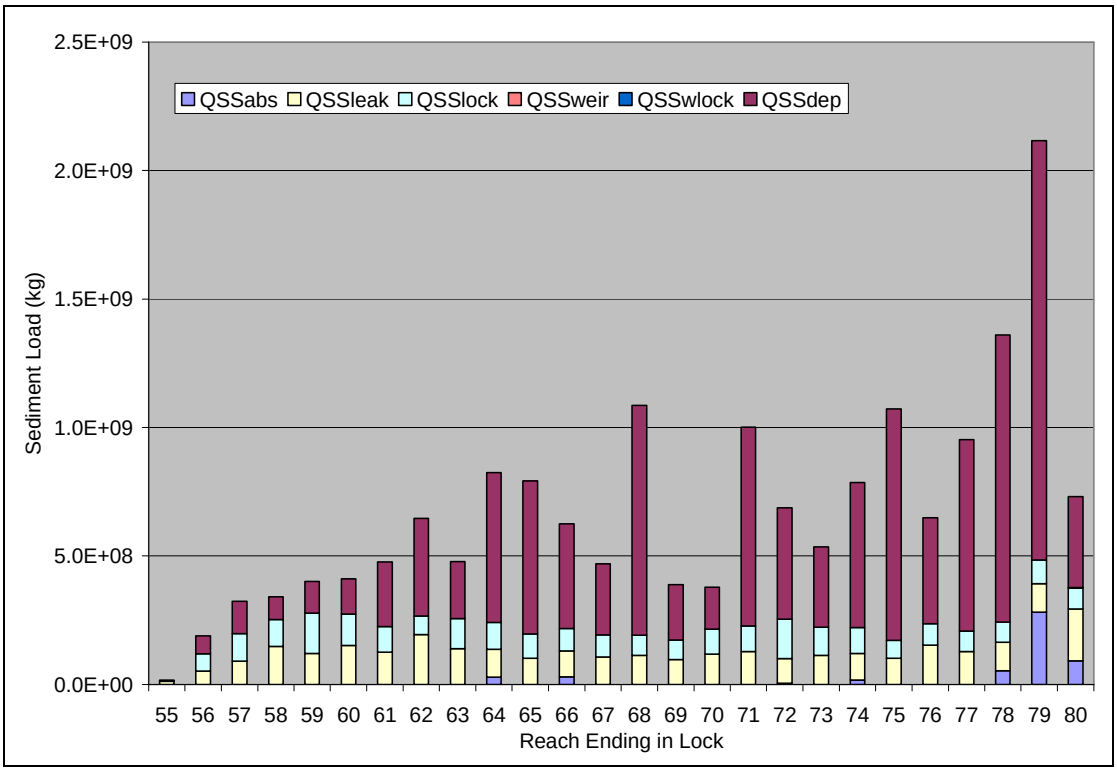

Figure 60. Breakdown of non-cohesive sediment outflows from each reach in the Kennet and Avon Canal.

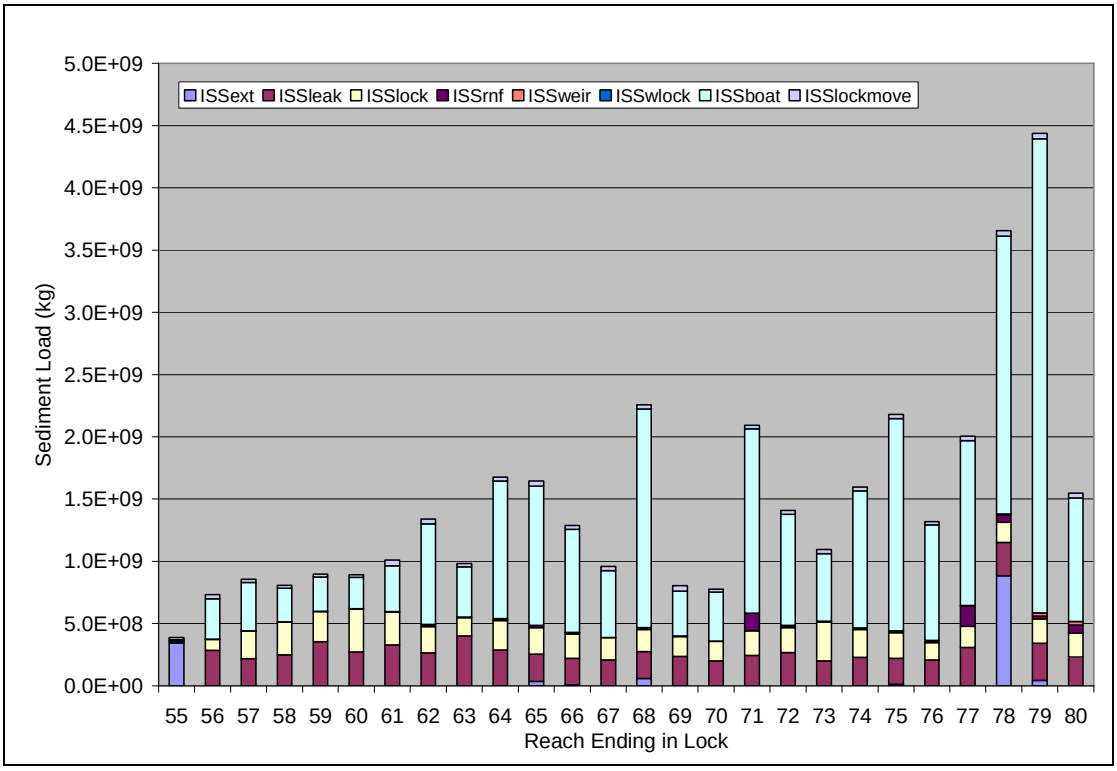

Figure 61. Breakdown of cohesive inflows to each reach in the Kennet and Avon Canal.

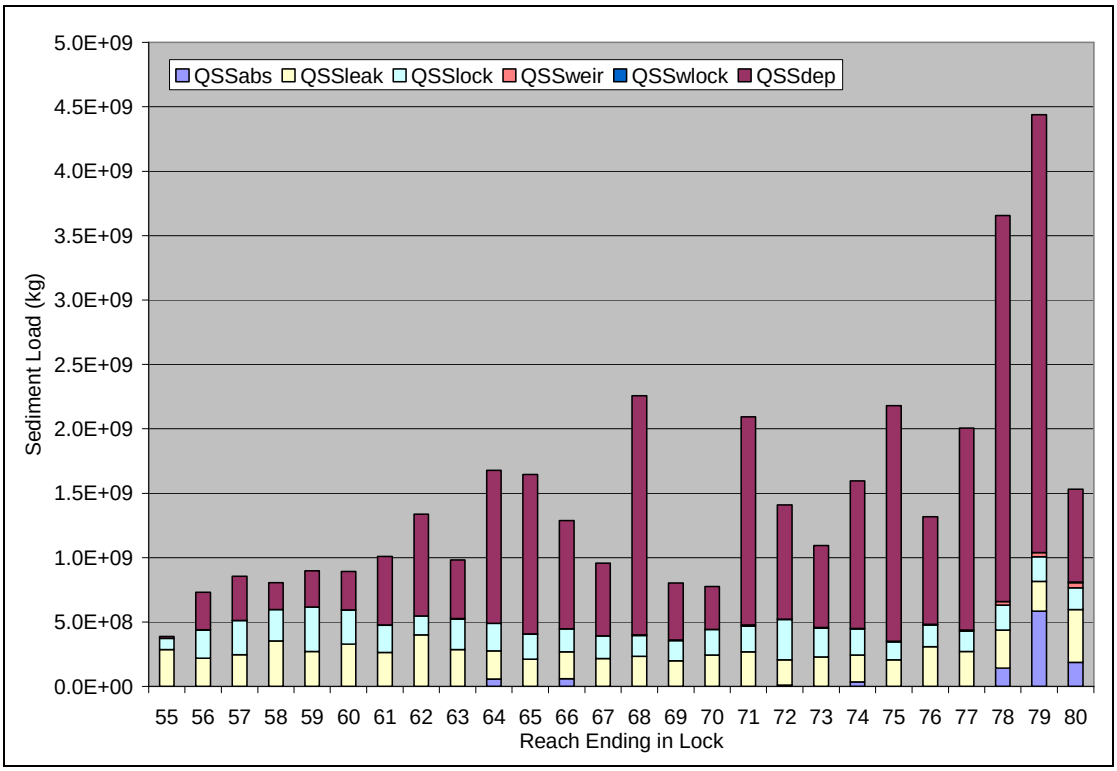

Figure 62. Breakdown of cohesive outflows from each reach in the Kennet and Avon Canal.

7.2.4.3. Algae

As would be expected with a constituent that remains suspended in the water column, the movement of algae from reach to reach largely follows the same pattern as that of the water (Figure 63, inflows; Figure 64, outflows) – weir flow dominates, followed by leakage and then lockage. The interesting thing to glean from Figure 63 is that the total movement of algae from reach to reach is governed primarily by growth in the reach. That is, at the summit reach, there are very little algae available to transport downstream; but in each reach, the total algae available for transport is increased by the amount of growth in the reach. Thus, the high transport seen in the most downstream reaches is simply a result of the growth that has occurred in the upstream reaches. If this growth can be slowed, the total algal transport will reduce throughout the system.

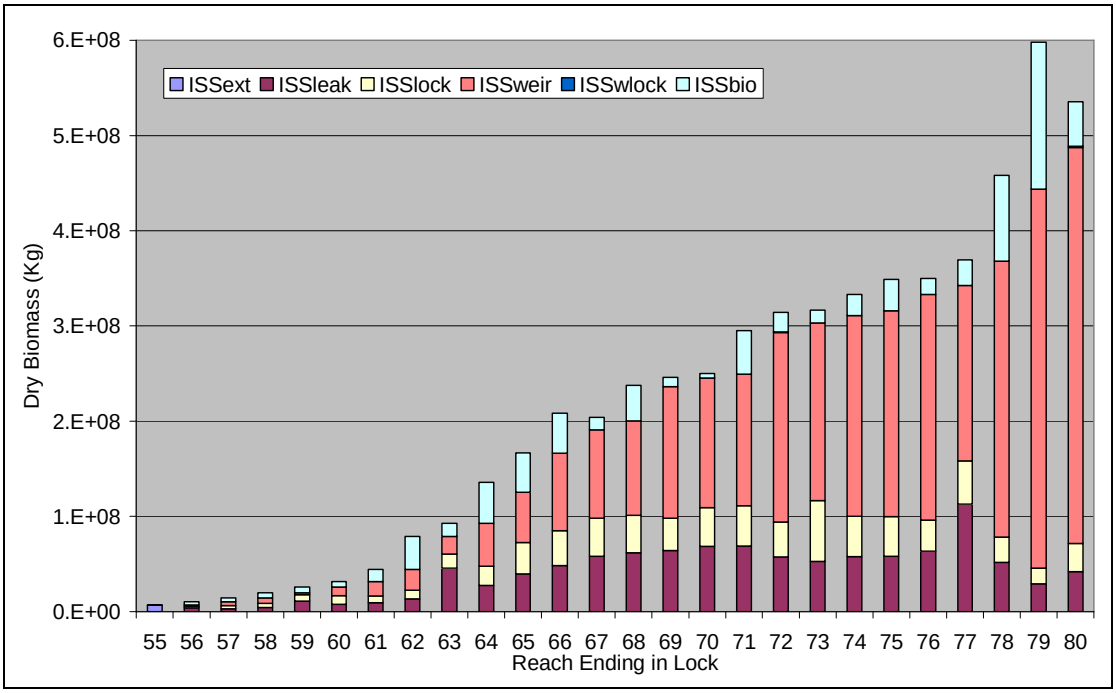

Figure 63. Breakdown of algal inflows to each reach in the Kennet and Avon Canal.

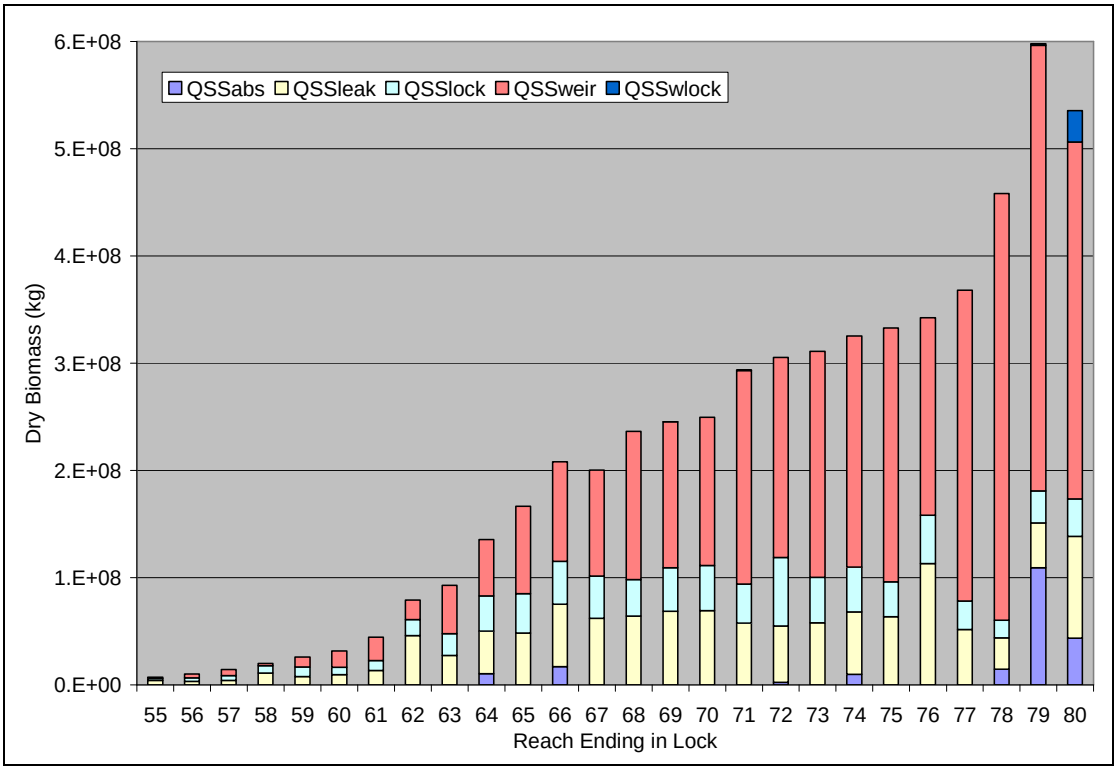

Figure 64. Breakdown of algal outflows from each reach in the Kennet and Avon Canal.

The components of algal growth rate at two points in the canal were investigated to further illuminate the factors involved in algal growth (at the reach ending in Lock 60 (Figure 65) and the reach ending in Lock 79 (Figure 66)). In both graphs, the top line (MuMaxT = $\mu_{max,T}$) represents the maximum growth rate as determined by temperature only; the middle line (MuMax = μ_{max}) represents the maximum growth rate as further modified by available light; and the bottom line (Mu = μ) represents the final growth rate used in Equation 55, as modified by available phosphorus. Light intensity (LI) is plotted on the right axis for reference. It is clear that the amount of sunlight available never allows the growth rate to reach its fullest potential as defined by the temperature; this is not surprising given the latitude of the study area, as insolation at 51ºN would commonly be half that found at even a latitude of 25ºN for many seasons of the year (Hamon et al. 1954). The differences in the trend in the 'Mu' curve for the two locations are interesting. Above Lock 60, the algal population is not great, and the growth rate is typically unhindered by phosphorus concentrations, with the exception of the peak of summer, when algal populations are at their peak while phosphorus concentrations are at their minimum. By contrast, phosphorus is noticeably limiting further downstream above Lock 79; with the exception of a couple months in the winter, the algal population continually pushes the cap imposed by

phosphorus, as evidenced by the degree to which μ is reduced year-round compared to μ_{max}. Thus, minor reductions of phosphorus in the upstream reaches of the canal will likely have little effect on algal populations, but the same reductions farther downstream would have a more noticeable effect.

The final component presented in the growth rate figures is the light intensity. This follows an interesting trend that bears analysis. The light intensity is driven both by solar radiation and by shading from sediment and algae within the stream (Appendix A.3). Thus, the light intensity reaches a trough during the winter months, when incoming solar radiation is at its lowest. Light intensity peaks in the spring, when days grow longer and boat traffic is not great. During the summer light intensity actually decreases, due to shading from the boat-disturbed sediment and self-shading from increased algal populations. The light intensity continues to generally decline through the autumn months as incoming solar radiation decreases, with an interesting mini-peak in October. In October the boat traffic noticeably drops off, thus significantly decreasing the shading due to sediment, so much that the light intensity available to algae in October is actually higher than in September even though solar radiation in October is lower than solar radiation in September. This is the reason for the perhaps higher-than-expected algal concentrations in the autumn months seen during model calibration. It is clear that boat traffic in these crucial 'swing' months (spring and autumn) will have a great influence on the amount of light available to the algae. A reduction in boat traffic, though beneficial in terms of reductions in the total sediment concentration, would actually increase the algal concentration by increasing light available for growth.

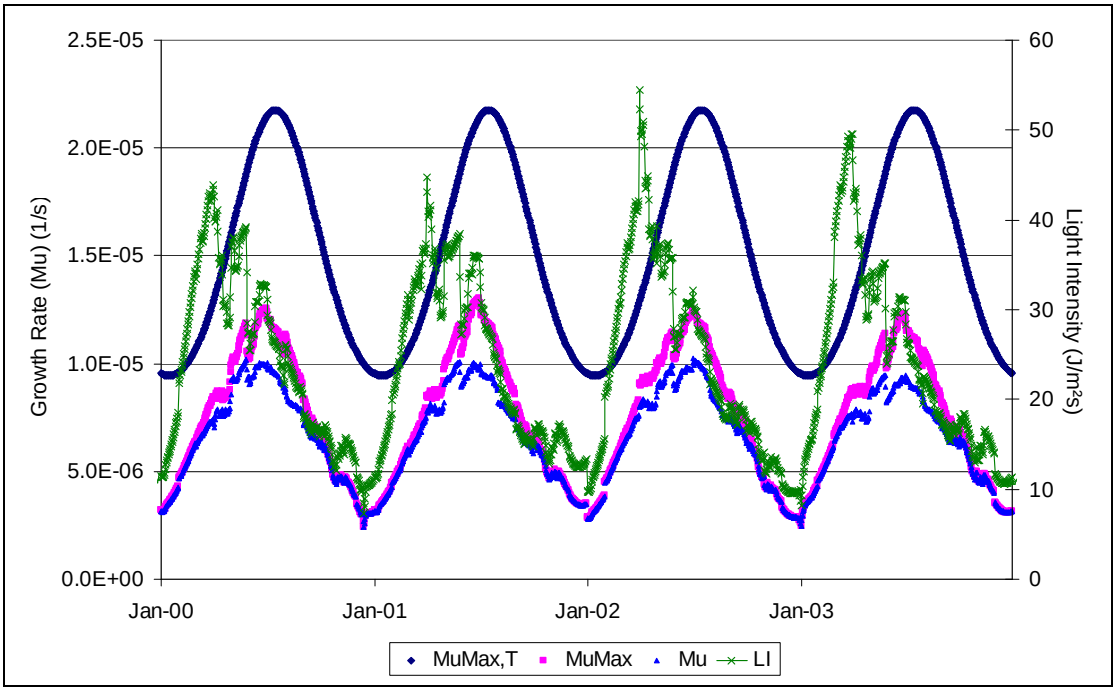

Figure 65. Seasonal trends of growth rates and light intensity for the reach ending in Lock 60.

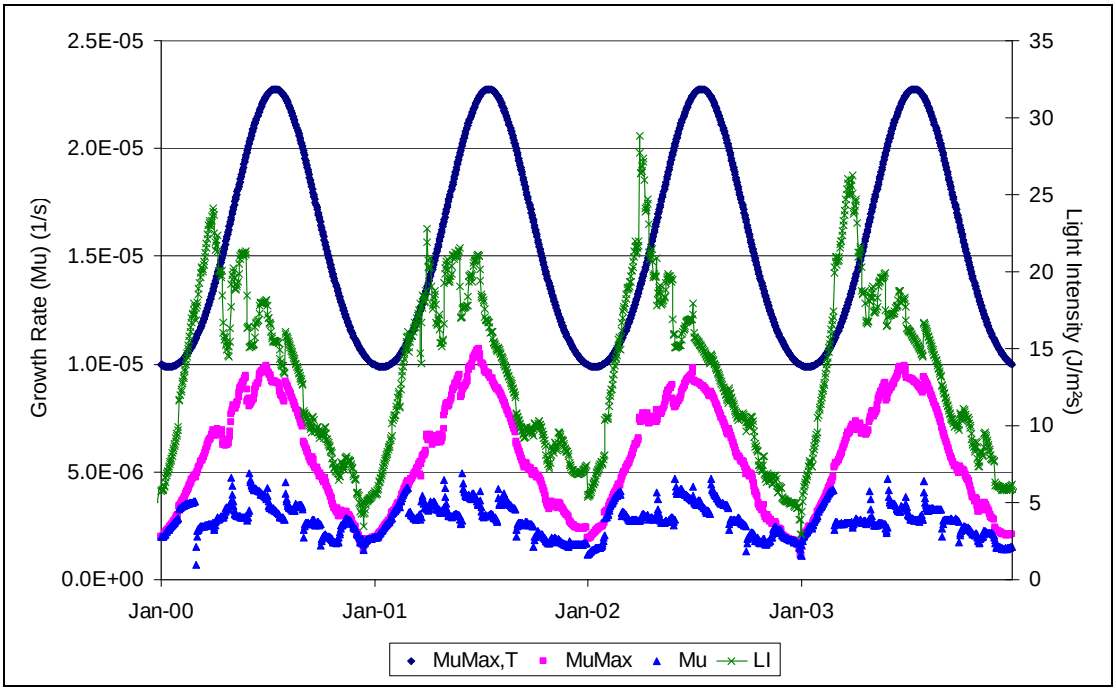

Figure 66. Seasonal trends of growth rates and light intensity for the reach ending in Lock 79.

7.3. Kennet and Avon Canal Management Options

As can be seen in the sensitivity analysis (Table 10) and the details of the calibrated model (Section 7.2.4), light intensity and phosphorus concentration in the Kennet and Avon Canal are key drivers of its algal concentration. Boat traffic is most influential

on the inorganic sediment concentration in the reach (Table 10, Figure 59, Figure 61), but decreases in boat traffic can be expected to have an adverse effect on the concentration of algae in the reach. Any successful management options must address these multiple and interrelated issues.

As has been previously discussed (Section 2.5.1), the primary area of concern in the studied system is the poor water quality brought from the Kennet and Avon Canal into the River Kennet where the two join just below Copse Lock (Lock 80). Officials at the Environment Agency have worked with an external contractor to arrive at a suite of potential management solutions to the water quality problem in the River Kennet downstream of Copse Lock (Halcrow Group Limited 2007). The short list of options presented in that report are:

1. 'Do minimum' - dredge reaches
2. Divert feeder streams
3. Install cross-drainage culverts
4. Install on-line filtration of canal flow
5. Reduce storm runoff entering canal
6. Reduce volume of poor quality water from canal into river
7. Control effluent discharge
8. Treat canal water
9. Separate canal and river

These will be addressed individually in this section. The results of the scenarios are first presented with reference to dry solids (being equivalent to what has been measured in the canal). Under existing conditions algae constitute about 15% of the observed total suspended solids (see Figure 67, where algal mass is calculated based on observed chlorophyll-a data modified by the conversion of chlorophyll-a to algal mass used in modeling, 60 mg dry algal mass/mg Chl-a). However, the dry mass of algae that contributes to the measured total suspended solids concentration is a factor of 16 lower than what might be expected for the *in situ* (wet) suspended solids (Table 1, page 38; Figure 68). This means that the water with high turbidity visually observed in the canal is composed of both the (dry) total suspended solids and an additional wet weight for the live algae, so that the actual effect visible to observers on the canal is worse than the effect expected from the laboratory analysis of the dessicated algae. In the scenarios discussed in the following subsections a

comparison is done both according to changes that might be observed solely from laboratory analysis of dried solids and changes that might be observed visually in the canal of sediment and live algal mass.

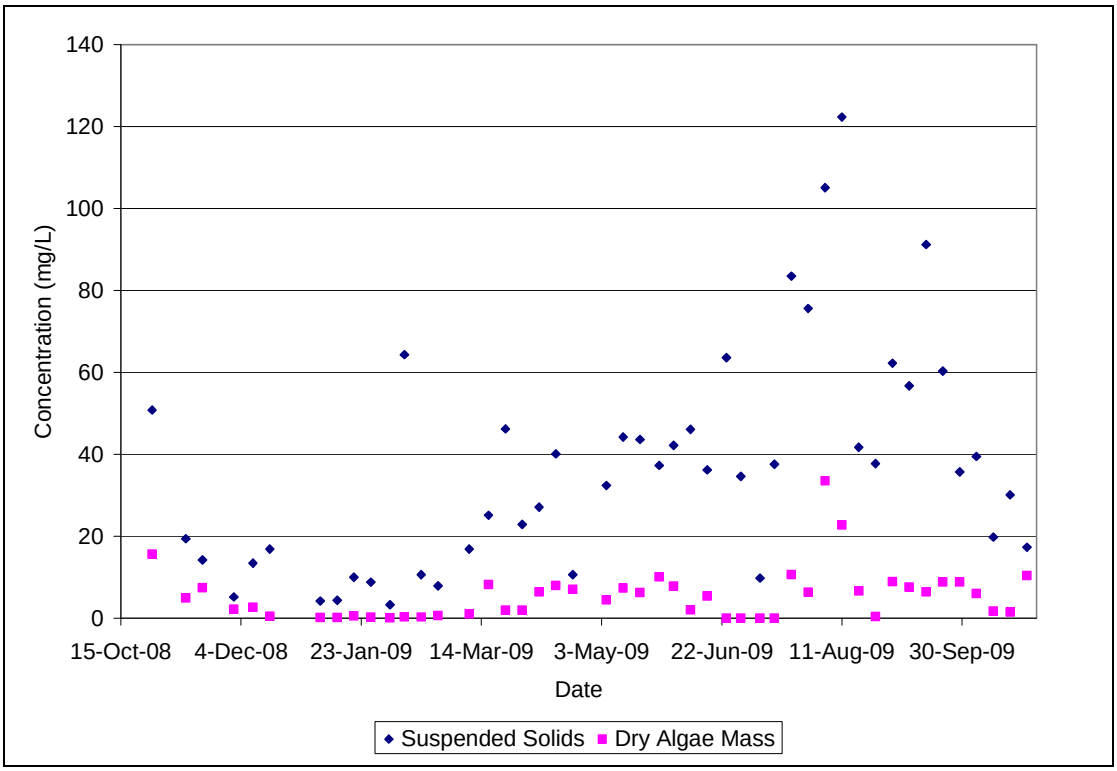

Figure 67. Observed algal dry mass and total suspended solids at the Copse Lock sampling station.

Note that because phosphorus is not modeled, any side effects that might result in a decrease in in-stream phosphorus concentrations (e.g., in a decrease in sediment-attached phosphorus in the water column due to less sediment disturbance by boats) are not evaluated. However, given the relatively non-fluctuating nature of the observed phosphorus concentrations, it is not expected that these potential side effect phosphorus influences would be significant.

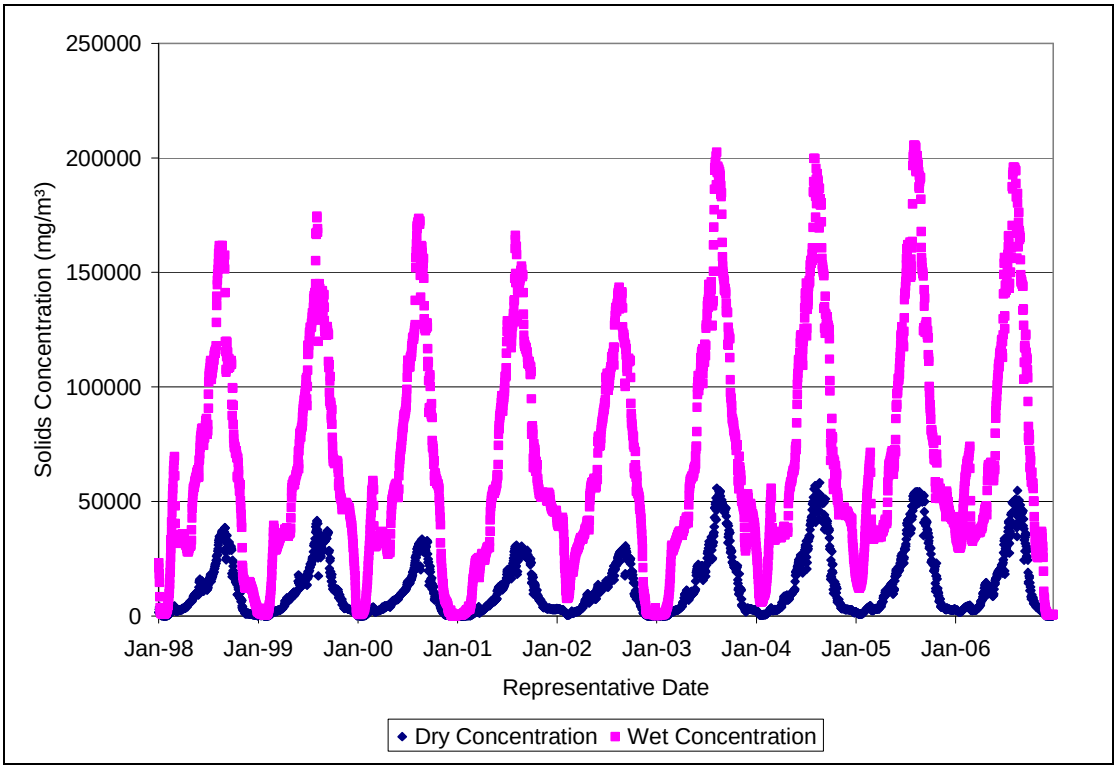

Figure 68. Wet and dry solids concentrations modeled in the Kennet and Avon Canal.

7.3.1. Do Minimum

The Environment Agency considers a 'do minimum' approach to involve dredging the canal reaches near Copse Lock. This would have the effect of increasing the depth of the canal, thus reducing the amount of sediment disturbed as boats pass, both by reducing the sediment available to disturb and by lowering the bottom of the canal away from the zone of disturbance caused by boat propellers. In consideration of this latter effect: it was previously demonstrated (Figure 17) that sediment disturbance generally happens intensively within the boat's width; a logical extrapolation of this would be that there is a circular pattern of disturbance around the propeller of the boat (case a, Figure 69, includes typical dimensions for the Kennet and Avon Canal under current conditions). If the canal can be dredged to the point where this zone of disturbance does not intersect the bottom of the canal (case b), the amount of sediment disturbed by boat passage might be greatly reduced. Even if this amount of dredging is not possible, if the area on the bottom of the canal that the zone of disturbance covers could be reduced (case c), some effect could be seen on boat-generated sediment.

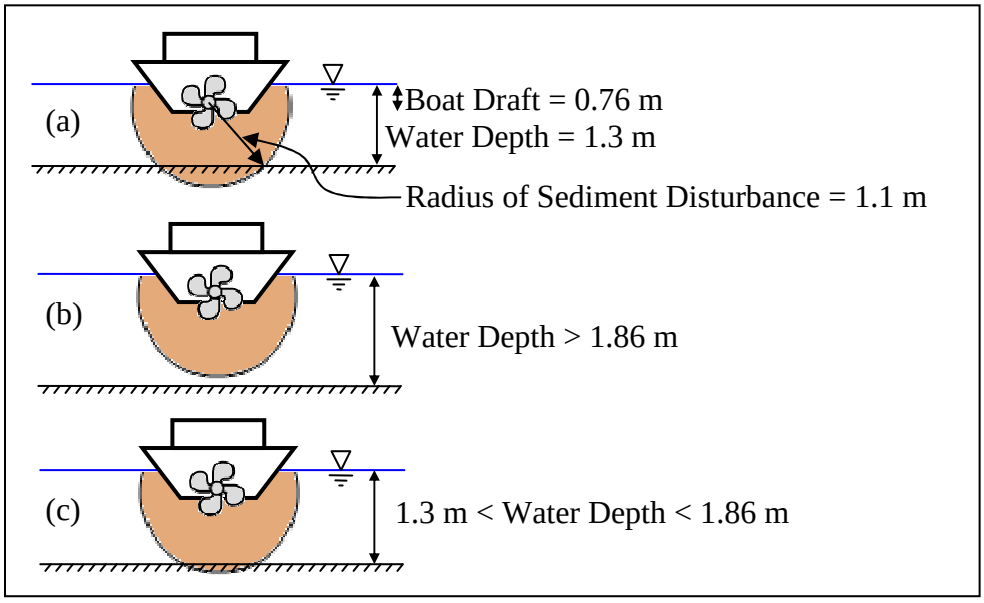

Figure 69. Influence of water depth on boat-disturbed sediment.

To evaluate the potential benefits of this scenario, the canal model was executed using a 50% and 90% reduction in CS_{boat} compared to the concentration of sediment disturbed by boat passage under existing conditions (this was applied to the entire length of the canal). The results of these scenarios on the sediment concentration at Copse Lock are shown in Figure 70. Clearly, this reduction in boat-generated sediment would have a sizeable impact on the total dry solids concentration in the canal, and thus on the total dry solids concentration entering the River Kennet. However, without an accompanying decrease in sediment entering the canal, sediment inputs from surface runoff, point sources, and upstream canal reaches would accumulate over time, eventually negating the impact of the dredging option. If the solids are considered including the live biomass of algae, the effect of this scenario is diminished, as the sizeable reduction in inorganic sediment concentration permits more light to penetrate the water column, allowing a higher growth rate for algae, so that the additional live biomass of algae nearly completely replace the sediment removed by this option.

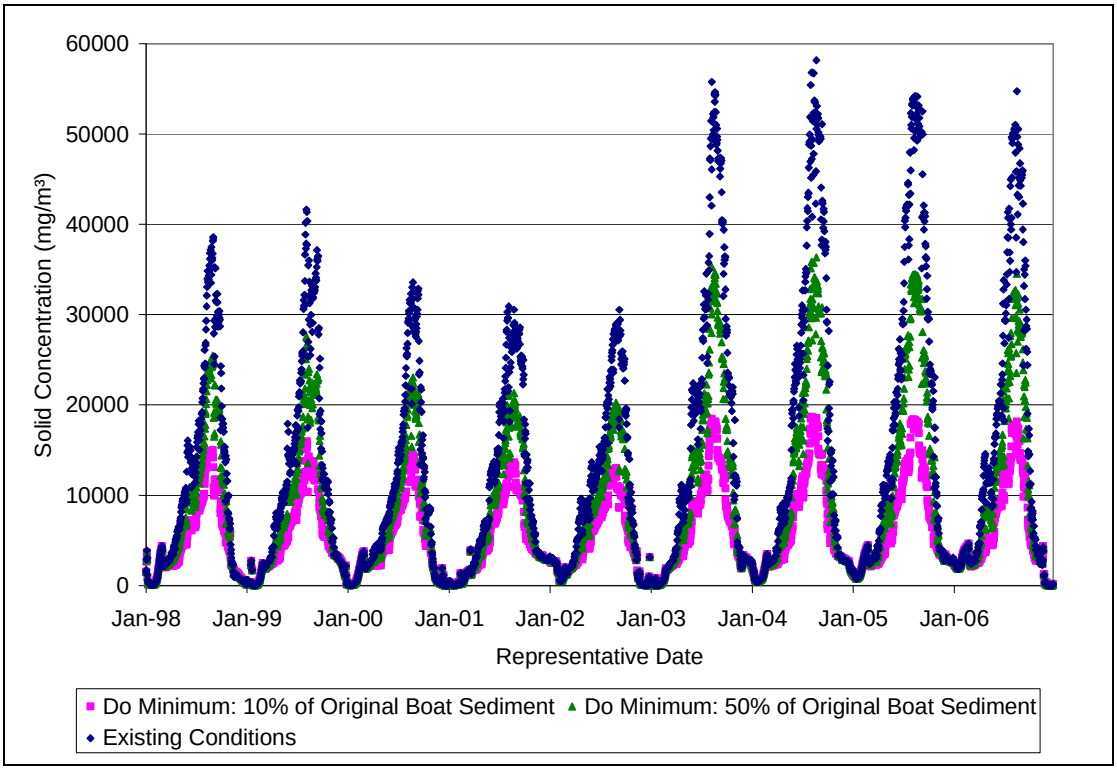

Figure 70. Reduction in dry solids concentration in outflows from Lock 80 under 'Do Minimum' management scenarios.

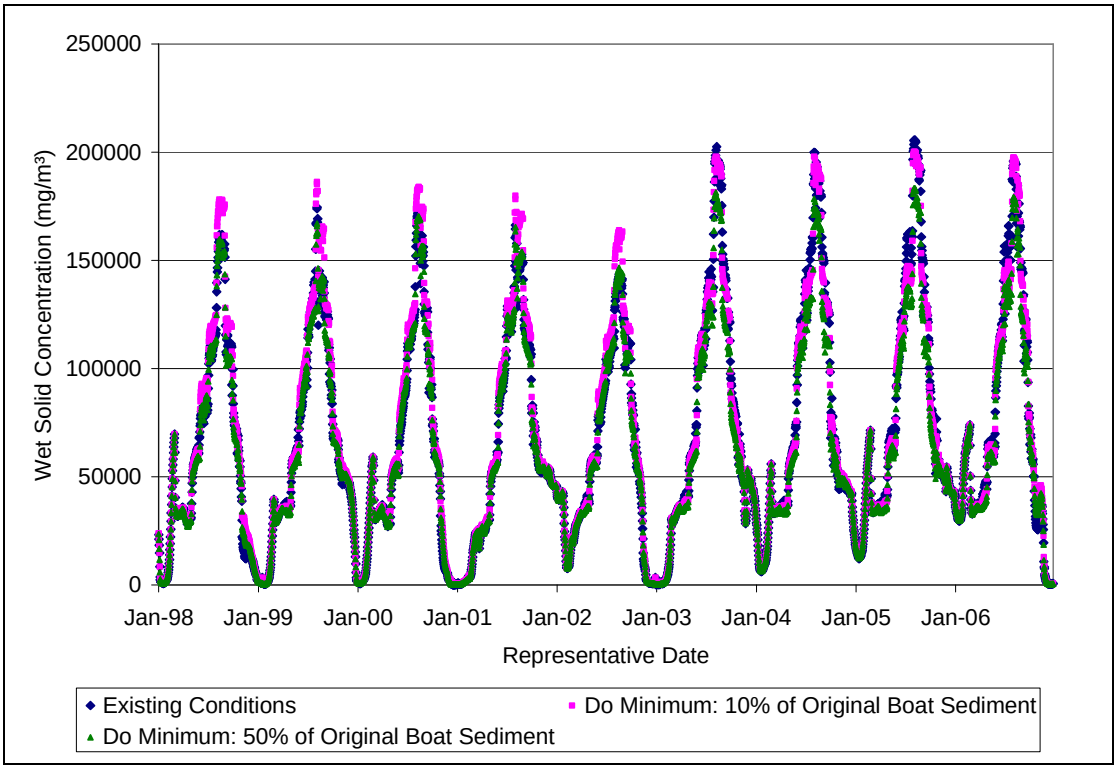

Figure 71. Reduction in wet solids concentration in outflows from Lock 80 under 'Do Minimum' management scenarios.

7.3.2. Divert Surface Flow

For modeling purposes, items 2, 3, and 5 from the short list of options have the same effect: reduce or divert surface flows to minimize the amount of sediment from the land surface entering the canal. In the canal model, this is effected by the reduction of runoff inputs and external inputs from the river to the canal. As was previously demonstrated in Figure 59 and Figure 61, runoff inputs of sediment to the canal are minimal compared to the sediment suspended by boat traffic. Thus, without the inclusion of the 'Do Minimum' option, this action can be expected to have little impact on the overall solids concentration in the canal, and in fact could have a detrimental effect by reducing the flow rate in the canal and thus providing a more hospitable environment for algal growth, a lower water depth (causing higher boat-generated sediment), and less dilution water for the boat- and lock-disturbed sediment and any remaining sediment transported from the land surface. The Halcrow Group proposal suggests that efforts might be targeted on the Kintbury Feeder (reach above Lock 78) and Peartree Bottom Stream (reach above Lock 80); thus, the effect of removing the feeder (external) input and the stream (runoff) input from only these two sources is shown in Figure 72 and Figure 73. Removing the considerable flow input from Kintbury Feeder and Peartree Bottom Stream causes a severe reduction in flow from Copse Lock, and thus the flow that does leave has a much higher concentration of solids, even though the load is lower (Figure 74). Because the Kintbury Feeder provides such a large volume of water to the canal, the input from Wilton Water to the summit reach must be tripled before the concentration of solids leaving Copse Lock under this scenario drops to the level of the existing conditions. Therefore, diversion of the Kintbury Feeder is considered undesirable.

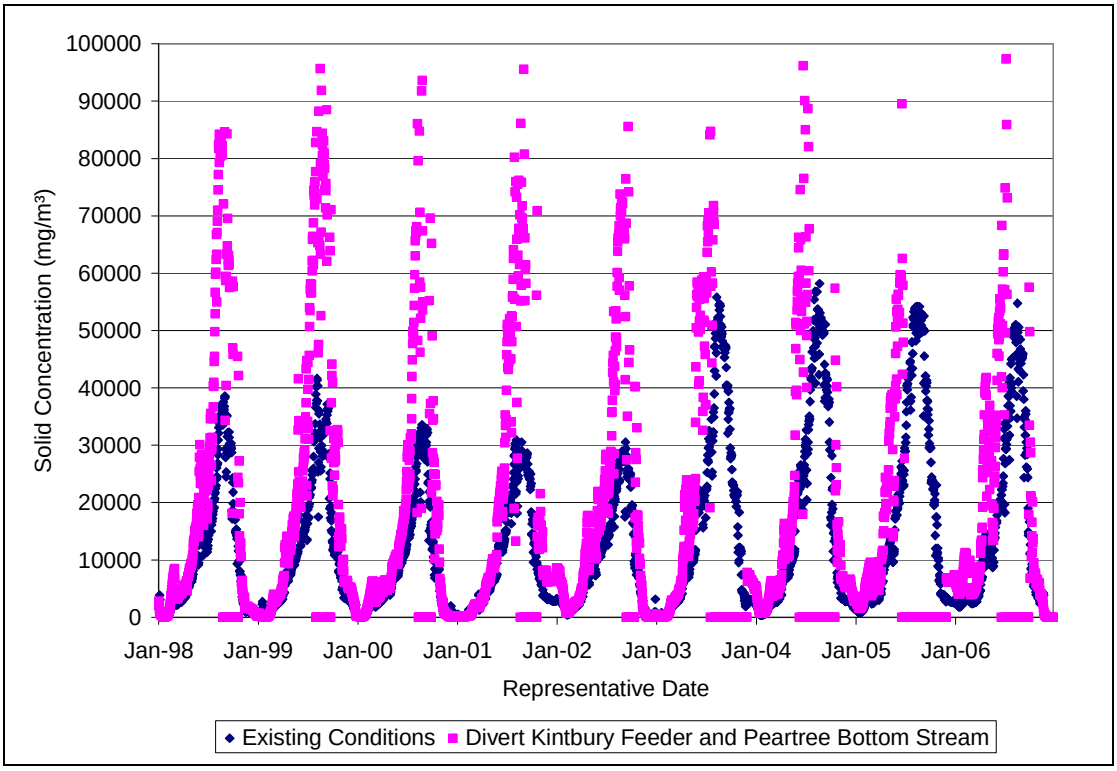

Figure 72. Change in dry solids concentration in outflows from Lock 80 under surface flow diversion management scenarios.

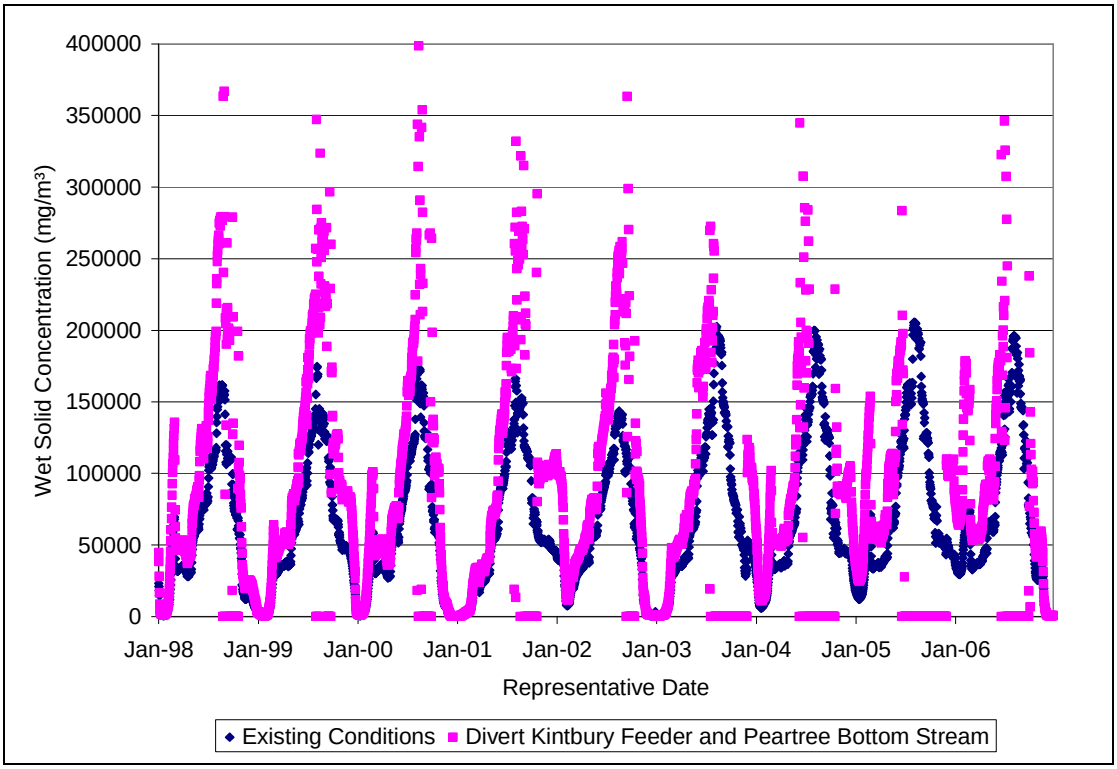

Figure 73. Change in wet solids concentration in outflows from Lock 80 under surface flow diversion management scenarios.

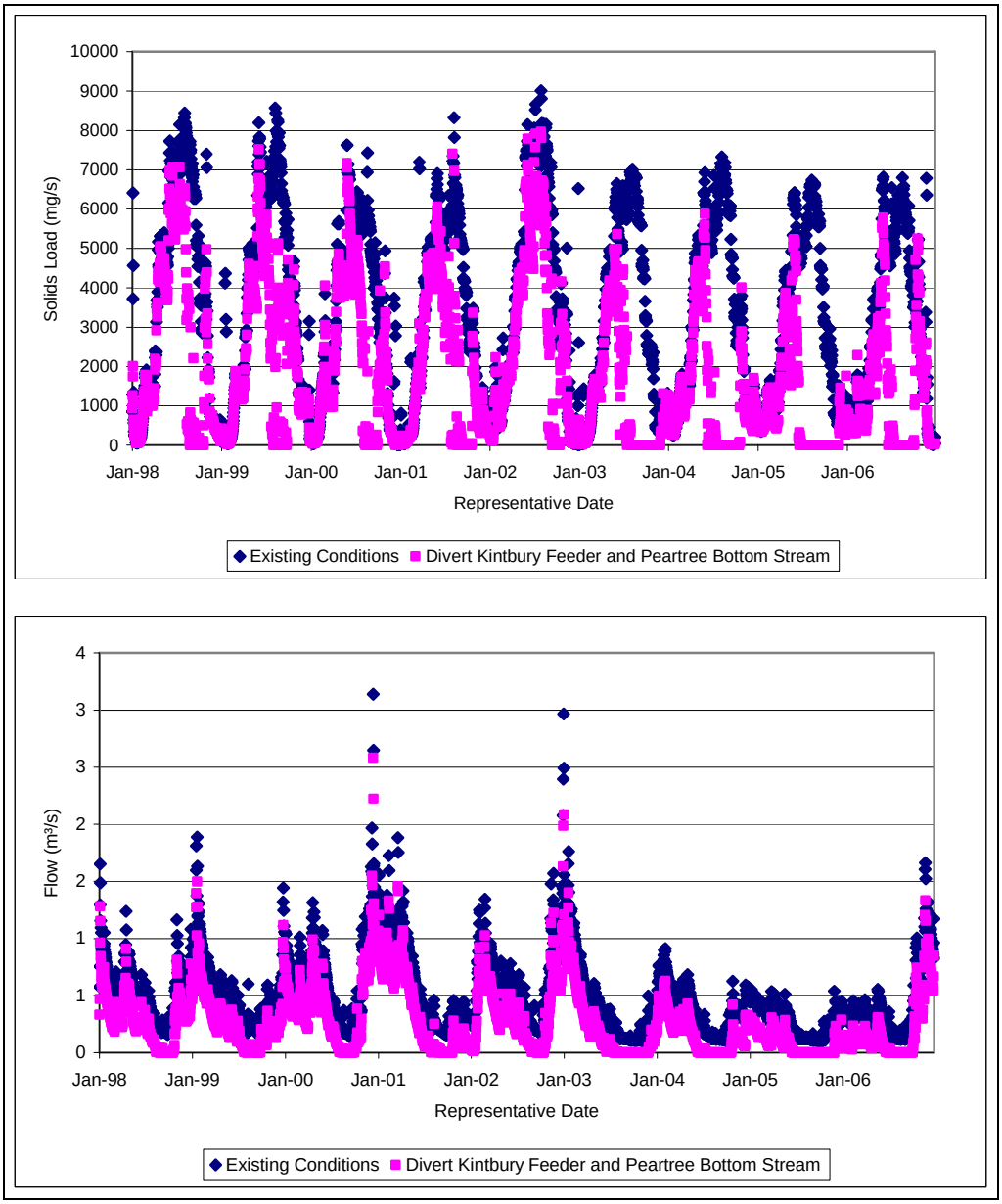

Figure 74. Change in dry solids load (top) and flow rate (bottom) from Lock 80 under surface flow diversion management scenarios.

7.3.3. Install On-line Filtration of Canal Flow

The Environment Agency proposes that the on-line filtration of canal flow option would involve installing reed beds in bypass channels around locks to filter nutrients and sediment from the water. This addresses filtration of the water involved in I_{weir} and thus the solids transported in ISS_{weir}. As was previously demonstrated in Figure 59 and Figure 61, inorganic sediment transported via weir flow is minimal due to deposition along the length of the reach. Thus, this can be expected to have a minimal effect on sediment transport and concentration. However, a large number of algae

pass through the overflow weir (Figure 63) and the reed beds would additionally filter out the phosphorus crucial to algal growth, so it is expected this scenario would have a noticeable effect on algal concentrations.

To evaluate the best possible implementation of this scenario, it was assumed that 65% of the water in the canal would pass through a reed bed (assuming a reed bed installed at each lock, with 65% of the total outflows due to weir flow (Figure 58)). Assuming phosphorus is fully mixed in the water column, this means 65% of phosphorus in the system will pass through a reed bed. Reed beds have a reported phosphorus removal efficiency of 3-85% (Green and Upton 1994; Gschlößl et al. 1998; Babatunde et al. 2008), with most values reported between 20-40%. For the purposes of this scenario, a removal efficiency of 30% was assumed for total phosphorus. Thus, the total phosphorus in each reach was assumed to be 19.5% (0.65*0.3) less than current levels. Additionally, sediment and algae were assumed to be filtered out of weir flows with the reported reed bed efficiency for sediment removal, 85% (reported literature values range from 72%-99%) (Green and Upton 1994; Gschlößl et al. 1998; Babatunde et al. 2008). The results of this scenario are shown in Figure 75 and Figure 76. This is the best case scenario; it is of course more likely that reed beds would be installed in (at best) only the weirs that are currently open to the air, significantly minimizing the effect of these measures. The scenario shows a significant drop in solids effluent from Copse Lock, particularly in the wet solids concentrations driven by algae, but requires a greater expenditure than many of the other options.

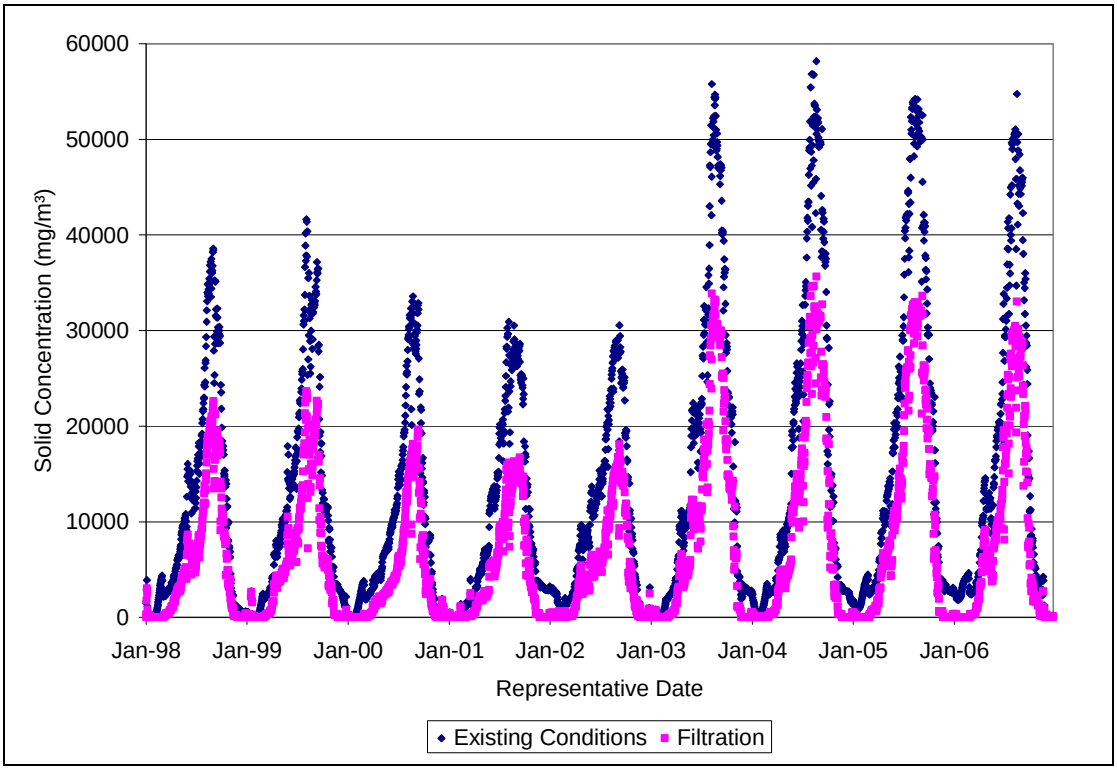

Figure 75. Reduction in dry solids concentrations discharged from Copse Lock for the filtration scenario.

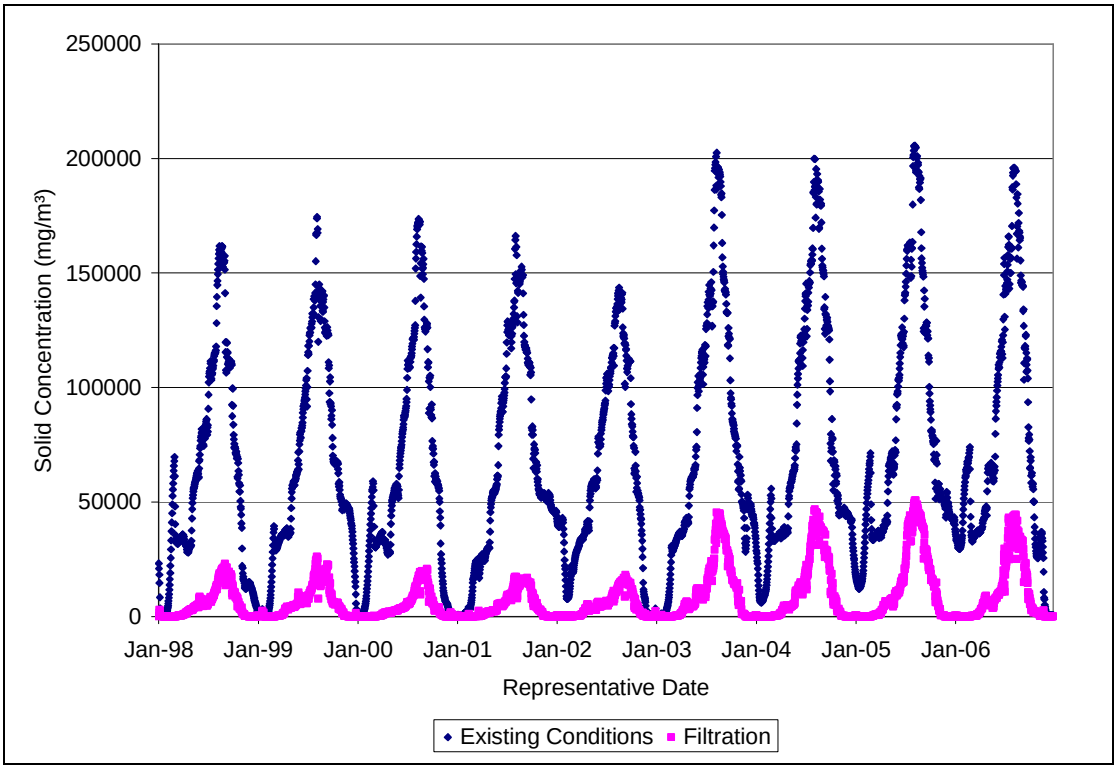

Figure 76. Reduction in wet solids concentrations discharged from Copse Lock for the filtration scenario.

7.3.4. Reduce Volume of Poor Quality Water from Canal into River

This scenario differs from the previous in that it proposes to route both weir and lock flow through a reed bed, but targets only areas like Copse Lock which would otherwise feed directly into the river. As this scenario addresses the transport of sediment with lockages, it has a greater potential than the previous scenario to attenuate inorganic sediment concentration. To implement this scenario in the model, it was assumed that all flow from Copse Lock would be routed through a reed bed, and thus sediment and algae were assumed filtered out of the flow from Copse Lock according to the reported reed bed efficiency for sediment removal, 85%. This procedure has the added benefit of targeting the problem just before its impact on the river, and can actually be evaluated in model post-processing, rather than by using the model itself. The results of this scenario are shown in Figure 77 (dry solids) and Figure 78 (wet solids). It is interesting to note that this scenario produces a comparable reduction in wet solids concentration and a much greater reduction in dry solids concentration flowing from Copse Lock compared to that of the 'filtration' scenario presented in Section 7.3.3; however, the current scenario requires only one reed bed to be installed, rather than twenty-six reed beds.

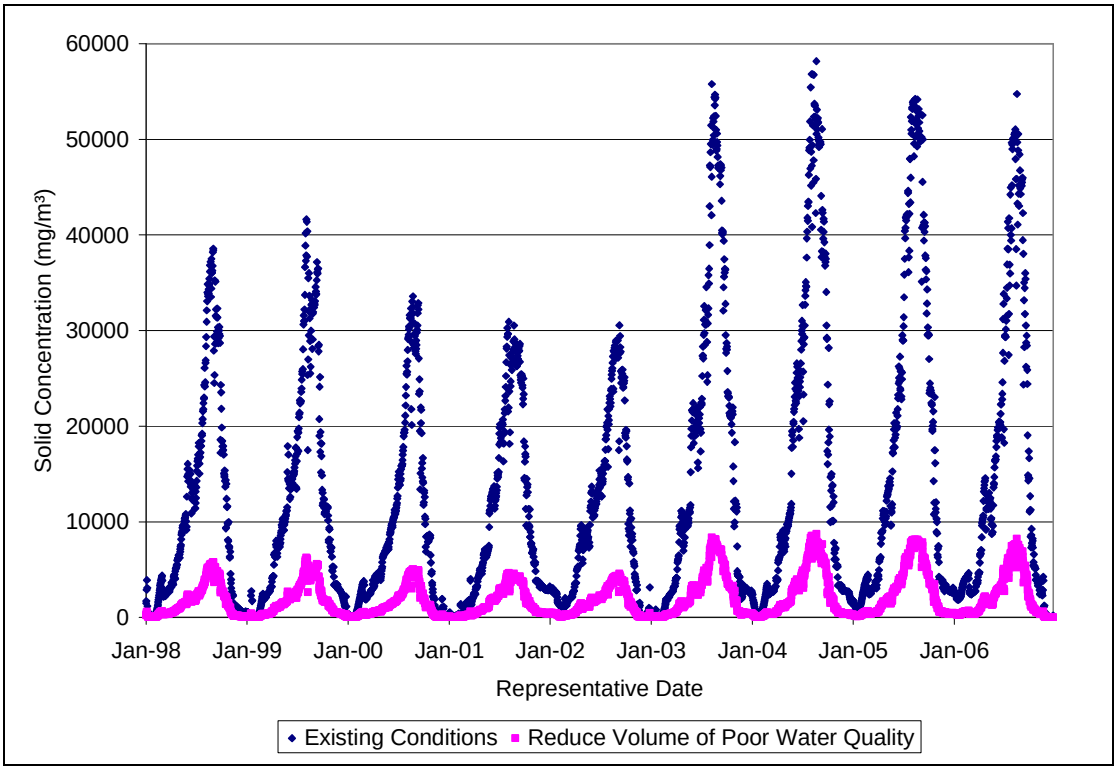

Figure 77. Reduction in dry solids concentrations discharged from Copse Lock for the poor water quality reduction scenario.

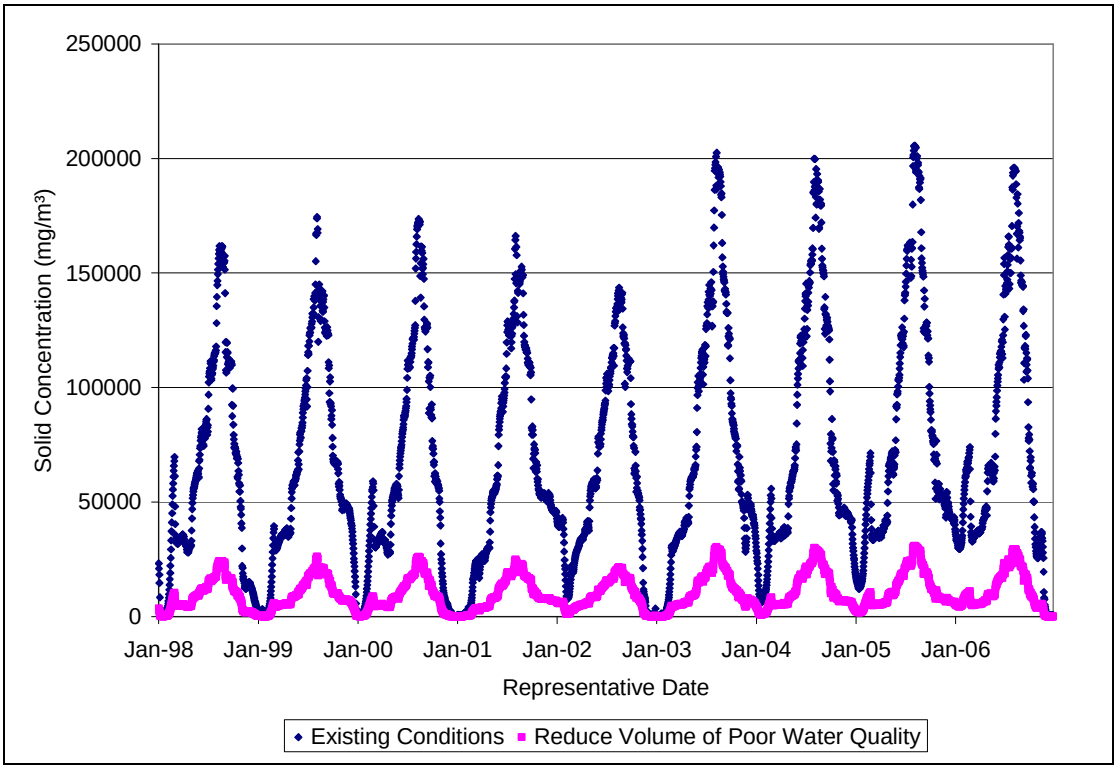

Figure 78. Reduction in wet solids concentrations discharged from Copse Lock for the poor water quality reduction scenario.

7.3.5. Control Effluent Discharge

This option proposes to target the flow from the sewage treatment works (STW) on the canal, either in improving discharge standards or in diversion of the effluent away from the canal to the river. The initial focus would be on the Kintbury sewage treatment works. As can be seen from Figure 59 and Figure 61, the inflow of sediment from the Kintbury sewage treatment works (represented in the figures by ISS_{ext} for the reach above Lock 79) is minimal, and thus any improvement in sediment discharge from the operation would have minimal effect on the canal water quality. However, reductions in phosphorus concentration could have a more noticeable impact through a control on algal growth. This impact was evaluated by reducing the total amount of phosphorus in the reach above Lock 79.

The Environment Agency has monitored the phosphorus concentration in the effluent from the Kintbury STW at an average of 5.7 mg/L. According to modeling efforts, the effluent water from the STW constitutes 1.6% of the total inflow to the reach above Lock 79. To evaluate the potential impact of improved phosphorus controls on the algal concentration in the canal, the model was executed, subtracting the concentration of phosphorus due to the Kintbury STW (0.016 * 5.7 mg/L) from the total phosphorus concentration in the reach above Lock 79 (Figure 79 (dry solids), Figure 80 (wet solids)). This is of course a best case scenario, removing all phosphorus originating from the Kintbury sewage treatment works; the actual result of phosphorus improvements would lie between the existing conditions and scenario presented in the figures. As can be seen from the results, the impact of this change is expected to be unnoticeable on the total dry solids concentration, and not very significant in terms of the wet solids concentration including the live biomass. In the reach above Lock 79, the algae have already become so abundant due to their growth in the previous 24 reaches that a minor setback to their growth in the reach above Lock 79 is nearly inconsequential. To evaluate the potential impact of diverting the STW flow from the canal, the same reduction in phosphorus was enacted, and the flows and sediment loads from the Kintbury STW were additionally removed from the canal (Figure 81). Removal of the Kintbury STW flows in this manner decreases the overall flow rate in the reach above Lock 79, thus increasing the hospitability of the water for algal growth. The effect on dry solids concentration is again

inconsequential; for wet solids, the flow and sediment diversion results in greater concentrations than when only phosphorus is reduced.

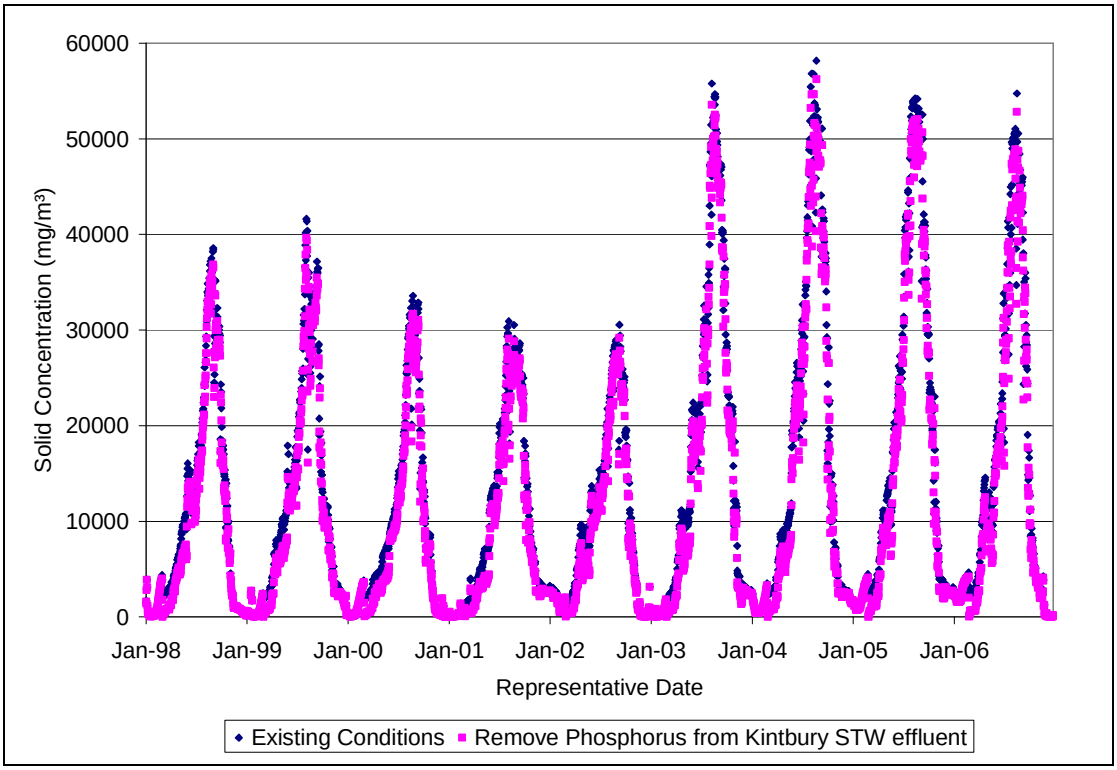

Figure 79. Reduction in dry solids concentration achieved by removing phosphorus from Kintbury STW effluent in the reach above Lock 79.

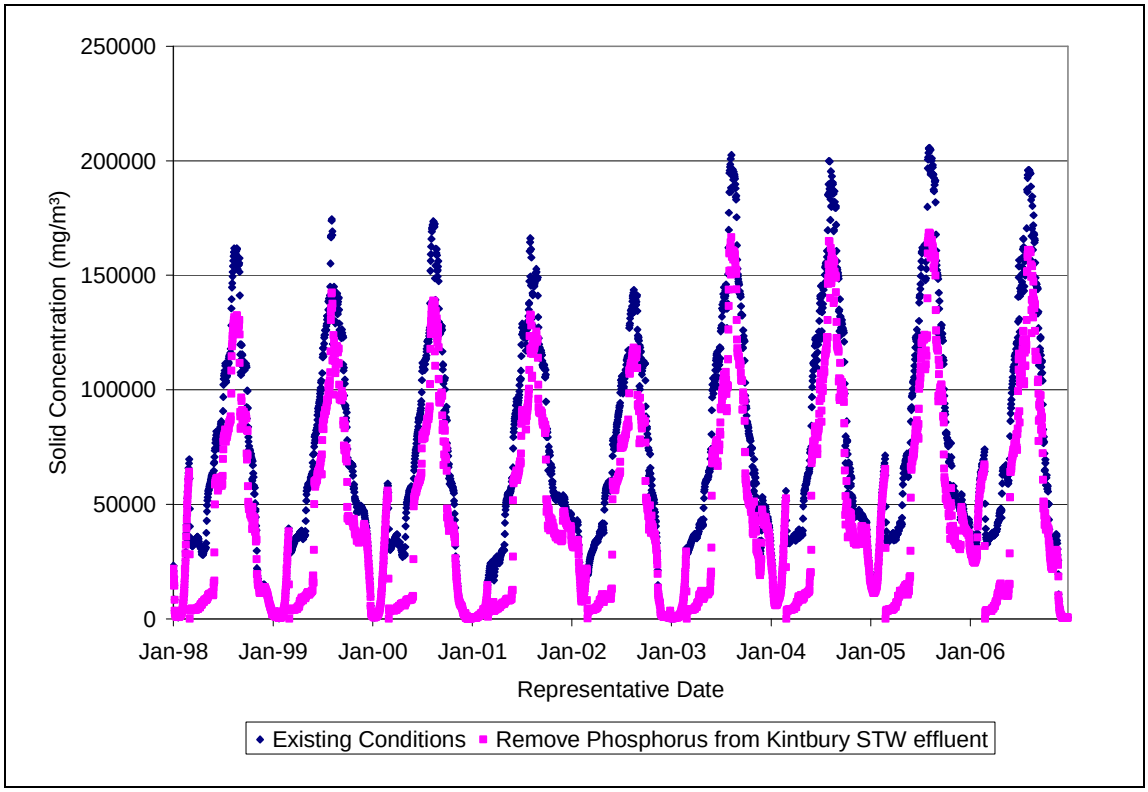

Figure 80. Reduction in wet solids concentration achieved by removing phosphorus from Kintbury STW effluent in the reach above Lock 79.

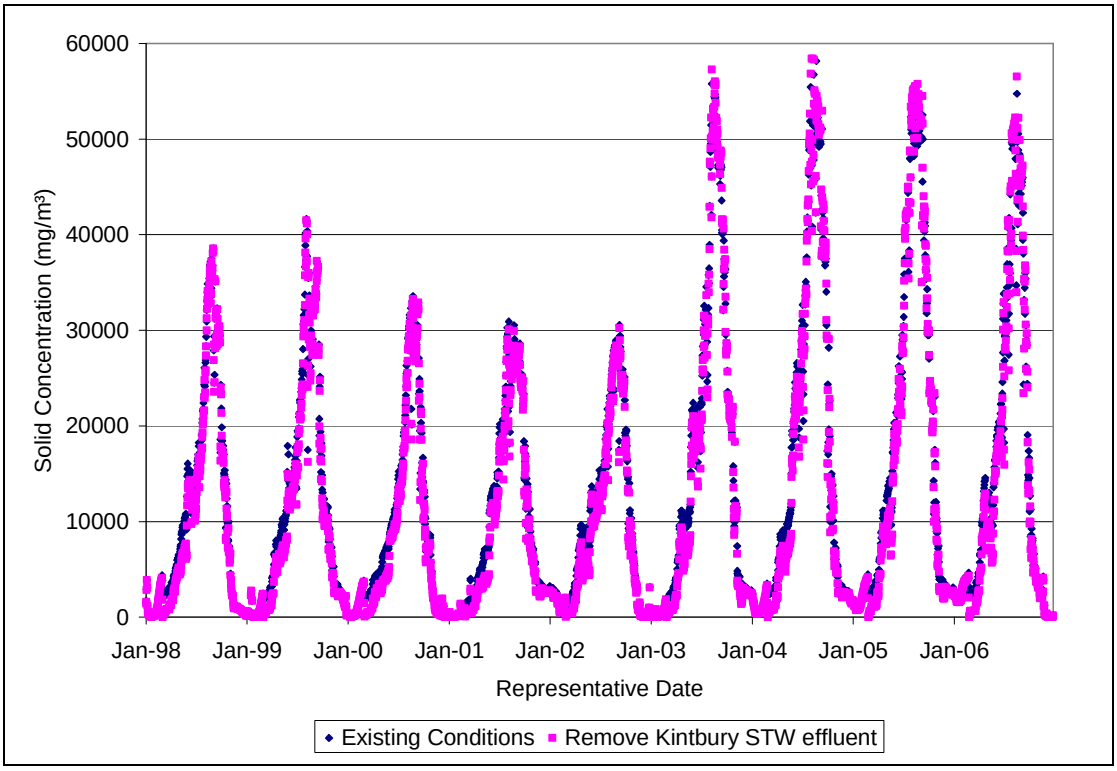

Figure 81. Effect (on dry solids concentration) of removing Kintbury STW flow, phosphorus, and sediment concentrations from the canal in the reach above Lock 79.

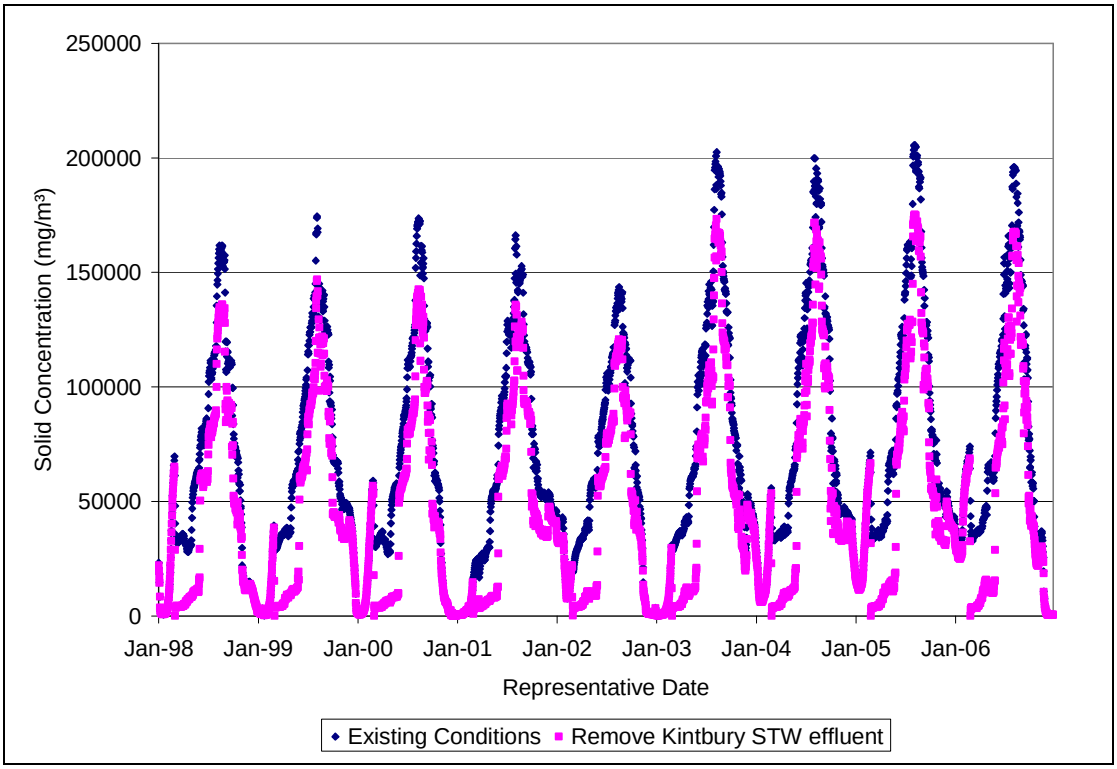

Figure 82. Effect (on wet solids concentration) of removing Kintbury STW flow, phosphorus, and sediment concentrations from the canal in the reach above Lock 79.

The phosphorus levels in the Kennet and Avon Canal are generally high and do not noticeably increase past the Kintbury STW (located in the reach above Lock 79) (Figure 83); in fact, the phosphorus concentrations observed at Kintbury and Copse Lock are typically the lowest recorded in the canal. Therefore, to restrict algal growth via phosphorus controls, it appears a systematic approach is needed, one that addresses all the elevated phosphorus concentrations in the canal. This could be accomplished by reducing phosphorus in effluents from all sewage treatment works contributing to the canal, as well as installing riparian buffer strips and/or implementing nutrient management planning in neighboring farmland to reduce phosphorus transported to the canal in surface runoff. The effect of reducing phosphorus concentration at all points in the canal to 0.05 mg/L (suggested as the level needed to reduce eutrophication in lakes and reservoirs) (Mueller and Helsel 1999) is shown in Figure 84 (dry solids) and Figure 85 (wet solids). As is evident, such a project would have a small effect on the measureable dry solids concentration, but a much larger effect on the wet solids concentration including the live algal biomass.

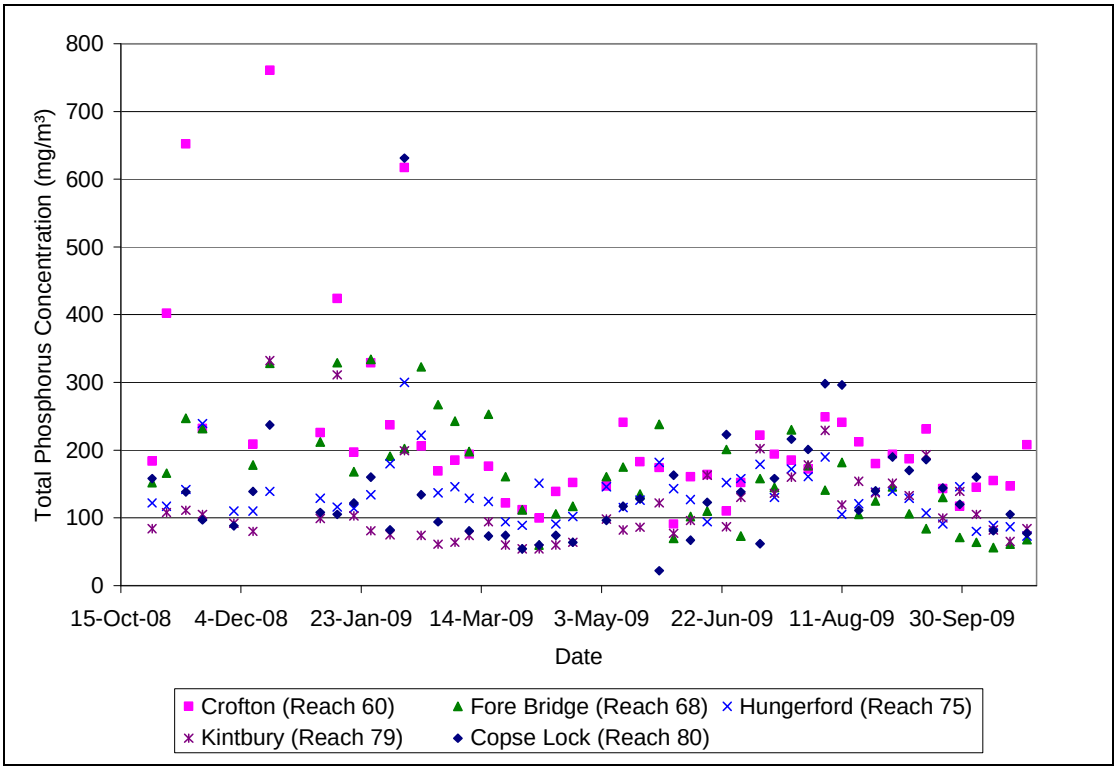

Figure 83. Observed Total Phosphorus concentrations in the canal. (Reach ##) indicates the reach above Lock ##.

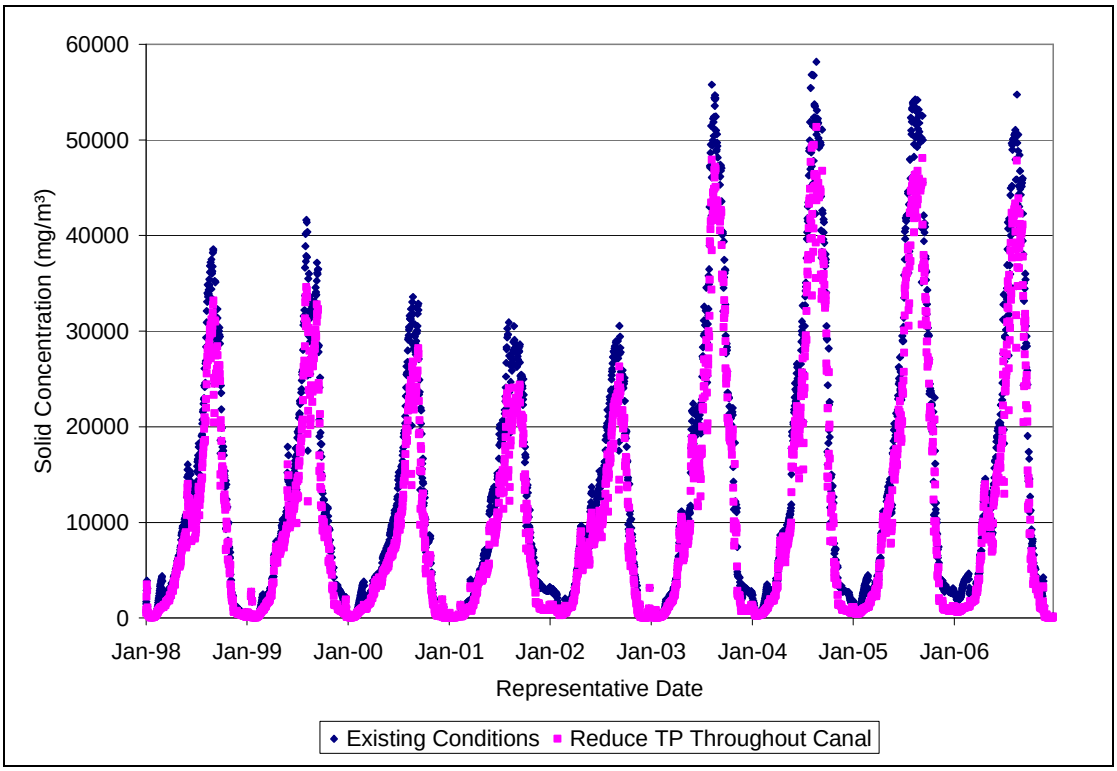

Figure 84. Reduction in dry solids concentration achieved by reducing phosphorus levels throughout the canal to 0.05 mg/L.

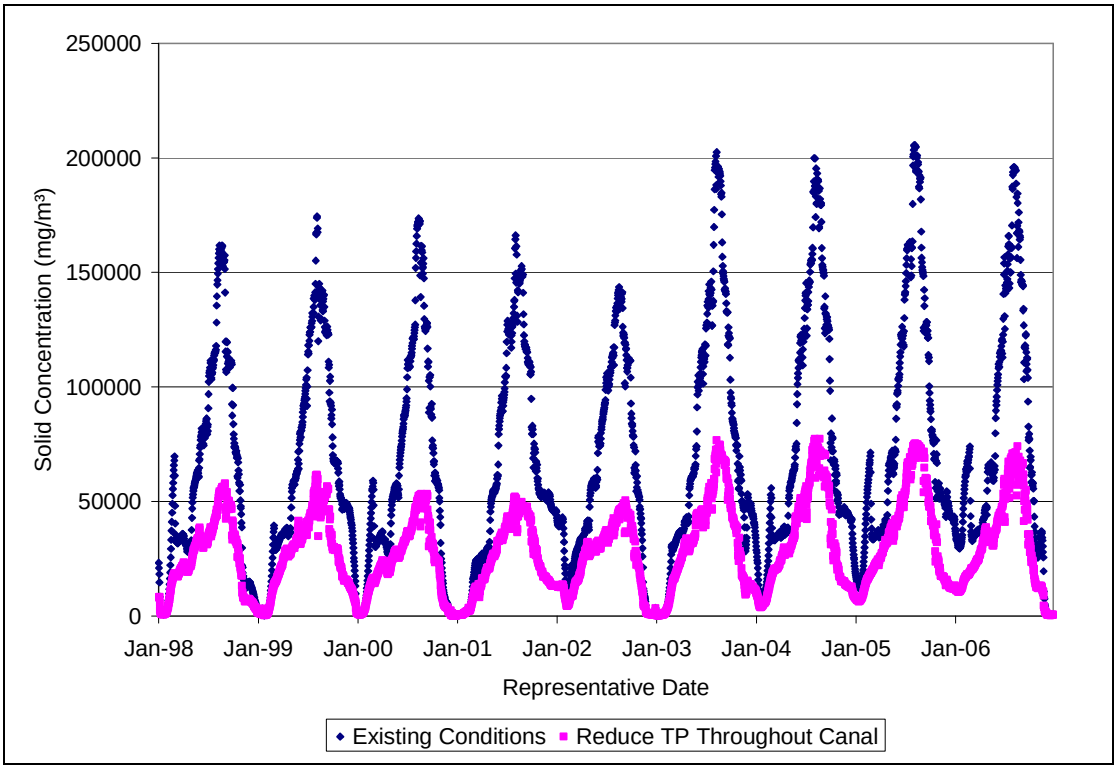

Figure 85. Reduction in wet solids concentration achieved by reducing phosphorus levels throughout the canal to 0.05 mg/L.

7.3.6. Treat Canal Water

The details of implementation of this option are vague in the Halcrow Group report, stating that further investigation is needed. However, the general idea behind this option is to biologically and/or chemically treat the canal water at some point(s) along the length of the Kennet and Avon Canal. The current canal model can be used to optimize the placement of such treatment. To represent this management option, the canal model was run separately 25 times, each time assuming a treatment mechanism has been put in place in the reach above one of the 25 locks, capable of removing 90% of sediment and algal concentrations. The final scenario, above Lock 80, was created in post-processing as was done in Section 7.3.4. Unsurprisingly, treatment mechanisms installed nearest to Copse Lock have the largest effect on the water quality entering the River Kennet. Treatment mechanisms installed anywhere upstream of Lock 74 have no noticeable effect on the concentration output from Copse Lock. Treatment mechanisms installed in the reaches between Lock 74 and Lock 79 have a slight effect on solids concentrations output from Copse Lock (Figure 86 (dry solids), Figure 87 (wet solids)). Unsurprisingly, the greatest effect is seen with treatment mechanisms installed in the reach above Lock 80 (Copse Lock)

(Figure 88); this last option is similar to the option presented in Section 7.3.4. However, if land availability for such treatment is better at a higher point in the canal, the evaluation in Figure 86 and Figure 87 may prove useful. The drastic change seen in dry solids concentration reductions achieved by installing treatment works above Lock 80 rather than above Lock 79 is due to the fact that most of the sediment suspended in a given reach comes from the boats traversing the reach; any sediment brought into a reach from the upstream lock will likely settle out of suspension before reaching the next downstream lock.

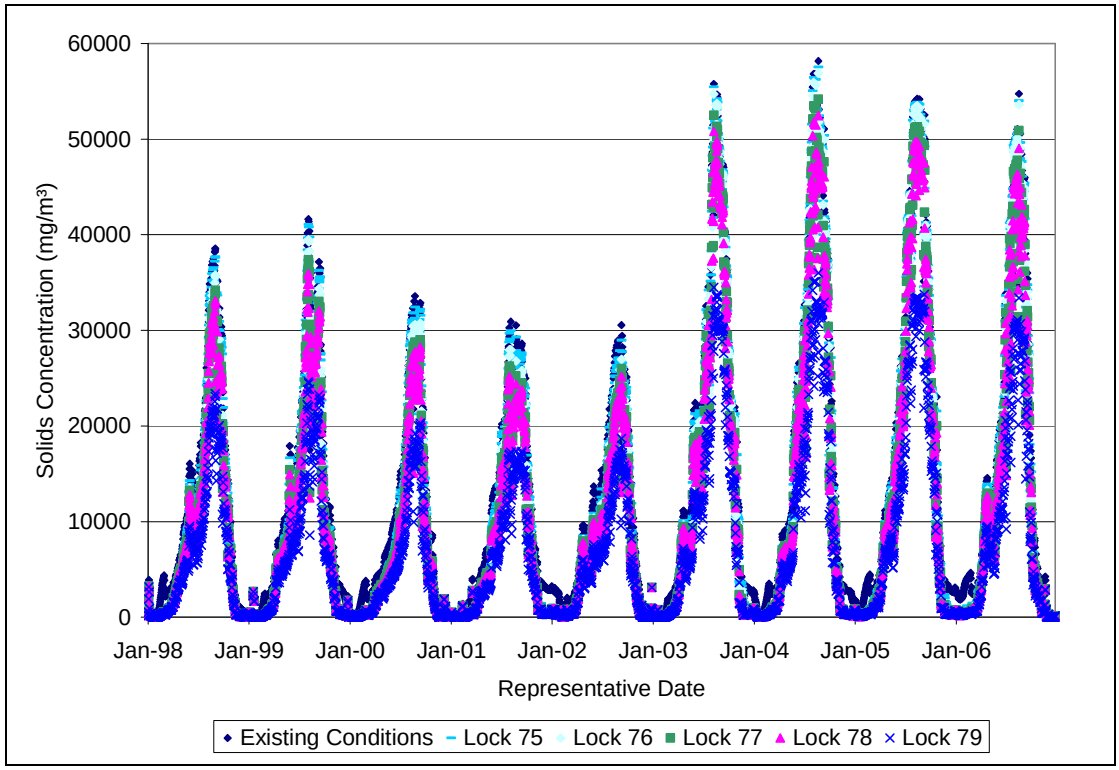

Figure 86. Dry solids concentrations output from Copse Lock when treatment works are installed at the indicated locks.

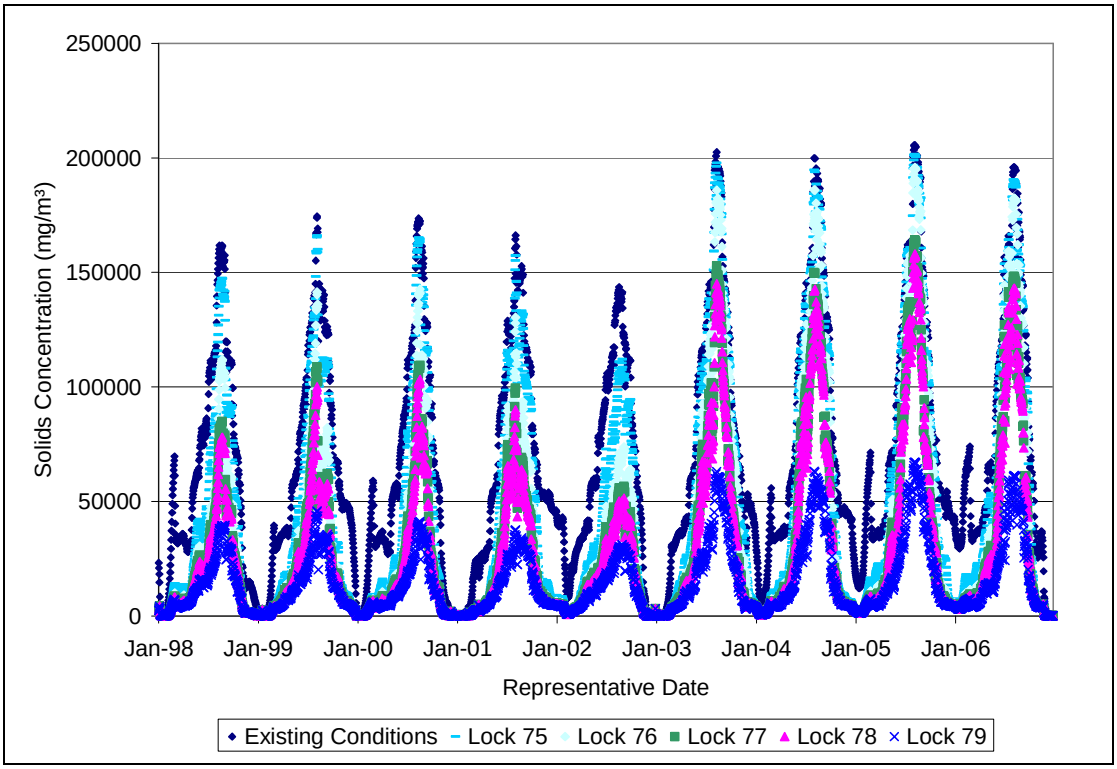

Figure 87. Wet solids concentrations output from Copse Lock when treatment works are installed at the indicated locks.

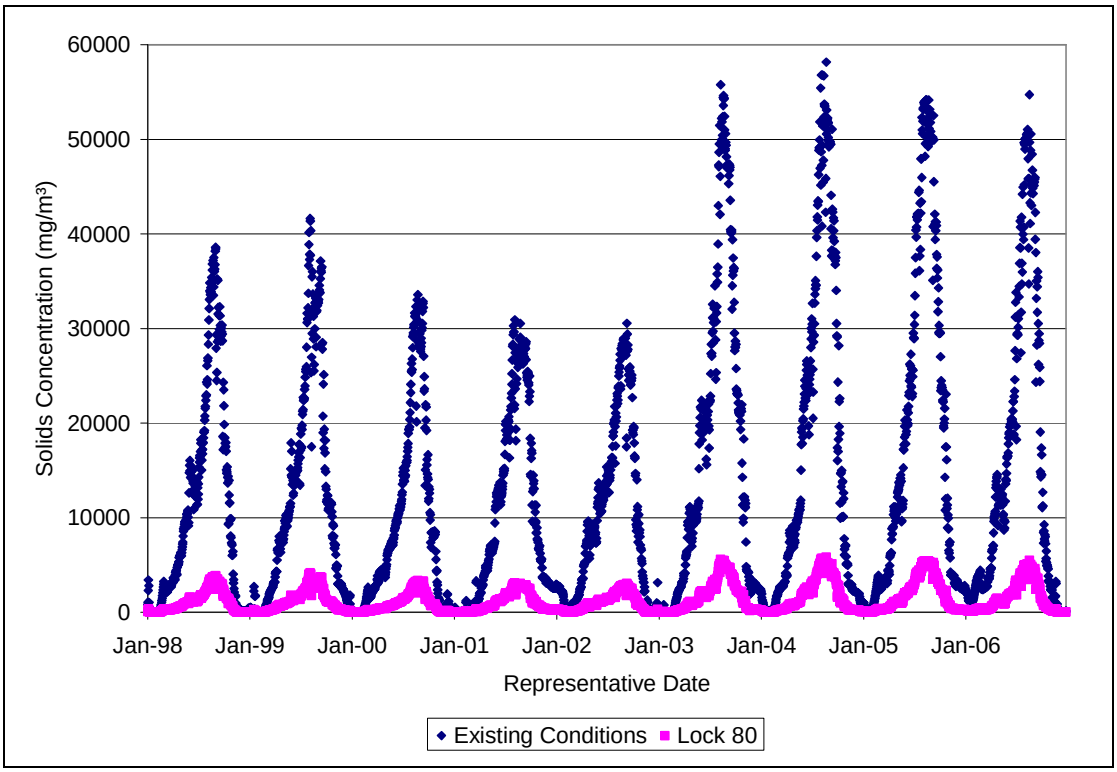

Figure 88. Dry solids concentrations output from Copse Lock when treatment works are installed at Lock 80.

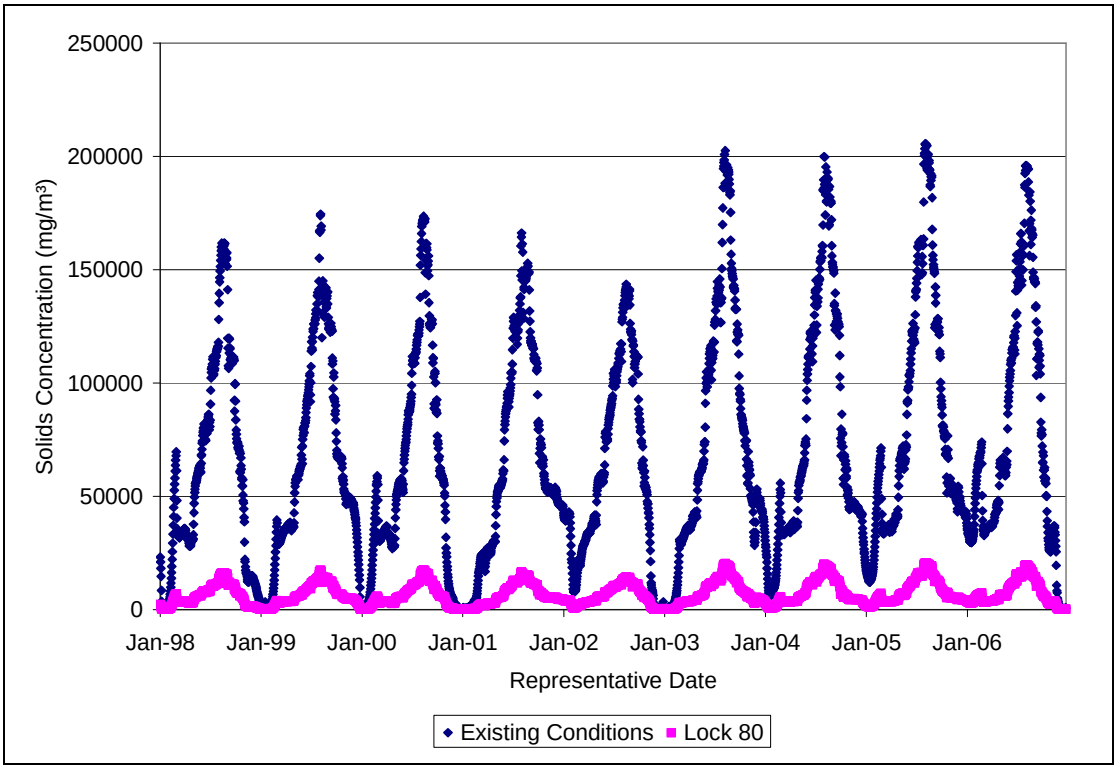

Figure 89. Wet solids concentrations output from Copse Lock when treatment works are installed at Lock 80.

7.3.7. Separation of Canal and River

This option involves separating the combined canal and river navigation below Copse Lock into a canal and a river. Modeling in this case using the canal model is not needed, as the water quality output from the canal becomes irrelevant in the new system. As this is a prohibitively expensive option, the Environment Agency will not likely consider it until all other options have been exhausted.

7.3.8. Summary

This previous sections have provided a description of the expected effects of various proposed management scenarios for the Kennet and Avon Canal based on the canal model predictions. The effects are summarized in Table 20.

Table 20. Summary of impacts of potential management scenarios.

Scenario	Average Dry Solids Concentration (mg/m^3)	Reduction in Average Dry Solids Concentration (%)	Average Wet Solids Concentration (mg/m^3)	Reduction in Average Wet Solids Concentration (%)
Baseline	13 000	--	67800	--
Do Minimum (90% reduction)	5 680	56	70300	-4
Do Minimum (50% reduction)	8 970	31	64700	5
Surface Flow Diversion	22 100	-70	105000	-55
On-line Filtration	6 840	47	7760	89
Poor Water Quality Reduction	1 950	85	10200	85
Effluent Discharge Control (treat effluent)	11 640	10	45900	32
Effluent Discharge Control (divert effluent)	12 100	7	47000	31
Effluent Discharge Control (reduce TP throughout canal)	10 600	18	28600	58
Treat Canal Water (treatment above Lock 75)	11 600	11	46200	32
Treat Canal Water (treatment above Lock 79)	7 350	43	14800	78
Treat Canal Water (treatment above Lock 80)	1 280	90	6780	90

The scenarios illustrated in Table 20 and in the previous figures suggest that the most effective management scenarios would focus on the reach directly upstream of Lock 80 (Copse Lock). These scenarios are most effective in part because so much of the inorganic sediment concentration leaving a reach is attributable to boat traffic within the reach in question; thus, dry solids concentrations contributed to a reach from the upstream reaches are not very significant. Additionally, by treating the water directly above the point in question (Copse Lock), one can be sure that all relevant sources of solids are indeed being addressed. Treatment of the canal water directly above Copse Lock seems a promising option, causing a major reduction in both inorganic sediment and algae; the ultimate success and viability of this option would depend on the

specific treatment method used. Alternatively, reducing the amount of poor water quality discharged from Copse Lock (which in practice may have a similar implementation) will provide a large impact. Because these options have a small spatial scope, it may be that they are the most practical to implement.

Treatment of water in reaches above Lock 79 may also provide a noticeable impact, and may be practical to implement should the preferred scenarios prove much more expensive than these treatment installed in reaches of the canal upstream from Lock 79. Although improving the quality of effluent from sewage treatment works will provide a beneficial effect on the water quality in the canal, this effect is focused only on the algal biomass and thus is ultimately limited in what it can achieve. The costs of implementing this scenario should be weighed against the costs of the treatment or poor water quality reduction scenarios, as those provide comprehensive treatment and achieve greater water quality improvements. Dredging of the canal has the potential to provide noticeable impact on the inorganic sediment discharged from Copse Lock, the magnitude of which is dependent upon the depth to which the canal can be dredged. However, a thorough dredging (e.g., a 90% reduction in boat sediment) may increase light availability and thus algal growth to a point that makes the reductions in inorganic sediment concentration unnoticeable. Even the effects of minor dredging may be offset by increased algal growth. However, it may be that dredging only in the reach above Copse Lock may minimize the potential for algal growth while still achieving a significant reduction in sediment concentrations. Surface flow diversion, particularly of the Kintbury Feeder, is not recommended due to the resultant severe decrease in flow rate in the canal and corresponding increased sediment concentration and algal growth.

8. Conclusions & Impact

The development, testing, and application of a new canal model have been presented in this document. This canal model satisfies the primary objective of this work: to determine and quantify the effect that canal operations have on water quality. In developing the new canal computer model, sources of solids were identified in a target canal, hydrological and water quality interactions between the canal and the natural landscape were quantified, algorithms were developed and coded to represent water quality processes within the canal, and the coded algorithms were tested on a target canal.

To identify sources of solids in the Kennet and Avon Canal, extensive data about the canal were collected. Field surveys involving the measurement of physical characteristics and water quality sample collection were conducted (Section 3.2). An external model, HSPF, was parameterized and used to quantify the effects on the canal from the natural landscape (Section 6).

The new canal model considers processes relevant specifically to inland navigational canals, namely lockage, leakage, seepage, boat traffic, and algal growth (Section 4.2). The processes in the new model were verified through process evaluation and sensitivity analysis using input parameters collected for the Kennet and Avon Canal (Section 5).

The effectiveness of new canal model has been demonstrated in predicting hydrology and inorganic sediment transport in canals. Its effectiveness has also been demonstrated in predicting the general trend of algal concentrations in a canal (Section 7.2). In satisfaction of the secondary objective of this research, the utility of the canal model has been further demonstrated through its application to the Kennet and Avon Canal to find solutions to the water quality problem in the River Kennet caused by the canal (Section 7.3).

In its application to the Kennet and Avon Canal, the new canal model showed:

- algal growth is most affected by light availability and phosphorus concentration;
- total algal concentration in a given reach reflects a combined impact of algal growth in all upstream reaches;
- inorganic sediment generation in a canal is primarily due to sediment disturbed by boat passage;
- inorganic sediment transport in a canal is primarily through the mechanisms of lockage and leakage; and
- a management scenario to address water quality problems must take a combined approach to restricting algal growth and minimizing sediment disturbance by boats.

Now that the model is complete, it will be passed along to the Environment Agency, who will use it in future planning efforts for the Kennet and Avon Canal. The model developed herein is sufficiently broad to allow application to other canals. After successful physical implementation of management efforts on the Kennet and Avon Canal, the Environment Agency will be able to use the new canal model to guide water quality improvement efforts in other canals in Britain.

Additional interest has been expressed in this model by the developers of the Integrated Catchments (INCA) model (Wade et al. 2002), who will be provided with the algorithms and source code in hopes they will be able to incorporate the canal model into their existing overland flow and receiving water model. As the canal model code and algorithms will be made freely available to any interested party, designers of other comprehensive land-surface and receiving water body models may also find a use for incorporating the canal model into their own models.

9. Future Research

Concurrent research being done by Mr. Attila Lazar at the University of Reading involves equation development to predict algal growth in detail. His work will include varied factors that may make it possible to predict nuances of algal growth with greater accuracy than the algorithms used here. It is hoped that his work can be incorporated into the canal model. However, the intrinsic simplicity in input development for the current canal model may be adversely affected by a detailed algal growth model, and thus the ability to implement the simple approach presented herein may be desired in a final combined model.

As has been mentioned throughout this report, there are many physical details of the canal that would have been useful in characterizing and evaluating the computer model: total flow rates, or even bypass weir flow rates monitored at multiple locations; algal concentration in the feed water to the summit reach; seepage rates; leakage rates; daily boat traffic; additional measurements of sediment disturbed by boat traffic; algal biomass measurements; and detailed time series of external inflows and abstractions to and from the canal. An intensive study of a canal, collecting all these data, would greatly enhance the utility of this model and any future efforts to refine it. In particular, measurement of seepage rates, leakage rates, daily boat traffic, and sediment disturbed by boat traffic could provide a useful suite of data currently lacking in the literature.

If the input requirements do not become prohibitive, the current canal model would benefit from a phosphorus simulation routine, rather than depending on phosphorus concentrations as input from the user. The addition of a phosphorus routine to the model would enable a daily-variable prediction of phosphorus concentration and could reduce the effect of excessive peaks or troughs in the monitored data that may not be indicative of the true condition of the canal. However, as phosphorus concentrations are so ubiquitously measured where water quality is measured, it seems that the current approach would put far less demand on modelers attempting to use the canal model.

10. References

Abril, J. M. and M. M. Abdel-Aal (2000). "A modelling study on hydrodynamics and pollutant dispersion in the Suez Canal." Ecological Modelling. **128**: 1-17.

Antia, N. J., C. D. McAllister, T. R. Parsons, K. Stephens and J. D. H. Strickland (1963). "Further measurements of primary production using a large-volume plastic sphere." Limnology and Oceanography. **8**(2): 166-183.

Babatunde, A. O., Y. Q. Zhao, M. O'Neill and B. O'Sullivan (2008). "Constructed wetlands for environmental pollution control: a review of developments, research and practice in Ireland." Environment International. **34**: 116-126.

Bakema, A. H. (1988). Empirical light modeling for a number of Dutch lakes., The Netherlands (in Dutch). Delft Hydraulics Report: T387.

Baugh, J. V. and A. J. Manning (2007). "An assessment of a new settling velocity parameterisation for cohesive sediment transport modeling." Continental Shelf Research. **27**: 1835-1855.

Beer, W. N. (2001). "Six parameter water temperature model.". Retrieved 3 September, 2009 from http://www.cbr.washington.edu/data/streams/six.param.white.pdf.

Benaman, J., C. A. Shoemaker and D. A. Haith (2005). "Calibration and validation of Soil and Water Assessment Tool on an agricultural watershed in upstate New York." Journal of Hydrologic Engineering. **10**(5): 363-374.

Berman, T. and U. Pollingher (1974). "Annual and seasonal variations of phytoplankton, chlorophyll, and photosynthesis in Lake Kinnerret." Limnology and Oceanography. **19**(1): 31-54.

Bicknell, B. R., J. C. Imhoff, J. L. Kittle Jr., T. H. Jobes and A. S. Donigian Jr. (2001). Hydrological Simulation Program - Fortran: HSPF, Version 12 User's Manual. AQUA TERRA Consultants, Mountain View, California.

Blom, G., E. H. S. Van Duin and L. Lijklema (1994). "Sediment resuspension and light conditions in some shallow Dutch lakes." Water Science and Technology. **30**: 243-252.

Boyce, W. E. and R. C. DiPrima (1986). Elementary Differential Equations and Boundary Value Problems. Chichester, John Wiley & Sons. 654 pp.

Brady, N. C. and R. R. Weil (1996). The Nature and Properties of Soils. London, Prentice-Hall International, Inc. 740 pp.

Brown, C. D., M. V. Hoyer, R. W. Bachmann and D. E. Canfield, Jr. (2000). "Nutrient-chlorophyll relationships: an evaluation of empirical nutrient-chlorophyll

models using Florida and north-temperate lake data." Canadian Journal of Fisheries and Aquatic Sciences. **57**(8): 1574-1583.

Buiteveld, H. (1995). "A model for calculation of diffuse light attenuation (PAR) and Secchi depth." Netherlands Journal of Aquatic Ecology. **29**: 55-65.

Byne, F. W. (2000). Predicting Sediment Detachment and Channel Scour in the Process-Based Planning Model ANSWERS-2000. Biological Systems Engineering, Virginia Tech, Blacksburg, Virginia. M.S. Thesis.

Clew, K. R. (1973). The Kennet and Avon Canal: An Illustrated History. Newton Abbot, David & Charles. 206 pp.

Cooper, L. H. N. (1937). "On the ratio of nitrogen to phosphorus in the sea." Journal of the Marine Biological Association. **22**: 177-182.

Copeland, R. R., D. D. Abraham, G. H. Nail, R. Seal and G. L. Brown (2001). Entrainment and Transport of Sediments by Towboats in the Upper Mississippi River and Illinois Waterway, Numerical Model Study. US Army Engineer Districts of Rock Island, St. Louis, and St. Paul. Upper Mississippi River - Illinois Waterway System Navigation Study: ENV Report 37. 91 pp.

Coraci, E., G. Umgiesser and R. Zonta (2007). "Hydrodynamic and sediment transport modelling in the canals of Venice (Italy)." Estuarine, Coastal, and Shelf Science. **75**: 250-260.

Corrie, E. (2002). The Kennet & Avon Canal: From the Thames to Bristol. Burton-on-Trent, Waterways World, Ltd.

Daugherty, R. L. (1937). Hydraulics: A Text on Practical Fluid Mechanics. London, McGraw-Hill Book Company, Inc. 460 pp.

de Vente, J., J. Poesen, G. Verstraeten, A. J. J. Van Rompaey and G. Govers (2008). "Spatially distributed modelling of soil erosion and sediment yield at regional scales in Spain." Global and Planetary Change. **60**(3-4): 393-415.

Dickman, M. (1969). "Some effects of lake renewal on phytoplankton productivity and species composition. ." Limnology and Oceanography. **14**(5): 660-666.

Dillon, P. J. and F. H. Rigler (1974). "The phosphorus-chlorophyll relationship in lakes." Limnology and Oceanography. **19**(5): 767-773.

DiToro, D. M. (1978). "Optics of turbid estuarine waters: approximations and applications." Water Research. **12**: 1059-1068.

Dugdale, R. C. and J. J. MacIsaac (1971). "A computation model for the uptake of nitrate in the Peru upwelling region." Investigatión Pesquera. **35**(1): 299-308.

Dun, R. W. (2006). "Reducing uncertainty in the hydraulic analysis of canals." Proceedings of the Institution of Civil Engineers, Water Management. **159**(WM4): 211-224.

EPA (1999). BASINS Technical Note 5: Using HSPEXP with BASINS/NPSM. United States Environmental Protection Agency Office of Water. EPA-823-R-99-010.

EPA (2000). BASINS Technical Note 6: Estimating Hydrology and Hydraulic Parameters for HSPF. United States Environmental Protection Agency Office of Water. EPA-823-R00-012.

EPA (2006). BASINS Technical Note 8: Sediment Parameter and Calibration Guidance for HSPF. United States Environmental Protection Agency Office of Water.

Eppley, R. W. (1972). "Temperature and phytoplankton growth in the sea." Fishery Bulletin. **70**(4): 1063-1085.

Eppley, R. W. and P. R. Sloan (1966). "Growth rates of marine phytoplankton: correlation wih light absorption by cell Chlorophyll-a." Physiologia Plantarum. **19**: 47-59.

Fleming, R. H. (1940). Composition of plankton and units for reporting populations and production. Proceedings of the Sixth Pacific Science Congress. 535-540.

Fogg, G. E. (1965). Algal Cultures and Phytoplankton Ecology. University of London, The Athlone Press. 126 pp.

Fox, P. (2010). Kennet and Avon Canal Weir Levels. Personal Communication received 23 March 2010 by R. W. Zeckoski.

Gerritsen, H., R. J. Vos, T. van der Kaaij, A. Lane and J. G. Boon (2000). "Suspended sediment modelling in a shelf sea (North Sea)." Coastal Engineering. **41**(1-3): 317-352.

Goldman, C. R., M. Gerletti, P. Javornický, U. Melchiorri-Santolini and E. de Amezaga (1968). "Primary productivity, bacteria, phyto- and zooplankton in Lake Maggiore: correlations and relationships with ecological factors." Memorie dell'Istituto Italiano di Idrobiologia. **23**: 49-127.

Green, M. B. and J. Upton (1994). "Constructed reed beds: a cost-effective way to polish wastewater effluents for small communities." Water Environment Research. **66**(3): 188-192.

Gschlößl, T., C. Steinmann, P. Schelypen and A. Melzer (1998). "Constructed wetlands for effluent polishing of lagoons." Water Research. **32**(9): 2639-2645.

Hadfield, C. (1981). The Canal Age. London, David and Charles, Ltd. 233 pp.

Halcrow Group Limited (2007). Kennet Chalkstream Restoration Project: Kennet Canal/River Scoping Final Report. 98 pp.

Hamming, R. W. (1973). Numerical Methods for Scientists and Engineers. New York, McGraw-Hill Book Company. 721 pp.

Hamon, R. W., L. L. Weiss and W. T. Wilson (1954). "Insolation as an empirical function of daily sunshine duration." Monthly Weather Review. **82**(6): 141-146.

Heatlie, F., J. Drake and D. Debski (2007). "Modelling the Manchester Ship Canal." Water and Environment Journal. **21**: 100-107.

Henderson, F. M. (1966). Open Channel Flow. London, Collier-Macmillan Ltd. 522 pp.

Hilton, J. and G. L. Phillips (1982). "The effect of boat activity on turbidity in a shallow broadland river." The Journal of Applied Ecology. **19**(1): 143-150.

Hummel, P., J. L. Kittle Jr. and M. Gray (2001). WDMUtil Version 2.0: A Tool for Managing Watershed Modeling Time-Series Data: User's Manual. AQUA TERRA Consultants, Decatur, Georgia. 165 pp.

Jarvis, M. G., R. H. Allen, S. J. Fordham, J. Hazelden, A. J. Moffat and R. G. Sturdy (1984). Soils and Their Use in South East England. Harpenden, Lawes Agricultural Trust. 405 pp.

Jarvis, M. G., J. Hazelden and D. Mackney (1979). Soils of Berkshire. Harpenden, Rothamsted Experimental Station, Lawes Agricultural Trust. 263 pp.

Johansen, C. and T. Larsen (1998). "Measurement of settling velocity of fine sediment using a recirculated settling column." Journal of Coastal Research. **14**(1): 132-139.

Jones, J. R. and R. W. Bachmann (1976). "Prediction of phosphorus and chlorophyll levels in lakes." Journal (Water Pollution Control Federation). **48**(9): 2176-2182.

Kennet and Avon Canal Trust Ltd. (1981). The Kennet and Avon Canal and its Trust.

Kennet and Avon Canal Trust Ltd. (1999). The Kennet and Avon Canal: a Pictorial Journey.

Kennet Chalkstream Monitoring Group (2008). Discussion at the Kennet Chalkstream Monitoring Group Team Meeting held 16 May 2008 at the Red Kite House in Wallingford.

Kim, S. M., B. L. Benham, K. M. Brannan, R. W. Zeckoski and J. Doherty (2007a). "Comparison of hydrologic calibration of HSPF using automatic and manual methods." Water Resources Research. **43**(1): W01402.

Kim, S. M., B. L. Benham, K. M. Brannan, R. W. Zeckoski and G. R. Yagow (2007b). "Water quality calibration criteria for bacteria TMDL development." Applied Engineering in Agriculture. **23**(2): 171-176.

Kimmel, B. L., O. T. Lind and L. J. Paulson (1990). Chapter 6: Reservoir Primary Production. Reservoir Limnology: Ecological Perspectives. K. W. Thornton, B. L. Kimmel and F. E. Payne, ed. New York, John Wiley & Sons. 133-193.

Kirkby, M. J., R. J. A. Jones, B. Irvine, A. Gobin, G. Govers, O. Cerdan, A. J. J. Van Rompaey, Y. Le Bissonnais, J. Daroussin, D. King, L. Montanarella, M. Grimm, V. Vieillefont, J. Puigdefabregas, M. Boer, C. Kosmas, N. Yassoglou, M. Tsara, S. Mantel, G. J. Van Lynden and J. Huting (2004). Pan-European Soil Erosion Risk Assessment: the PESERA Map, Version 1. Luxembourg. Office for Official Publications of the European Communities.

Krone, R. B. (1962). Flume Studies of the Transport of Sediment in Estuarial Shoaling Processes. Hydraulic Engineering Laboratory and Sanitary Engineering Research Laboratory, Berkeley, California.

Lal, A. M. W. (2001). "Modification of canal flow due to stream-aquifer interaction." Journal of Hydraulic Engineering. **127**(7): 567-576.

Langridge, J. (2004). Kennet & Avon Canal Sustainability Monitoring Report 2003-2004. British Waterways. 90 pp.

Lau, Y. L. (1994). "Temperature effect on settling velocity and deposition of cohesive sediments." Journal of Hydraulic Research. **32**(1): 41-51.

Lau, Y. L. and B. G. Krishnappan (1992). "Size distribution and settling velocity of cohesive sediments during settling." Journal of Hydraulic Research. **30**(5): 673-684.

Lee, R. W. and W. Rast (1997). Light Attenuation in a Shallow, Turbid Reservoir, Lake Houston, Texas. United States Geological Survey. USGS Water-Resources Investigations Report: 97-4064.

Lucas, L. V., J. K. Thompson and L. R. Brown (2009). "Why are diverse relationships observed between phytoplankton biomass and transportation?" Limnology and Oceanography. **54**(1): 381-390.

Lumb, A. M., R. B. McCammon and J. L. Kittle Jr. (1994). Users manual for an expert system (HSPexp) for calibration of the Hydrologic Simulation Program--Fortran. United States Geological Survey. Water Resources Investigations Report 94-4168.

Malone, T. C. (1980). Chapter 12: Algal Size. The Physiological Ecology of Phytoplankton. I. Morris, ed. Oxford, Blackwell Scientific Publications. Studies in Ecology, Volume 7: 433-463.

Malone, T. C., M. B. Chervin and D. B. Boardman (1979). "Effects of 22-μm screens on size-frequency distributions of suspended particles and biomass estimates of phytoplankton size fractions." Limnology and Oceanography. **24**(5): 956-960.

Manning, A. J. (2004). The development of new algorithms to parametise the mass settling flux of flocculated estaurine sediments. HR Wallingford. Report TR145.

Marsh, T. J. and J. Hannaford, Eds. (2008). UK Hydrometric Register. Hydrological Data UK, Centre for Ecology & Hydrology. 210 pp.

Maynord, S. T., S. K. Knight, S. Bourne, M. R. Graves and K. J. Landwehr (2004). Upper Mississippi River-Illinois Waterway System Models Report - Physical Effects Models. U.S. Army Engineer District, Rock Island, St. Louis, and St. Paul. Upper Mississippi River-Illinois Waterway System Navigation Study: ENV Report 42. 109 pp.

Mehta, A. J., E. J. Hayter, W. R. Parker, R. B. Krone and A. M. Teeter (1989). "Cohesive Sediment Transport 1: Process Description." Journal of Hydraulic Engineering. **115**(8): 1076-1093.

MetOffice (2010). "Oxford Data." Retrieved 11 March, 2010 from http://www.metoffice.gov.uk/climate/uk/stationdata/oxforddata.txt. Last Updated February 2010.

Milburn, D. and B. G. Krishnappan (2003). "Modelling erosion and deposition of cohesive sediments from Hay River, Northwest Territories, Canada." Nordic Hydrology. **34**(1/2): 125-138.

Minikin, R. C. R. (1920). Practical River and Canal Engineering. London, Charles Griffin & Company. 123 pp.

Mishra, A., S. Kar and V. P. Singh (2007). "Determination of runoff and sediment yield from a small watershed in sub-humid subtropics using the HSPF." Hydrological Processes. **21**(22): 3035-3045.

Misra, R., K. Sridharan and M. S. M. Kumar (1991). "Transients in canal network." Journal of Irrigation and Drainage Engineering. **118**(5): 690-707.

Mueller, D. K. and D. R. Helsel (1999). "Nutrients in the Nation's Waters -- Too Much of a Good Thing?" National Water-Quality Assessment Program. Retrieved 27 May 2010 from http://pubs.usgs.gov/circ/circ1136/.

Mullin, M. M., P. R. Sloan and R. W. Eppley (1966). "Relationship between carbon content, cell volume, and area in phytoplankton." Limnology and Oceanography. **11**(2): 307-311.

Murphy, K. J. and J. W. Eaton (1983). "Effects of pleasure-boat traffic on macrophyte growth in canals." The Journal of Applied Ecology. **20**(3): 713-729.

Nash, J. E. and J. V. Sutcliffe (1970). "River flow forecasting through conceptual models: Part I - A discussion of principles." Journal of Hydrology. **10**: 282-290.

National Rivers Authority, Thames Region (1992). Kennet and Avon Canal: Survey of Interaction with the River Kennet. National Rivers Authority, Thames Region. 27 pp.

Neal, C., J. Hilton, A. J. Wade, M. Neal and H. Wickham (2006a). "Chlorophyll-a in the rivers of eastern England." Science of the Total Environment. **365**: 84-104.

Neal, C., W. A. House, N. P. Jarritt, M. Neal, L. Hill and H. Wickham (2006b). "The water quality of the River Dun and the Kennet and Avon Canal." Journal of Hydrology. **330**: 155-170.

Neal, C., W. A. House, H. P. Jarvie, M. Neal, L. Hill and H. Wickham (2005a). "Phosphorus concentrations in the River Dun, the Kennet and Avon Canal and the River Kennet, southern England." Science of the Total Environment. **344**(1-3): 107-128.

Neal, C., H. P. Jarvie, S. M. Howarth, P. G. Whitehead, R. J. Williams, M. Neal, M. Harrow and H. Wickham (2000). "The water quality of the River Kennet: initial observations on a lowland chalk stream impacted by sewage inputs and phosphorus remediation." Science of the Total Environment. **251/252**: 477-495.

Neal, C., H. P. Jarvie, A. Love, M. Neal, H. Wickham and S. Harman (2007). "Water quality along a river continuum subject to point and diffuse sources." Journal of Hydrology. **350**(3-4): 154-165.

Neal, C., H. P. Jarvie, M. Neal, A. Love, L. Hill and H. Wickham (2005b). "Water quality of treated sewage effluent in a rural area of the upper Thames Basin, southern England, and the impacts of such effluents on riverine phosphorus concentrations." Journal of Hydrology. **304**: 103-117.

Neal, C., M. Neal, G. J. L. Leeks, G. Old, L. Hill and H. Wickham (2006c). "Suspended sediment and particulate phosphorus in surface waters of the upper Thames Basin, UK." Journal of Hydrology. **330**: 142-154.

Neumeier, U., C. Ferrarin, C. L. Amos, G. Umgiesser and M. Z. Li (2008). "Sedtrans05: An improved sediment-transport model for continental shelves and coastal waters with a new algorithm for coastal sediments." Computers and Geosciences. **34**(10): 1223-1242.

Nicholson, J. and B. A. O'Connor (1986). "Cohesive sediment transport model." Journal of Hydraulic Engineering. **112**(7): 621-640.

Pinkett, A. J. (1995). "Basingstoke Canal Hydrological Study: A Water Balance." Journal of the Chartered Institution of Water and Environmental Management. **9**(4): 376-384.

Pridmore, R. D. and G. B. McBride (1984). "Prediction of Chlorophyll *a* concentrations in impoundments of short hydraulic retention time." Journal of Environmental Management. **19**(4): 343-350.

Redfield, A. C. (1958). "The biological control of chemical factors in the environment." American Scientist. **46**(3): 205-221.

Reid, N. J. and S. K. Hamilton (2007). "Controls on algal abundance in a eutrophic river with varying degrees of impoundment (Kalamazoo River, Michigan, USA)." Lake and Reservoir Management. **23**(3): 219-230.

Reynolds, C. S. (1984). The Ecology of Freshwater Phytoplankton. Cambridge, Cambridge University Press. 384 pp.

Rodhe, W. (1948). "Environmental requirements of freshwater plankton algae. Experiment studies in the ecology of phytoplankton." Symbolae Botanica Upsalienses. **X**(1): 1-149.

Roehl, J. W. (1962). "Sediment source areas, delivery ratios and influencing morphological factors. ." International Association of Scientific Hydrology. **59**: 202-213.

Schindler, D. W. (1978). "Factors regulating phytoplankton production and standing crop in the world's freshwaters." Limnology and Oceanography. **23**(3): 478-486.

Schwab, G. O., D. D. Fangmeier, W. J. Elliot and R. K. Frevert (1993). Soil and Water Conservation Engineering. Chichester, John Wiley & Sons, Inc. 507 pp.

Simons, D. B. and F. Şentürk (1977). Chapter 4: Properties of Sediment. Sediment Transport Technology. Fort Collins, CO, Water Resources Publications. 807.

Søballe, D. M. and B. L. Kimmel (1987). "A large-scale comparison of factors influencing phytoplankton abundance in rivers, lakes, and impoundments." Ecology. **68**(6): 1943-1954.

Søballe, D. M. and S. T. Threlkeld (1985). "Advection, phytoplankton biomass, and nutrient transformations in a rapidly flushed impoundment." Archiv für Hydrobiologie. **105**(2): 187-203.

Soeder, C. J., J. F. Talling and I. Baak (1974). Section 2.14: Chemical Components (b) Dry weight and ash content. . A Manual on Methods for Measuring Primary Production in Aquatic Environments. R. A. Vollenweider, ed. Oxford, Blackwell Scientific Publications. IBP Handbook No. 12: 18-21.

Soulsby, R. (1997). Dynamics of Marine Sands: A Manual for Practical Application. London, ThomasTelford. 249 pp.

Strickland, J. D. H. and T. R. Parsons (1968). A Practical Handbook of Seawater Analysis. Ottawa.

Sutcliffe, J. V. and Y. P. Parks (1987). "Hydrological modelling of the Sudd and Jonglei Canal." Hydrological Sciences Journal. **32**(2): 143-159.

Swanson, L. A., R. J. Lunn and S. G. Wallis (2004). "Management of canal systems under the Water Framework Directive: determining fundamental properties governing water quality." Hydrology: Science and Practice for the 21st Century. **II**: 160-167.

Talling, J. F. (1955). "The relative growth rates of three plankton diatoms in relation to underwater radiation and temperature." Annals of Botany. **19**(75): 329-341.

Thomas, W. H. and A. N. Dodson (1972). "On nitrogen deficiency in tropical Pacific oceanic phytoplankton. II. Photosynthetic and cellular characteristics of a chemostat-grown diatom." Limnology and Oceanography. **17**(4): 515-523.

Tyagi, J. V., S. K. Mishra, R. Singh and V. P. Singh (2008). "SCS-CN based time-distributed yield model." Journal of Hydrology. **352**(3-4): 388-403.

U. S. Naval Observatory, Astronomical Applications Department (2010). "US Naval Oceanography Portal: Sun or Moon Rise/Set Table for One Year." Retrieved 8 February, 2010 from http://aa.usno.navy.mil/data/docs/RS_OneYear.php.

Van Duin, E. H. S., G. Blom, F. J. Los, R. Maffione, R. Zimmerman, C. F. Cerco, M. Dortch and E. P. H. Best (2001). "Modeling underwater light climate in relation to sedimentation, resuspension, water quality and autotrophic growth." Hydrobiologia. **444**: 25-42.

van Rijn, L. C. (1984). "Sediment transport, part II: Suspended load transport." Journal of Hydraulic Engineering. **110**(11): 1613-1641.

Vanoni, V. A., Ed. (1975). Sedimentation Engineering. New York, American Society of Civil Engineers. 745 pp.

Vollenweider, R. A. (1974). Section 2.18: 'Conversion factors' between different criteria. A Manual on Methods for Measuring Primary Productivity in Aquatic Environments. R. A. Vollenweider, ed. Oxford, Blackwell Scientific Publications. IBP Handbook No. 12: 31-32.

Vollenweider, R. A. (1976). "Advances in defining critical loading levels for phosphorus in lake eutrophication." Memorie dell'Istituto Italiano di Idrobiologia. **33**: 53-83.

Wade, A. J., P. Durand, V. Beaujouan, W. W. Wessel, K. J. Raat, P. G. Whitehead, D. Butterfield, K. Rankinen and A. Lepistö (2002). "A nitrogen model for European catchments: INCA, new model structure and equations." Hydrology and Earth System Sciences. **6**(3): 559-582.

Walker, W. W., Jr. (1984). "Empirical prediction of chlorophyll in reservoirs." Lake and Reservoir Management. **1**(1): 292-297.

Wallingford Software (2008). "ISIS Flow/Hydrology." Retrieved 15 August, 2008 from http://www.wallingfordsoftware.com/products/isis/.

West Berkshire Heritage Service (1999). Working Waterway: the Kennet and Avon Canal through West Berkshire.

Wienke, S. M. and J. E. Cloern (1987). "The phytoplankton component of seston in San Francisco Bay." Netherlands Journal of Sea Research. **21**(1): 25-33.

Willby, N. J., J. R. Pygott and J. W. Eaton (2001). "Inter-relationships between standing crop, biodiversity and trait attributes of hydrophytic vegetation in artificial waterways." Freshwater Biology. **46**: 883-902.

Winter, C. (2007). "On the evaluation of sediment transport models in tidal environments." Sedimentary Geology. **202**(3): 562-571.

Zeckoski, R. W., A. N. Lazar, D. L. Liang and A. J. Wade (2009). Comparison of the HSPF and HBV-INCA Models: Crossing the Atlantic Divide. Paper presented to ASABE International Meeting held in Reno, Nevada from June 21-June 24, 2009. Paper No. 096591.

Zhang, Y., B. Qin, W. Hu, S. Wang, Y. Chen and W. Chen (2006). "Temporal-spatial variations of euphotic depth of typical lake regions in Lake Taihu and its ecological environmental significance." Science in China: Series D Earth Sciences. **49**(4): 431-442.

Appendices

Appendix A. Supporting Information for Algorithm Development

A.1. Cohesive Sediment Deposition

The mass settling flux is calculated according to the equations developed by Manning (2004) and tested by Baugh and Manning (2007). The equations depend on the separation of flocs into macrofloc (>160 μm diameter) and microflocs (<160 μm diameter). Manning found the settling velocity for macroflocs to be dependent on both suspended solids concentration and shear stress at the bed, as was previously described in the literature review (Equations 7-10 in Section 2.2). The macrofloc fall velocity equations will be modified to calculate SPM according to Equation 72, to work with model variables.

$$SPM = \frac{SS_{alg} + SS_{coh}}{S * 1000} \tag{72}$$

Where: SS_{alg} = dry mass of algal solids (mg);
SS_{coh} = mass of cohesive solids (mg); and
1000 = conversion from m^3 to L.

Manning was working with silt- and clay-dominated bottom material, and his equations assume that all suspended material is in the form of either macro- or microflocs. Therefore, only the concentration of cohesive sediments and algae (a form of organic matter) will be used in calculating $w_{s,macro}$, SPM_{ratio}, and MSF. Although the algae will not deposit noticeably, organic matter is known to have an effect on flocculation and indeed to be a part of flocs that are formed (Mehta et al., 1989), and so algae will be included in the MSF calculations.

The shear stress used in the $w_{s,macro}$ and $w_{s,micro}$ equations will be calculated with Equation 73 (Soulsby 1997).

$$\tau = \rho C_{d,drag} v_w^2 \tag{73}$$

Where: ρ = water density (kg/m^3);
$C_{d,drag}$ = drag coefficient (unitless); and
v_w = velocity of water (m/s).

Soulsby suggests that where detailed data are not available (as will be the case in most hydrological modeling cases), a value for $C_{d,drag}$ of 0.0025 be used; this will be used in this case.

The canal model will also use the modification to fall velocity suggested by Mehta et al. (1989) to include the probability that a "grain reaching the bed will remain there" (Equation 74).

$$p = 1 - \frac{\tau_b}{\tau_{cd}} \tag{74}$$

This helps account for the effect of turbulence on the resuspension of cohesive particles: when shear stress is low, most sediment will be deposited, but as shear stress rises, there will be enough energy in the water to keep cohesive sediments suspended. This is similar to the modification to deposition used in Krone's Equation (Equation 2). Because p cannot be allowed to be negative, if $\tau_b > \tau_{cd}$, p will be 0. τ_{cd} should be measured where possible but is typically in the range of 0.04-0.08 kg/(m·s²) (Krone 1962; Nicholson and O'Connor 1986; Mehta et al. 1989; Milburn and Krishnappan 2003), so can be estimated by the user.

A problem with Manning's method arises when the SPM concentration is extremely large (greater than 10000 mg/L). The behavior of the SPM_{ratio} equation (Equation 8) at these extreme concentrations is undesirable (Figure 90).

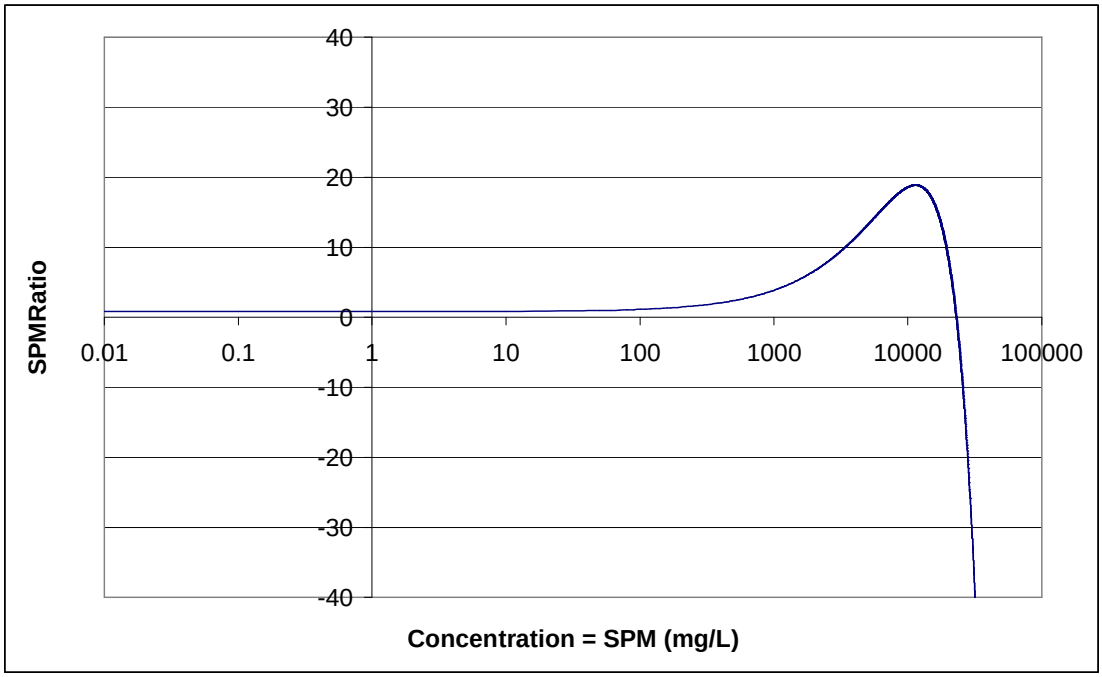

Figure 90. Equation 8, showing the undesirable behavior at high solids concentrations.

The peak of the curve in Figure 90 occurs when $dSPM_{ratio}/dSPM = 0$, or at 11357 mg/L. To prevent against illogical calculations during extreme conditions, a method was introduced to account for these extreme concentrations: because the figure presented in Manning's original document (2004) implies a constant asymptote as concentrations rise above 10000, above 11357 mg/L the SPM_{ratio} calculated for SPM = 11357 mg/L will be used in the model. It should be noted that these extreme concentrations are not expected in a properly functioning canal.

A.2. Boat-Generated Sediment and Weir Flow

Only a portion of the sediment generated by boats as they traverse the reach will make it out of the reach via the overflow weir – that is, the portion that stays in suspension near the top of the water column at the location of the overflow weir (or the top of the lock gates). For boats moving upstream, this effect is summarized in Figure 91 (v_b = boat velocity; v_w = water velocity; D = water depth; H_{weir} = depth of water above weir bottom; t_1 defined later).

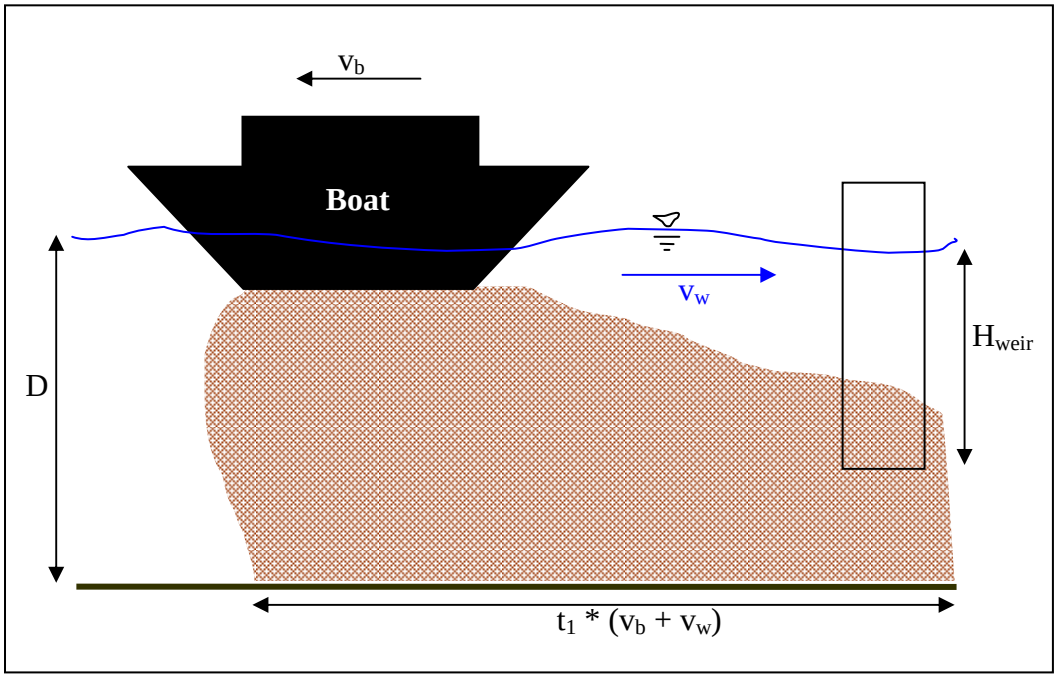

Figure 91. Concentration profile for sediment generated by a boat as it passes a weir. Weir elongated for effect. Brown shading represents suspended sediment.

A complication arises in that the sediment will appear to settle faster at a given point in the reach (i.e., the weir) than the deposition equation would predict, because while the sediment falls it is also being carried down the reach by the flowing water. In the case of a boat moving downstream, sediment is being washed out of the weir area faster than one would expect; for a boat moving upstream, sediment is being moved into the weir area faster than one would expect.

An equation is needed that can calculate the concentration at a given point in space as a function of the time since boat passage. However, use of the deposition equation without modification would neglect the action of the flow rate, which moves sediment into or out of the weir cross section in addition to the actions of gravity causing the sediment to settle out of suspension.

Thus, the time parameter in the deposition equation must be modified so that the input to the equation can be <time since boat passage> while the time parameter in the exponent in the equation remains the <time since the boat deposited the sediment>. Note that the time since the boat passed a given point in space is not the same as the time since the sediment currently occupying that space was deposited.

Consider a boat and point of interest as given in Figure 92.

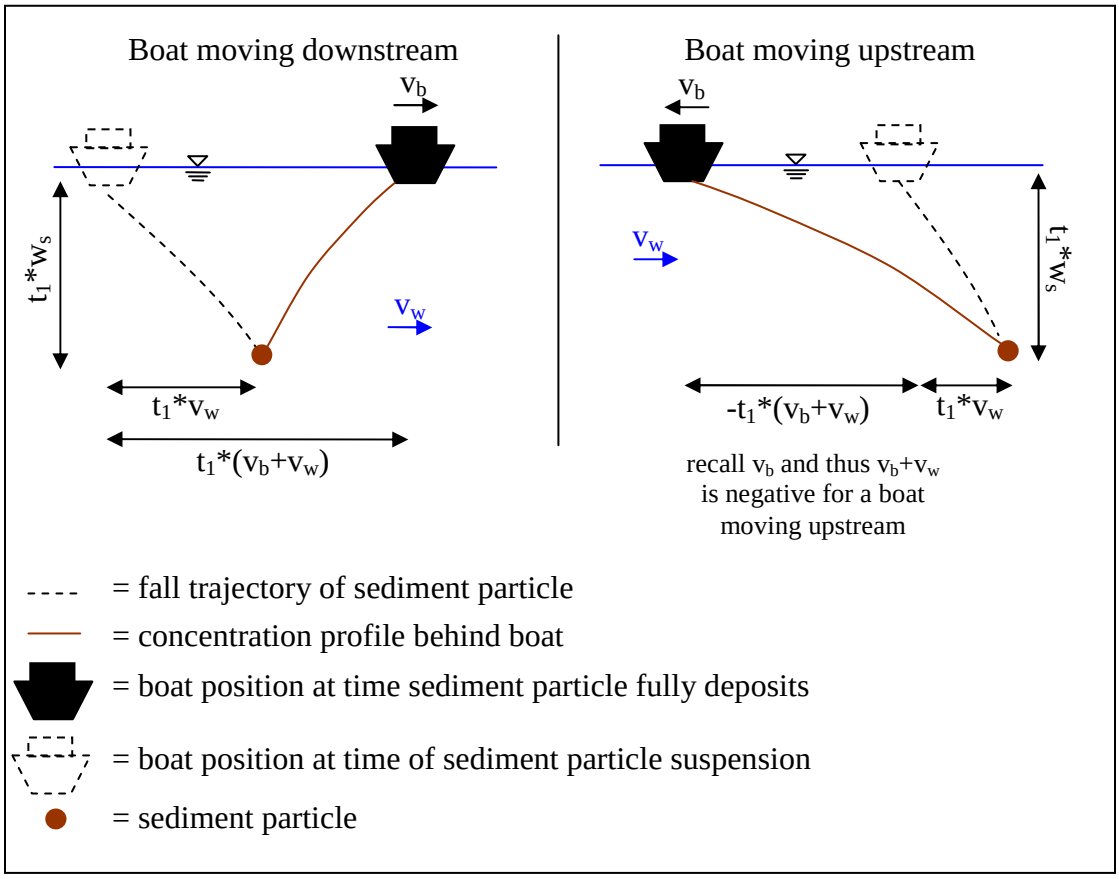

Figure 92. Diagram of boat and sediment movement in relation to a point of interest.

Considering the case of the boat moving downstream, to be at the level at which it is located, the sediment must have been deposited t_1 ago. In that time, the sediment has moved along the reach t_1*v_w from its point of origin. In that same time, the boat has moved $t_1*(v_b+v_w)$ downstream from its point of origin. Thus, the sediment is currently t_1*v_b behind the boat and the peak concentration at the moment. However, the boat actually passed the point of interest longer ago than t_1. Given that the boat has travelled $t_1*(v_w+v_b)$ since depositing a given sediment particle in the weir cross-section, and that same sediment particle was originally deposited t_1*v_w before the weir, the boat must have travelled $t_1*(v_w+v_b-v_w)$ since passing the weir, or t_1*v_b. The time it took to do this (t_2) is this distance divided by its rate of travel (Equation 75).

$$t_2 = \frac{t_1 \cdot v_b}{v_b + v_w} \tag{75}$$

So, it is desired to input t_2 into the deposition equation, but have it come out as t_1 in the exponent. That is, it is necessary to define $f(t_2) = t_1$ (Equation 76).

$$t_1 = t_2 \frac{v_b + v_w}{v_b} \tag{76}$$

If the time variable in the exponent of the solution to the deposition equation is modified according to Equation 76, the deposition equation becomes Equation 77.

$$C = C_0 e^{\frac{-w_s}{D}\left(\frac{v_b+v_w}{v_b}\right)t} \tag{77}$$

This equation considers the effects of water movement on the decrease in concentration at a given point in space, modifying the time parameter to account for the effects of advection by the moving water. The time input to this equation is the time since the boat passed the point of interest.

Returning to the issue at hand – the increased amount of sediment that moves through the overflow weir (or overtops the lock gates) due to a boat that stirs up sediment as it passes. The sediment concentration in the top few centimeters of flow is not constant but rather is decreasing as the boat moves farther away. To determine the amount of sediment lost, one must first determine the length of time (say, t_3) that passes between the time of boat passage and the time that the concentration above the weir becomes negligible (assumed to occur when $C/C_o = 0.001$). This can be determined from Equation 77 with the appropriate substitutions (Equations 78-79).

$$\ln(0.001) = -\frac{w_s}{H_{weir}} t_3 * \left(\frac{v_b + v_w}{v_b}\right) \tag{78}$$

$$t_3 = -\frac{H_{weir}}{w_s} * \ln(0.001) * \left(\frac{v_b}{v_b + v_w}\right) \tag{79}$$

The total amount of sediment lost while under boat effects is thus $BSS = \int_0^{t_3} Q_{weir} C \, dt$.

The equations above simplify to Equation 80.

$$BSS = Q_{weir} C_0 * \left(-\frac{H_{weir}}{w_s} \frac{v_b}{v_b + v_w}\right) * \left(e^{\ln(0.001)} - 1\right) \tag{80}$$

Considering that 0.001 was just the arbitrary ‘just greater than zero’ value used to represent zero in a formula that would not allow a zero, this can be simplified further to Equation 81.

$$BSS = Q_{weir} CS_{boat} * \left(\frac{H_{weir}}{w_s} \frac{v_b}{v_b + v_w} \right) \quad (81)$$

In this case, C_o is the increase in the concentration of solids caused by boat passage, CS_{boat}, an input by the user.

This description has been for a boat moving downstream past the weir. If the boat is moving upstream, the value held by the v_b variable becomes negative. The time that has passed since the boat crossed the weir is greater than the time the sediment has been settling, as illustrated in Figure 92. The distance travelled by the boat since being deposited becomes $-t_1*(v_w+v_b)$ but in turn the total distance travelled by the boat since crossing the weir becomes $t_1*v_w + -t_1*(v_w+v_b)$, and the equations work out the same as for a boat moving downstream. When the equations are combined in Equation 45, the amount of boat-contributed sediment is thus based on the entire F_{boat} of the downstream lock, regardless of whether the boats are moving upstream or downstream.

Finally, all these equations have used Q_{weir} and H_{weir}; substituting $Q_{w,lock}$ and H_{lock} for these values gives the equivalent scenario for flow over the lock gates.

A.3. Algal Growth

A key component of the algal growth algorithm presented in Section 4.2.4.2 is the estimation of light intensity (LI). The HSPF model uses Equations 82-84 to predict available light intensity.

$$LI = 0.97 * C_{rad} * RAD * e^{(-EXTCO*0.5*Min(ED,D))} \quad (82)$$

$$EXTCO = 0.000452 * \lfloor SS_{alg} \rfloor + LITSED * \lfloor SS_{inorg} \rfloor + EXTB \quad (83)$$

$$ED = \frac{4.60517}{EXTCO} \quad (84)$$

Where: C_{rad} = coefficient for radiation, accounts for the effects of shading of the water (unitless);
RAD = incoming radiation (Langleys/min);
ED = euphotic depth (ft);
D = water depth (ft);
EXTCO = light extinction coefficient (1/ft);
0.000452 = light extinction due to algae (L ft^{-1} µmol Chl-a^{-1});
$[SS_{alg}]$= phytoplankton concentration (µmol Chl-a/L);
LITSED = light extinction due to inorganic sediment (L ft^{-1} mg^{-1});

$[SS_{inorg}]$ = inorganic sediment concentration (mg/L);
EXTB = base light extinction coefficient (1/ft); and
4.60517 = ln(100).

The 0.5 in Equation 82 captures the light available to phytoplankton at half the euphotic depth, used to represent the average light availability for all plankton in the euphotic depth. The 0.97 in Equation 82 accounts for an assumed 3% surface reflection of radiation.

These basic formulae, which match those presented elsewhere in the literature (Equations 21 and 22), are used in the canal model. However, in order to make the canal model more generic, the factor 0.000452 is replaced by an input variable LITALG. Additionally, all units are changed to metric units, and the concentration of phytoplankton (algae) is tracked in milligrams of dry biomass rather than μmol of chlorophyll-a. The concentrations of algae and inorganic sediment are calculated as Equations 85 and 86, respectively.

$$\left[SS_{a\lg}\right] = \frac{SS_{a\lg}}{Vol_{ED}} \tag{85}$$

$$\left[SS_{inorg}\right] = \frac{SS_{coh} + SS_{non}}{S} \tag{86}$$

The concentration of algae is limited to the euphotic depth, as that is where algae are assumed to remain, and thus that is the concentration that will affect light available to them.

Because euphotic depth is dependent upon algal concentration (through EXTCO, Equation 83), but algal concentration is, in turn, dependent on euphotic depth (Equation 85), the use of Equation 82 for LI is not straightforward. If euphotic depth is less than the water depth, Equation 82 simplifies to Equation 87.

$$LI = 0.97 * C_{rad} * RAD * e^{(-0.5*\ln(100))} \tag{87}$$

However, in this case, every time an algal concentration is used in the code (e.g., Equation 52), the euphotic depth must be calculated and used to determine the volume (Vol_{ED}) used in the concentration calculation. If, by contrast, euphotic depth is greater than the water depth, the LI equation becomes complicated – with the terms in

the exponent of the LI equation requiring input of the algal concentration, which in turn is dependent on the available light intensity. In this case Vol_{ED} becomes equal to depth in calculating the algal concentration. These two cases require separate solutions, presented in Appendix A.4.

As a final note, it may seem odd to use the value 0.5*ED to represent the average light intensity available to algae, as Equation 82 is readily integrated to obtain the actual average LI over the euphotic depth (Equation 88 for ED<D, Equation 89 for ED>D).

$$LI_{avg} = \frac{0.97 * C_{rad} * RAD}{4.60517}\left(1 - e^{-4.60517}\right) \tag{88}$$

$$LI_{avg} = \frac{0.97 * C_{rad} * RAD}{EXTCO}\left(1 - e^{-EXTCO \cdot D}\right) \tag{89}$$

However, finding an average maximum growth rate over the euphotic depth from Equation 58 is somewhat more problematic as Equation 58 is not readily integrated. To evaluate the relative merits of discretizing Equations 58 and 88 vs. simply using the light intensity calculated at half the euphotic depth, a comparison was performed in Microsoft Excel. The light intensity was calculated for 3500 increments between the water surface and a sample euphotic depth. With 3500 increments, the average LI over the water depth was calculated within 0.04% of the actual value obtained through integration. $LI/(K_{s,l}+LI)$ was then calculated for each of these 3500 depths. Given the accuracy of the LI estimate with 3500 increments, it was assumed the average $LI/(K_{s,l}+LI)$ estimate would be equally representative of the true average value over the water depth. This 'true' average $LI/(K_{s,l}+LI)$ was then compared to the single values of $LI/(K_{s,l}+LI)$ obtained using the depth-averaged LI from integration (Equation 88) and the LI calculated at half the euphotic depth (Equation 82). In most cases the single value for $LI/(K_{s,l}+LI)$ obtained using HSPF's method of estimating a representative LI was actually much closer to the true mean value for $LI/(K_{s,l}+LI)$ than the value obtained using the true average LI – typically errors less than 10% for the former vs. greater than 30% for the latter. The only exception to this was when the radiation dropped very low – less than 50 ly/day. However, even at latitudes of 50º, the radiation never drops beneath 100 ly/day (Hamon et al. 1954), so this extreme case was considered unlikely to occur, and thus HSPF's method of estimating average LI as the value at half the euphotic depth is used in the new canal model.

A.4. Solution Details

In this section, detailed information regarding the solution to the complex series of equations presented in Section 4.1 is presented. If through these processes the hydrologic storage falls below 1 cm, water quality processes cease to be simulated; this is consistent with what is done by some other models (e.g., Bicknell et al. 2001) and prevents in particular unrealistic estimation of shear stress (which propagates to unrealistic estimates of deposition). In this case, solids loads are held constant at the value from the previous time step and inflows and outflows are calculated based on that constant value.

(i) Detailed Q and QSS formulae

Equations 90-92 present detailed Q and QSS formulae for hydrology, non-cohesive sediment, cohesive sediment, and algae, respectively, including all the components presented in the appropriate subsections of Section 4.1.

$$Q = \left[\left(1 - E_{boat}\right) + \frac{E_{boat}}{2} + \frac{E_{boat} * Empty}{2} \right] * F_{boat} * V_{lock} + Q_{abs} + PE * SA$$
$$Seep * \left(\frac{2S_{j+1}}{W} + W * L \right) + \frac{2}{3} C_d \sqrt{2g} \left[\left(L_{weir} - 0.2 \left(\frac{S_{j+1}}{W * L} - D_{weir} \right) \right) \right. \quad (90)$$
$$\left. * \left(\frac{S_{j+1}}{W * L} - D_{weir} \right)^{3/2} + L_{lock} * \left(\frac{S_{j+1}}{W * L} - D_{lock} \right)^{3/2} \right] + Leak * Min\left(D, D_{lock}\right)$$

$$QSS_{non} = \frac{F_{boat}}{\Delta t} * Q_{weir} * CS_{boat} * \left(\frac{H_{weir}}{w_s} \frac{v_b}{v_b + v_w} \right) + Q_{weir} * \frac{SS - ISS_{boat}}{S} * e^{\frac{-w_s}{H_{weir}} \frac{L}{v_w}} +$$
$$\frac{F_{boat}}{\Delta t} * Q_{w,lock} * CS_{boat} * \left(\frac{H_{lock}}{w_s} \frac{v_b}{v_b + v_w} \right) + Q_{w,lock} * \frac{SS - ISS_{boat}}{S} * e^{\frac{-w_s}{H_{lock}} \frac{L}{v_w}} + (91)$$
$$\frac{SS}{S} * Q_{lock} + \frac{SS}{\Delta t} * \left(1 - e^{\frac{-w_s}{D} \Delta t} \right) + \frac{SS}{S} * Q_{abs} + \frac{SS}{S} * Q_{leak}$$

$$QSS_{coh} = \frac{F_{boat}}{\Delta t} * Q_{weir} * CS_{boat} * \left(\frac{H_{weir}}{w_s(SS)} \frac{v_b}{v_b + v_w} \right) +$$
$$Q_{weir} * \frac{SS - ISS_{boat}}{S} * e^{\frac{-p \cdot w_s(SS)}{H_{weir}} \frac{L}{v_w}} +$$
$$\frac{F_{boat}}{\Delta t} * Q_{w,lock} * CS_{boat} * \left(\frac{H_{lock}}{w_s(SS)} \frac{v_b}{v_b + v_w} \right) + \quad (92)$$
$$Q_{w,lock} * \frac{SS - ISS_{boat}}{S} * e^{\frac{-p \cdot w_s(SS)}{H_{lock}} \frac{L}{v_w}} + \frac{SS}{S} * Q_{lock} +$$
$$\frac{SS}{\Delta t} * \left(1 - e^{\frac{-p \cdot w_s(SS)}{D} \Delta t} \right) + \frac{SS}{S} * Q_{abs} + \frac{SS}{S} * Q_{leak}$$

The term $w_s(SS)$ indicates that the fall velocity for cohesive sediments is a function of the sediment concentration.

$$QSS_{alg} = \frac{SS \cdot D}{ED \cdot S} * \left(Q_{weir} + Q_{w,lock} + Q_{abs} + (ED - H_{lock}) \cdot Leak \right) + \frac{SS}{S} * Q_{lock} \quad (93)$$

Note that the equation for QSS_{alg} includes a leak term slightly different from that presented in Equation 54. To simplify the calculations, ED is first determined using QSS_{alg} in Equation 93; then the minimum and maximum comparisons are performed and QSS_{alg} and ED are recalculated if necessary.

(ii) Solving the System of Equations

A formula for Q_{j+1} or QSS_{j+1} having been defined for each constituent (Equations 90-93), the next step is to put these outflow formulae back into their respective continuity equation formulae (Equations 32, 33, and 55) to solve for the storage of each constituent at each time step. With the exception of non-cohesive sediment, this is not a straightforward procedure and Newton's Method must be used.

The solutions presented next assume that the sum of inflows for a constituent are constant, as well as some values that do not depend on the reach storage (for example, Q_{lock} and Q_{abs}). In some cases this assumption may cause the solution to the system of equations to be unattainable, as the 'fixed' outflow demand may exceed the available inflow plus storage. In these cases, the 'fixed' outflow demands are reduced so that they do not exceed the available inflows plus storage. Additionally, if for any reason

any of the storages are calculated to be negative, they are set to zero (water, inorganic sediment) or 1 (algae). Algal storage is always maintained above 0 so that a 'seed' exists to start growth at the next time step.

In all cases that use Newton's Method, if the cap on iterations is reached before the value for 'f(x)' falls below the error threshold, the final absolute value for f(x) is compared to that of the initial estimate; if the value for the final f(x) is less than that for the initial estimate, the final storage estimate is used even though the threshold was not met, as it is a better estimator than the initial estimate.

For the hydrology, the 'f(x)' (or f(S)) used for Newton's Method is given as Equation 94. The iteration of Newton's Method continues until the absolute value of the function is less than 0.00001 m^3/s. The derivative of the function with respect to storage is given in Equation 95. The initial guess for S_{j+1} is the value at the previous time step.

$$\begin{aligned} 0 = {} & \frac{2S_{j+1}}{\Delta t} - \left(\left(I_j + I_{j+1}\right) + \left[\frac{2S_j}{\Delta t} - Q_j \right] \right) + \\ & \left[\left(1 - E_{boat}\right) + \frac{E_{boat}}{2} + \frac{E_{boat} * Empty}{2} \right] * F_{boat} * V_{lock} + Q_{abs} + PE * SA \\ & + Seep * \left(\frac{2S_{j+1}}{W} + W * L \right) + \frac{2}{3} C_d \sqrt{2g} \left[\left(L_{weir} - 0.2 \left(\frac{S_{j+1}}{W * L} - D_{weir} \right) \right) \right. \\ & \left. * \left(\frac{S_{j+1}}{W * L} - D_{weir} \right)^{3/2} + L_{lock} * \left(\frac{S_{j+1}}{W * L} - D_{lock} \right)^{3/2} \right] \end{aligned} \tag{94}$$

$$\begin{aligned} 0 = {} & \frac{2}{\Delta t} + \frac{2 * Seep}{W} + \frac{2 * C_d \sqrt{2g}}{3 * W * L} \left[-0.2 * \left(\frac{S_{j+1}}{W * L} - D_{weir} \right)^{3/2} \right. \\ & + \frac{3}{2} \left(\frac{S_{j+1}}{W * L} - D_{weir} \right)^{1/2} \left(L_{weir} - 0.2 \left(\frac{S_{j+1}}{W * L} - D_{weir} \right) \right) \\ & \left. + \frac{3}{2} L_{lock} \left(\frac{S_{j+1}}{W * L} - D_{lock} \right)^{1/2} \right] \end{aligned} \tag{95}$$

For non-cohesive sediment, no iteration is required. The value for storage of non-cohesive sediment is a straightforward calculation (Equation 96).

$$SS_{j+1} = \left[S_{j+1} * \left(ISS_j \Delta t + ISS_{j+1} \Delta t + 2SS_j - QSS_j \Delta t - \right.\right.$$
$$F_{boat} Q_{weir,j+1} CS_{boat} \left(\frac{H_{weir} v_b}{w_s (v_b + v_w)} \right) - F_{boat} Q_{w,lock.j+1} CS_{boat} \left(\frac{H_{lock} v_b}{w_s (v_b + v_w)} \right) \Bigg)$$
$$\left. + Q_{weir,j+1} ISS_{boat,j+1} \Delta t \cdot e^{\frac{-w_s L}{H_{weir} v_w}} + Q_{w,lock,j+1} ISS_{boat,j+1} \Delta t \cdot e^{\frac{-w_s L}{H_{lock} v_w}} \right] \div \qquad (96)$$
$$\left[2S_{j+1} + Q_{weir,j+1} e^{\frac{-w_s L}{H_{weir} v_w}} \Delta t + Q_{w,lock,j+1} e^{\frac{-w_s L}{H_{lock} v_w}} \Delta t + \right.$$
$$\left. Q_{lock,j+1} \Delta t + S_{j+1} \left(1 - e^{\frac{-w_s}{D} \Delta t} \right) + Q_{abs,j+1} \Delta t + Q_{leak,j+1} \Delta t \right]$$

The storages for cohesive sediments and algae must be solved simultaneously, as the algal concentration affects the fall velocity used in computing cohesive sediment storage, and the cohesive sediment concentration is used in computing the light intensity used in computing algal storage. The storages are solved using Newton's Method. For the simple condition, when ED<D, the first step is to calculate $g(SS_{alg})$ (Equation 97), which is simply the algal equation rearranged to solve for cohesive sediment concentration (that is, $g(SS_{alg}) = SS_{coh}$). The initial guess for $SS_{alg,j+1}$ is set to half the value that causes $g(SS_{alg,j+1})$ to be zero; this is done to prevent the initial estimate from inadvertently landing outside the narrowly defined range for the ED>D function (discussed momentarily).

$$g\left(SS_{alg,j+1}\right) = \left\{ \left[\frac{-2S_{j+1}}{D_{j+1} SS_{bio,j+1}} \left(\frac{SS_{alg,j+1} - SS_{alg,j}}{\Delta t} - \frac{ISS_j + ISS_{j+1}}{2} + \frac{QSS_j}{2} - \frac{\mu_j SS_{alg,j}}{2} \right) + \right.\right.$$
$$\left. \left. \frac{-Q_{lock,j+1} + \mu_{\max,j+1} S_{j+1}}{D_{j+1}} - Leak \right] * \left(4.60517 \cdot S_{j+1} - LITALG \cdot SS_{bio,j+1} D_{j+1} / CHL\right) \right\} \div$$
$$\left[LITSED \left(\frac{\mu_{\max,j+1} SS_{alg,j+1}}{K_{j+1}} + Q_{weir,j+1} + Q_{w,lock,j+1} + Q_{abs,j+1} - H_{lock} Leak \right) \right] -$$
$$SS_{non,j+1} - \frac{EXTB \cdot S_{j+1}}{LITSED}$$

(97)

This $g(SS_{alg})$ can then be used in place of SS_{coh} to solve the set of cohesive sediment equations as a function of SS_{alg}. In this way, f(SS) for Newton's Method becomes Equation 98.

$$0 = -S_{j+1}\left(ISS_j + ISS_{j+1} + 2\frac{SS_{coh,j}}{\Delta t} - QSS_j \right) +$$
$$\frac{F_{boat} CS_{boat} v_b S_{j+1}}{\Delta t \cdot p \cdot w_s (SS_{coh,j+1} + SS_{a\lg,j+1}) \cdot (v_b + v_w)} \left(Q_{weir,j+1} H_{weir} + Q_{w,lock,j+1} H_{lock} \right) +$$
$$\left(g\left(SS_{a\lg,j+1}\right) - ISS_{boat,j+1} \right) \left(Q_{weir,j+1} e^{\frac{-p \cdot w_s (SS_{coh,j+1} + SS_{a\lg,j+1}) \frac{L}{v_w}}{H_{weir}}} + Q_{w,lock,j+1} e^{\frac{-p \cdot w_s (SS_{coh,j+1} + SS_{a\lg,j+1}) \frac{L}{v_w}}{H_{lock}}} \right) +$$
$$g\left(SS_{a\lg,j+1}\right) \left(Q_{lock,j+1} - \frac{S_{j+1}}{\Delta t} e^{\frac{-p \cdot w_s (SS_{coh,j+1} + SS_{s\lg,j+1})}{D} \Delta t} + Q_{abs,j+1} + 3\frac{S_{j+1}}{\Delta t} + Q_{leak,j+1} \right)$$

(98)

Where:

$$w_s(SS) = \left[1 - \frac{1}{1.815 + 0.00318\frac{SS}{S} - 0.00000014\left(\frac{SS}{S}\right)^2} \right] * w_{s,macro} + \frac{w_{s,micro}}{1.815 + 0.00318\frac{SS}{S} - 0.00000014\left(\frac{SS}{S}\right)^2} \quad (99)$$

Equation 100 presents the derivative of f(SS).

$$f'(SS_{j+1}) = 0 = \frac{F_{boat} CS_{boat} v_b S_{j+1}}{\Delta t \cdot (v_b + v_w) \cdot (w_s(SS))^2} \left(Q_{weir,j+1} H_{weir} + Q_{w,lock,j+1} H_{lock} \right) * \frac{d(w_s)}{dSS_{j+1}} +$$
$$\left(g\left(SS_{a\lg,j+1}\right) - ISS_{boat,j+1} \right) \left(Q_{weir,j+1} \frac{-L \cdot p}{H_{weir} v_w} \frac{d(w_s)}{dSS_{j+1}} e^{\frac{-p \cdot w_s(SS)}{H_{weir}} \frac{L}{v_w}} + \right.$$
$$\left. Q_{w,lock,j+1} \frac{-L \cdot p}{H_{lock} v_w} \frac{d(w_s)}{dSS_{j+1}} e^{\frac{-p \cdot w_s(SS)}{H_{lock}} \frac{L}{v_w}} \right) +$$
$$\left(Q_{weir,j+1} e^{\frac{-p \cdot w_s(SS)}{H_{weir}} \frac{L}{v_w}} + Q_{w,lock,j+1} e^{\frac{-p \cdot w_s(SS)}{H_{lock}} \frac{L}{v_w}} \right) \left(g'\left(SS_{a\lg,j+1}\right) \right) +$$
$$g\left(SS_{a\lg,j+1}\right) \left(S_{j+1} \frac{p}{D} \frac{d(w_s)}{dSS_{j+1}} e^{\frac{-p \cdot w_s(SS)}{D} \Delta t} \right) +$$
$$g'\left(SS_{a\lg,j+1}\right) \left(Q_{lock,j+1} - \frac{S_{j+1}}{\Delta t} e^{\frac{-p \cdot w_s(SS)}{D} \Delta t} + Q_{abs,j+1} + 3\frac{S_{j+1}}{\Delta t} + Q_{leak,j+1} \right) \quad (100)$$

Where:

$$g'\left(SS_{a\lg,j+1}\right)=\left\{\left(\left[\frac{-2S_{j+1}}{D_{j+1}SS_{a\lg,j+1}}\left(\frac{SS_{a\lg,j+1}-SS_{a\lg,j}}{\Delta t}-\frac{ISS_j+ISS_{j+1}}{2}+\frac{QSS_j}{2}-\frac{\mu_j SS_{a\lg,j}}{2}\right)+\right.\right.$$

$$\left.\frac{-Q_{lock,j+1}+\mu_{\max,j+1}S_{j+1}}{D_{j+1}}-Leak\right]\cdot\left(-LITALG\cdot D_{j+1}/CHL\right)+$$

$$\left(4.60517\cdot S_{j+1}-LITALG\cdot SS_{a\lg,j+1}\cdot D_{j+1}/CHL\right)*$$

$$\left.\left(\frac{-2S_{j+1}\left(\frac{SS_{a\lg,j}}{\Delta t}+\frac{ISS_j+ISS_{j+1}}{2}-\frac{QSS_j}{2}+\frac{\mu_j SS_{a\lg,j}}{2}\right)}{D_{j+1}\left(SS_{a\lg,j+1}\right)^2}\right)\right)*$$

$$LITSED\left(\frac{\mu_{\max,j+1}SS_{a\lg,j+1}}{K_{j+1}}+Q_{weir,j+1}+Q_{w,lock,j+1}+Q_{abs,j+1}-Leak\left(D_{j+1}-D_{lock}\right)\right)-$$

$$\left[\frac{-2S_{j+1}}{D_{j+1}SS_{a\lg,j+1}}\left(\frac{SS_{a\lg,j+1}-SS_{a\lg,j}}{\Delta t}-\frac{ISS_j+ISS_{j+1}}{2}+\frac{QSS_j}{2}-\frac{\mu_j SS_{a\lg,j}}{2}\right)+\right.$$

$$\left.\frac{-Q_{lock,j+1}+\mu_{\max,j+1}S_{j+1}}{D_{j+1}}-Leak\right]*$$

$$\left.\left(4.60517\cdot S_{j+1}-LITALG\cdot SS_{a\lg,j+1}D_{j+1}/CHL\right)\cdot\frac{LITSED\cdot\mu_{\max,j+1}}{K_{j+1}}\right\}\div$$

$$\left[LITSED\left(\frac{\mu_{\max,j+1}SS_{a\lg,j+1}}{K_{j+1}}+Q_{weir,j+1}+Q_{w,lock,j+1}+Q_{abs,j+1}-Leak\left(D_{j+1}-D_{lock}\right)\right)\right]^2$$

(101)

and

$$\frac{d\left(w_s\right)}{dSS_{a\lg}}=\frac{d\left(w_{s,macro}\right)}{dSS_{a\lg}}-\left[\frac{d\left(w_{s,macro}\right)}{dSS_{a\lg}}*\right.$$

$$\left(1.815+0.00318\frac{SS_{a\lg}+SS_{coh}}{S\cdot1000}-0.00000014\left(\frac{SS_{a\lg}+SS_{coh}}{S\cdot1000}\right)^2\right)$$

$$\left.-\left(w_{s,macro}-w_{s,micro}\right)\left(\frac{0.00318}{S\cdot1000}-\frac{0.00000028\left(SS_{a\lg}+SS_{coh}\right)}{\left(S\cdot1000\right)^2}\right)\right]\div \quad (102)$$

$$\left[1.815+0.00318\frac{SS_{a\lg}+SS_{coh}}{S\cdot1000}-0.00000014\left(\frac{SS_{a\lg}+SS_{coh}}{S\cdot1000}\right)^2\right]^2$$

And finally,

$$\frac{d\left(w_{s,macro}\right)}{dSS_{a\lg}} = \begin{cases} 0.00471 \div \left(S \cdot 1000\right) & 0.04 < \tau < 0.7 \\ 0.000346 \div \left(S \cdot 1000\right) & 0.6 < \tau < 1.5 \\ 0.000303 \div \left(S \cdot 1000\right) & 1.4 < \tau < 5 \end{cases} \tag{103}$$

If ED>D, then g(SS_{alg}) must be rewritten as Equation 104. Typically the f(SS) calculated in Equation 98 becomes negative when ED>D (Figure 93); this transition to a negative value for f(SS) is used in the model as an indication to switch to ED>D calculations. The relationship between ED and D is verified once Newton's Method converges on a solution.

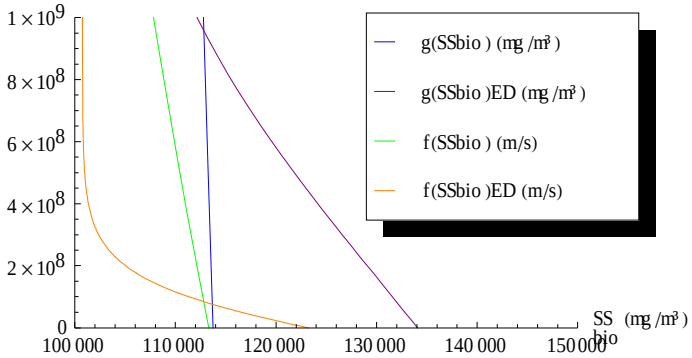

Figure 93. Typical zeros of f(SS_{alg}) and g(SS_{alg}) when euphotic depth is greater than (indicated by subscript ED) and less than water depth. (SSbio = SS_{alg} in this figure)

$$\begin{aligned} g\left(SS_{a\lg,j+1}\right) = & -\frac{EXTB \cdot S_{j+1}}{LITSED} - \frac{LITALG \cdot SS_{a\lg,j+1}}{Chl \cdot LITSED} + \\ & \ln\left[0.97C_{rad} \cdot RAD\left(\Delta t \cdot K \cdot \chi \cdot S_{j+1} - \Delta t \cdot K \cdot Q \cdot SS_{a\lg,j+1} - \right.\right. \\ & 2 \cdot K \cdot S_{j+1} SS_{a\lg,j+1} + \Delta t \cdot K \cdot \mu_{\max,T} \cdot S_{j+1} SS_{a\lg,j+1} \\ & \left.\left. - \Delta t \cdot \mu_{\max,T} \cdot SS^2_{a\lg,j+1}\right) \div \right. \\ & \left. K \cdot K_{s,l} \cdot \left(-\Delta t \cdot \chi \cdot S_{j+1} + \Delta t \cdot Q \cdot SS_{a\lg,j+1} + 2 \cdot S_{j+1} \cdot SS_{a\lg,j+1}\right)\right] * \\ & \frac{2 \cdot S_{j+1}}{D \cdot LITSED} - SS_{non,j+1} \end{aligned} \tag{104}$$

Where: $\chi = ISS_{a\lg,j} + ISS_{a\lg,j+1} + \frac{2 \cdot SS_{a\lg,j}}{\Delta t} - QSS_{a\lg,j} + \mu_j SS_{a\lg,j}$; and

$$Q = Q_{weir,j+1} + Q_{w,lock,j+1} + Q_{abs,j+1} + Q_{leak,j+1} + Q_{lock,j+1}$$

And the derivative of g(SS_{alg}) becomes Equation 105. Because f(SS) only deals with inflows and outflows related to cohesive sediment, it remains unchanged.

$$g'\left(SS_{a\lg,j+1}\right)=\frac{-LITALG}{Chl\cdot LITSED}-\frac{2S_{j+1}}{D\cdot LITSED}\cdot$$
$$\left[\frac{2S_{j+1}+\Delta t\cdot Q}{2S_{j+1}SS_{a\lg,j+1}+\Delta t\cdot Q\cdot SS_{a\lg,j+1}-\Delta t\cdot\chi\cdot S_{j+1}}-\right.$$
$$\left(-\Delta t\cdot K\cdot Q-2K\cdot S_{j+1}+\Delta t\cdot K\cdot\mu_{\max,T}\cdot S_{j+1}-2\Delta t\cdot\mu_{\max,T}\cdot SS_{bio,j+1}\right)\div$$
$$\left(\Delta t\cdot K\cdot\chi\cdot S_{j+1}-\Delta t\cdot K\cdot Q\cdot SS_{a\lg.j+1}-2\cdot K\cdot S_{j+1}\cdot SS_{a\lg,j+1}+\right.$$
$$\left.\left.\Delta t\cdot K\cdot\mu_{\max,T}\cdot SS_{a\lg,j+1}\cdot S_{j+1}-\Delta t\cdot\mu_{\max,T}SS^{2}_{a\lg,j+1}\right)\right]$$

(105)

In both cases (ED>D and ED<D), the iterations for Newton's Method continue until the absolute value of f(x) is less than 0.1 mg·m³/s.

Note that should the input phosphorus concentration for a given time step be zero, all equations involving 'K' in the denominator would be undefined; therefore, if the input phosphorus concentration is zero, algal growth is set to zero and all terms in the formulae related to algal growth are removed.

If the calculated euphotic depth is negative or zero, the algae are assumed uniformly distributed in the water column and the algal and cohesive solids storages are recalculated.

Appendix B. Model Verification Inputs

Table 21. Reach parameters for the verification scenario.

Parameter	Value		
Reach Number	1	2	3
Length (m)	536.33	402.25	804.5
Width (m)	13.33	11.67	14
Overflow weir location (upstream of lock) (m)	1	2	3
Height of overflow weir above bottom of reach (m)	3	3.2	2.9
Length of overflow weir crest (m)	0.33	0.67	0.5
Height of sides of overflow weir (m)	0.167	0.173	0.15
Height of lock gates above bottom of reach (m)	3.5	3.9	3.4
Weir Constant (Ø)	0.611	0.61	0.612
Seepage losses ($m^3/m^2/s$)	1.08×10^{-7}	1.15×10^{-7}	1.05×10^{-7}
Number of locks contributing flow at upstream end	0	1	1
ID number of downstream lock	1	2	3
ID number of upstream lock	0	1	2
ID number of upstream reach	0	1	2
Mean reach temperature (ºC)	12.1	11.5	12.6
Correction to incoming radiation (Ø)	0.7	0.65	0.75

Table 22. Lock parameters for the verification scenario.

Parameter	Value		
Lock Number	1	2	3
Is the lock left empty after use?	Yes	No	Yes
Efficiency of lock use by boats (Ø)	0.5	0.75	0.4
Volume (m^3)	1777.78	1347.5	2272.5
Length of lock gates (m)	13.33	11.67	15
Gate leakage rate (m^3/m)	0.010031	0.000893	0.010896
Fraction of boats moving upstream (Ø)	0.5	0.4	0.6
Fraction of boats moving downstream (Ø)	0.5	0.6	0.4
Non-cohesive sediment concentration stirred up by lock gate movement (mg/m^3)	30000	32000	28000
Cohesive sediment concentration stirred up by lock gate movement (mg/m^3)	10000	12000	11000

Table 23. Solids parameters for the verification scenario.

Parameter	Value
Non-cohesive particle diameter (m)	0.0002
Specific gravity of sediment (Ø)	2.65
Critical shear stress for the deposition of sediment (kg m^{-1} s^{-2})	0.06
Drag coefficient (Ø)	0.0025
Concentration of non-cohesive sediment stirred up by boat passage (mg/m^3)	14500
Concentration of cohesive sediment stirred up by boat passage (mg/m^3)	29000
Average boat velocity (including water velocity) (m/s)	1.8
Fraction of sediment in runoff that is non-cohesive (Ø)	0.6
Fraction of sediment in runoff that is cohesive (Ø)	0.4
Fraction of sediment from external sources that is non-cohesive (Ø)	0.3
Fraction of sediment from external sources that is cohesive (Ø)	0.7
Base light extinction coefficient (m^{-1})	1
Michaelis-Menton constant for light-limited growth (J/m^2s)	23.012
Magnitude parameter for temperature equation	6.28
Phase shift parameter for temperature equation	4.46
Conversion from chlorophyll-a mass to total biomass (mg biomass/mg Chl-a)	1.5
Factor to convert sediment concentration to light extinction (m^2/mg)	0.000025
Factor to convert algal concentration to light extinction (m^2/(mg Chl-a))	0.00002

Table 24. Sample time series inputs for the first five timesteps for the verification scenario.

Parameter	Value				
Timestep	Day 1	Day 2	Day 3	Day 4	Day 5
Precipitation (m)	0.0048	0.0054	0.0027	0	0
Radiation (J/m²/s)	121.06	96.851	193.7	121.06	121.06
Potential evaporation (m)	0.0008	0	0.0005	0.0012	0.0004
Frequency of boat movement – reach 1 (Ø)	4	4	4	4	4
Frequency of boat movement – reach 2 (Ø)	5	5	5	5	5
Frequency of boat movement – reach 3 (Ø)	7	7	7	7	7
External hydrologic inputs – reach 1 (m³/s)	0.125	0.127	0.123	0.125	0.124
External hydrologic inputs – reach 2 (m³/s)	0.002	0.003	0.002	0.004	0.002
External hydrologic inputs – reach 3 (m³/s)	0.003	0.005	0.001	0.001	0.002
External sediment inputs – reach 1 (mg/m³)	0.125	0.127	0.123	0.125	0.124
External sediment inputs – reach 2 (mg/m³)	0.002	0.003	0.002	0.004	0.002
External sediment inputs – reach 3 (mg/m³)	0.003	0.005	0.001	0.001	0.002
External algal inputs – reach 1 (mg/m³)	0.125	0.127	0.123	0.125	0.124
External algal inputs – reach 2 (mg/m³)	0.002	0.003	0.002	0.004	0.002
External algal inputs – reach 3 (mg/m³)	0.003	0.005	0.001	0.001	0.002
Runoff hydrologic inputs – reach 1 (m³/s)	0.001	0	0.003	0	0.002
Runoff hydrologic inputs – reach 2 (m³/s)	0.002	0.004	0	0.005	0.001
Runoff hydrologic inputs – reach 3 (m³/s)	0	0.001	0.003	0.002	0.001
Runoff sediment inputs – reach 1 (mg/m³)	0.01	0	0.03	0	0.02
Runoff sediment inputs – reach 2 (mg/m³)	0.013	0.015	0	0.01	0.025
Runoff sediment inputs – reach 3 (mg/m³)	0	0.007	0.022	0.04	0.036
Hydrologic abstractions – reach 1 (m³/s)	0.0001	0	0	0.0001	0.0001
Hydrologic abstractions – reach 2 (m³/s)	0.0003	0	0.0003	0	0.0003
Hydrologic abstractions – reach 3 (m³/s)	0.0002	0.0002	0	0.0002	0.0002
Total phosphorus concentration – reach 1 (mg/m³)	186	219	176	166	483
Total phosphorus concentration – reach 2 (mg/m³)	139.5	164.25	132	124.5	362.25
Total phosphorus concentration – reach 3 (mg/m³)	232.5	273.75	220	207.5	603.75

Appendix C. Sensitivity Analysis Baseline Parameters

$C_e = 0.7$

Table 25. Reach parameters for the sensitivity analysis.

Parameter	Value		
Reach Number	1	2	3
Length (m)	18.00	270.68	322.11
Width (m)	9.98	9.03	7.85
Overflow weir location (upstream of lock) (m)	0	0	0
Height of overflow weir above bottom of reach (m)	1.37	1.42	1.425
Length of overflow weir crest (m)	2.44	1.83	1.88
Height of sides of overflow weir (m)	0.14	0.33	0.20
Height of lock gates above bottom of reach (m)	1.55	1.6	1.6
Weir Constant (Ø)	0.611	0.611	0.611
Seepage losses ($m^3/m^2/s$)	3.72×10^{-7}	3.72×10^{-7}	3.72×10^{-7}
Mean reach temperature (ºC)	11.5	11.5	11.5
Correction to incoming radiation (Ø)	1.0	0.92	0.89

Table 26. Lock parameters for the sensitivity analysis.

Parameter	Value		
Lock Number	1	2	3
Is the lock left empty after use?	Yes	Yes	Yes
Efficiency of lock use by boats (Ø)	0.67	0.67	0.67
Volume (m^3)	173.02	229.27	201.52
Length of lock gates (m)	17.67	17.33	16.00
Gate leakage rate (m^3/m)	0.044	0.021	0.021
Non-cohesive sediment concentration stirred up by lock gate movement (mg/m^3)	1000	1000	1000
Cohesive sediment concentration stirred up by lock gate movement (mg/m^3)	2600	2600	2600

Table 27. Solids parameters for the sensitivity analysis.

Parameter	Value
Non-cohesive particle diameter (m)	0.0002
Specific gravity of sediment (Ø)	2.65
Critical shear stress for the deposition of sediment (kg m^{-1} s^{-2})	0.06
Drag coefficient (Ø)	0.0025
Concentration of non-cohesive sediment stirred up by boat passage (mg/m^3)	4500
Concentration of cohesive sediment stirred up by boat passage (mg/m^3)	9000
Average boat velocity (including water velocity) (m/s)	1.79
Fraction of sediment in runoff that is non-cohesive (Ø)	0.2
Fraction of sediment in runoff that is cohesive (Ø)	0.8
Fraction of sediment from external sources that is non-cohesive (Ø)	0.15
Fraction of sediment from external sources that is cohesive (Ø)	0.85
Base light extinction coefficient (m^{-1})	1.67
Michaelis-Menton constant for light-limited growth (J/m^2s)	23.012
Magnitude parameter for temperature equation	6.54
Phase shift parameter for temperature equation	4.46
Conversion from chlorophyll-a mass to total biomass (mg biomass/mg Chl-a)	60
Factor to convert sediment concentration to light extinction (m^2/mg)	0.000025
Factor to convert algal concentration to light extinction (m^2/(mg Chl-a))	0.00002

Table 28. Sample time series inputs for the first five timesteps of the sensitivity analysis.

Parameter	Value				
Timestep	Day 1	Day 2	Day 3	Day 4	Day 5
Precipitation (m/d)	0.0021	0.0049	0.0094	0.0073	0.0014
Radiation ($J/m^2/s$)	29.7	30.0	30.3	30.6	30.9
Potential evaporation (m/d)	0.00047	0.00042	0.00040	0.00051	0.00055
Frequency of boat movement (Ø)	1	1	1	1	1
External hydrologic inputs – reach 1 (m^3/s)	0.063	0.063	0.063	0.063	0.063
External hydrologic inputs – reach 2 (m^3/s)	0	0	0	0	0
External hydrologic inputs – reach 3 (m^3/s)	0	0	0	0	0
External sediment inputs – reach 1 (mg/s)	630	630	630	630	630
External sediment inputs – reach 2 (mg/s)	0	0	0	0	0
External sediment inputs – reach 3 (mg/s)	0	0	0	0	0
External algal inputs – reach 1 (mg/s)	2.29	2.32	2.35	2.38	2.41
External algal inputs – reach 2 (mg/s)	0	0	0	0	0
External algal inputs – reach 3 (mg/s)	0	0	0	0	0
Runoff hydrologic inputs – reach 1 (m^3/s)	0.0239	0.0255	0.0310	0.0311	0.0277
Runoff hydrologic inputs – reach 2 (m^3/s)	0.00255	0.00228	0.00331	0.00332	0.00296
Runoff hydrologic inputs – reach 3 (m^3/s)	0.00228	0.00242	0.00295	0.00296	0.00264
Runoff sediment inputs – reach 1 (mg/s)	0.708	7.06	246	82.3	0.176
Runoff sediment inputs – reach 2 (mg/s)	0.0755	0.753	26.2	8.78	0.0188
Runoff sediment inputs – reach 3 (mg/s)	0.0673	0.672	23.4	7.83	0.0168
Hydrologic abstractions – reach 1 (m^3/s)	0.008	0.008	0.008	0.008	0.008
Hydrologic abstractions – reach 2 (m^3/s)	0	0	0	0	0
Hydrologic abstractions – reach 3 (m^3/s)	0.009	0.009	0.009	0.009	0.009
Total phosphorus concentration (mg/m^3)	302.4	302.4	302.4	302.4	302.4

Appendix D. Sensitivity Analysis – Results

D.1. Non-cohesive Sediment Variables

The key parameters to which the non-cohesive sediment variables are most sensitive are listed in Table 29. Table 30 complements the data for SS_{non} in Table 10 on page 111, showing relative sensitivities of the concentration of non-cohesive sediment to the remaining parameters where $|S_r| < 0.5$.

Table 29. Key parameters to which the non-cohesive sediment variables are most sensitive.

Var.	Most Sig. Param.	Average Sensitivities									
		Avg	Max	Min	1Q	2Q	3Q	W	Sp	Su	A
SS_{non}	I_{ext}	0.41	0.28	0.03	0.04	0.54	0.40	0.01	0.07	0.58	0.46
	L	1.30	1.38	-0.04	0.81	1.13	1.36	0.14	1.26	1.39	1.32
	W	0.58	0.67	-0.04	0.27	0.50	0.62	0.02	0.54	0.64	0.59
	D_{weir} ‡	1.15	1.26	0.22	0.77	1.08	1.21	0.31	1.08	1.23	1.16
	D_{lock} †	0.83	0.84	1.05	0.60	0.82	0.86	0.35	0.83	0.86	0.82
	V_{lock}	-0.35	-0.46	<0.01	<0.01	-0.21	-0.41	<0.01	-0.20	-0.47	-0.33
	$CS_{boat,non}$	0.82	0.86	<0.01	0.62	0.79	0.85	0.13	0.82	0.85	0.84
	F_{boat}	0.52	0.49	<0.01	0.00	0.68	0.53	<0.01	0.66	0.45	0.56
QSS_{abs}	Q_{abs}	0.91	0.93	0.79	0.86	0.91	0.92	0.82	0.91	0.92	0.91
	$CS_{boat,non}$	0.82	0.86	<0.01	0.62	0.79	0.85	0.13	0.82	0.85	0.84
	F_{boat}	0.61	0.60	0.00	0.00	0.71	0.68	0.00	0.68	0.59	0.66
QSS_{weir}	I_{runoff}	0.94	1.00	0.00	2.79	1.36	0.84	1.28	0.90	1.21	0.66
	I_{ext}	5.43	3.59	0.00	6.82	16.77	4.90	2.32	3.74	7.90	6.16
	Q_{abs}	-0.92	-0.60	0.00	-3.77	-2.41	-0.84	-0.63	-0.63	-1.32	-1.06
	D_{weir} ‡	-2.81	-2.67	0.00	-5.07	-5.40	-2.51	-2.88	-2.72	-2.92	-2.87
	L_{weir}	-0.66	-0.68	0.00	-0.48	-0.66	-0.64	-0.63	-0.66	-0.65	-0.65
	Empty	-0.88	-0.49	0.00	-0.23	-5.07	-0.73	-0.03	-0.42	-1.68	-0.92
	V_{lock}	-2.05	-1.19	0.00	-4.08	-7.03	-1.71	-0.09	-1.14	-3.63	-2.14
	diam	-1.62	-1.62	0.00	-1.62	-1.62	-1.62	-1.62	-1.62	-1.62	-1.62
	sg	-1.48	-1.48	0.00	-1.48	-1.48	-1.48	-1.48	-1.48	-1.48	-1.48
	$CS_{boat,non}$	1.00	1.00	0.00	1.00	1.00	1.00	1.00	1.00	1.00	1.00
	$C_{d,weir}$	-0.65	-0.68	0.00	-0.47	-0.66	-0.63	-0.63	-0.66	-0.65	-0.65
	Leak	-1.67	-1.10	0.00	-4.87	-4.02	-1.54	-1.15	-1.17	-2.37	-1.92
	F_{boat}	-0.98	-0.13	0.00	-4.00	-5.03	-0.65	0.00	-0.12	-2.45	-1.06
QSS_{dep}	I_{ext}	0.41	0.28	0.03	0.04	0.54	0.40	0.01	0.07	0.58	0.46
	L	1.30	1.38	-0.04	0.81	1.13	1.36	0.14	1.26	1.39	1.32
	W	0.58	0.67	-0.04	0.27	0.50	0.62	0.02	0.54	0.64	0.59
	D_{weir} ‡	1.15	1.26	0.22	0.77	1.08	1.21	0.31	1.08	1.23	1.16
	D_{lock} †	0.83	0.84	1.05	0.60	0.82	0.86	0.35	0.83	0.86	0.82
	V_{lock}	-0.35	-0.46	<0.01	<0.01	-0.21	-0.41	0.00	-0.20	-0.47	-0.33
	$CS_{boat,non}$	0.82	0.86	<0.01	0.62	0.79	0.85	0.13	0.82	0.85	0.84
	F_{boat}	0.52	0.49	<0.01	0.00	0.68	0.53	<0.01	0.66	0.45	0.56
QSS_{leak}	I_{ext}	0.41	0.28	0.03	0.04	0.54	0.40	0.01	0.07	0.58	0.46
	D_{weir} ‡	1.14	1.26	0.21	0.77	1.07	1.21	0.29	1.07	1.23	1.15
	D_{lock} †	0.85	0.86	1.05	0.64	0.85	0.89	0.41	0.87	0.88	0.85
	V_{lock}	-0.35	-0.46	<0.01	<0.01	-0.21	-0.41	<0.01	-0.20	-0.47	-0.33
	$CS_{boat,non}$	0.82	0.86	0.00	0.62	0.79	0.85	0.13	0.82	0.85	0.84
	Leak	0.78	0.75	1.32	0.92	0.81	0.78	1.18	0.80	0.76	0.77
	F_{boat}	0.52	0.49	0.00	0.00	0.68	0.53	<0.01	0.66	0.45	0.56
QSS_{lock}	I_{ext}	0.17	0.25	0.00	0.00	0.02	0.10	-0.01	0.02	0.22	0.18
	V_{lock}	0.68	0.56	0.00	1.00	0.81	0.73	1.00	0.80	0.63	0.70
	$CS_{boat,non}$	0.85	0.86	0.00	0.63	0.83	0.85	0.60	0.84	0.85	0.85
	F_{boat}	1.58	1.61	0.00	0.00	1.70	1.76	0.00	1.64	1.54	1.61
QSS_{tot}	I_{ext}	0.31	0.30	0.02	0.03	0.13	0.31	0.01	0.05	0.42	0.35
	L	0.67	0.73	-0.53	0.32	0.61	0.71	-0.36	0.65	0.72	0.69
	D_{weir} ‡	0.80	0.82	0.11	0.65	0.72	0.83	0.20	0.77	0.82	0.81
	D_{lock} †	0.58	0.56	0.15	0.51	0.58	0.59	0.27	0.61	0.58	0.59
	$CS_{boat,non}$	0.83	0.86	<0.01	0.62	0.82	0.85	0.13	0.83	0.85	0.84
	F_{boat}	0.87	0.93	<0.01	0.00	0.93	0.96	<0.01	0.93	0.87	0.89

† Only significant at the -25% level, when $D_{lock} < D_{weir}$.

‡ Average sensitivity for D_{weir} ±10% and -25%; at D_{weir} +25%, the weir depth exceeded lock depth and caused an excessive sensitivity.

Table 30. Sensitivity of non-cohesive sediment concentration to variables which cause an absolute value for S_r less than 0.5.

Sensitivity	Variable (sign of S_r)	
$S_r > 0.1$ or $S_r < -0.1$	I_{ext} (+) L (+) W (-) D_{weir} (+) V_{lock} (-) Leak (-)	
$0 < S_r < 0.1$ or $0 > S_r > -0.1$	PREC (+) I_{runoff} (+) PE (-) Q_{abs} (-) L_{weir} (-) Empty (-) L_{lock} (+) $CS_{lock,non}$ (+)	Diam (+) SG (+) v_b (-) ISS_{runoff} (+) ISS_{ext} (+) C_e (-) $C_{d,weir}$ (-) Seep (-)
$S_r = 0$	H_{sides} T_{mean} C_{rad} $CS_{lock,coh}$ $Boat_{coh}$ τ_{cd} $C_{d,drag}$ $K_{s,l}$ C_{chl}	$ISS_{ext,alg}$ TP RAD T_{mag} T_{phase} E_{boat} EXTB LITSED LITALG

D.2. Cohesive Sediment Variables

The key parameters to which the cohesive sediment variables are most sensitive are listed in Table 31. Table 32 complements the data for SS_{coh} in Table 10 on page 111, showing relative sensitivities of the concentration of cohesive sediment to the remaining parameters where $|S_r| < 0.5$.

Table 31. Key parameters to which the cohesive sediment variables are most sensitive.

Var.	Most Sig. Params.	Average Sensitivities									
		Avg	Max	Min	1Q	2Q	3Q	W	Sp	Su	A
SS_{coh}	I_{ext}	0.37	<0.01	0.03	0.04	0.52	0.37	0.01	0.06	0.55	0.43
	L	1.14	-0.07	-0.04	0.49	1.00	1.26	0.03	1.10	1.28	1.18
	W	0.55	-0.22	-0.04	0.16	0.49	0.62	-0.02	0.51	0.64	0.57
	D_{weir}	1.03	0.15	0.22	0.57	0.99	1.14	0.25	0.97	1.16	1.06
	D_{lock}	0.75	0.17	4.00	0.45	0.75	0.81	0.31	0.74	0.81	0.75
	$CS_{boat,coh}$	0.70	<0.01	0.01	0.39	0.68	0.76	0.06	0.70	0.76	0.73
	F_{boat}	0.45	0.00	<0.01	<0.01	0.55	0.48	<0.01	0.58	0.40	0.50
QSS_{abs}	Q_{abs}	0.91	0.85	0.79	0.84	0.90	0.92	0.81	0.90	0.92	0.91
	W	-0.45	-1.23	-1.04	-0.86	-0.54	-0.38	-1.05	-0.50	-0.36	-0.44
	$CS_{boat,coh}$	0.70	0.02	0.01	0.39	0.66	0.76	0.06	0.70	0.76	0.73
	F_{boat}	0.54	0.00	0.00	0.00	0.59	0.63	0.00	0.59	0.55	0.59
QSS_{weir}	I_{runoff}	0.93	0.96	+‡	3.55	1.33	0.89	1.28	0.90	1.21	0.66
	I_{ext}	5.36	3.54	+‡	8.23	16.3	5.03	2.33	3.72	7.86	6.09
	Q_{abs}	-0.90	-0.55	-‡	-4.72	-2.02	-0.85	-0.62	-0.62	-1.30	-1.04
	D_{weir}*	-2.83	-2.67	-‡	-6.50	-5.68	-2.65	-2.87	-2.74	-2.96	-2.88
	L_{weir}	-0.66	-0.66	-‡	-0.50	-0.60	-0.65	-0.63	-0.66	-0.65	-0.65
	Empty	-0.83	-0.47	0.66	-0.48	-4.86	-0.65	-0.03	-0.40	-1.62	-0.88
	V_{lock}	-1.97	-1.12	-4.87	-4.93	-6.48	-1.73	-0.09	-1.10	-3.55	-2.06
	$CS_{boat,coh}$	0.90	0.90	-3.41	0.85	0.87	0.91	0.99	0.91	0.87	0.90
	$C_{d,weir}$	-0.65	-0.66	-‡	-0.49	-0.60	-0.65	-0.63	-0.66	-0.65	-0.65
	Leak	-1.63	-1.03	-‡	-5.91	-4.04	-1.59	-1.16	-1.14	-2.33	-1.88
	F_{boat}	-1.03	-0.18	-1.59	-4.82	-4.82	-0.81	0.00	-0.19	-2.55	-1.11
QSS_{dep}	I_{ext}	0.37	<0.01	0.03	0.04	0.52	0.37	0.01	0.06	0.55	0.43
	L	1.14	-0.07	-0.04	0.49	1.00	1.26	0.03	1.10	1.28	1.18
	W	0.55	-0.22	-0.04	0.16	0.49	0.62	-0.02	0.51	0.64	0.57
	D_{weir}*	1.03	0.15	0.22	0.57	0.99	1.14	0.25	0.97	1.16	1.06
	D_{lock}†	0.75	0.17	4.00	0.45	0.75	0.81	0.31	0.74	0.81	0.75
	$CS_{boat,coh}$	0.70	<0.01	0.01	0.39	0.68	0.76	0.06	0.70	0.76	0.73
	F_{boat}	0.45	0.00	<0.01	<0.01	0.55	0.48	<0.01	0.58	0.40	0.50
QSS_{leak}	I_{ext}	0.37	<0.01	0.03	0.04	0.52	0.37	0.01	0.06	0.55	0.43
	W	-0.46	-1.26	-1.04	-0.87	-0.51	-0.39	-1.06	-0.50	-0.36	-0.44
	D_{weir}*	1.03	0.12	0.21	0.57	0.98	1.14	0.23	0.96	1.16	1.05
	D_{lock}†	0.78	0.25	4.00	0.49	0.78	0.83	0.36	0.78	0.83	0.78
	$CS_{boat,coh}$	0.70	<0.01	0.01	0.39	0.68	0.76	0.06	0.70	0.76	0.73
	Leak	0.82	1.38	1.32	1.04	0.84	0.80	1.23	0.84	0.77	0.80
	F_{boat}	0.45	0.00	<0.01	<0.01	0.55	0.48	0.00	0.58	0.40	0.50
QSS_{lock}	V_{lock}	0.71	0.59	0.00	1.00	0.83	0.75	1.01	0.82	0.66	0.73
	$CS_{boat,coh}$	0.76	0.78	0.00	0.39	0.72	0.76	0.37	0.73	0.77	0.75
	F_{boat}	1.53	1.57	0.00	0.00	1.63	1.70	0.00	1.57	1.50	1.55
QSS_{tot}	I_{ext}	0.28	0.28	0.02	0.03	0.10	0.29	0.01	0.05	0.38	0.32
	L	0.53	0.61	-0.52	-0.01	0.49	0.60	-0.47	0.50	0.61	0.56
	D_{weir}*	0.69	0.75	0.11	0.44	0.65	0.74	0.14	0.66	0.74	0.71
	D_{lock}†	0.51	0.51	4.00	0.36	0.52	0.54	0.22	0.53	0.53	0.52
	$CS_{boat,coh}$	0.72	0.78	<0.01	0.39	0.69	0.76	0.06	0.71	0.77	0.73
	F_{boat}	0.79	0.88	0.00	0.00	0.84	0.91	<0.01	0.84	0.83	0.83

* Average sensitivity for D_{weir} ±10% and -25%; at D_{weir} +25%, the weir depth exceeded lock depth and caused an excessive sensitivity.

† Only significant at the -25% level, when $D_{lock} < D_{weir}$.

‡ Model output minimum Q_{weir}s are all <<0.00001 so sensitivity calculation is skewed; sign indicates the sign of the change.

Table 32. Sensitivity of cohesive sediment concentration to variables which cause an absolute value for S_r less than 0.5.

Sensitivity	Variable (sign of S_r)	
$S_r > 0.1$ or $S_r < -0.1$	L (+) V_{lock} (-) L_{lock} (+) $CS_{lock,coh}$ (+) ISS_{ext} (+) Leak (-)	
$0 < S_r < 0.1$ or $0 > S_r > -0.1$	PREC (-) PE (-) I_{runoff} (+) I_{ext} (+) Q_{abs} (-) D_{weir} (+) L_{weir} (-) D_{lock} (+) T_{mean} (+) C_{rad} (+) Empty (-) $CS_{lock,non}$ (-) diam (-) sg (+) $CS_{boat,non}$ (-) v_b (-)	ISS_{runoff} (+) $ISS_{ext,alg}$ (+) TP (+) RAD (+) T_{mag} (+) T_{phase} (+) C_e (+) $C_{d,weir}$ (-) Seep (+) τ_{cd} (+) $C_{d,drag}$ (-) EXTB (-) $K_{s,l}$ (-) C_{chl} (+) LITSED (-) LITALG (+)
$S_r = 0$	H_{sides}	E_{boat}

D.3. Algal Variables

The key parameters to which the algal variables are most sensitive are listed in Table 33. Table 34 complements the data for SS_{alg} in Table 10 on page 111, showing relative sensitivities of the concentration of algal mass to the remaining parameters where $|S_r| < 0.5$.

Table 33. Key parameters to which the algal variables are most sensitive. (continues next page)

Var.	Most Sig. Params.	Average Sensitivities									
		Avg	Max	Min	1Q	2Q	3Q	W	Sp	Su	A
SS_{alg}	I_{ext}	-1.25	-0.39	-¶	-1.20	-0.93	-1.17	-0.76	-1.42	-1.40	-1.02
	L	1.86	1.37	+¶	1.55	1.74	1.89	1.68	1.73	2.07	1.64
	W	2.02	1.36	+¶	1.57	1.81	2.10	1.67	1.83	2.33	1.78
	D_{weir} †	1.12	1.36	0.00	0.99	1.06	1.02	1.54	1.04	1.05	0.93
	D_{lock} ‡	0.85	-0.40	0.00	0.82	0.93	0.82	1.12	0.85	0.80	0.70
	T_{mean}	0.60	0.05	0.00	0.34	0.52	0.70	0.13	0.54	0.84	0.47
	$ISS_{ext,alg}$	0.85	0.00	0.00	1.00	0.98	0.98	0.26	0.98	0.96	0.99
	EXTB	-0.47	-0.05	0.00	-0.39	-0.45	-0.56	-0.14	-0.42	-0.62	-0.45
QSS_{abs}	I_{ext}	-1.57	-0.44	-¶	-1.31	-1.49	-1.57	-0.81	-1.48	-1.90	-1.55
	Q_{abs}	1.08	1.04	1.00	1.07	1.08	1.09	1.08	1.06	1.10	1.07
	L	0.85	0.39	+¶	0.55	0.73	0.88	0.68	0.72	1.05	0.63
	W	1.00	0.38	+¶	0.58	0.80	1.05	0.67	0.81	1.29	0.76
	T_{mean}	0.60	0.05	0.00	0.36	0.53	0.69	0.13	0.54	0.84	0.47
	$ISS_{ext,alg}$	0.85	0.00	0.00	1.00	0.98	0.98	0.26	0.98	0.96	0.99
	EXTB	-0.44	-0.05	0.00	-0.39	-0.43	-0.50	-0.14	-0.42	-0.57	-0.43
QSS_{weir}	I_{ext}	1.65	1.24	3.92	3.70	2.35	1.83	0.85	0.83	3.08	2.78
	Q_{abs}	-0.51	-0.42	-1.13	-1.39	-0.50	-0.51	-0.36	-0.33	-0.79	-0.75
	L	0.67	0.19	+¶	0.41	0.46	0.74	0.51	0.65	0.93	0.46
	W	0.80	0.22	+¶	0.54	0.57	0.96	0.52	0.75	1.19	0.60
	D_{weir} †	-1.65	-1.81	-2.70	-3.08	-1.90	-1.81	-1.57	-1.65	-1.64	-1.89
	T_{mean}	0.49	0.05	0.00	0.42	0.38	0.67	0.12	0.53	0.85	0.42
	V_{lock}	-0.99	-0.06	-3.52	-2.64	-1.31	-1.32	-0.04	-0.54	-2.29	-1.61
	$ISS_{ext,alg}$	0.77	0.00	0.00	1.00	1.00	0.96	0.23	0.98	0.96	0.99
	Leak	-0.96	-0.59	-3.73	-2.44	-1.11	-1.00	-0.60	-0.68	-1.52	-1.42
	F_{boat}	-1.11	0.00	-3.50	-2.64	-1.41	-1.55	0.00	-0.62	-2.61	-1.76
QSS_{leak}	I_{ext}	-1.25	-0.39	-¶	-1.20	-0.93	-1.17	-0.76	-1.42	-1.40	-1.02
	L	0.85	0.38	+¶	0.55	0.73	0.87	0.68	0.72	1.04	0.63
	W	0.99	0.37	+¶	0.56	0.80	1.07	0.67	0.81	1.28	0.76
	D_{weir} †	1.11	1.34	<0.01	0.99	1.04	1.02	1.52	1.03	1.05	0.93
	D_{lock} ‡	0.88	-0.31	0.00	0.85	0.95	0.84	1.17	0.89	0.82	0.73
	T_{mean}	0.60	0.05	0.00	0.34	0.52	0.70	0.13	0.54	0.84	0.47
	$ISS_{ext,alg}$	0.85	0.00	0.00	1.00	0.98	0.98	0.26	0.98	0.96	0.99
	Leak	1.05	1.20	1.00	0.98	1.00	1.03	1.15	1.02	1.04	1.02
	EXTB	-0.47	-0.05	0.00	-0.39	-0.45	-0.56	-0.14	-0.42	-0.62	-0.45
QSS_{lock}	I_{ext}	-1.76	-2.17	0.00	-0.89	-1.40	-1.33	-0.75	-1.56	-1.87	-1.57
	L	0.92	1.13	0.00	0.33	0.61	0.80	0.77	0.73	1.04	0.66
	W	1.13	1.42	0.00	0.32	0.66	1.03	0.75	0.84	1.28	0.82
	T_{mean}	0.73	0.92	0.00	0.16	0.43	0.65	0.09	0.56	0.83	0.51
	V_{lock}	1.09	1.13	0.00	1.00	1.01	1.08	1.00	1.05	1.11	1.08
	$ISS_{ext,alg}$	0.96	0.96	0.00	1.00	0.98	0.95	0.03	0.98	0.96	0.99
	EXTB	-0.56	-0.67	0.00	-0.20	-0.34	-0.54	-0.10	-0.43	-0.62	-0.47
	$K_{s,l}$	-0.48	-0.58	0.00	-0.17	-0.28	-0.48	-0.10	-0.36	-0.53	-0.40
	F_{boat}	0.80	0.69	0.00	0.00	0.93	0.76	0.00	0.83	0.79	0.86
QSS_{tot}	I_{ext}	-0.60	0.60	-¶	-0.33	-0.50	-0.64	0.11	-0.56	-0.88	-0.48
	L	0.82	0.26	+¶	0.46	0.66	0.81	0.59	0.69	1.02	0.60
	W	0.98	0.28	+¶	0.48	0.77	1.03	0.59	0.79	1.27	0.75
	T_{mean}	0.61	0.05	0.00	0.29	0.54	0.67	0.12	0.54	0.84	0.47
	$ISS_{ext,alg}$	0.86	0.00	0.00	1.00	0.98	0.98	0.24	0.98	0.96	0.99
	EXTB	-0.47	-0.05	0.00	-0.31	-0.47	-0.51	-0.13	-0.42	-0.61	-0.44

Var.	Most Sig. Params.	Average Sensitivities									
		Avg	Max	Min	1Q	2Q	3Q	W	Sp	Su	A
ISS_{bio}	I_{ext}	-1.59	-0.21	-[¶]	-1.29	-1.27	-1.36	-0.75	-1.45	-1.75	-1.43
	L	1.77	1.18	+[¶]	1.54	1.71	1.69	1.59	1.66	1.88	1.51
	W	2.24	1.20	+[¶]	1.67	2.03	2.25	1.59	1.95	2.45	1.99
	T_{mean}	1.43	0.76	0.74	1.11	1.27	1.42	0.91	1.28	1.57	1.23
	C_{rad}	0.96	0.79	0.77	0.99	0.91	1.01	0.85	0.84	1.01	1.00
	$ISS_{ext,alg}$	0.91	0.00	<0.01	0.99	0.82	0.94	0.44	0.95	0.92	0.97
	RAD	0.96	0.79	0.77	0.99	0.91	1.01	0.85	0.84	1.01	1.00
	T_{mag}	0.52	-0.42	-0.41	-0.32	-0.04	0.60	-0.47	0.15	0.81	0.23
	T_{phase}	0.49	-0.45	-0.34	-1.49	0.30	0.74	0.14	2.59	0.15	-2.33
	EXTB	-1.13	-0.98	-0.95	-1.21	-1.10	-1.13	-1.04	-1.02	-1.17	-1.19
	$K_{s,l}$	-0.99	-0.81	-0.79	-1.03	-0.94	-1.03	-0.87	-0.85	-1.04	-1.04
	LITSED	-0.68	-0.05	-0.09	-0.19	-0.37	-0.76	-0.07	-0.47	-0.80	-0.71

[†] Average sensitivity for D_{weir} ±10% and -25%; at D_{weir} +25%, the weir depth exceeded lock depth and caused an excessive sensitivity.

[‡] Only significant at the -25% level, when $D_{lock} < D_{weir}$.

[¶] Because the minimum algae concentration was nearly zero, extreme values of S_r were frequently calculated whenever any change in minimum algae concentration was seen; in these cases, this column is simply marked '+' or '-' to indicate a positive or negative correlation, respectively.

Table 34. Sensitivity of algal dry mass concentration to variables which cause an absolute value for S_r less than 0.5.

Sensitivity	Variable (sign of S_r)	
$S_r > 0.1$ or $S_r < -0.1$	I_{runoff} (-) D_{weir} (+) C_{rad} (+) $CS_{boat,coh}$ (-) TP (+) RAD (+)	T_{mag} (+) T_{phase} (+) $K_{s,l}$ (-) C_{chl} (+) LITSED (-) F_{boat} (-)
$0 < S_r < 0.1$ or $0 > S_r > -0.1$	PREC (-) PE (+) Q_{abs} (+) L_{weir} (-) D_{lock} (+) Empty (+) V_{lock} (+) L_{lock} (-) $CS_{lock,non}$ (-) $CS_{lock,coh}$ (-) Diam (-) SG (-)	$CS_{boat,non}$ (-) v_b (+) ISS_{runoff} (-) ISS_{ext} (-) C_e (+) $C_{d,weir}$ (-) Seep (+) Leak (+) τ_{cd} (-) $C_{d,drag}$ (+) LITALG (-)
$S_r = 0$	H_{sides}	E_{boat}

Appendix E. Calibrated Parameters for HSPF

This section provides tables of the calibrated parameters for HSPF. Table 35 lists the hydrologic parameters, and Table 36 lists the sediment parameters. Table 38 lists the parameters associated with the reaches, where the most upstream reach is reach 25. Table 39 lists the land surface parameters that vary monthly.

Table 35. Hydrologic land surface parameters for HSPF.

Parameter	Forest	Arable	Other Ag	Grassland	Urban
Pervious Land Parameters					
LZSN (in)	6				
INFILT (in/hr)	0.11				
LSUR (ft)	405.9	417.0	373.7	414.7	434.4
SLSUR	0.054	0.049	0.069	0.050	0.041
AGWRC (1/day)	0.99	0.975	0.975	0.975	0.975
INFEXP	2				
INFILD	2				
DEEPFR	0.31				
BASETP	0.04				
AGWETP	0.04				
UZSN (in)	0.1				
NSUR	0.30	0.15	0.20	0.20	0.15
INTFW	1				
IRC	0.3				
Impervious Land Parameters					
LSUR (ft)					150
SLSUR					0.041
NSUR					0.05
RETSC					0.10

Table 36. Sediment land surface parameters for HSPF.

Parameter	Value
Pervious Land Parameters	
SMPF	1
KRER	0.32
JRER	2.0
AFFIX (1/day)	0.01
NVSI (lb-ac/day)	1.0
KSER	10
JSER	1.73
KGER	0
JGER	2.5
Impervious Land Parameters	
KEIM	1.0
JEIM	2.1
ACCSDP	0.01
REMSDP	0.05

Table 37. Reach parameters for HSPF constant for all reaches.

Parameter	Value
KS	0.5
DB50	0.01
POR	0.5
SAND-D (in)	0.01
SAND-W (in/sec)	0.4
SAND-RHO (g/cm^3)	2.65
SAND-KSAND	0.5
SAND-EXPSAND	2.0
SILT-D (in)	0.0006
SILT-W (in/sec)	0.0005
SILT-RHO (g/cm^3)	2.3
CLAY-D (in)	0.0001
CLAY-W (in/sec)	0.00001
CLAY-RHO (g/cm^3)	2.0

Table 38. HSPF reach parameters that vary by reach.

Reach #	LEN (mi)	DELTH (ft)	BEDWID (ft)	TAUCD – SILT (lb/ft²)	TAUCS – SILT (lb/ft²)	M – SILT (lb/ft²d)	TAUCD – CLAY (lb/ft²)	TAUCS – CLAY (lb/ft²)	M – CLAY (lb/ft²d)
13	1.35	9.84	42.65	0.25	0.85	0.010	0.18	0.75	0.010
14	2.07	26.25	39.37	0.44	0.85	0.010	0.32	0.75	0.010
15	1.52	16.41	36.09	0.37	0.85	0.010	0.27	0.75	0.010
16	2.64	19.69	32.81	0.3	0.85	0.010	0.25	0.75	0.010
17	0.59	9.84	32.81	0.51	0.85	0.010	0.36	0.75	0.010
18	0.99	3.28	32.81	0.3	0.85	0.010	0.25	0.75	0.010
19	0.40	9.84	26.25	0.75	1.75	0.010	0.53	1.50	0.010
20	1.53	6.56	24.61	0.3	1.00	0.010	0.25	0.90	0.010
21	2.16	26.25	22.97	0.27	1.00	0.010	0.25	0.90	0.010
22	0.72	9.84	19.69	0.28	0.75	0.015	0.17	0.65	0.015
23	4.36	52.50	19.69	0.25	0.75	0.015	0.15	0.65	0.015
24	2.94	32.81	16.41	0.2	0.75	0.015	0.12	0.65	0.015
25	1.69	32.81	13.12	0.28	0.75	0.015	0.17	0.65	0.015

Table 39. Land surface parameters for HSPF that vary monthly.

Parameter	Land Use	Jan	Feb	Mar	April	May	Jun	Jul	Aug	Sep	Oct	Nov	Dec
CEPSC	Forest	0.03	0.03	0.05	0.09	0.14	0.18	0.18	0.14	0.09	0.07	0.05	0.03
	Arable	0.02	0.02	0.09	0.1	0.15	0.2	0.2	0.15	0.1	0.08	0.03	0.03
	Other Ag	0.03	0.03	0.08	0.1	0.15	0.2	0.2	0.15	0.1	0.08	0.05	0.03
	Grassland	0.04	0.05	0.06	0.07	0.08	0.09	0.09	0.09	0.08	0.07	0.06	0.05
	Urban	0.04	0.05	0.06	0.07	0.08	0.09	0.09	0.09	0.08	0.07	0.06	0.05
LZETP	Forest	0.3	0.35	0.4	0.45	0.5	0.65	0.65	0.6	0.5	0.45	0.4	0.35
	Arable	0.1	0.1	0.1	0.2	0.2	0.65	0.65	0.6	0.5	0.45	0.2	0.1
	Other Ag	0.1	0.1	0.1	0.2	0.2	0.65	0.65	0.6	0.5	0.45	0.2	0.1
	Grassland	0.3	0.35	0.4	0.45	0.5	0.65	0.65	0.6	0.5	0.45	0.4	0.35
	Urban	0.3	0.35	0.4	0.45	0.5	0.65	0.65	0.6	0.5	0.45	0.4	0.35
COVER	Forest	0.75	0.75	0.75	0.8	0.8	0.8	0.8	0.8	0.8	0.8	0.75	0.75
	Arable	0.55	0.55	0.55	0.6	0.65	0.65	0.65	0.65	0.65	0.65	0.55	0.55
	Other Ag	0.25	0.25	0.25	0.3	0.35	0.35	0.35	0.35	0.35	0.35	0.25	0.25
	Grassland	0.7	0.7	0.7	0.75	0.8	0.8	0.8	0.8	0.8	0.8	0.7	0.7
	Urban	0.7	0.7	0.7	0.75	0.8	0.8	0.8	0.8	0.8	0.8	0.7	0.7